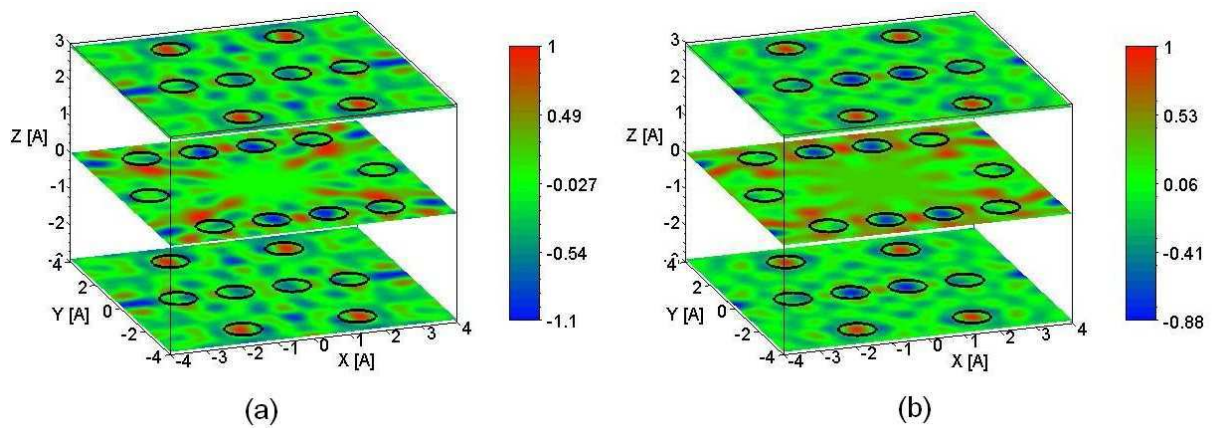# PROGRESS REPORT

ON THE
ACTIVITIES
AT THE

BUDAPEST RESEARCH REACTOR

2008 - 2009

September 2011

Budapest Neutron Centre
Progress report 2008-2009
Edited by R. Baranyai, M. Makai, L. Rosta
Budapest, September 2011

Postal address and contact persons:

KFKI Atomic Energy Research Institute
Hungarian Academy of Sciences
1525 Budapest 114, POB 49, Hungary
Dr. Rózsa F. Baranyai
Phone: 36-1-392-2222
Fax: 36-1-395-9293
e-mail: baranyai@aeki.kfki.hu

Institute of Isotopes
1525 Budapest 114, POB 49, Hungary
Dr. Tamás BELGYA
Phone: 36-1-392-2539
Fax: 36-1-392-2584
e-mail: belgya@iki.kfki.hu

Research Institute for Solide State Physics and Optics
Hungarian Academy of Sciences
1525 Budapest 114, BOB 49, Hungary
Dr. László ROSTA
Phone: 36-1-392-2296
Fax: 36-1-395-9293
e-mail: rosta@szfki.hu

KFKI Research Institute for Particle and Nuclear Physics
Hungarian Academy of Sciences
1525 Budapest 114, BOB 49, Hungary
Dr. Bottyán László
Phone: 36-1-392-2761
Fax: 36-1-392-2598
e-mail: bottyan@nucssp.rmki.kfki.hu

Location:

Budapest Research Reactor
1121 Budapest, Konkoly Thege út 29-33
KFKI, Bld, 10.

Cover page figure:
 Real part of the reconstructed measured (a) and calculated (b) neutron hologram of SnCd sample

CONTENTS

PREFACE

The Budapest Research Reactor (BRR) was operated according to its usual regime, resuming 12 and 11 ten-day cycles in 2008 and 2009, respectively. This is somewhat less than in the previous years (15-16 cycles), since the reactor core conversion programme was started. Following the commitment to join the Russian Research Reactor Fuel Return (RRRFR) programme, BRR signed an agreement to repatriate spent and fresh HEU nuclear fuel stored at our site to Russia and made a commitment to convert the BRR's core from high enriched uranium (HEU) to low enriched uranium (LEU). The first spent nuclear fuel shipment (all assemblies irradiated before 2005) was performed in autumn of 2008. The *fresh* HEU fuel stored at BRR's site was shipped back to Russia in July 2009. The preparation for the core conversion has been running since 2007. The selected type of LEU was the Russian made VVR-M2 fuel, similar to the previously used VVR-M and -M2 HEU fuel elements. In this way the core conversion scenario was including HEU and LEU fuels with gradually decreasing HEU fuel assembly numbers. During the core conversion 4 cycles with mixed HEU-LEU cores takes place (over 8 months), then the utilisation of HEU fuel will be finished in early 2012 and later on only 20% enriched fuel will be used. No significant loss in neutron flux is expected.

The BNC facilities – a suit of reactor irradiation equipment, thermal neutron beam instruments and cold neutron spectrometers in the neutron guide hall – are open for the international user community. Research proposals can be submitted twice a year, an international selection panel takes care of the review of the proposals. This panel meets ones a year, the proposals are, however, evaluated after the submission by the panel members and even "fast-track" processing of proposals is possible thanks to the electronic communication. BNC was involved in the EU FP6 Neutron and Muon Integrated Infrastructure Initiative (NMI3) access programme providing the possibility for many experiments, which have been performed by EU partner users. The NMI3 project was closed in June 2008. Resuming the 4 years activity we were very pleased to realize, that the international community has highly appreciated the BNC contribution: at the concluding general assembly meeting 4 European experts presented in different fields a selection of highlights out of the nearly 1000 experiments performed in the frame of NMI3. Eleven of the presented 32 highlight were performed at our reactor! Another success of BNC: In 2009 another FP7 project was started, we have been invited as the "neutron facility" in the CHARISMA projects, which puts together a consortium of large European museums (Louvre, British Museum, Prado…) and scientific facilities to join efforts for the investigation of objects of cultural heritage.

Thus BNC services are available for researchers both from member states and associated states of the European Community. A table showing the experimental stations is given in the Appendix. The call for proposals including the conditions how one can make use of the EC travel support is regularly advertised in the journal Neutron News and on the web (www.bnc.hu). The web site of BNC offers also the possibility of reading reports on BNC activities, e.g. the present Report. We assume that BNC plays an important role as a regional hub for neutron beam experiments, and our aim is to boost growing interest and competence in applied materials science in Central Europe.

The instrument development programme was progressed, mostly thanks to a domestic project (named Large International Projects, with Hungarian acronym NAP) financed by the Hungarian Innovation Fund. Within this NAP project the installation of a new reflectometer was realized and the extension of the PGAA stations has been performed. The TOF diffractometer has also reached a routine operation mode. In the first part of this volume a selection of topics and highlights on the research avtivity is presented. This booklet gives also the description of our experimental stations. A list of publications concerning this two years activity is also attached.

Budapest, October 2011

János Gadó
Chairman of the BNC
Board of Directors

5

1. BUDAPEST RESEARCH REACTOR

Sándor Tőzsér, Ferenc Gajdos

The Budapest Research Reactor (BRR) is a tank-type reactor, moderated and cooled by light water. The reactor, which went critical in 1959, is of Soviet origin. The initial thermal power was 2 MW. The first upgrade took place in 1967 when the power was increased to 5 MW, using a new type of fuel and a beryllium reflector. A full-scale reactor reconstruction and upgrade project started in 1986. The upgraded 10 MW reactor received the operation license in November 1993. In line with Hungarian safety regulations a periodic safety review (PSR) was conducted in 2002-2003, as a result of which the operation license was renewed in November 2003, it is now valid until further notice, however PSRs are foreseen every ten years.

The BRR site, the Reactor Hall and the Control Room can be seen in the photo below.

1: Reactor Building with the Control Room being on the 2nd floor   ♦   2: Reactor Hall   ♦   3: Engine Room with air filters of the Air Ventilation System   ♦   4: Secondary Pump Room   ♦   5: Cooling Towers   ♦   6: Auxiliary Building accommodating the Diesel Generators and Compressed Air System   ♦   7: Building of the Liquid Waste Storage Facilities (under the foreground area two storage tanks are accommodated   ♦   8: AFR-pool Service Hall (with solid waste storage wells in the foreground area)   ♦   9: CNS's Measuring Hall   ♦   10: TOF's Measuring Hall

Bird's eye view of the BRR site

Panorama view of Reactor Hall   *Control Room*
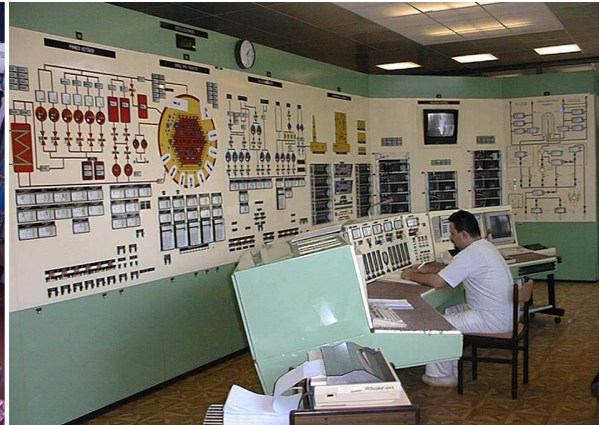
1.1. Main technical data

Reactor type: ....Light-water cooled and moderated tank-type reactor with beryllium reflector

Fuel:..Mixed core: 190 pcs. VVR-SM(-M2) with 36 % ^{235}U initial enrichment and 38 pcs. VVR-SM with less than 20 % ^{235}U

Core geometry:...............................Hexagonal (height: 600 mm; $\varnothing$ 1000 mm)

Equilibrium core: ....228 fuel assemblies (in single equivalent)

Control: ....• 3 safety rods (B4C); • 14 shim rods (B4C); • 1 automatic (fine) rod (SS)

Nominal thermal power: ....10 MW

Mean power density in the core: .....39,7 kW/litre

Neutron flux density in the core:.....   2.1 * 10^{14} n/cm^{2}s (thermal in the flux trap, measured by the gold foil)

       1 * 10^{14} n/cm^{2}s (approx. max. fast flux in the fast channel)

Operation in 2009
The operation time record (scheduled and performed) and the operation cycles performed in 2009 are shown below.
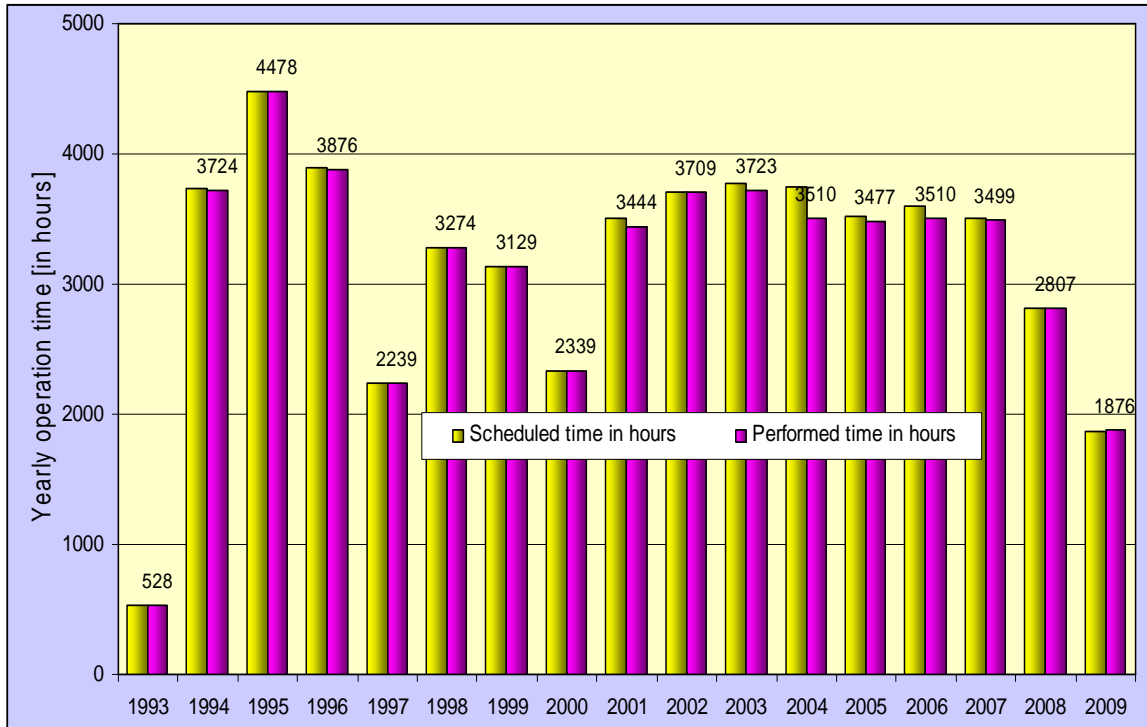
Operation time record
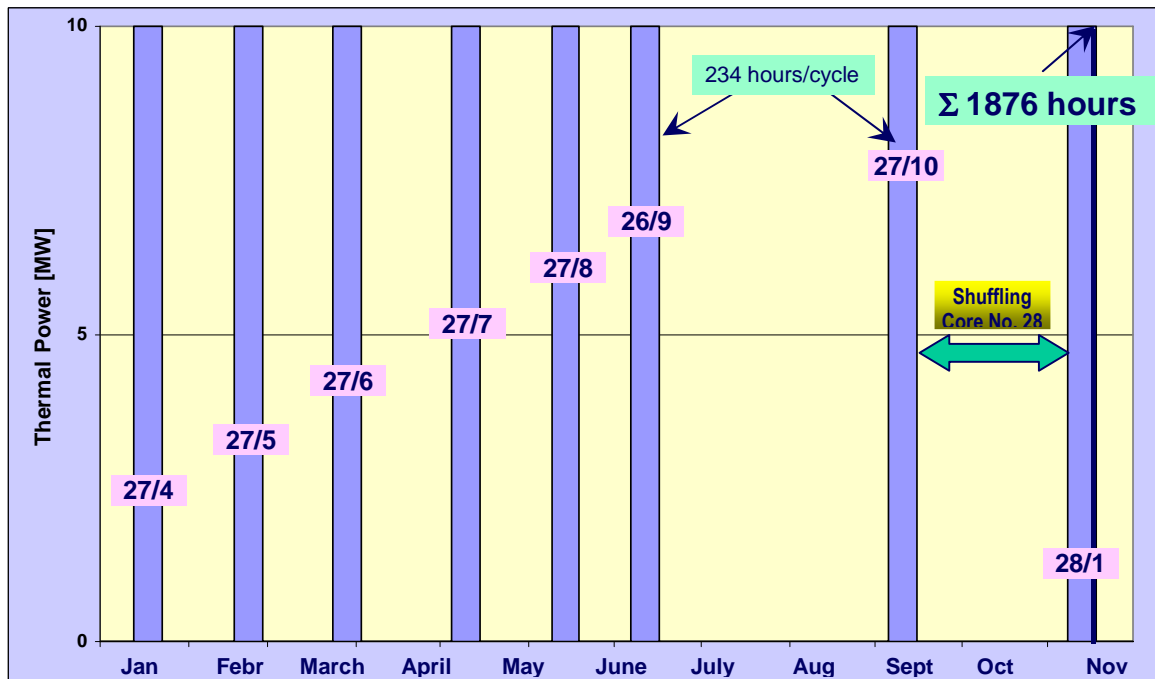
Operation cycles in 2009

1.2. Core conversion from HEU to LEU

BRR joined the Russian Research Reactor Fuel Return (RRRFR) project. The project was financed by US DOE National Nuclear Security Administration's Global Threat Reduction Program. In 2008, all the spent HEU fuel, used before 2005 was repatriated to the Russian Federation, and in 2009 the fresh HEU as well. It was declared, that exclusively LEU fuel assemblies will be used in the future. The core conversion is in progress, currently mixed cores with HEU and LEU assemblies are used. The last HEU assemblies will be reloaded late 2012 according to reactor schedule. The last spent HEU fuel is foreseen to be returned to Russia in 2014 in the frameworks of RRRFR project as well.

During these periods (repatriations and procurement) the operating personal was overloaded with work; consequently the reactor operation time had to be decreased.
As the spent fuel storage pool had been emptied, the cleaning and inspection of the pool could be carried out. The inspection allowed to make the statement, that the pool is suitable for at least 30 more years of use.

1.3. Utilization

Since its initial criticality, the BRR has been utilized as a neutron source for research and various industrial and health care applications. Irradiations are performed in vertical channels (the reactor has now more than 40 channels, they can be used for isotope production and material testing) whereas physical experiments are carried out at the horizontal neutron beam ports. The reactor has ten beam ports (eight radial and two tangential) and nearly all of them are constantly in use. There are a total of thirteen so called 'larger scale experimental facilities' installed at the BRR's beam ports. The utilization matters are coordinated and managed by the Budapest Neutron Centre, which is a consortium founded by four academic institutions in 1993. Under the guidance of the BNC the 13 measuring sites opened a possibility for operating the BRR as a regional centre. In promoting that activity, the European Framework Programs helped substantially. In 2008 within the scope of the European Union FP-7 research program, the NMI3 international co-operation gave the possibility for hundreds of users to carry out their research plans partly or entirely at the BRR.

1.4. Accommodation to the changing word - East European Research Reactor Initiative (EERRI)

While the reactor has been fulfilling its traditional mission duties since its first criticality, the operating environment – especially financial, safety, and security requirements – as well as user and public demands, were significantly changed in recent years. Thus, perceiving these changing demands a research reactor coalition was launched under the name of EERRI by the initiation of BRR. The exploratory meeting was held in Budapest, Hungary on January 28-29, 2008 at the invitation of the KFKI Atomic Energy Research Institute (AEKI). This coalition original was founded by 5 reactors but by the end of 2008 it has 8 research and education/training reactors with two observers institutions (see table below).

Strategic goal of the coalition is that improved services for the user communities are offered which will prepare themselves for the time of using leading-edge European facilities based on the synergy effect of the existing facilities participating in the coalition. Areas of Cooperation and Collaboration are: (1) education and training; (2) neutron beam application, (3) isotope production, and finally (4) irradiation of fuel and materials/PIE.

Summarizing the activities of the EERRI coalition, a formalized and regular dialogue among the RR operators can be mentioned as the most important achievement. Beyond the sharing of information, a kind of joint thinking and planning has been started since the first meeting. It is expected that this process will strengthen and develop.

List of EERRI's members

Country	Organization	Reactor	Satus	Specific EERRI duties
Austria	TU Vienna	TRIGA 250 kW	EERRI member	Coordinator on training activities
Czech Republic	NRI Rez	LWR-15 10 MW	EERRI member	Coordinator fuel and material irradiation and PIE
Czech Republic	CTU Prague	VR-1 (1 kW)	EERRI member	–
Hungary	AEKI	BRR 10 MW	EERRI member	General coordination of EERRI matters
				Coordinator on neutron scattering and beam application
Hungary	TU Budapest	100 kW	EERRI member	–
Poland	IAE Swierk	MARIA 30 MW	EERRI member	Coordinator on isotope production
Romania	ICN Pitesti	TRIGA 14 MW	EERRI member	–
Slovenia	JSI Ljubjana	TRIGA 250 kW	EERRI member	–
Austria	IAEA	–	Observer	Organizational issues
Serbia	Vinca Institute	–	Observer	

2. INTERNATIONAL SCIENTIFIC ADVISORY BOARD

Ferenc Mezei chairman	Los Alamos National Laboratory, USA KFKI, Research institute for Solid State Physics and Optics, Hungary
Alexander Ioffe	Forschungszentrum Jülich, Germany
Béla Faragó	Institute Laue-Langevin, France
Gerard Pepy	Laboratorie Leon Brillouin, France
Gerhard Krexner	Institute of Experimental Physics, Austria
Helmut Schober	Institute Laue-Langevin, France
János Major	Max-Planck Institute für Metallforschung,Germany
Josef Plestil	Institute of Macromolecular Chemistry, Czech Republic
László Cser	MTA, Research Institute for Solide State Physics and Optics
László Rosta	MTA, Research Institute for Solide State Physics and Optics
Massimo Rogante	Rogante Engeering Office, Italy
Matthias Rossbach	Forschungszentrum Juelich GmbH, Germany
Michael Jentschel	Institute Laue-Langevin, France
Mihály Makai	MTA KFKI Atomic Energy Research Institute
Pavol Mikula	Nuclear Physics Institute, Czech Republic
Rózsa F. Baranyai	MTA KFKI Atomic Energy Research Institute
Tamás Belgya	MTA Institute of Isotopes
Thomas Geue	Paul Sherrer Institute, Switzerland
Viktor L. Aksenov	Joint Institute for Nuclear Research, Russia

3. USER SELECTION PANEL

Gerard Pepy chairman	Laboratorie Leon Brillouin, France
Charles de Novion	Laboratorie Leon Brillouin, France
Flavio Carsughi	Universita Politechnica delle Marche, Italy
Gerhard Krexner	Institute of Experimental Physics, Austria
János Major	Max-Planck Institute für Metallforschung,Germany
Josef Plestil	Institute of Macromolecular Chemistry, Czech Republic
Matthias Rossbach	Forschungszentrum Juelich GmbH, Germany
Michael Jentschel	Institute Laue-Langevin, France
Mihály Makai	Budapest Technical University, Hungary
Tamás Grósz	Chemical Research Centre, Hungary

4. RESULTS OF RESEARCH ACTIVITIES
(Highlights)

4.1. Condensed Matter Research by Neutron Spectroscopy

L. Rosta, L. Almásy, L. Cser, I. Füzesy, J. Füzi, A. Len, M. Markó, A. Meiszterics, F. Mezei, G. Nagy, J. Orbán, E. Rétfalvi, L. Riecsánszky, Zs. Sánta, N. Székely, Gy. Török, T. Veres

Research Institute for Solid State Physics and Optics, Neutron Spectroscopy Department

The activity of our Department is directly related to the 10 MW Budapest Research Reactor (BRR), which recently was classified as Strategic Research Infrastructure by the National Infrastructure Roadmap programme (NEKIFUT) and in fact, this is a unique large-scale facility in the Central European region. Our Department is one of the laboratories of the associate institutes forming the Budapest Neutron Centre, open for domestic and international users. Out of the 15 experimental stations of BRR, we operate several of them: on cold neutron beams – a small angle scattering (SANS) spectrometer, a reflectometer (REFL) and a three axis spectrometer (TAS), a new SANS instrument is under construction; on thermal beams – another TAS and a diffractometer (TOF-D).

Our thematic research is mainly focused on topics that may find industrial application already on the short run: we study the structure and dynamics of polymers, glasses, ceramics, geological and archaeological objects. Some highlights to be mentioned from the past few years (published in high impact journals): Direct observation of local distortion of crystal lattice with picometer accuracy using atomic resolution neutron holography *(PRL),* structural features of molecular-colloidal solutions of C60 fullerenes *(Langmuir, J.Chem.Phys.),* studies in artificial photosynthesis: effect of phosphorylation on the thermal- and light-stability of thylakoid membranes (*Photosyn.Res),* SANS investigation of swelling conditions for nanophase separation in epoxy hydrogels (*Eur.Polymer J.).*

Considerable effort has been always devoted to methodical-instrumental development. To balance in the situation of using large scale instrumentation and modest financing, we had to practice to design and build spectrometers by our own effort with using minimum commercial components. Thus, our experimental equipment consists of at a large extent home-made optical and electronics component, selectors, detectors, shielding elements etc. The other aspect of the methodical development programme is the commercialisation of neutron equipment via technology transfer to high-tech, spin-off companies. Several SMEs at the KFKI site (ANTE, Mirrotron, RegTron….) form the industrial ensemble to provide a sizable production volume in neutron instrumentation. This strategy is also confirmed by numerous successful grant applications, in accordance with the policy of funding agencies (NKTH, NFÜ) to sponsor collaboration of the academic sector with industry. Education and professional training is an important mission for us: we are involved in graduate and professional training, (teaching at several universities, performing PhD works, organising international training courses). The first comprehensive text-book on neutron scattering in Hungarian was recently published (L. Cser, Tipotex, 2009).
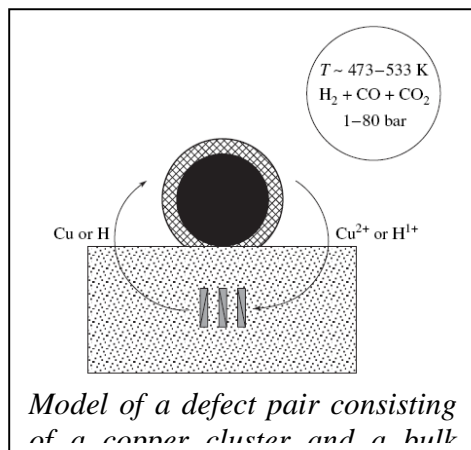
Organization and co-ordination of international relations at BNC level is also in the scope of our activity. The Hungarian membership to ILL in the context of the Central European Neutron Initiative (CENI, co-operation with AU, CZ, HU, SK) is managed also by our Department. Collaboration projects have been running, for example with the Joint Institute for Nuclear Research (Dubna) and the Kurchatov Institute Russian Research Center.

Condensed matter properties
Structure of condensed matter. Bioactive glass-ceramics and composites have been successfully used

for the repair, reconstruction, and replacement of diseased or damaged parts of the body, especially bones. The aim of our study was to prepare a bulk calcium silicate system that exhibits suitable properties to be used for biomedical applications. Glass-ceramics of composition CaO·SiO2 were produced by sol-gel technique starting from tetraethoxysilane and calcium nitrate tetrahydrate as well as by melt-quenching technique using a mixture of CaCO3 and SiO2. The traditional power technology requires 1500 °C temperature to produce ceramic bulks; contrarily the sol-gel technique 700 °C. Their structures were compared by means of thermo-analysis, X-ray diffraction, small angle X-ray and neutron scattering. The compactness of these materials is the key feature for biocompatibility, in this respect SANS measurements revealed important information on the temperature dependence of the fractal structure in various stages of the sample preparation. In the melt-quenched samples, the crystalline feature is dominated; the gel-derived samples are rather amorphous. The mechanical property of the calcium silicate materials obtained by different preparation routes were characterized by Brinell-hardness tests. The melt-quenching technology yields the glass-ceramics product with good mechanical strength at 1500 °C; while the gel derived products achieve this mechanical strength already after a heat treatment at 700 °C. The gel derived product prepared with ammonia catalyst proved to be the hardest and most compact matter.

*Applied research with neutrons – Structural features of H$_2$-containing catalysts.* The presence of hydrogen determines the activity of ZnOCuH(D) catalysts, widely used for methanol synthesis, however, the catalysis mechanism governed by hydrogen behavior inside and on the surface of copper inclusions (clusters) in the ZnO matrix remains unclear. The aim of this work is to determine Cu ordering at atomic and nano-scale level as well as the location and arrangement of hydrogen atoms in the structure, related to possible influence on catalytic activity. We prepared pairs of isotopic samples Zn0.9263Cu0.08O(H), Zn 0.92 63Cu0.08O(D), Zn0.9265Cu0.08O(H) and Zn 0.9265Cu 0.08 O(D), characterized by contrast according to the amplitudes of scattering on H, D, 63Cu and 65Cu isotopes. The migration and condensation of hydrogen in the vicinity and inside nanosized defects in the CuH(D)ZnO catalyst powders were investigated by using small-angle neutron scattering. We have obtained that the inclusions at the surface of ZnO particles and inside ZnO matrix have a complex structure: a hydrogen-rich core with radius ~ 4 nm is located in the center of the Cu cluster, surrounded by a hydrogen shell with external radius ~ 14 nm. The characteristic H(D) concentration in the core is ~15 % at., while in the shell only ~ 1 % at. with respect to metallic copper (Cu ~ 8.5x10^{22}cm^{-3}). The integral ratio on cluster volume of number of atoms is H(D) : Cu = 1 : 10. From the calculated correlation functions the hydrogen distribution model is the following: hydrogen occupies two different positions: (i) near the defects in the ZnO matrix volume and (ii) on the surface of a defect near a copper cluster. These two coupled defects can form an electrochemical pair and cause a Cu – H exchange, effective direction of which depends on the composition and temperature of the gas medium, where the catalyst is placed. Such pairs assist the decomposition of molecular hydrogen into atomic hydrogen involved in the methanol synthesis reaction.


Model of a defect pair consisting of a copper cluster and a bulk

Neutron holographic measurement on ammonium-chloride. We have made a succesfull neutron holographic measurement on ammonium-chloride (NH$_4$Cl) on the thermal three-axes

spectrometer (TAST) at the 8-th thermal neutron channel of the Budapest Research Reactor (BRR). In this measurement the protons act as internal detector and internal source of neutrons also. The simultaneously appearing inside detector and inside source holograms cause false peaks, but increase the signal-to-noise ratio. We have measured the hologram at 45° scattering angle, and rotated the sample around two axes using an Eulerian cradle. The plane of the cradle was parallel to the scattered beam. For the better signal-to-noise ratio we have put the detector close to the sample. Its total viewing angle was near 5°. The angular steps were also 5° in both directions. The reconstructed holographic peaks of the first nitrogen and first hydrogen neighbours of the hydrogen atoms are in good agreement with the model calculations.
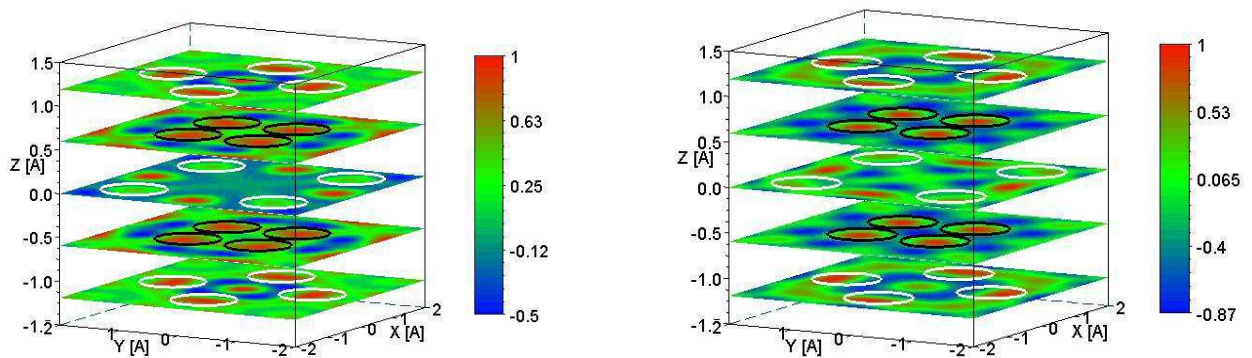

Reconstructed holographic image of ammonium-chloride from the measurement (left side) and from the model calculation (right side). The positions of hydrogen and nitrogen atoms are signed by white and black circles respectively. In the middle layer the false peaks out of the circles are the artefacts caused by the simultaneously appearing inside detector and inside source hologram.

Investigation of periodic multilayers. The recipe used nowadays in the neutron supermirror production give aperiodic multilayers. The thickness of the consecutive layers is changing from bilayer to bilayer. A new algorithm proposed by V. Ignatovich and I. Carron gives periodic supermirrors in the sense, that they are composed of periodic stacks of bilayers. The realization began in the cooperation of SZFKI, Mirrotron Ltd (Budapest) and JINR (Dubna). Already the first produced supermirrors have similar (sometimes better) reflectivity as the traditional ones under the same conditions (same sputtering machine, similar number of layers).
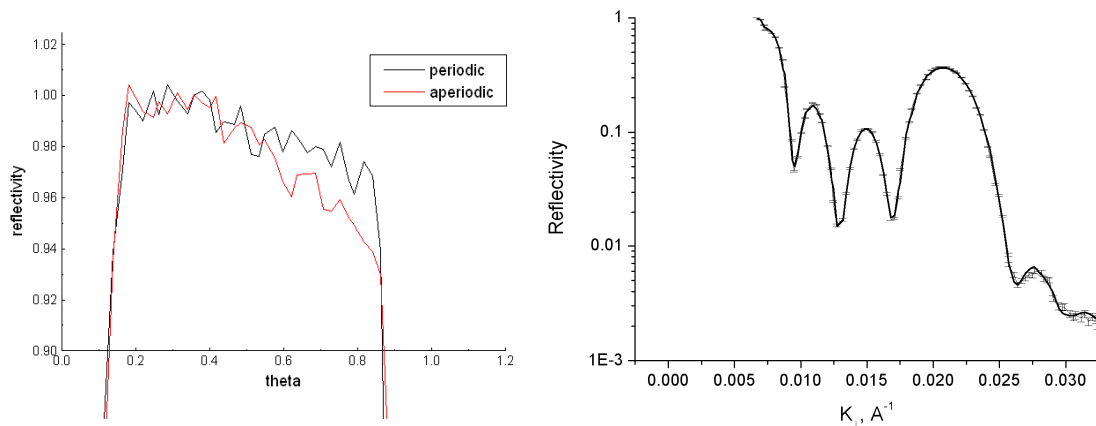
The left figure above shows the reflectivity of a periodic and aperiodic supermirror as function of incidence angle, λ=4.28 Å. The figure on the right shows the measured (bars) and fitted (line) reflectivity of a periodic multilayer. To study the imperfectness of the produced layers simple periodic multilayers were also produced which give Bragg reflection at 2 $\theta_{crit\ Ni}$. According to this condition, the thickness of Ni layers is 84 Å, and 70 Å for the Ti layers. The number of layers is 4, 8 and 16. From these specular reflectivity curves, measured at BNC, the real layer thicknesses and scattering densities were calculated (J.7). To investigate the roughness of the interfaces we also measured the offspecular scattering at GKSS, Geesthacht.

Investigation of steels. We have investigated by small angle neutron scattering (SANS) a duplex steel (containing two different phases) of industrial interest subjected to various ageing processes. Supposing that the scattering objects in steels have cuboid or rombohedral form, the scattering law obeys known formulae (in the case of monodisperse size distribution) and the cahracteristic size of these particles can be determined. The form factor and the contrast factor of the objects relative to the basic material give information also on the angle of orientation of the diagonal of the rhombes relatively to the main axes of investigation. We have observed the growth of cuboids with size changes from a ≈ 17 nm to a≈ 20.5 ± 6.6 nm due to thermal treatment. Further thermal treatment causes a developing of polydispersity of scattering particles. Therefore in this case only an average size was estimated. It was shown that this system becomes very polydisperse and the scattering data can be approximated by average parameter of particles as a ≈ 17 nm.

| a. | b. | c. |
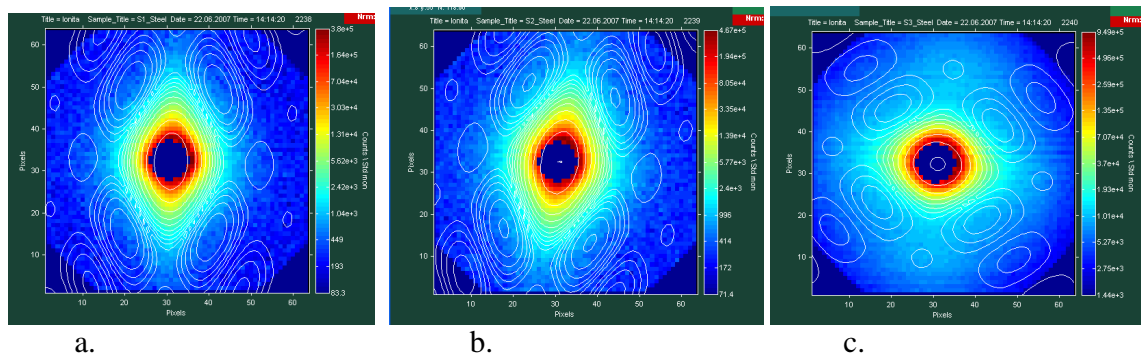
SANS analysis of steel samples (a) S1 as received, (b) S2 aged at low temperature, (c) S3 aged at high temperature. This yields the characteristic thermal treatment to evaluate the aging process.

## 4.2. Structure analyses of amorhous and crystalline materials by neutron diffraction

Margit Fábián, György Mészáros, Erzsébet Sváb
Research Institute for Solid State Physics and Optics, Neutron Physics Department

Borosilicate waste glasses [1,2]– Multi-component alkali borosilicate glasses are known as most

promising host materials for immobilizing high-level radioactive wastes, like U-, Pu-, Th-oxides. We have successfully prepared $(65-x)SiO_2 \cdot xB_2O_3 \cdot 25Na_2O \cdot 5BaO \cdot 5ZrO_2$ (x=5-20mol%) matrix glasses (hereafter denoted as Bx) and the same compositions loaded with 30 wt% UO_3 (UBx). Both systems have been investigated by neutron diffraction (ND) and high energy X-ray diffraction (XD), Figure 1 shows a characteristic set of structure factors, S(Q) for B10 and UB10 glasses. The short range atomic structure has been analysed by direct Fourier-transformation method and reverse Monte Carlo (RMC) modelling. The RMC minimizes the squared difference between the experimental S(Q) and the calculated one from a 3-dimensional atomic configuration. The structure of this computer configuration is modified by moving the atoms randomly until the calculated S(Q) agrees with the experimental data within the experimental errors. Moves are only accepted if they are in accordance with certain constraints, like cut-off distance, connectivity.

It was established that the Si-O network consists from tetrahedral SiO_4 units with characteristic first neighbour distances $r_{Si-O}=1.60$ Å and $r_{Si-Si}=3.0$ Å. The boron surrounding contains two well-resolved B-O distances at 1.40 and 1.60 Å and, both 3- and 4-fold oxygen coordinations are present. A chemically mixed network structure is proposed including [4]B-O-[4]Si and [3]B-O-[4]Si chain segments as illustrated in Fig. 2.
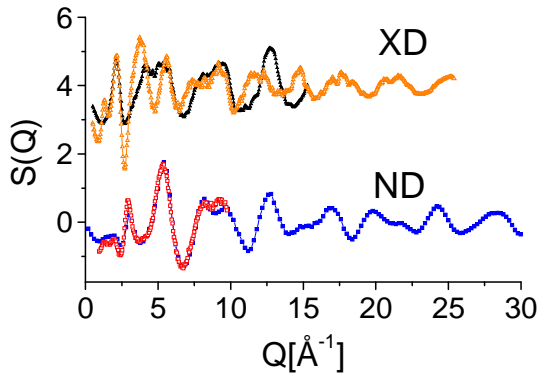

Figure 1. Experimental neutron (blue square) and high-energy X-ray (black triangle) structure factors, S(Q) for B10 (red filled) and UB10 (orange open) glasses.
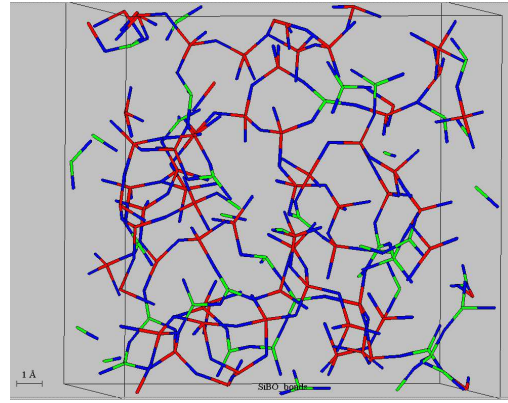
Figure 2. Schematic representation of the basic network structure of B10 borosilicate glass,: Si(red), B(green) and O (blue) bond lines.

The O-O and Na-O distributions suggest partial segregation of silicon and boron rich regions. The highly effective ability of Zr to stabilize the glass and hydrolytic properties of sodium-borosilicate host materials is argumented by the network forming role of Zr ions.
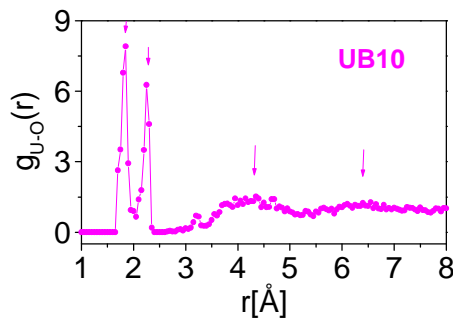
Figure 3. Uranium-oxygen pair correlation function in UB10 glass. The arrows show the two first neighbour distances, and the two others indicate the presence of intermediate short range order (see text for the actual values).

For the U-O correlations two distinct peaks were resolved at 1.84 Å and 2.24 Å, and for higher distances

well pronounced correlations are present at ~4.3 Å and at ~6.4 Å, as it is shown in Fig. 3. Furthermore, significant atomic pair correlations have been revealed between uranium and the network former Si and B atoms centred at 3.4 Å and 3 Å, respectively, and for the modifier Na ions at 3.7 Å and Zr at 3.8 Å, as well (see Fig. 4). From these finding we have concluded that uranium ions take part in the network forming, which may be the reason for the observed good glass stability and hydrolytic properties.
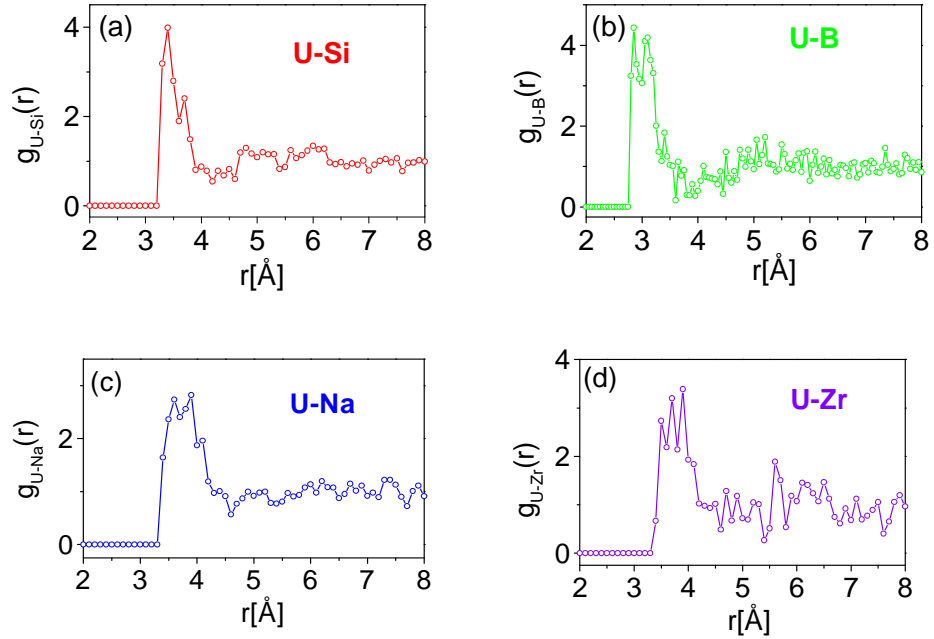
Figure 4. *U-Y (Y=Si (a); B (b); Na (c) and Zr (d)) partial atomic pair correlation functions in the UB10 glass.*

Crystalline and magnetic structure of novel functional materials [3-6] - The experiments questioned the correlations between structure and magneto-transport properties of the new perovskite family $(Bi_{1-y}R_y)_{1-x}A_xMnO_3$ (x, y=0.5; R = La, Nd, Ho, Tm; A=Ca, Sr) as well as the role that bismuth plays in these half-doped manganites, the charge order (CO) stability in $Bi_{0.5}A_{0.5}Mn_{1-x}Fe_xO_3$, ($0 \leq x \leq 1$; $R=La^{3+}$, Nd^{3+}, Ho^{3+}, Er^{3+}, Tm^{3+}; $A = Ca^{2+}$, Sr^{2+}), the loss of the colossal magnetorestive (CMR) properties of ordered double perovskites due to substitution effects in $Ba_2MSbO_{6-\delta}$ (M= Fe, Co), the magnetic moments arrangements in Y-Fe-Cr-O perovskite-like system and the loss of multiferroic properties as compared with the multiferroic parent phase $YbMn_2O_5$ due to substitution effects in its derivative $YbFeMnO_5$.

- A substantial body of our research was focused on the replacement of Mn with Fe, because it is an intricate problem from structural point of view. Ionic radii of high spin Fe^{3+} and Mn^{3+} in oxides are practically equal ($r_i \approx 0.645$ Å) so that one should not expect key structural changes. However, the number of d-electrons and the effective magnetic moments are different for Fe^{3+} and Mn^{3+}. Thus, the magnetic interactions and other electronic properties could be affected so as the compound to display unexpected properties.

Neutron and X-ray diffraction structural data and magneto-transport data were obtained for the system $Bi_{0.5}Sr_{0.5}Fe_xMn_{1-x}O_3$ ($0 \leq x \leq 1.0$) contributing to the clarification of the orbital and charge-ordering phenomena in transition metal oxides. The crystal structure was established as rhombic for $x \leq 0.3$ and cubic for $x > 0.4$. The unit cell volume increases with increasing Fe content. The magnetic properties were studied from 5K to 1300 K in magnetic fields up to 16 KOe for the compositions with x

≤ 0.8, which remain stable at high temperatures. The characteristic signs of orbital and charge ordering effects are exhibited only for the composition without Fe. In dependence on the Fe-amount the magnetic state changes from paramagnetic to weak ferromagnetic under a characteristic temperature in the interval 116 K ÷ 155 K. The coexistence of antiferromagnetic and ferromagnetic fluctuations much above this characteristic T entails unusual thermomagnetic behaviour in the paramagnetic region. Below 50 K there are indications for the presence of small ferromagnetic clusters. The electrical conductivity of the compound between 90 K and 600 K exhibit semiconductor behaviour, and application of magnetic fields up to 7 kOe does not induce changes in the electrical conductivity (no magnetoresistive effect).

- Mixed oxides with perovskites-like structure prepared from the system Y-Fe-Cr-O were investigated by neutron and X-ray doffraction, and we carried out a multipattern profile analysis. These mixed oxides with perovskite structure were successfully synthesized by an original combustion route. They are orthorhombic perovskites believed to be monoclinic at room temperature when produced by the ceramic route. The end member $CrFeO_3$ of this family is known for its clearly pronounced magneto-electric link at low temperature. Figure 1 shows the Rietveld-refined diffraction patterns demonstrating single phase character. The parameters of the crystalline (orthorhombic Pnma) and magnetic (GyFx) structures at 295 K were determined. Figure 5 illustrates the refinement of crystal and magnetic structure. The conventional factors for assessment of the quality of structural solution are also given.
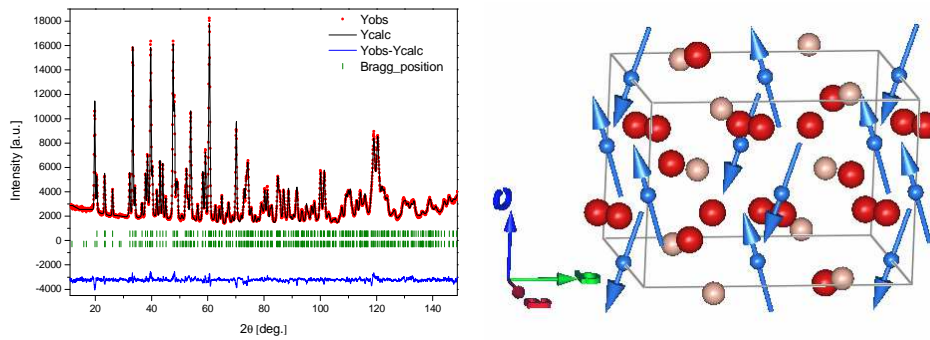

Figure 5. *left panel: Observed (crosses), calculated (full line) and difference (bottom) Rietveld profiles for $YCr_{0.25}Fe_{0.75}O_3$ at 295 K. Reliability factors $R_p = 6.09$; $R_{wp} = 6.15$; $R_B = 2.23$; $R_M = 5.11$; $\chi^2 = 3.08$, right panel – effective magnetic moments of Fe/Cr atoms within the refined unit cell.*

Chalcogenide glasses [7-11] - Chalcogenide glasses are transparent in the infrared region and exhibit high third order nonlinear optical properties. Thus, they are very attractive as high-speed optical elements for applications such as data processing devices, electronic switches, and optical memories. We have performed neutron and X-ray diffraction measurements and reverse Monte Carlo modelling on $As_{40}Se_{60}$ and $As_{40}Se_{50}Te_{10}$ glasses. A possible 3-dimensional structure model has been obtained which is consistent with the experimental data. The partial atomic correlation functions (see Fig. 6), coordination number distributions and three-atom-bond angle distributions have been revealed. We have established that addition of Te does not change the basic network structure of the two component glass. For the As-Se first neighbour distance 2.42 Å was revealed with 2.6 Se atoms around As atoms, while Se atoms are surrounded by 1.8 As atoms, the corresponding coordination number distributions are displaed in Fig. 7. The average three-particle <Se-As-Se> and <As-Se-As> bond angle is 95 Å° as obtained from the RMC calculations.
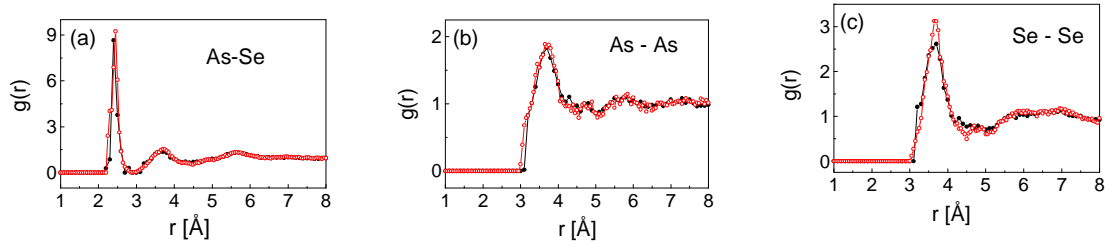
Figure 6. *Partial atomic correlation functions obtained from the RMC modelling of As-Se (a), As-As (b) and Se-Se (c) atom pairs for As$_{40}$Se$_{60}$ (full circles) and As$_{40}$Se$_{50}$Te$_{10}$ (open circles) glasses.*
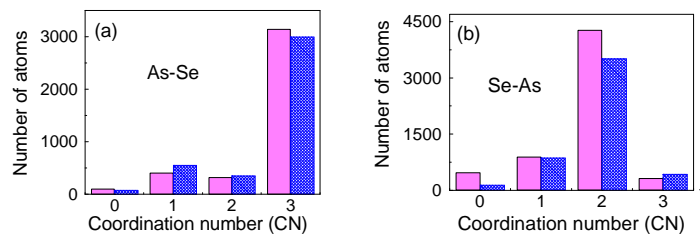
Figure 7. *Coordination number distribution for As$_{40}$Se$_{60}$ (magenta filled) and As$_{40}$Se$_{50}$Te$_{10}$ (blue crossed) glasses from RMC modelling of As-Se (a) and Se-As (b) atom pairs.*

4.3. Role of hydrogen species in palladium-catalyzed alkyne hydrogenation

Detre Teschner[1,2], János Borsodi[1,2], Zoltán Kis[2], László Szentmiklósi[2], Zsolt Révay[2], Axel Knop-Gericke[1], Robert Schlögl[1], Daniel Torres[3] and Philippe Sautet[3]

[1]Fritz-Haber-Institut der Max-Planck-Gesellschaft, Faradayweg 4-6, Berlin, D-14195, Germany
[2]Institute of Isotopes, Hung. Acad. Sci., POB 77, Budapest, H-1525, Hungary
[3]Université de Lyon, Institut de Chimie, Laboratoire de Chimie, Ecole Normale Supérieure de Lyon and CNRS, 46 Allée d'Italie, 69364 Lyon, Cedex 07, France

Removal of traces of alkynes or multiple unsaturated hydrocarbons from ethylene or propylene feed to produce polymer-grade alkenes are achieved by selective hydrogenation. Selective alkyne hydrogenation in the presence of carbon-carbon double bond compounds, for which Pd is the mostly applied catalyst, is a strategically important large-scale industrial process.

Although in palladium, functionality and structure are closely interrelated, knowledge of the structure of Pd is insufficient, as the interaction with the chemical environment causes drastic compositional changes near the sub-surface region [1]. To shed some light on the role of the hydride phase on the reactivity of Pd catalyst, the amount of hydrogen dissolved in Pd and the thermodynamic aspects of H incorporation during selective hydrogenation of short chain alkynes (here propyne) have been studied by means of *in situ* PGAA and periodic density functional calculations.

One of the few possibilities to detect and quantify hydrogen being dissolved in palladium is if the interaction with the atomic nucleus of hydrogen is utilized in the process of observation. We have recently developed in situ Prompt Gamma Activation Analysis (PGAA) to follow the hydrogen content of palladium during hydrogenation [2]. With this technique the total number of hydrogen atoms, either dissolved in palladium or adsorbed on the surface, can be counted during the hydrogenation event, and this can be directly related to the hydrogenation chemistry. (The hydrogen content of the gaseous phase proved to be negligible in these experiments.)

We employed unsupported Pd black in the PGAA experiments, in order to eliminate the likely effect of adsorbates and/or OH groups on the support material, and thus simplifying data evolution. A fresh sample exposed to H_2 absorbs hydrogen and forms the β-hydride phase, with a well known stoichiometry of $PdH_{0.75}$. After more than 24 hours in contact with various hydrogenation feeds and directly before the propyne hydrogenation experiments shown here, the H/Pd ratio in H_2 was 0.86, slightly higher than in the β-hydride phase, indicating the presence of remaining H-containing (adsorbates) on the surface (Figure 1, *right*). A sequence of selective hydrogenation events was carried out with increasing hydrogen flow rate (8-20 ml/min), however at constant (4 ml/min) propyne flow. The amount of hydrogen (being dissolved in palladium, adsorbed on the surface and in adsorbates/deposits) decreased only very slightly during selective hydrogenation compared to pure H_2, and its amount was independent of the hydrogen flow rate (Figure 1). When the hydrogen flow was

increased to 32 ml/min, full conversion (above 99.99 %) was observed and the only product was propane. This was accompanied by a temperature runaway (from 293 to 333 K) and a slight increase of the H/Pd ratio, back to the original level. These results show that the presence of a high H content and hence of the β-hydride bulk phase is compatible with both selective and non selective reaction, and that the reaction rate of selective hydrogenation is not linked to the bulk H/Pd ratio. High-pressure XPS experiments (not shown here) indicate that carbon occupies the interstitial lattice sites in the top few Pd layers, depleting hydrogen from the near-surface region, without affecting here the bulk.
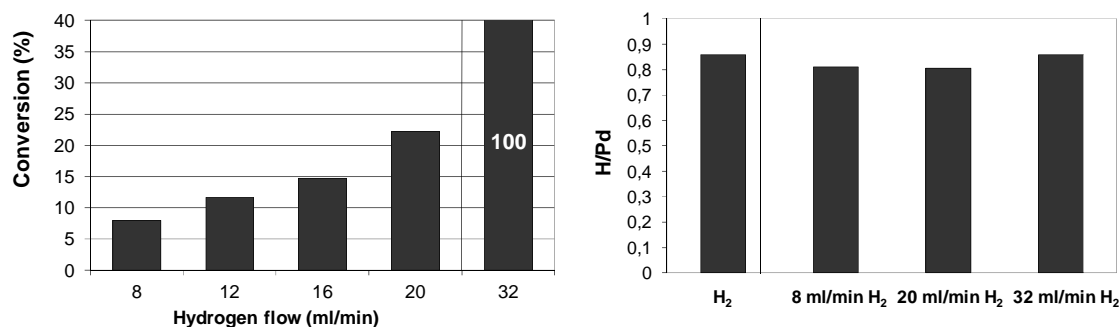
Figure 1. (*left*): Propyne conversion during PGAA experiments with Pd black catalyst. Selective hydrogenation (toward propene with higher than 97%) was observed with 8-20 ml/min H_2. Using 32 ml/min H_2 hydrogenation is unselective with full conversion to propane. (*right*): Atomic H/Pd ratios by PGAA in H_2 and under propyne hydrogenation at the indicated hydrogen flow rates. Propyne flow: 4 ml/min.

By using DFT calculation we have analysed hydrogen migration from the surface to the bulk (and vice versa) and the energetics of hydrogen adsorption at different surface, subsurface and bulk sites. Energy profiles associated to migration are shown in Figure 2. We found that the hydrogen binding energy increases (or decreases in absolute value) progressively with the depth of the interlayer to be populated, towards a limit of -0.1 eV corresponding to the bulk adsorption value. The energy barrier to move from surface to subsurface is ~0.4 eV, being almost zero for the reverse process. Since even bulk absorption is exothermic once hydrogen enters the subsurface it will easily migrate towards the bulk.

With carbon occupying the subsurface octahedral sites, the presence of this interstitial carbon atoms has a strong influence of the H adsorption energy (Figure 2). The surface adsorption energy is strongly reduced (by ~0.3 eV compared to Pd(111)). The adsorption of H in the first interlayer is reduced in a similar amount, becoming endothermic by at least 0.2 eV (in the least unstable site). Furthermore, in the Pd-C phase, hydrogen migration barriers towards the bulk tend to be higher, for both diffusion directions. As a result the H concentration will be low on the surface, in qualitative agreement with the kinetic data, and H will not be present as a stable species in the Pd-C region. Below this region, however hydrogen is stabilized as with pure palladium.
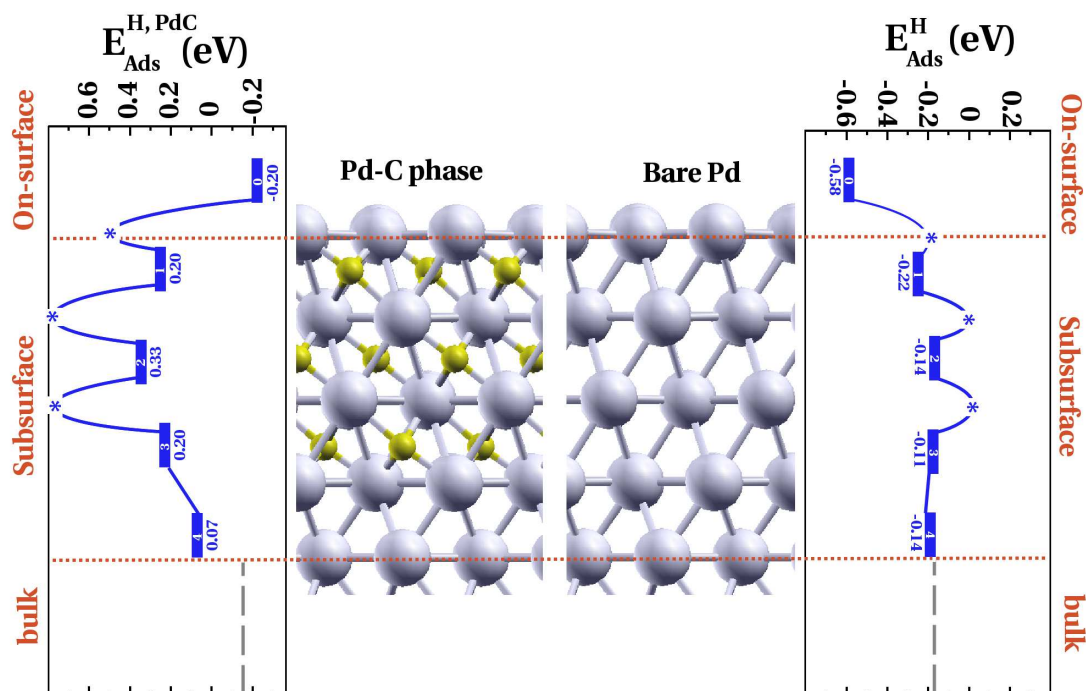
Figure 2: (*Right panel*) Energy profile for the adsorption and migration of H towards the bulk for pure Pd(111). (*Left panel*) Energy profile for the adsorption and migration of H towards the bulk in the presence of a 3-layer *Pd-C* phase. First, second and third interlayers are populated by C atoms (concentration 1 C for 3 Pd). The vertical dashed lines indicate hydrogen binding energy in the bulk of Pd.

In summary, we have demonstrated by means of PGAA experiments and DFT simulations that although the presence of surface and subsurface carbon accumulated under selective alkyne hydrogenation conditions imply a strong restructuring of the near-surface hydride phase, the bulk of palladium can still be populated by hydrogen. Due to the middle-sized barrier of approx. 0.8 eV for hydrogen emerging from the bulk through Pd-C to the surface, bulk and surface is still in a dynamic equilibrium, at least at the time scale of hydrogenation. The reaction rate of selective hydrogenation is nevertheless independent of the H/Pd ratio of the bulk. The binding energy of surface H is strongly reduced in the presence of Pd-C, and hence its coverage is low. On the other hand during unselective total hydrogenation the subsurface is populated by hydrogen rendering the surface concentration of H high.

References:

1. Teschner, D.; Borsodi, J.; Wootsch, A.; Révay, Z.; Hävecker, M.; Knop-Gericke, A.; Jackson, S. D.; Schlögl, R. *Science* **2008**, *320*, 86.

2. Révay, Z.; Belgya, T.; Szentmiklósi, L.; Kis, Z.; Wootsch, A.; Teschner, D.; Swoboda, M.; Schlögl, R.; Borsodi, J.; Zepernick, R. *Analytical Chemistry* **2008**, *80*, 6066.

5. DETAILED RESULTS

(Experimental reports)

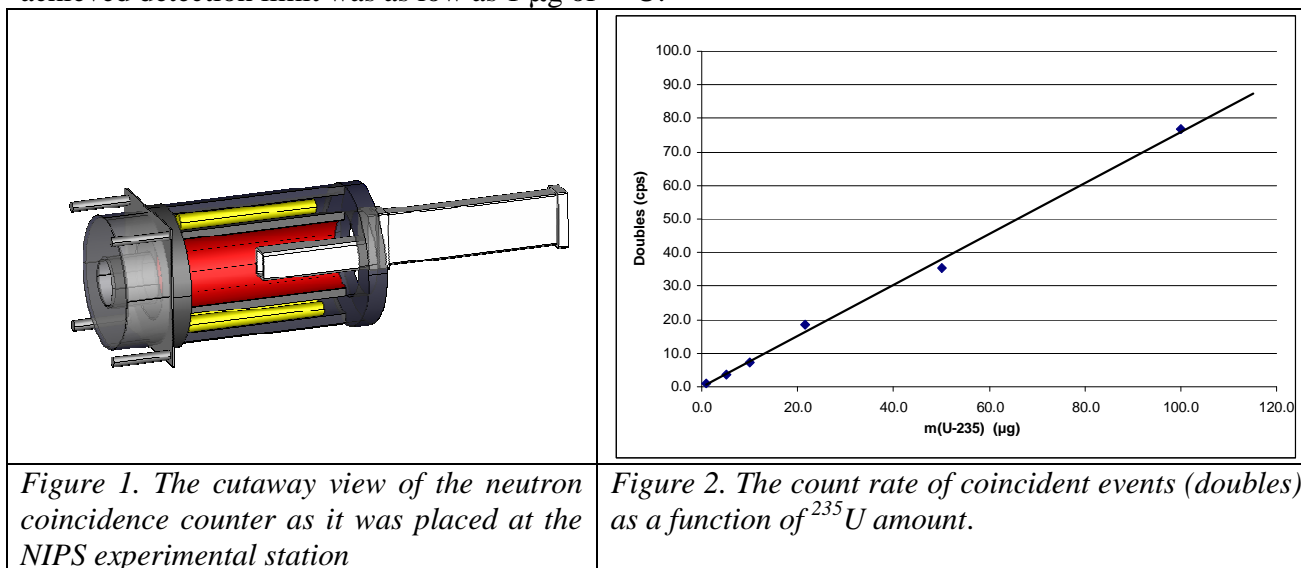| B N C **Experimental Report**	*Experiment title* Active neutron multiplicity counting with guided cold neutrons	*Instrument* *NIPS* *Local contact* *L. Szentmiklósi*
Principal proposer: J Bagi – Institute of Isotopes, HAS *Experimental team:* L. Szentmiklósi, Z. Hlavathy, Zs. Révay. E. Serf		*Experiment Number* *BRR_236* *Date* 25-27 Feb 2009

Objectives:

To establish the active neutron multiplicity counting technique with guided neutrons, and investigate its performance in quantification of ^{235}U in various samples.

Results:

Successful experiments have been performed at the NIPS facility to establish the cold-neutron based neutron multiplicity counting technique. It is aimed at determining low amounts of nuclear material in different matrices, based on the detection of fission neutrons. The device consists of 19 pieces of ^{3}He neutron detector tubes embedded in a cylindrical polyethylene moderator (Figure 1.). The inside cavity – where the neutron beam passed through – was lined with Cd to shield against scattered slow neutrons. The sample, in form of a powder or liquid, was placed to the end of the NIPS flight tube. As the neutrons from neutron-induced fission are emitted in coincidence, contrary to the guided neutrons, a highly-selective discrimination is possible. The events were recorded with a digital pulse-train reader. For normalization, the incoming neutron flux was also monitored.

With the optimization of the shielding and geometry, the background was already low enough for useful experiments. A calibration curve was measured with a series of solid and liquid samples, containing ^{235}U from 1-250 µg, which was found to be a linear over most of the investigated range. It was proven that the rate of coincidences (also called as doubles) is independent of the matrix and the volume of the sample. The achieved detection limit was as low as 1 µg of ^{235}U.

Figure 1. The cutaway view of the neutron coincidence counter as it was placed at the NIPS experimental station	*Figure 2. The count rate of coincident events (doubles) as a function of ^{235}U amount.*

Future prospects:

The achieved DL could be further improved by employing a detector with better counting efficiency. The more precise sample positioning could also reduce the scattering of the measured points, as the beam was measured to be spatially inhomogeneous.

References:

János Bagi, László Szentmiklósi, Zoltán Hlavathy, Zsolt Révay, Egyed Serf: Determination of Uranium with Neutron Coincidence Counting at a guided beam of the Budapest Research Reactor, to appear

B N C **Experimental Report**	*Experiment title* In situ PGAA: a new method to unravel mechanistic details of heterogeneous catalytic processes	*Instrument* PGAA *Local contact* Zs. Révay
Principal proposer: D. Teschner – Fritz-Haber-Institut der MPG *Experimental team:* D. Teschner, L. Szentmiklósi, Zs. Révay, Z. Kis		*Experiment Number* *BRR_197* *Date* 16-30 June 2008 13-17 July 2009

Introduction and Objectives:

Recently, PGAA has been further developed by us to analyze reacting components inside a chemical reactor to unravel mechanistic details of heterogeneous catalytic processes [1]. Up to now, two groups of catalytic reactions have been studied, hydrogenation reactions and the so called Deacon reaction for chlorine production. In both cases, the uptake of a reactant fragment (H and Cl, respectively) were investigated under reaction conditions (*in situ*) to correlate the abundance of these species with the activity (and selectivity) of the studied process.

Results:

The standard PGAA experiment has been modified in such a way that we placed a continuous-flow catalytic micro-reactor instead of a normal specimen into the neutron beam and recorded the emitted gamma radiation by a Compton suppressed Ge detector. By performing careful reference experiments, we were able to accurately quantify the hydrogen uptake of catalysts (palladium, palladium-based intermetallic compounds as well as complex metallic alloys) in alkyne hydrogenation, being an important group of industrial processes. From the experiments we concluded that – when pure palladium catalysts are used – unselective alkyne hydrogenation proceeds over palladium in the form of hydrogen-saturated β-hydride, whereas selective hydrogenation was independent of the amount of dissolved H in palladium [2-4]. Since the subsurface hydrogen content is critical for the selectivity [2], the observed lack of correlation with bulk H can be explained with the occupation of subsurface sites by carbon atoms (in line with our earlier in situ XPS results) disturbing the equilibrium between surface and bulk-dissolved H. When palladium intermetallic compounds (e.g. PdGa, Pd_3Ga_7) were used as catalyst, the modified electronic structure of these materials with filled *d*-band resulted in the weakening of hydrogen *ad*sorption and no hydrogen was *ab*sorbed in the subsurface and bulk of these materials, giving rise to selective hydrogenation. A similar situation was observed with a noble metal free iron-based complex mixed alloy sample [5], making it to a cheaper alternative to the Pd system.

References:

[1] Zs. Revay, T. Belgya, L. Szentmiklosi, Z. Kis, A. Wootsch, D. Teschner, M. Swoboda, R Schlögl, R. Zepernick, *Anal. Chem.*, **2008**, *80*, 6066.

[2] D. Teschner, J. Borsodi, A. Wootsch, Zs. Revay, M. Hävecker, A. Knop-Gericke, S. David Jackson, R. Schlögl, *Science*, **2008**, *320*, 86.

[3] D. Teschner , Zs Revay, J. Borsodi, A. Knop-Gericke, R. Schlögl, D. Milroy, S. David Jackson, D. Torres, P. Sautet, *Angew. Chem.*, **2008**, *120*, 9414.

[4] D. Teschner, J. Borsodi, Z. Kis, L. Szentmiklosi, Zs. Revay, A. Knop-Gericke, R. Schlögl, D. Torres, P. Sautet, *J.Phys. Chem.C*, **2010**, *114*, 2294.

[5] M. Armbrüster, D. Teschner, et al., in preparation.

B N C Experimental Report	*Experiment title* **Quantifying phosphorus in archaeological iron and steel**	*Instrument.* PGAA *Local contact* Zs. Kasztovszky
Principal proposer: Evelyne Godfrey - ISIS, Rutherford Appleton Laboratory, UK *Experimental team:* Zs. Kasztovszky, V. Szilágyi, L. Szentmiklósi, M. Balaskó, A. Willemsen, E. Godfrey		*Experiment Number* *BRR_201* *Date* 07.2008-12.2008

Objectives:

Prompt Gamma Activation Analysis (PGAA) of various iron objects produced in the Early Iron Age Western Europe, was proposed. The aim of the PGAA experiments was to determine chemical composition - first of all C, P and As content - of the bulk of these precious ancient objects. From the composition data, together with previous TOF-ND experiments at ISIS, we hoped to obtain important information on ancient metallurgy.

Since most of the iron swords to be analysed are heavily corroded, we proposed X-ray radiography of the objects at the BNC, prior to PGAA. Ten archaeological phosphoric iron and steel samples were selected from the Late Roman-Iron Age (300-500 AD) site of Heeten-Raalte in the Netherlands. In these, we would again like to measure P and As (similar range as standards) by PGAA.

The proposed PGAA experiment aimed to be a step towards the development of a new, non-invasive protocol for the characterisation of phosphoric iron objects. Such objects are commonly seen in the archaeological record of most European countries from the Early Iron Age onwards. Time-of-flight neutron diffraction (TOF ND) has been carried out by the proposers on the samples already, in order to quantify carbon contents.

Results:

We analysed seven iron swords and knives from the Early Medieval site of Rhenen-Donderberg in the Netherlands, provided by the National Museum of Antiquities, Leiden and five modern 'standard' experimental materials. The PGAA results indicate that all of the Rhenen objects are made from phosphoric iron. The whole phosphoric iron compositional range is represented, up to around the maximum amount of phosphorus seen in early iron. One of the knives has 1.2 wt% P, and would have been a bright silver colour when polished. We will compare these results with the crystallographic TOF-ND data collected at ISIS. By direct correlation the ISIS data with the PGAA and SEM-EDS, we can account non-destructively for the two most important chemical elements regularly seen in archaeological iron (P and C). In addition, we analysed 6 other archaeological phosphoric iron and steel samples from the Late Roman-Iron Age (ca. 300-500 AD) iron production site of Heeten-Raalte in the Netherlands, along with one smelting slag sample from Heeten and 2 iron samples from the contemporary Late Roman-Iron Age iron production site of Snorup in Denmark. We collected data on two samples of bog iron ore excavated at a Medieval site in the Netherlands (the Ooyerhoek), and three metal and ore samples excavated at Medieval smelting sites in North and West Yorkshire in England (Kyloe Cow Beck and Myers Wood). PGAA presents an effective method to quantify P in archaeological materials, particularly small ones (ca. 5 g powder samples or metal fragments the size of metallographic sections).

Fig. 1 PGAA setup for iron sword sword

Fig. 2 X-ray radiography setup for iron sword

B N C **Experimental Report**	*Experiment title* **Boron, chlorine and sulphur concentration measurements on serpentinized ultramafic rocks from present day ocean-floor and high pressure metamorphic environments**	*Instrument.* *PGAA* *Local contact* *Katalin Gméling*
Principal proposer: dr. János Kodolányi *Experimental team:* Prof. Thomas Pettke, dr. Carl Spendler		*Experiment Number* *BRR_206* *Date* March 2009

Objectives:

Examination of B, Cl and S content of serpentinized ultramafic rocks can give information about hydration and dehydration reactions. The determination of the above mentioned trace or minor elements in whole-rock samples are *1)* analytically challenging; and *2)* may easily be biased by contamination introduced during sample preparation for analysis by traditional analytical methods. This project aimed at determining B, Cl and S contents of serpentinized ultramafic rocks to trace and potentially quantify chemical changes related to hydration and dehydration reactions that affected these rocks on the ocean-floor and in subduction zones. This knowledge contributed to the understanding of water exchange among the Earth's mantle, crust and hydrosphere.

Results:

At the subduction zones great quantities of material are transferred to the Earth's mantle. This process is accompanied by significant volcanism along island arcs. Mass transfer in subduction zones is directly related to mineral-mineral as well as mineral-fluid interactions caused by increasing pressure and temperature in and around the submerging lithospheric slab. Water dragged down during subduction is stored in hydrous minerals, whose relative abundance and stability in turn determines the rate at which H_2O gets released from the subducting plate as well as the absolute quantity of H_2O released during dehydration. One important group of these H_2O-bearing phases is serpentines (chrysotile, lizardite and antigorite). They contain up to 13 wt % H_2O, which makes them the most important carrier of H_2O in subduction zones.

This work focused on the major and trace element geochemistry of serpentinites, hydrated ultramafic rocks consisting almost entirely of serpentine. They form through hydration of mantle olivine and orthopyroxene on the ocean floor and in the mantle wedge above subduction zones. Hydration of ultramafic rocks on the ocean floor is accompanied by the uptake of not only H_2O, but B, Cl, S, as well as Sr.

Analysis of Cl and S by techniques traditionally used for trace element analysis (e.g. ICP-MS) is very difficult or requires time-consuming special sample preparation. PGAA is a good alternative of mass spectrometry for B, Cl and S analysis. Further more it is a non-destructive method, which does not require sample preparation, thus contamination can be avoided.

Boron is the second-most enriched trace element in serpentinites after Cl. Serpentine is the major carrier of B in serpentinites. We note that aragonite may also contain substantial amounts of B (9.2-49 μg/g). Serpentinites have refractory major element compositions and are generally depleted in trace elements. However, they show up to

several orders of magnitude enrichments in Cl, B, (and few other trace elements: Sr, U, Sb, Pb, Rb, Cs and Li) relative to elements of similar compatibility during mantle melting. The trace element enrichments are the product of serpentinization and/or carbonate precipitation. Serpentinites show compositional variability as a function of the tectonic setting of serpentinization. Serpentinites from mid-ocean ridge environments are characterized by high relative enrichments in Cl, B, U, Sr, Sb, Pb and Li superposed on overall strongly depleted trace element compositions. Passive margin serpentinites show the highest B contents and prominent U enrichments, with a generally less-depleted precursor composition. Forearc serpentinites are similar to mid-ocean ridge serpentinites with respect to overall trace element depletion as well as B, Sb, Pb and Li enrichment but lack the U-enrichment commonly observed for mid-ocean ridge and passive margin serpentinites.

References:
Kodolányi, J., Pettke, T., Spandler, C., Kamber, B., Gméling, K. (2011): Geochemistry of ocean floor and forearc serpentinites: Constraints on the ultramafic input to subduction zones. Journal of Petrology (accepted)

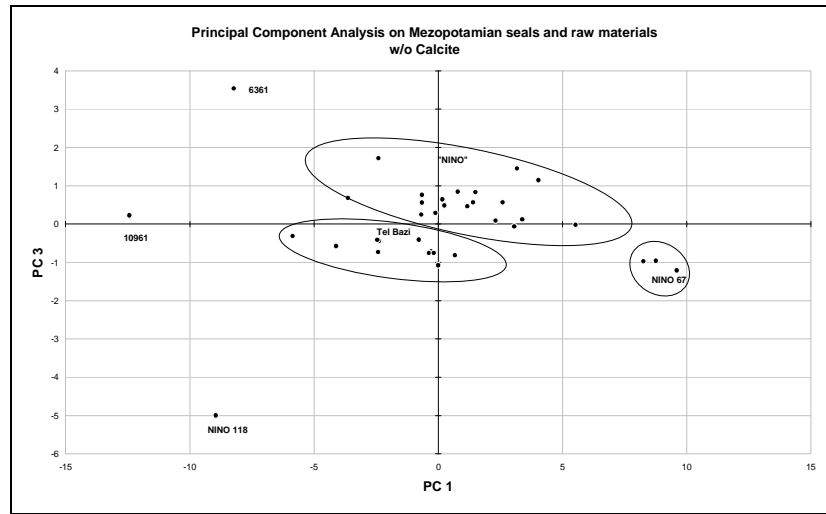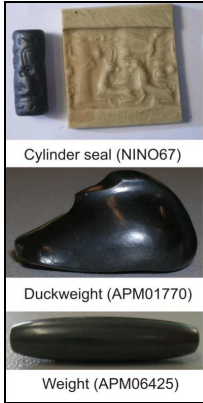| B N C Experimental Report	*Experiment title* **PGAA elemental analysis of Mesopotamian seals, weights half fabricates and raw material consisting of haematite.**	*Instrument.* PGAA *Local contact* Zs. Kasztovszky
Principal proposer: Martine de Vries-Melein - Institute for Geo- and Bioarcheology, VU University, Amsterdam *Experimental team:* Zs. Kasztovszky, V. Szilágyi, D. Visser		*Experiment Number* BRR_213 *Date* 02.2008-07.2009

Objectives:

Archaeologists tend to call all black to grey-black stones with a metallic luster "hematite". Previous research already demonstrated that this is often incorrect. To properly identify the material some kind of material analysis has to be done. The popularity of "hematite" for seals and weights during the Old Babylonian Period, ca. 2000-1600 BC may have been caused by the provenance of the raw material. To determine this provenance we want to identify a mineralogical or chemical marker, with which to connect artifacts to natural sources. The individual markers of these groups also provide information about the geological genesis of the stone. The experiments focus on the potential of PGAA in the 'haematite' matrix of Mesopotamian iron stone seals. Indications of the type of additional inclusion material next to haematite, magnetite and goethite can be obtained, as well as trace material important for provenancing purposes. The proposed objects are material from an excavation at Selenkahiye, Tall Bazi (Syria) and unprovenanced material made available by the Allard Pierson Museum, RMO Leiden and LMU-München. We measured 31 artifacts from two Dutch collections, NINO and Allard Pierson Museum. All artifacts were identified as "hematite" or "goethite" by archaeologists, on the basis of their macroscopic appearance. The sample set consisted of 17 cylinder seals, 1 stamp seal, 2 duck weights, 3 other weights and 5 half-fabricates. Furthermore, we measured 3 pieces of raw material from the Tell Bazi area.

Results:

The results could be plotted into three groups based on the major element distribution (excluding CaO and CO_3): one containing the Bazi samples, 2 seals, and 2 half-fabricates. This group was specified as "goethite" by earlier ND measurements. The second group consists of a Mitanni seal, and 2 weights (Fig. 2). The third group is the largest with 12 seals, 2 weights and 2 half-fabricates. Five outliers were identified: the two calcite seals, and three objects that turned out to have high goethite content: a Sasanian stampseal a half-fabricate and a cylinder seal.

As preliminary conclusions, we can say that the sample could be divided into different groups, based on their chemical composition. Raw material from one location (Tell Bazi) all belonged to one group. PGAA seems to be a suitable technique for fingerprinting this material in order to provenance it. In addition we can distinguish between hematite, goetite and magnetite. However, groups based on PGAA results often but not always resemble groups based on XRF or ND measurements. The techniques supplement one another. Material groups do not follow artifact groups; seals and weights were made from the same material.

Cylinder seal (NINO67)

Duckweight (APM01770)

Weight (APM06425)

Principal Component Analysis on Mezopotamian seals and raw materials w/o Calcite

PC 3 (y-axis: -6 to 4)
PC 1 (x-axis: -15 to 15)

6361

"NINO"

10961

Tel Bazi

NINO 67

NINO 118

References:
Proceedings of 7th International Congress on the Archaeology of the Ancient Middle East, 2010, London

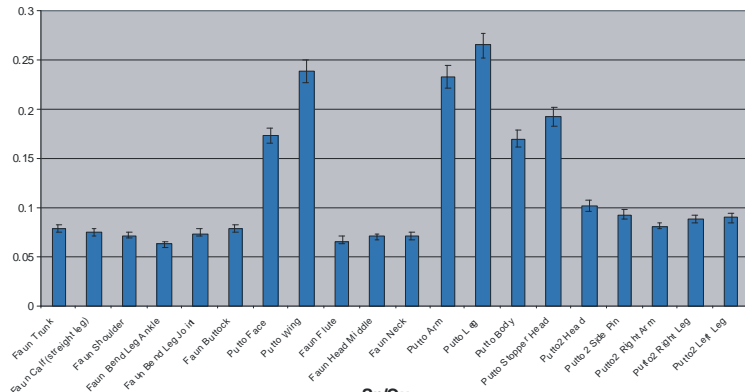| B N C Experimental Report	*Experiment title* **PGAA as an Investigative Tool for the Provenance of Renaissance Bronze Statuettes**	*Instrument.* PGAA *Local contact* Zs. Kasztovszky
Principal proposer: Dirk Visser - Reactor Institute Delft, TU-Delft *Experimental team:* Zs. Kasztovszky, D. Visser, L. Szentmiklósi		*Experiment Number* BRR_215 *Date* 07.2009

Objectives:

We investigated three Renaissance Bronzes from a period dated around 1620-40 with PGAA to determine the composition of the bronze and core material. The objects are a Flute playing Faun and two Puttos. On stylistic and art historical bases, the provenance for these objects points the famous and influential Flemish sculptor Francois Duquesnoy. We aimed to determine the bronze composition for different parts of the statuettes and relate the results to previous neutron computer tomography studies.
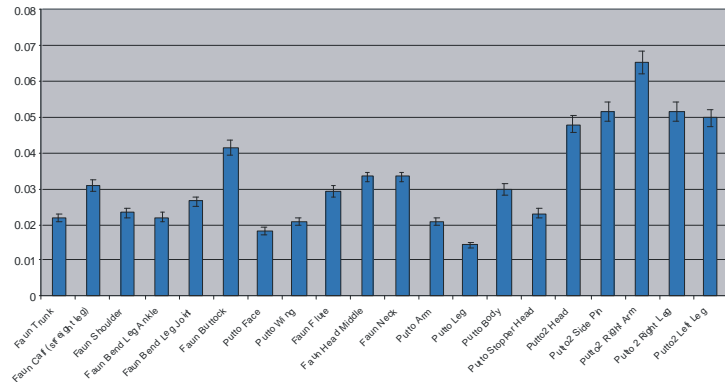
Results:

We analyzed several areas on the objects, and quantified major Cu, Zn, Sn and Pb; traces of Cl, Ag and Cd. The positions were selected on the basis of previous neutron tomography. We established that the alloy mixture for all objects, the Faun and the Puttos, was unusual. Large amounts of Zn were present as well as As and relatively small percentages of Sn. In one objects (Faun) we could not detect lead. In one of the putto's we found a difference in the alloy composition for the head and the body. Two of the objects contained original core material. The measured high percentages of As is very unusual in Renaissance bronzes. It indicates a particular usage of antique material for the manifacture of the sculptures. With this set of experiments we have evidence to underwrite statements made in archieval material to support the attribution of these objects to the sculptor Duquesnoy.

Zn/Cu

Sn/Cu

B N C Experimental Report	*Experiment title* **Studying the Deacon process using in-situ Prompt Gamma Activation Analysis**	*Instrument* *PGAA* *Local contact* *Zs. Révay*
Principal proposer: D. Teschner – Fritz-Haber-Institut der MPG *Experimental team:* D. Teschner, E.Varga, L. Szentmiklósi, Zs. Révay, Z. Kis		*Experiment Number* *BRR_221* *Date* 6-16 Oct 2009

Objectives:

The aim of the experiments was to correlate the reaction rate of chlorine production and the degree of surface chlorination and hence to enable us to build up a realistic model of the active surface.

Results:

We have built up a modified version of reaction environment of our in situ prompt gamma activation analysis (PGAA) setup [1] to handle the needs of the Deacon reaction ($4HCl + O_2 = 2Cl_2 + 2H_2O$). Three RuO_2 samples from different suppliers after calcination in air have been investigated; the reaction rate has been followed by iodometric titration whereas the degree of chlorination has been measured by in situ PGAA. Since it was known that the rate of chlorine production over RuO_2-based catalyst is positively affected by the oxygen content of the feed (reaction order of O_2: +0.5), we have varied the feed O_2/HCl ratio at constant HCl as well as constant total flow rate by balancing the O_2 flow with inert N_2. Our reaction data precisely re-

produced the formal +0.5 oxygen order of previous RuO_2 experiments and Deacon catalysts, and hence our RuO_2 samples can be considered as valid model catalysts for the reaction. The Cl uptake was typically close to its maximum; decreasing with increasing reaction rate. Hence, Cl is clearly a poison of the reaction; however, small amount of Cl removal induced high relative changes of reaction rate. This indicates that only a small part of the surface liberated from Cl contributes to the reaction. Furthermore, a catalytic material stable under this
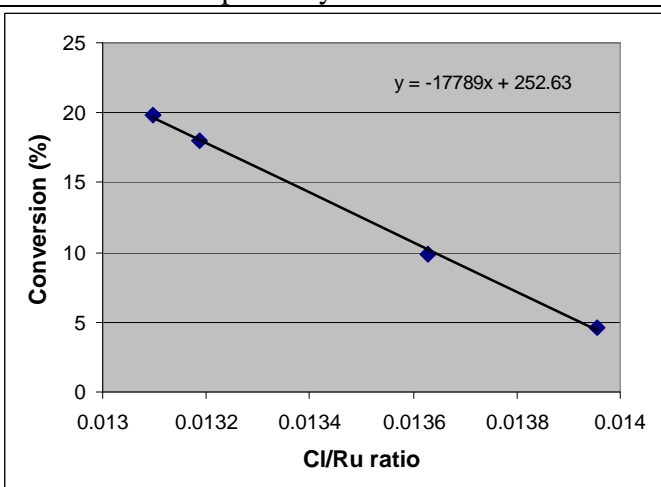

Fig. 1: The effect of degree of chlorination on the activity of Aldrich RuO_2. Degree of chlorination is expressed as the molar ratio of Cl uptake and total amount of RuO_2 (that is, not only surface Ru).

corrosive condition but binding chlorine somewhat weaker than RuO_2 could be a very effective catalyst.

Future prospects:

The proposed model has to be validated by measuring real equilibrated catalysts.

References:
[1] Zs. Révay, T. Belgya, L. Szentmiklósi, Z. Kis, A. Wootsch, D. Teschner, M. Swoboda, R. Schlögl, J. Borsodi, R. Zepernick: In situ determination of hydrogen inside a catalytic reactor using prompt gamma activation analysis, Anal. Chem. 80 (2008) 6066.
[2] D. Teschner, J. Borsodi, A. Wootsch, Zs. Révay, M. Hävecker, A. Knop-Gericke, S.D. Jackson, R. Schlögl: The Roles Of Subsurface Carbon And Hydrogen In Palladium-Catalyzed Alkyne Hydrogenation Science, 320 (2008) 86.
[3] D. Teschner, R. Farra, L. Yao, R. Schlögl, H. Soerijanto, R. Schomäcker, T. Schmidt, L. Szentmiklósi, A.P. Amrute, C. Mondelli, J. Pérez-Ramírez, G. Novell-Leruth, N. López, submitted to Journal of the American Chemical Society (2011)

B N C Experimental Report	*Experiment title* **Provenance study of Croatian and Bosnian archaeological obsidian artefacts with PGAA**	*Instrument.* PGAA *Local contact* Zs. Kasztovszky
Principal proposer: Marcel Buric – Dept. of Archaeology, University of Zagreb *Experimental team:* Zs. Kasztovszky, V. Szilágyi		*Experiment Number* *PGAA_08_03_IC* *Date* 05.2008-01.2009

Objectives:

In 2008-2009 we started to work on archaeological obsidians from Croatia and Bosnia-Herzegovina within the frame of a Croatian-Hungarian project. The main objective of our work was to perform a provenance study of these obsidian artefacts. The chemical compositions of the systematically collected samples have been determined non-destructively with Prompt Gamma Activation Analysis. Obsidian is among the important raw materials of prehistoric tool production in the Carpathian Basin, and a popular subject of archaeometric studies. According to previous studies, three main groups could be separated. The main categories are the transparent-translucent Carpathian 1 (C1 – Slovakian) type, the non-transparent Carpathian 2 (C2 – Hungarian) and the Carpathian 3 (C3) type from Ukraine. In order to determine the origin of obsidian raw materials, we have analysed Carpathian (C1 and C2) and Mediterranean (Melos, Lipari, Sardinia) geological samples as well as archaeological pieces from Hungary and Romania. Our PGAA database on obsidian is continuously expanding with the new analytical results.

Results:

We have analysed archaeological obsidians from Croatia and Bosnia-Herzegovina, and comparative raw materials, collected on field trips in Tokaj-Eperjes Mountains. We have analysed geological samples from the Mediterranean region (Melos, Lipari, Sardinia), from Armenia (Sevan) and from France (Auvregne), too, as comparative material. Other pieces of macroscopically similar appearance were also measured, which turned out to be modern slag.

Based on the PGAA results, we were able to differentiate between Carpathian (also between C1 and C2) and Mediterranean obsidians, based on PGAA results. When we added the new analytical data to our library, we found that some of the Croatian obsidians are similar to C1, while the others are similar to Mediterranean (Lipari) ones in composition, which makes it possible to determine the raw material sources of the archaeological pieces with high probability
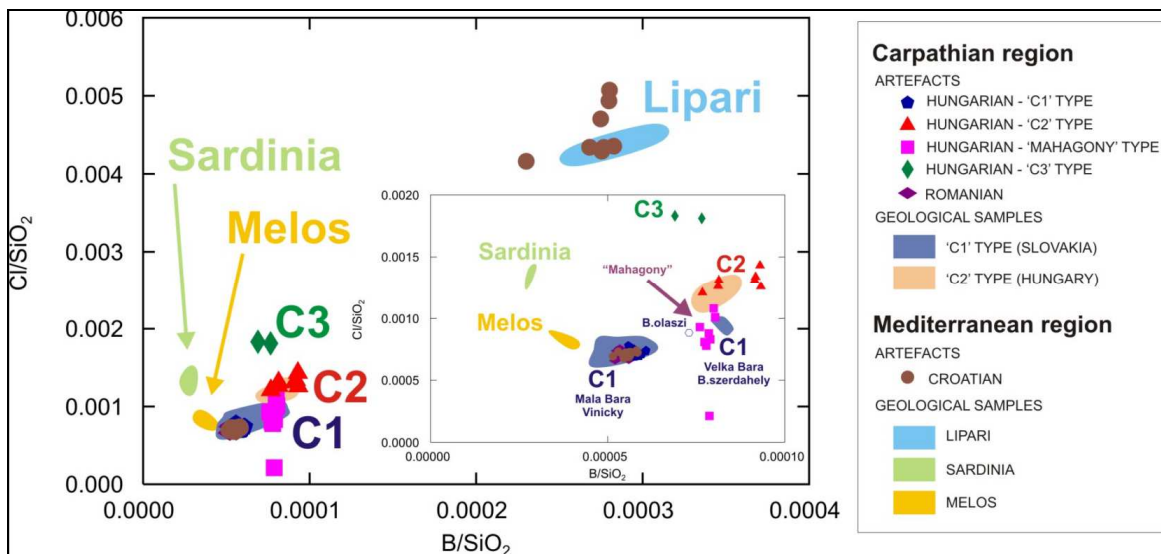
Fig. 1: Separation of Croatian and Bosnian archaeological obsidian samples on the basis of boron (B/SiO$_2$) and chlorine (Cl/SiO$_2$) content.

References:

Zs. Kasztovszky et al. – Archaeometry Workshop 2009/3. pp. 5-14.

B N C **Experimental Report**	*Experiment title* **New data on the characterisation of radiolarite sources of the Carpathian Basin**	*Instrument.* PGAA *Local contact* Zs. Kasztovszky
Principal proposer: Tihomila Težak-Gregl – Dept. of Archaeology, University of Zagreb *Experimental team:* Zs. Kasztovszky, V. Szilágyi		*Experiment Number* *PGAA_08_01_IC* *Date* 12.2008-05.2009

Objectives:

As raw material for chipped stone tools, radiolarite – a siliceous rock formed in the deep sea and ocean environment – is frequently used. On the average, it is the most frequent component of lithic inventories in Hungary and even more, in Transdanubia. There are macroscopically separable types among the radiolarites, mainly on the basis of colour and other physical properties. They are currently named after the most characteristic geological source locality. It remains a question though, how much the 'raw material types' represent really different sources; how variability within each source is reflected in the archaeological lithic material and how much we can separate regional varieties, supported by objective methods of analysis. It is also imperative to know radiolarites from sources outside the present territory of Hungary that may have played a role in the raw material supply and 'fingerprint' the individual sources and regions.

Results:

New analytical data and characteristic major element distributions of radiolarite raw materials from Gerecse, Bakony and Mecsek mountains were obtained. By the comparison with chemical data on archaeological radiolarite artefacts from sites in Hungary, Croatia and Bosnia and Herzegovina, preliminary suggestions for the provenance of archaeological radiolarites were provided. Stone tools of sites in the Gerecse and at Nadap are possibly originated from the Gerecse source. Radiolarite artefacts of site Vörs may be related to raw material of Bakony. Archaeological finds of Szálka site have similar chemical character to the Mecsek raw materials. Chert artefacts of Fajsz can not be directly connected neither to the Mecsek nor to the Gerecse source. Chipped stone tools from Croatia and Bosnia can not be compared chemically to the radiolarite types of Hungary. However, the carbonate-free Bosnian radiolarite seems to serve as a potential "new" raw material source.
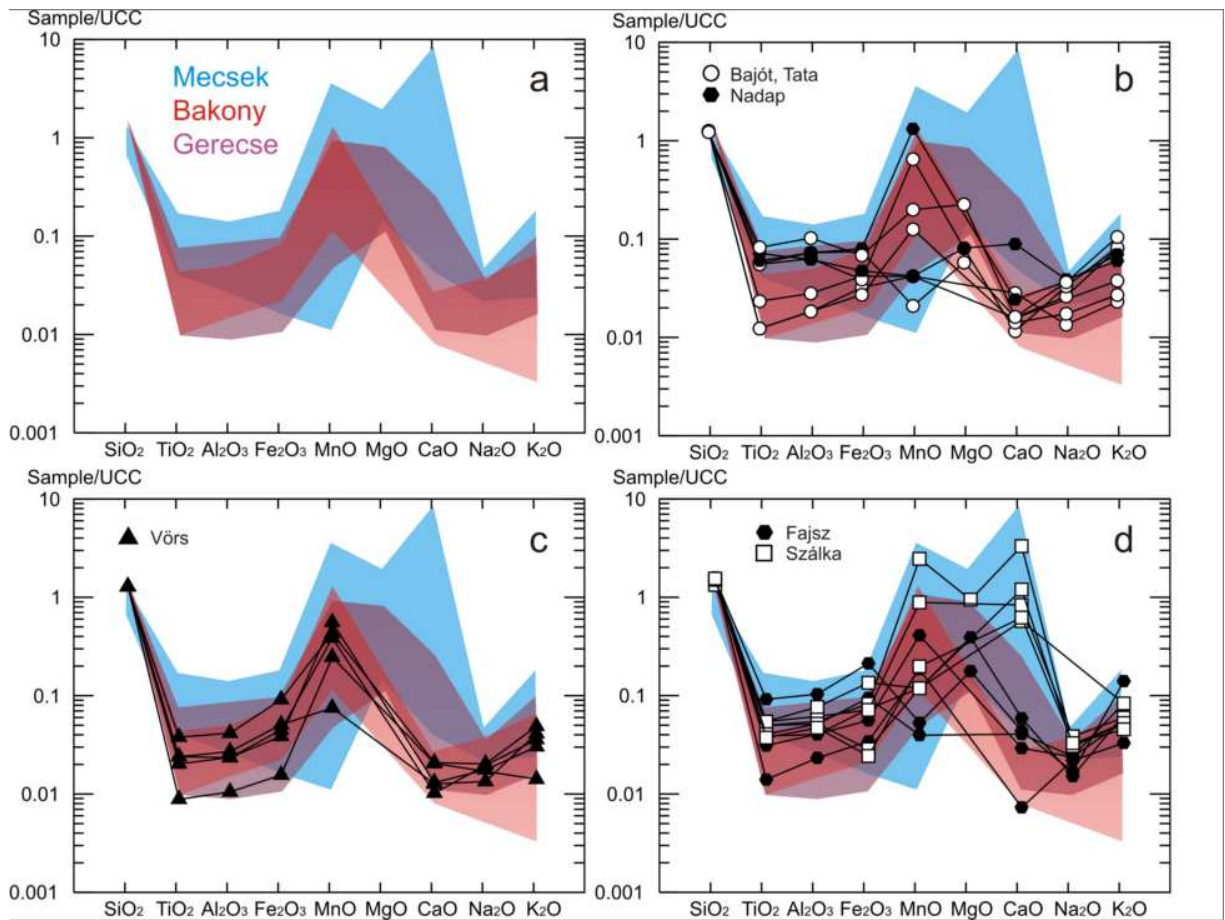
Fig. 1: Major element distribution of Hungarian archaeological radiolarites normalised for UCC (average composition of the upper continental crust) presented in the same context as the geological sources
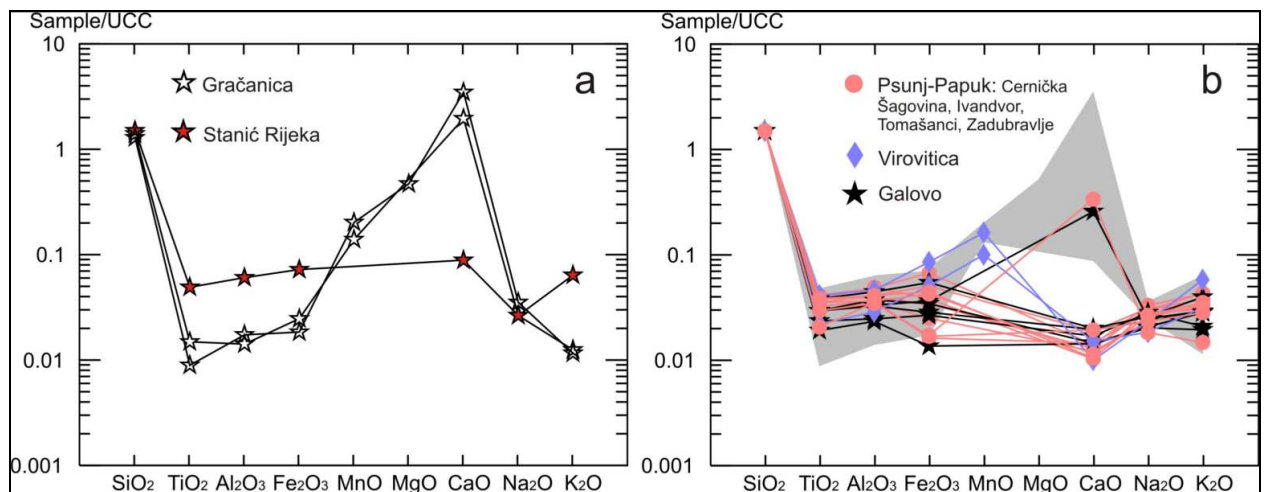

Fig. 2: Major element distribution of Bosnian and Croatian samples normalised for UCC, (a) Bosnian geological samples (n_{geo}=3), (b) Bosnian and Croatian archaeological samples (n_{arch}=6+12)

References:

K.T. Biró, V. Szilágyi, Zs. Kasztovszky – Archaeometry Workshop 2009/3. pp. 25-43.

	BNC Experimental Report	Experiment title Measuring cross-sections ($\square_\square$) and k0-factors of short- and medium-lived radionuclides	Instrument PGAA Local contact L. Szentmiklósi
Principal proposer: L. Szentmiklósi – Institute of Isotopes, HAS Experimental team: L. Szentmiklósi			Experiment Number PGAA_08_04_IH Date 11-17. Nov 2008

Objectives:

To determine the partial gamma-ray production cross-sections (σ_γ) and k_0-factors of short- and medium-lived radionuclides

Results:

As a continuation of our previous experiments, the partial gamma-ray production cross-sections (σ_γ) and k_0-factors of 12 short- and medium-lived radionuclides were determined using a chopped beam of cold neutrons. This technique avoids several problems associated with epithermal activation, sample transportation and dead-time effects in NAA measurements. Our k_0-values were determined with internal standardization, using stoichiometric compounds or water solutions of known compositions. The peaks of hydrogen or chlorine served here as comparators because their nuclear data are accurately known.

The neutron beam is periodically switched on and off using a chopper, a four-sector rotating blade with two open and two closed quadrants. In the open phase the sample is irradiated and the prompt spectrum is recorded, while in the closed phase the prompt photons are absent and only the decay radiation is detected. A dedicated unit controls the chopper and provides the timing signals to route the events. The data listed in the Table were obtained.

Good agreement was found between the measurements and various literature sources for the ^{52}V,

Sample	Nuclide	Half-life* (Abs. Unc)	Decay Peak Energy, keV	Sigma, barn (Abs. Unc)
NaCl	^{24m}Na	20.20 (7) ms	472.202	0.504 (11)
VF$_4$+H$_2$O	^{52}V	3.75 (1) m	1434.10	4.78 (8)
CuCl$_2$	^{64}Cu	12.700 (2) h	1345.77	0.0156 (11)
	^{66}Cu	5.120 (14) m	1038.97	0.0596 (14)
	^{38m}Cl	0.715 (3) s	671.355	0.0141(4)
	^{38}Cl	37.24 (5) m	1642.5	0.0356 (8)
			2166.90	0.0459 (10)
SeO$_2$+H$_2$O	^{77m}Se	17.36 (5) s	161.922	0.859 (18)
NH$_4$TcO$_4$	^{100}Tc	15.27 (5) s	539.5	1.482 (22)
			590.7	1.259 (19)
RhCl$_3$	^{104m}Rh	4.34 (5) m	51.50	3.44 (8)
			97.14	0.222 (8)
	^{104}Rh	42.3 (4) s	555.81	3.33 (7)
			1237.05	0.138 (8)
InCl$_3$	^{116m2}In	2.18 (4) s	162.393	23.5 (7)
	^{116m}In	54.41 (6) m	416.86	41.3 (11)
			1097.30	85.4 (23)
			1293.4	124 (3)
			463.14	1.37 (9)
			818.70	18.1 (5)
			1507.40	14.6 (5)
			1753.8	3.40 (19)
			2112.3	22.6 (7)
Sb(CH$_3$COO)$_3$	^{122}Sb	2.7238 (2) d	564.24	2.535 (23)
			564.24	2.494 (23)
			692.65	0.136 (5)
			692.65	0.134 (5)

	124m2Sb	93 (5) s	498.40	*0.00807 (23)*
	124Sb	60.20 d	1690.98	*0.85 (6)*
CsCl	134mCs	2.903 (8) h	127.500	*0.313 (3)*

116mIn and for the copper isotopes. Thanks to the higher neutron flux, we could improve our data for ^{38}Cl. For ^{77m}Se we measured a lower value than in the literature, while its is higher than EGAF. The same is true for the ^{134m}Cs.

The partial gamma-ray production cross-sections of the measured radionuclides

Reference:

L. Szentmiklósi, Zs. Révay, T. Belgya, Measurement of partial gamma-ray production cross-sections and k_0-factors for radionuclides with chopped-beam PGAA - Part II, Nucl. Instr. Meth. A **622** (2010) 468–472

B N C Experimental Report	Experiment title **Measuring partial gamma-ray production cross-sections (σ_γ) of selected elements**	Instrument *PGAA* *Local contact* *Zs. Révay*
Principal proposer: Zs. Révay – Institute of Isotopes, HAS *Experimental team:* L. Szentmiklósi, Z. Kis		*Experiment Number* *PGAA_08_05_IH* *Date* 16-31. Jan 2008

Objectives:

To improve the accuracy of the partial gamma-ray production cross-sections (σ_γ) of selected elements

Results:

      Standardization measurements were carried out at the PGAA station of the BRR. Two HPGe detectors were used in parallel, one was the standard PGAA detector, the other was a Canberra LeGe detector with excellent energy resolution for low-energies. This latter was useful to resolve the low-energy multiplets in the elemental spectra.

      After a careful calibration of the spectrometers, the following materials were measured: Ni-acetate, Zn-acetate, Mg-acetate, K-acetate, Li-acetate, Sb-acetate, Tl-acetate, Rb-acetate, Fe-acetate, Bi-oxide, Hg-oxide, Ru-oxide, Mn-chloride, Pt-chloride, Rh-chloride, Mo-chloride, In-chloride, Sc-chloride, Ta-chloride, Hg-chloride, Sr-sulphate, Te-hydroxide, phosphor pentoxide, ammonium-hydrogen phosphate, ammonium fluoride, Zr-oxide.

      Certain measurements have been repeated at the cold neutron PGAA instrument of the FRM-II reactor at Garching bei München, Germany. This other facility was run at a thermal equivalent flux of 3×10^9cm^{-2} s^{-1}. Their HPGe detector had a relative efficiency of 36% and was also surrounded by a BGO Compton suppressor. The values deduced from the two set of measurements are listed in the following table:

Element	Energy (keV)	Cross-section (barn)	Stat. Unc %	Total Unc%
F	1633	0.00932	1.6	1.9
Na	472	0.5008	0.6	0.9
Mg	585	0.0324	0.3	0.6
Mg	1808	0.0184	1	1
Al	1779	0.237	1	1.1
P	637	0.032	0.7	0.9
K	770	0.916	0.8	1
Ca	1942	0.0353	0.45	0.5
Sc	627	2.49	1.1	1.3
Mn	314	1.497	0.8	1.1
Ni	465	0.876	0.4	0.6
Zn	1077	0.365	0.3	0.6
Se	614	2.34	0.7	0.8
Sr	851	0.266	0.8	0.9
Sb	332	0.102	2.7	2.7
Te	602	2.7	0.5	0.7
Pt	356	6.52	0.7	1
Ta	402	2.22	1.5	1.7
Pb	7368	0.132	0.7	1.4
Bi	319	0.0128	1.4	1.7

Reference:

Zs. Révay, L. Szentmiklósi, Z. Kis, Determination of new k_0 values for prompt gamma activation analysis at Budapest, Nucl. Instr. Meth. A **622** (2010) 464–467

B N C **Experimental Report**	*Experiment title* Measuring the Compton-suppressed response function of the PGAA detector	*Instrument* PGAA *Local contact* L. Szentmiklósi
Principal proposer: L. Szentmiklósi *Experimental team:* L. Szentmiklósi		*Experiment Number* PGAA_08_06_IH *Date* 6-7 May 2009

Objectives:

To measure the response function of the new Budapest PGAA detector.

Results:

The present PGAA detector system consists of an n-type HPGe detector (Canberra GR 2720) and a Bismuth Germanate (BGO) guard detector arranged in a coaxial geometry. The eight main segments of the suppressor are complemented by two additional "catchers" behind the HPGe crystal. The whole detector is surrounded by a 10 cm-thick lead shielding.

The interpretation of the highly complicated elemental PGAA spectra and the prediction of the spectroscopic conditions for multi-component analytes require the accurate knowledge of the detector response function. The first step towards the characterization of our spectrometer was the accurate measurements of well known and simple gamma spectra. Unfortunately there are only a few commercially available radioactive sources for this purpose, while some additional nuclides with short half-lives could be prepared by activation in the neutron beam, and could be measured with the chopped-beam technique. A few, simple PGAA spectra were also involved in the study.

The earlier studies on the previous detector were repeated and extended. Now the Compton-suppressed spectra could also be well reproduced. The measurements compare well to the calculations.
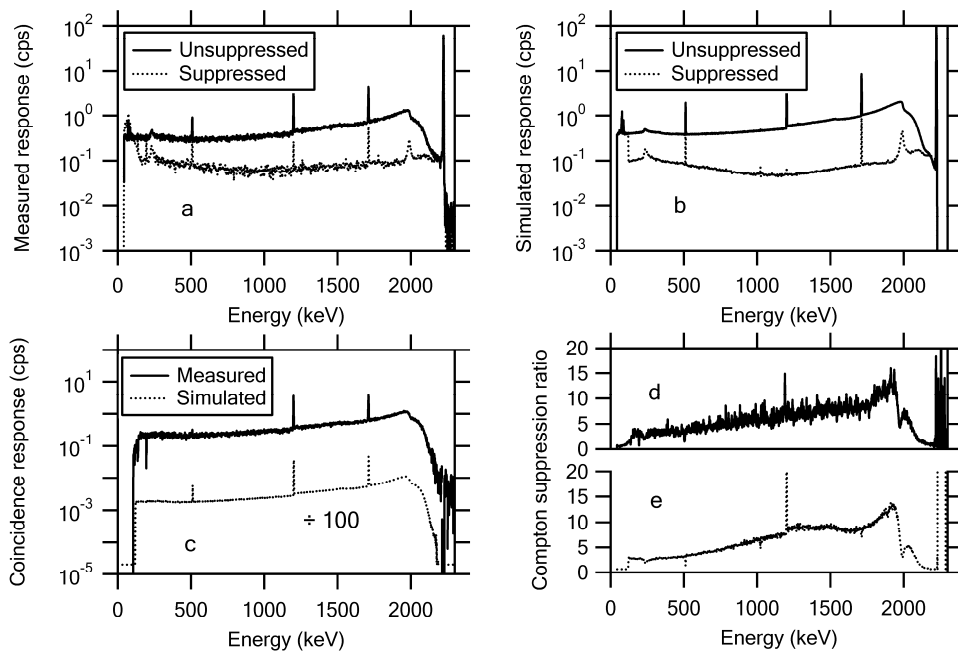
Fig. 1. The spectra of the 2223-keV gamma-rays from the $^{1}H(n,\gamma)^{2}H$ reaction. Panel a): the measured spectra in unsuppressed and suppressed mode. Panel b): the corresponding calculations. Panel c): the measured and simulated spectrum of rejected events (latter divided by a factor of hundred to visually separate the curves). Panels d) and e): The measured and simulated Compton suppression ratios as functions of energy.

Reference:

L. Szentmiklósi, A.N. Berlizov, Characterization of the Budapest Prompt Gamma Spectrometer by Monte Carlo Simulations, Nucl. Instr. Meth. A **612** (2009) 122–126

Objectives:

The Central European Cenozoic volcanic province forms an arc about 350 km long, from the Bohemian Massif to Lower Silesia and Moravia. Geochemical analysis of Tertiary alkali basaltic rocks from six regions of Lower Silesia: Luban, Jawor, Strzelin, Opole, Ladek Zdroj and Raciborz were measured by PGAA.

Results:

The SiO_2 content of the rocks vary between 38 and 62 wt%. 59 samples were analyzed; most of them fall in the tephrite and basanite field on the SiO_2 vs total alkali diagram. All the studied samples are alkaline in composition. The examined rocks are SiO_2-undersaturated and are characterized by their high MgO and low K_2O contents.

MgO show negative correlation with increasing differentiation index indicates fractionation of magnesian minerals, like olivin and clinopiroxen. Strong increase in Al_2O_3 indicates less significant feldspar fractionation. TiO_2 and Na_2O show positive correlation especially in Luban and Strzelin. Samples from Jawor, Opole and Ladek Zdroj are not that strongly fractionated. K_2O show no systematic variation with the Fe_2O_3T/MgO ratio. CaO is increasing in the older samples from Luban and Opole, due to plagioclase fractionation. CaO is stable with increasing Fe_2O_3T/MgO ratios in younger samples from Jawor, Strzelin and Landek Zdroj.

Samples from Lower Silesia show REE enrichment compared to the primitive mantle. LREE enrichment are more significant, then HREE. All mafic rocks are enriched in incompatible (Rb, Ba, Th, U, Nb) elements compared to primitive mantle. B is highly incompatible and fluid mobile element, but show negative anomaly in the Lower Silasian samples, as B is only enriched in the mantle by subduction fluids. Samples from all location show similar trace element pattern. Small differences visible only. The differences between the trace element patter of the samples are more visible separating them by their age. Older samples (23.8-33 million year (Ma)) have small variation in U content and they are more enriched in Ba, La, Nb, Ce, Sr, Nd then the younger samples (16.4-23.8 Ma). Old samples have K trough, which is together with high U content is typical for volcanic rocks originating from locally enriched lithospheric mantle source. Younger samples have also relatively low K content and even higher and more variable U data. The relatively high content of Sr and Ba are probably associated with glass phase and apatite, and also higher Ti content can refer for plagioclase fractionation (however Eu was not measured in the samples). Apatite represents a solitary host mineral concentrating incompatible elements (REE, U, Th). Sr and Ba contents are higher in older samples, but not as variably as in the younger once. There is a positive correlation between Ba and Sr in the Luban and Jawor areas. There is a great Sr variation in the Strzelin samples with limited fluctuation in Ba content. Sr is high, while Ba is low in Landek Zdroj. Ba and Sr content variation also reflect source variation under the

different areas. It is interesting to see the variation of B vs. Sr contents of the samples. There is a positive correlation between B and Sr in the samples from Landek Zdroj and a slight positive correlation in Strzelin. There is no B variation in Luban and Jawor with Sr increase. Plagioclase fractionation did not influence the B content. B content is not changing systematically with fractionation. The less fractionated samples (Jawor, Opole, Ladek Zdroj Raciborz) have the most variable B content. Ladek Zdroj and Raciborz show the highest B content (> 3 µg/g). Other samples have lower B content (< 3 µg/g), which is stable during increasing fractionation. Fractionation is not influencing the B content; it refers to source variation under the less differentiated volcanic structures.

B N C **Experimental Report**	*Experiment title* **Boron concentration measurement of andesite samples from Mátra Mts, North Hungary by PGAA**	*Instrument.* PGAA *Local contact* Katalin Gméling
Principal proposer: Katalin Gméling *Experimental team:* Katalin Gméling		*Experiment Number* PGAA_08_08_IH *Date* March 2008

Objectives:

In a frame work of a PhD research (Gméling 2010) the B content of the Neogene-Quaternary calc-alkaline volcanic rocks of the Carpathian Pannonian Basin were measured by PGAA. Most of the samples analysed with PGAA were measured before with different analytical methods to prove the accuracy and reliability of PGAA in geochemical analysis. We did not have previous chemical analysis from some of the calc-alkaline areas, for example the Mátra Mts. PGAA measurement of the andesites from the Mátra Mts were extended with LA-ICP-MS measurements.

Results:

Trace element data of the Mátra andesites show similar pattern to that of the other calc-alkaline rocks from the West Carpathians. The B content of the older (> 14 Ma) volcanic rocks of the Mátra Mts is increasing with increasing fractionation, B/Zr ratios did not show changes, referring to that the B/incompatible elemental ratios do not change with increasing fractionation. The variable Zr/Nb ratios between the samples are showing wide range in the partial melting of the source region. The Ba/Sm ratios of the samples are relatively higher then the B/Sm ratios referring to the fluid mobile element enrichment originates more from the crust, then the subducted sediments.

References:

Gméling, K. (2010): A Kárpát-Pannon térség miocén-kvarter mészalkáli vulkáni kőzeteinek bór geokémiai összetétele és kapcsolata a szubdukciós folyamatokkal: promptgamma aktivációs analitikai vizsgálatok. Doktori értekezés, ELTE TTK. / Boron geochemistry of the Miocene-Quaternary calc-alkaline volcanic rocks of the Carpathian Pannonian Region and its relation to subduction processes: prompt gamma activation analytical measurements. PhD dissertation Eötvös University, Budapest, Hungary; in Hungarian./

B N C **Experimental Report**	*Experiment title* **Neogen andesite intrusions along the Carpathian calc-alkaline volcanic arc, Toroiaga**	*Instrument.* PGAA *Local contact* *Katalin Gméling*
Principal proposer: Katalin Gméling and dr. Zoltán Pécskay *Experimental team:* Katalin Gméling		*Experiment Number* *PGAA_08_09_NC* *Date* December 2008

Objectives:

The Carpathian-Pannonian Region was formed during the Neogene-Quaternary by combined processes of large-scale block translation, subduction and extension, related to the collision of the European and African plates. We measured the B content, and examined the B geochemistry of andesite intrusions along the Carpathian arc from Toroiaga (Gméling et al. 2010). For comparison, B content of the Carpathian-Pannonian calc-alkaline volcanic rocks originating from different volcanic eruptions of various ages, were also measured. Numerous magmatic intrusions follow the Inner-Carpathian calc-alkaline volcanic arc with decreasing age towards the East-Southeast.

Results:

At the internal East Carpathians a big volume subvolcanic body (Tibles-Toroiaga-Rodna-Bârgau) found between the Gutâi and the Calimani volcanic massifs. The Toroiaga intrusive area situated north of the Rodna Mts., consist of a complex subvolcanic intrusions with pierce metamorphic rocks and its southern part, Paleogene to Miocene sedimentary deposits, suggesting a multiphase intrusive activity. The Toroiaga intrusive magmatism took place in between 9.7–9 Ma, much later then in the Western Carpathians.

The K_2O/Sm ratio of the Toroiaga samples are higher than in the Pieniny intrusions in the West Carpathians, and show positive correlation with the B/Sm ratio. The higher K_2O/Sm ratio is referring to metasomatising fluids originating from the crust. The Toroiaga intrusive rocks are slightly older, than the volcanics from the Calimani and Gurghiu Mts., which consistent with the age migration of volcanic activity from north towards the south.

Thanks for the support of OTKA K-68153 grant.

References:

Gméling K., Pécskay Z., Lexa J., Konečny V., Birkenmajer K. (2010): Neogene andesite intrusions along the Carpathian calc-alkaline volcanic arc. XIXth CBGA. Thessaloniki, Greece.

B N C **Experimental Report**	*Experiment title* **Whole rock analysis of basalts from a lava flow of Patagonia, Argentina**	*Instrument.* *PGAA* *Local contact* *Katalin Gméling*
Principal proposer: dr. Miguel Haller and dr. Károly Németh, Organizers of 3rd International Maar Conference *Experimental team:* *Katalin Gméling*		*Experiment Number* *PGAA_08_10_IC* *Date* February 2008

Objectives:

Patagonian basalt samples from different lava flows had to be measured by PGAA to give whole rock geoanalytical results of the rarely analysed volcanic formations which are located in that part of Patagonia, where the field trips of the 3rd International Maar Conference were organized.

Results:

Concentrations of major components and their oxides (except P and P_2O_5) and some trace elements (B, S, Cl, Sc, V, Cr, Co, Ni, Nd, Sm and Gd) have been determined in 18 samples using the PGAA facility at the BRR. Small pieces of each 18 powdered basalts and basaltic andesite sample were heat-sealed in FEP foils. The samples were irradiated in a cold neutron beam with a flux of 1.2×10^8 $cm^{-2}s^{-1}$. The cross-section of the neutron beam was collimated mostly to 1×1 cm^2 or 44 mm^2 during the measurements. The neutron flux has been proved to be stable during the reactor cycles and homogeneous in the area of the beam. Because the samples are practically transparent to neutrons, average bulk compositions of the investigated volume are obtained. All the samples were thinner than 10 mm; thus the corrections for the self-absorption of neutrons and γ-photons were negligible. The measurement time for each individual sample varied between 1440 and 4540 s. The measurement times were set to achieve acceptable accuracies for the major components. The spectra were fitted with Hypermet-PC software; the element identification was performed using our prompt-gamma library and evaluated with an Excel macro developed by Dr. Zsolt Révay.

Major oxides and B, Cl, Nd, Sm, and Gd were determined in all of the samples. In some of the samples Sc and V were below detection limits. The S, Co, Ni and Cr content could be measured only in three samples. PGAA is highly sensitive of B, Cl, Gd and H, and provides more satisfactory and reliable results, than other analytical methods. The B content of the analyzed rocks shows wide variety (1.6 – 33.1 μg/g). Samples from Los Loros (Argentina) have much higher B content then all other measured samples.

The relative uncertainties of the major oxides are typically range between 2 to 10 %. Those elements have the highest uncertainty, which concentrations are close to the detection limit of PGAA. Uncertainties of the B data are around 1%. The Cl content is relatively low (<50 μg/g) in these samples, thus their relative uncertainty is higher (mostly above 5%). The uncertainty depends on the analytical sensitivity of the element, its amount in the sample and the conditions of the measurement.

References:

Haller, M. & Németh, K. (2009): Malacara tuff cone and Carapacho tuff ring. Field trip guide.
Haller, M. & Németh, K. (2009): Llancanelo and Payun Matru volcanic fields. Field trip guide.

B N C **Experimental Report**	*Experiment title* **Measuring whole rock Cl content, all major oxide and trace element contents in silicate samples**	*Instrument.* *PGAA* *Local contact* *Katalin Gméling*
Principal proposer: Dr. Christoph Schnabel, NERC Cosmogenic Isotope Analysis Facility, SUERC *Experimental team:* *Katalin Gméling*		*Experiment Number* *PGAA_08_11_IC* *Date* April-July 2008

Objectives:

Measurement of whole rock Cl contents by PGAA needed to the analytical results for the interpretation of Cl-36 concentrations in the samples (Di Nicola et al. 2009). This was a collaboration, in which 34 silicate samples were measured from unknown destinations. Not only Cl, but also Si, Ti, Al, Fe, Mn, Mg, Ca, Na, K, C, H, B, Cl, Cr, Sm, Gd were measured.

Results:

Concentrations of major components and their oxides and some trace elements (B, Cl, Sc, V, Sm and Gd, plus in some cases Sc, V, Cr, Co, Ni, Nd) have been determined in 18 rock samples using the PGAA facility at the BRR. PGAA is especially useful for analyzing B, H, Cl and Gd concentrations in whole rocks. In contrast to other geoanalytical methods, no sample preparation is necessary, and hence contamination problems can be avoided. Accuracy of major and trace element analyses by PGAA has been verified by measurements of geological reference materials. Hydrogen can be measured using PGAA with a high sensitivity, thus the H_2O content of the whole rock can also be determined.

The received 34 powdered rock samples (silicates). 1.5–2.5 g of each sample were heat-sealed in FEP foils with the sizes of about 20×30 mm^2. The samples were irradiated in a cold neutron beam with a flux of 1.2×10^8 cm^{-2}s^{-1}. The cross-section of the neutron was collimated to 1×1 cm^2 during the measurements. The neutron flux has been proved to be stable during the reactor cycles and homogeneous in the area of the beam. Because the samples are practically transparent to neutrons, average bulk compositions of the investigated volume are obtained. All the samples were thinner than 5 mm; thus the corrections for the self-absorption of neutrons and γ-photons were negligible. The measurement time for each individual sample varied between 2100 and 5100 s. The measurement times were set to achieve acceptable accuracies for the major components. The spectra were fitted with Hypermet-PC software; the element identification was performed using our prompt-gamma library and evaluated with an Excel macro developed by dr. Zsolt Révay.

In some of the samples the Cr, Co, Ni and Nd contents were below detection limits. The B, Cl, Sc, V, Sm and Gd contents could be determined in all of the samples. PGAA is highly sensitive of B, Cl, H and Gd, and provides more satisfactory and reliable results, than other analytical methods. Sm results of the PGAA measurements proved to be slightly, but systematically higher, than given by other methods. Sample series "B" have a higher silica and water content, but lower Al_2O_3, MnO, CaO, Na_2O content, than series "A"). There is a visible difference in the B content between the two series ("A" <0.7 μg/g, while "B" >8 μg/g)

The relative uncertainties of the major oxides are typically range between 1 to 5 %. Between the major oxides the MgO has the highest uncertainty as its concentration is

close to the detection limit of PGAA. Uncertainties of the B data are around 1%. The Cl content is relatively low (<100 μg/g) in these samples, thus their relative uncertainty is higher (mostly above 20%). Uncertainty of the Sm data is around 2%, while for Gd it is higher, but below 10%. The uncertainty depends on the analytical sensitivity of the element, its amount in the sample and the conditions of the measurement.

References:

Di Nicola, L., Schnabel, C., Wilcken, K.M., Gméling, K. (2009): Determination of chlorine concentrations in whole rock: Comparison between prompt-gamma activation and isotope-dilution AMS analysis. *Quaternary Geochronology*, 4, 6, 501-507.

B N C **Experimental Report**	*Experiment title* **Boron concentration measurement of xenoliths originating from the mantle of the Earth by PGAA**	*Instrument.* *PGAA* *Local contact* *Katalin Gméling*
Principal proposer: Katalin Gméling and dr. Gábor Dobosi *Experimental team:* Katalin Gméling		*Experiment Number* *PGAA_08_12_IH* *Date* *March 2008*

Objectives:

Volcanic rocks solidify from a magma, which can originate from the asthenosphere, from the upper part of the mantle, or from the lower part of the lower crust. To get farther conclusion about the origin of the boron content of different volcanic rocks, good to know the boron concentration of possible source regions. Searching the boron geochemical systematics of the Neogene-Quaternary calc-alkaline volcanic rocks of the Carpathian Pannonian basin in a frame work of a PhD research (Gméling 2010), I measured the boron content of 8 xenolith samples originating from the upper mantle (Balaton Highland: 0.04-0.27 μg/g).

Results:

The average B content of the mantle is very low (0,05−0,8 μg/g), similar to B content of meteorites. Thus it is very difficult the measure the whole rock B content of mantle xenoliths. PGAA is very sensitive to measure the B content of whole rocks precisely, even in low concentration.

The boron content of the measured 8 upper mantle xenoliths (lherzolites and harzburgites) is very low, between 0.04 and 0.27 μg/g. These data are published in a PhD thesis (Gméling 2010), which gives good basic information about the average B content of the upper mantle under the Bakony-Balaton Highland, and can be used in petrogenetical models. B data of the Bakony Balaton Highland upper mantle xenoliths do not show enrichment by B rich subduction fluids.

References:

Gméling, K. (2010): A Kárpát-Pannon térség miocén-kvarter mészalkáli vulkáni k zeteinek bór geokémiai összetétele és kapcsolata a szubdukciós folyamatokkal: promptgamma aktivációs analitikai vizsgálatok. Doktori értekezés, ELTE TTK. / Boron geochemistry of the Miocene-Quaternary calc-alkaline volcanic rocks of the Carpathian Pannonian Region and its relation to subduction processes: prompt gamma activation analytical measurements. PhD dissertation Eötvös University, Budapest, Hungary; in Hungarian./

Objectives:

2008 (BRR-191)

Sea(marine)-related samples may suffer from mainly Na-originating effects from scattering. Some techniques can significantly decrease the analytical sensitivities of many elements of interest due to the high backgrounds arising form Cl-38 and Na-24. Samples with high concentrations of Na and Cl were used as samples from remote places with vestigial concentration, e.g. lichens, particulate matter, fish powder, soil from Pico mountain (Portugal), tree bark, synthetic wood and estuarine sediments. The results will be compared to the results obtained by other analytical techniques. These results are the preliminary data included on the PhD work: "Biomonitor-Reflection of Large Distance air mass transported trace elements" by BSc Bruno Vieira, PhD student.

2009-2010

Through the project IAEA-TCR-05632 RER/4/032 (supported by the IAEA - International Atomic Energy Agency), a team of 3 members of the NANE (Neutron Activation in Environment, Epidemiology and Nutrition) went for 1 month training at the Budapest PGAA facility with the main goal of learning the technique. The final objective of this project is to implement a PGNAA (Prompt Gamma Neutron Activation Analysis) facility at the RPI-ITN (Portugal) in order to enhance its facilities and experimental techniques offer to the users.

Results:

2008

No problems were encountered. In-situ Prompt Gamma Activation Analysis on biological and geological materials was used for quantification of light elements, lead, cadmium, sulphur, phosphorus, silicon, among others. Paper 1 was done with results obtained in this visit.

2009-2010

It was possible to learn about the technique and to understand the processes of irradiation, measurement, spectra analysis (by Hypermet-PC software) and how the results are calculated using the macro Excel. It was learnt how to perform the non linearity calibration and the efficiency calibrations using the Hypermet-PC software. PGAA analysis of soil samples allowed to obtain information for light elements, such as B and Si. Possibilities of set ups for the future PGAA facility at

PGAA Facility Set Up
Maximum Change with
remove of all Polyethylene (PE)
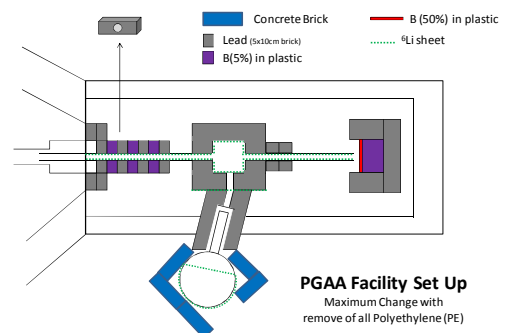
ITN (Portugal) were designed and the necessary materials for its construction were discussed. Paper 2 was written within this work.

References:

1) M.C. Freitas, Z. Révay, L. Szentmiklósi, I. Dionísio, H.M. Dung, A.M.G. Pacheco, Different methodologies in neutron activation to approach the full analysis of environmental and nutritional samples, J Radioanal Nucl Chem (2008) 278(2): 381–386 (DOI 10.1007/s10967-008-0804-6)

2) D. G. Beasley, A. Alghamdi, M.C. Freitas, A. Fernandes, Z. Révay, Simulating the introduction of a sapphire crystal into an epithermal neutron beamline, J Radioanal Nucl Chem (2009) 281:307–311 (DOI 10.1007/s10967-009-0096-5)

Objectives:

To determine the elemental composition of mussel reference material candidate.

Results:

The *Perna perna* mussel is abundant along most of the Brazilian coast and is important as it is consumed as seafood and as it is used in environment biomonitoring studies. The raw material was purchased from a mussel farm in the São Paulo State North Coast and it was processed following the ISO Guide 35 recommendations for the preparation of reference materials. The material was freeze-dried and particle size was adjusted to be less than 105 µm. Once homogenized, the material was bottled in amber glass vials with approximately 13 g and was finally gamma ray sterilized. Two vials of the material were analyzed. As the material was hygroscopic, an independent aliquot from each vial were dried in an oven at 85 ºC until constant weight.

The following elements were determined with PGAA:

	TM1-144				**TM1-37**			
	c% atom	unc %	c% el/el	unc %	c% atom	unc %	c% el/el	unc %
H	37.4	6	3.90	9	36.9	3.5	3.80	6.
B	8.43 ppm	6	9.43 ppm	9	8.49 ppm	3.5	9.39 ppm	6.
C	24		630	9	23		4.28	6.
N	5.1	6	7.4	9	5.0	3.9	7.2	6.
O	31		1252	9	33		7.54	5.
Na	0.58	6	1.38	9	0.58	3.9	1.37	6.
Mg	0.18	16	0.5	18	0.18	8.	0.46	10.
Si	0.084	7	0.24	10	0.056	8.	0.16	9.
P	0.30	9	1.0	11	0.25	7.	0.79	8.
S	0.32	6	1.06	9	0.32	3.9	1.05	6.
Cl	0.63	6	2.3	9	0.64	3.7	2.31	6.
K	0.133	6	0.54	9	0.147	4.	0.59	6.
Ca	0.05	12	0.23	14	500 ppm	28.	0.2	29.
V					6 ppm	16.	30 ppm	17.
Cd	0.025 ppm	11	0.29 ppm	13	0.031 ppm	12.	0.35 ppm	13.

In parallel, ICP-MS measurements have also been completed to quantify the trace elements of the samples.

Future prospects:

The results of several laboratories will be cross-checked and analyzed with statistical methods. The homogeneity of the batches will be scrutinized. The merged

dataset will form the basis of the certification procedure.

B N C **Experimental Report**	*Experiment title* Composition characterization materials using PGAA at Budapest cold neutron beam facility	*Instrument.* *PGAA* *Local contact* *Zs. Révay*
Principal proposer: R. Acharya, K. Sudarshan, P.K. Pujari, Radiochemistry Division, Bhabha Atomic Research Centre, Mumbai – 400 085, India *Experimental team*: Zs. Révay, L Szentmiklósi, T. Belgya Department of Nuclear Research, Institute of Isotopes, 1121 Budapest, Hungary		*Experiment Number* *PGAA_09_03_IC* *Date:* *2009 Oct.*

Objectives: Composition characterization of materials using PGNAA at Budapest cold neutron beam facility

Samples analyzed: (i) Composition analysis in Zircaloy 2, 4 and Zr-Nb alloy samples, (ii) Determination of H and B in zirconium samples, (iii) Impurity determination graphite and (iv) Composition analysis of meteoritic soil

Experimental:

The PGAA facility of was used for composition analysis of samples such as Zircaloy 2 and 4, Zr-2.5%Nb alloy, Graphite, C-C composite, aluminium oxide and soil. The thermal equivalent neutron flux at this position is 1.2×10^8 cm^{-2} s^{-1}. Samples in the mass range of 0.1-0.5 g, kept inside thin Teflon bag were irradiated and on-line measurement of prompt γ-rays were measured for 3-10 h with a HPGe detector (sample-to-detector distance 23 cm) surrounded by a Compton-suppressor and passive shielding. The absolute counting efficiency of the detector was determined using ^{133}Ba and ^{152}Eu and prompt gamma rays from ^{14}N(n,γ)^{15}N and ^{37}Cl(n,γ)^{38}Cl. The γ –ray spectra were complex due to presence of multi-γ producing elements/isotopes and they were analyzed for peak areas by Hypermet PC (MS DOS Version 5.01). Since all the major and minor elements were amenable to PGAA, the absolute concentrations of all the elements were determined using mass balance procedure i.e., without using concentration of any external or internal standard.

Results:

In zirconium alloys, in addition major Zr, the minor elements detected in three different zircaloys are Sn, Fe, Cr and Ni in zircaloy 2, Sn, Fe and Cr in zircaloy 4, and Nb, Fe and Cr in Zr-2.5% Nb alloy. The trace elements detected in general are B, Hf, Ti, Mn and Co. Trace amounts of Cl were also detected in zircaloy 2 and 4. Hydrogen concentrations were determined by k_0-PGAA utilizing 2223 keV prompt gamma rays obtained from ^{1}H(n$_{th}$, γ) reaction. Boron concentrations (0.1 mg kg^{-1} to 0.4%) were determined in zirconium matrix using 478 keV Doppler broadened γ-ray. The concentrations in the range of 20-160 mg kg^{-1} were determined.

In the case graphite, in addition to C, trace concentrations of neutron poisons, REEs and Sc, Na and Al were determined. Complete composition analysis of three meteoritic soil samples was carried out. The major to trace elements determined included Fe, Si, Ti, Al, Mg, Ca, Na, K, Mn, V, B, Cl, Sc, Cr, Co, Ni, Sm and Gd. Concentrations of Fe and Si were 23-25% and 13-15%, indicating Fe concentrations were higher and Si concentrations were lower than normal soil, which is signature of meteoritic impact in soil.

The advantages of the PGNAA method used are: (i) it is non-destructive, (ii) it could detect trace amounts of important elements like H,B, Cl, Cd, Sm, Gd, Eu and Hf in the presence of major/minor elements, and (iii) all elements determined except for B have multiple γ-rays, which help in self-validation of methodology.

The work was carried out under Indian National Science Academy and Hungarian Academy of Sciences (INSA-HAS) Bilateral Exchange Programme during October 2009 – March 2010 (INSA Ref: IA/Misc. 2009-2010/4237).

International Symposium Publications:

Composition analysis of zirconium alloys using k_0-based PGAA using Budapest cold neutron beam facility, R. Acharya, Zs. Révay, R.V. Kulkarni, A.V.R Reddy, 16th Radiochemical Conference (RadChem 2010), April 18-23, 2010, Prague.

Non-destructive determination of hydrogen contents in zircaloy samples by k_0-based Prompt Gamma-ray NAA, K. Sudarshan, R. Acharya, Zs. Revay, L Szentmiklósi, T. Belgya, R.V. Kulkarni, V. D. Alur, G.K. Mallik, P.K. Pujari, 4th International Symposium on Nuclear analytical Chemistry (NAC-IV), November 15-19, 2010, BARC, Mumbai

B N C **Experimental Report**	*Experiment title* **Measuring whole rock geochemical composition of carbonate and silicate samples**	*Instrument.* *PGAA* *Local contact* *Katalin Gméling*
Principal proposer: dr. Steven Binnie, Institute of Geography, School of Geosciences, University of Edinburgh *Experimental team:*		*Experiment Number* *PGAA_09_04_CW* *Date* January 2009

Objectives:

Measurement of whole rock major oxide and trace elements by PGAA were ordered for scientific reason from a research group of the Edinburgh University. This was a work of contract, in which 25 carbonates, basalts and other silicate samples were measured from unknown destinations.

Results:

Concentrations of major components and their oxides and some trace elements (B, Cl, S, Sc, V, Cr, Ni, Ge, Cd, Nd, Sm, Gd) have been determined in 25 rock samples using the PGAA facility at the BRR. PGAA is especially useful for analyzing B, H, Cl and Gd concentrations in whole rocks. In contrast to other geoanalytical methods, no sample preparation is necessary, and hence contamination problems can be avoided. Accuracy of major and trace element analyses by PGAA has been verified by measurements of geological reference materials. Hydrogen can be measured using PGAA with a high sensitivity, thus the H_2O content of the whole rock can also be determined.

The received 25 powdered rock samples (carbonates, basalt and other silicates). 1.4–2.9 g of each sample were heat-sealed in FEP foils with the sizes of about $20{\times}30$ mm^2. The samples were irradiated in a cold neutron beam with a flux of $1.2{\times}10^8$ $cm^{-2}s^{-1}$. The cross-section of the neutron was collimated to $1{\times}1$ cm^2 or 44 mm^2 during the measurements. Because the samples are practically transparent to neutrons, average bulk compositions of the investigated volume are obtained. All the samples were thinner than 5 mm; thus the corrections for the self-absorption of neutrons and γ-photons were negligible. The measurement time for each individual sample varied between 1140 and 4200 s. The measurement times were set to achieve acceptable accuracies for the major components. The spectra were fitted with Hypermet-PC software; the element identification was performed using our prompt-gamma library and evaluated with an Excel macro developed by dr. Zsolt Révay.

The Al_2O_3, MgO, CaO, H_2O, CO and B, Cd could be determined in measured limestones (16 samples). Most of the limestones have SiO_2, TiO_2, MnO, K_2O, and Cl content above the detection limit of PGAA, while Cr, Ni, Ge, Nd, Sm and Gd could be measured only in some of the limestone samples. In all basalts and other silicate samples we could determine all major oxides (SiO_2, TiO_2, Al_2O_3, Fe_2O_3T, MnO, MgO, CaO, Na_2O, K_2O and H_2O) and some trace elements (B, Cl, Nd, Sm and Gd). S, Sc, V, Cr could be measured above detection limit only in few silicates. The measured limestones have low B and Cl content (0.29-1.21 and 5.6-23.1 μg/g respectively), much lower than the measured basalts and silicates (19.4-58.2 and 165-1960 μg/g respectively).

In case of the basalts and other silicates the relative uncertainties of the major oxides are typically range between 1 to 8 %. Those elements have the highest uncertainty, which concentrations are close to the detection limit of PGAA. Uncertainties of the B data are between 0.7-1.2%. Analytical results of the limestones have higher uncertainties, between 2 and 20% for major oxides and it can reach even higher values in case of trace elements.

The uncertainties of the boron content of limestones are between 1.8 and 5%, even though the boron contents of these samples are quite low. The uncertainty depends on the analytical sensitivity of the element, its amount in the sample and the conditions of the measurement.

References:

B N C	*Experiment title*	*Instrument.*
Experimental Report	**Geochemical investigation of flisch sediments hosting the Pieniny andesite intrusion in the West Carpathians**	*PGAA* *Local contact* *Katalin Gméling*
Principal proposer: Katalin Gméling, dr. Zoltán Pécskay *Experimental team:* Katalin Gméling		*Experiment Number* *PGAA_09_05_NC* *Date* *April 2009*

Objectives:

Calc-alkaline volcanic rocks situated in the West Carpathians are proposed to form following the subduction of the European plate. Subducting sediments can influence the chemical composition of the volcanic rocks following the edge of the continental crust. Subduction processes finished by the continent-continent collision and slab break off. Sediments could be partly subducted and other part folded up in great amount following the outer Carpathians. The folded flisch sediments host andesite intrusions following an about 20 km long line. Thus it is interesting to examine the chemical composition of the flisch sediments in many reasons, like as host sediment of intrusive rocks and also as possible subducting sediment. Modern geophysical investigations suppose that, there was no subuction under the West Carpathians, which can be overview also by the boron geochemical research of the volcanic rocks, measured by PGAA.

Results:

The melt moving towards the surface can assimilate matters from the surrounding rocks and become contaminated with the lower crustal, upper mantle materials, and with the subducted sediment or slab materials and fluids originated from them. We tried to determine the average B content of the possible contaminants, and the host sediments of intrusive rocks in the West Carpathians. The B content measured in the flisch sediments gives good basic information about the average B content of possible subduting sediments, and can be used in petrogenetical models. The B content of the flisch sediments is between 112 and 121 μg/g. This result shows good agreement with the average B content of the Black Sea sediment measured previously by PGAA (129 μg/g, Cristache et al. 2009), and also with the literature data of sediments from the Pacific Ocean (96-132 μg/g, Ishikawa & Nakamura 1993). We made calculations about the B content of fluids originating from the subducted sediments, to show that the B concentration of fluids (5200-5600 μg/g) are much higher than the B content of the sediments (Gméling 2010). The B data of flisch were also used in petrological models tracing the origin of fluid mobile elements in the calc-alkaline volcanic rocks (Gméling 2010), and intrusive andesites in the Pieniny Andesite Line (Pécskay & Gméling 2010).

References:

Cristache, C., Gméling, K., Culicov, O., Frontasyeva, M.V., Toma, M. Duliu, O.G. (2009): An ENAA and PGAA comparative study of anoxic Black Sea sediments. J. of Radioanal. and Nucl. Chem., 279, 1, 7-12.
Gméling, K. (2010): A Kárpát-Pannon térség miocén-kvarter mészalkáli vulkáni k zeteinek bór geokémiai összetétele és kapcsolata a szubdukciós folyamatokkal: promptgamma aktivációs analitikai vizsgálatok. Doktori értekezés, ELTE TTK. / Boron geochemistry of the Miocene-Quaternary calc-alkaline volcanic rocks of the Carpathian Pannonian Region and its relation to subduction processes: prompt gamma

activation analytical measurements. PhD dissertation Eötvös University, Budapest, Hungary; in Hungarian./

Ishikawa, T., Nakamura, E. (1993): Boron isotope systematics of marine sediments. Earth Planet. Sci. Lett., 117, 3-4, 567-580.

Pécskay, Z., Gméling, K. (2010): Role of the intrusive processes within the evolution of the Neogene-Quaternary calc-alkaline volcanism of the Carpathians. New Advances in Maar-Diatreme Research in Hungary, Germany and New Zealand. Results and Perspectives International Maar Workshop Tapolca, Hungary, 13-15 August 2010 (Eds) Károly Németh, Balatonlelle, Hungary, ISBN 978-963-06-5638-2

B N C **Experimental Report**	*Experiment title* Characterisation of polished stone tools' raw materials from Hungary by non-destructive chemical analyses (PGAA)	*Instrument.* PGAA *Local contact* Zs. Kasztovszky
Principal proposer: György Szakmány - Dept. of Petrology and Geochemistry, Eötvös L. University, Budapest *Experimental team:* Zs. Kasztovszky, Zs. Szilágyi		*Experiment Number* PGAA_08_02_NC *Date* 01.2008-06.2009

Objectives:

Polished stone tools with fine to very fine grained texture may show striking similarities in their macroscopic appearance by texture and colour. Therefore, it is very difficult to distinguish the different rock types by the naked eye. PGAA is one of the powerful, absolutely non-destructive chemical methods for the analysis of archaeological materials. 189 polished stone tools from different collections and localities of Hungary, moreover 25 geological samples from potential raw material sources were analyzed by PGAA to obtain chemical composition of the analyzed artifacts for provenance study purposes and to create an initial database of PGAA results of the most important polished stone tools' raw materials occurring in Hungary

Results:

As a result, several types of raw materials (basalt-dolerite-metadolerite, greenschist-metabasite-amphibolite, blueschist, hornfels, 'white stone', ultrabasic rocks, acidic-intermediate volcanites) could be separated from each other. Moreover, we can distinguish different compositional groups within rock types (e.g. greenschist-metabasite, basalt-dolerite). It turned out that weathering or alteration can essentially change the chemical composition beyond the limit of recognisability of the rock. Macroscopic description together with PGAA will help to determine raw material types of polished stone tools. However, in some cases other methods are also necessary to achive precise determination.

PCA 1 and 3 (49%) for major elements
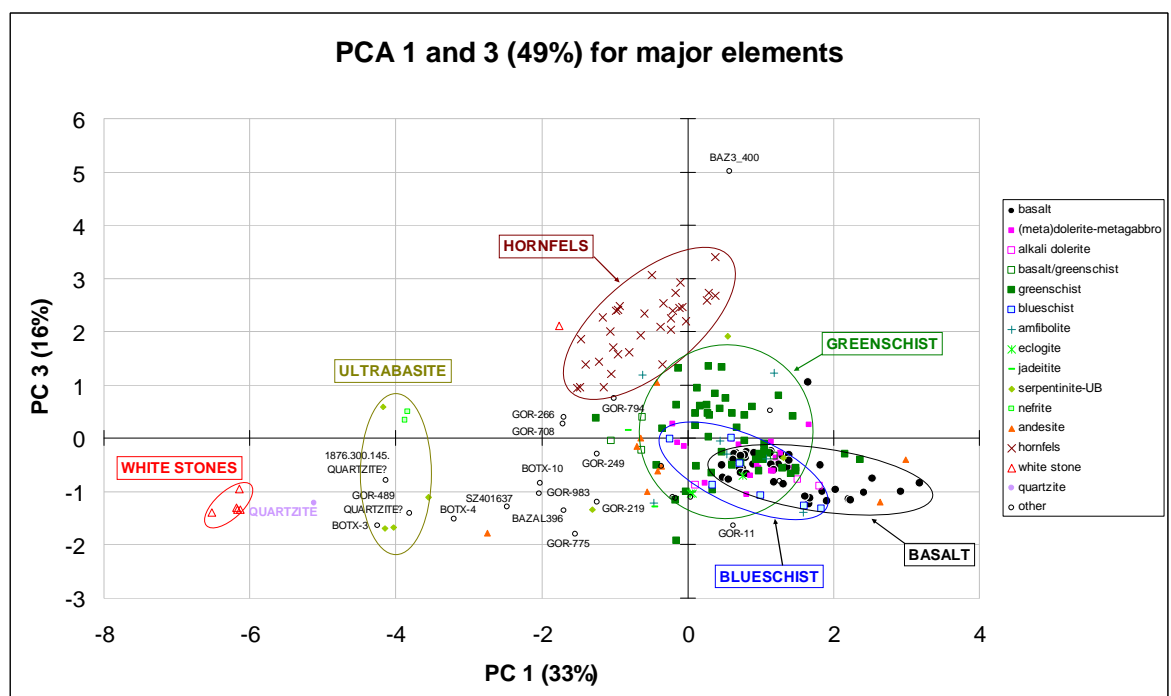
Fig.1 Clustering of the samples by principal component analysis of the major elements

References:

Szakmány et al.: Discrimination of prehistoric polished stone tools from Hungary by non-destructive chemical analyses (European Journal of Mineralogy – in prep.)

B N C **Experimental Report**	*Experiment title* Neutron holographic measurement on Sn-Cd alloy	*Instrument* TAST *Local contact* *Márton Markó*
Principal proposer: *Márton Markó,* *Experimental team:* *László Cser, Gyula Török*		*Experiment Number* *TAST_08_01_IH* *Date(s) of Exper.* *2008*

Objectives

Atomic resolution neutron holography is a relatively new method for investigating the immediate neighbourhood of impurities in a single crystal. Here gamma-conversion neutron holography (GNH) is used to explore positions of cadmium atoms in a tin-cadmium alloy.

Results

In GNH, a strong neutron absorber (in this measurement cadmium) absorbs neutron and emits a prompt-gamma photon. The measured gamma-yield is proportional to the mean neutron intensity at the place of the absorber nuclei. In a single crystal sample the neutron intensity at a given position of the unit cell is determined by the interference between the incoming beam coming from a distant source (reference beam), and the part of the beam coherently scattered by the neighbouring atoms (target beam). Thus changing the direction of the beam relative to the crystallographic orientation (i.e. rotating the sample) causes a shift of the interference fringes in the sample, thus holographic modulation appears in the measured gamma yield as a function of the direction of the direct beam relative to the crystallographic orientation. After applying Helmholtz-Kirchoff transformation (three dimensional Fourier-transformation restricted to a sphere centered in the origin and with a radius of the wavenumber of the neutron beam) on the measured data, high intensity points are appearing at the position of the neighbours of the absorber atoms.

We used BGO-scintillator detector for detecting the prompt gamma intensity coming from the sample. The discriminator level was set over the gamma energy of the boron-line, thus the background coming from the neutron shielding of the instrument was eliminated. The detector was carefully shielded by lead and by lithium containing plastic at the side looking at the sample. The sample-detector distance was set to 15 cm.

The measurement took 15 days. During this time more than 10^9 counts were collected. The spherically shaped sample of 7 mm diameter was rotated by an Eulerian-cradle. The plane of the cradle was parallel to the direct neutron beam. The sample was rotated around the chi axis (horizontal axis perpendicular to the direct beam) over the angular range of -60° +60°, and at each chi position a full round rotation was done around the phi axis (the axis of the sample holder). The angular steps were 1° in both directions.
Fourier-filters were applied to suppress the modulation coming from the imperfectly aligned sample. The measured hologram treated in that way was then reconstructed using the Helmholtz-Kirchoff integral. We applied mirror symmetry operations on the

reconstructed image (each symmetry plane was perpendicular to a main crystallographic axis in a tetragonal system). Due to the holographic central symmetry (holographic symmetry is the symmetry of the mean neighbourhood of the detector atoms) the imaginary part of the reconstructed image does not carry any holographic information i.e. applying the central symmetry operation either on the measured data or on the reconstructed image, the imaginary part of the image will disappear.

The real part of the reconstructed measured hologram is seen in Fig. 1.(a). The result of the model calculations is shown in Fig.1.(b). The amplitude of a reconstructed atomic peak varies as

$-2b/(R) \cos(kR)$

where b is the scattering length, R is the distance of the given atom from the probe atom, and k is the absolute value of the wavenumber of the incoming neutrons. This is the explanation why the signs of reconstructed atomic peaks of the first neighbours are negative (blue spots), while that of the fourth neighbours are positive (red spots).The same rule is the reason of disappearing of the atomic spots of the second and third neighbours at the given wavelength.
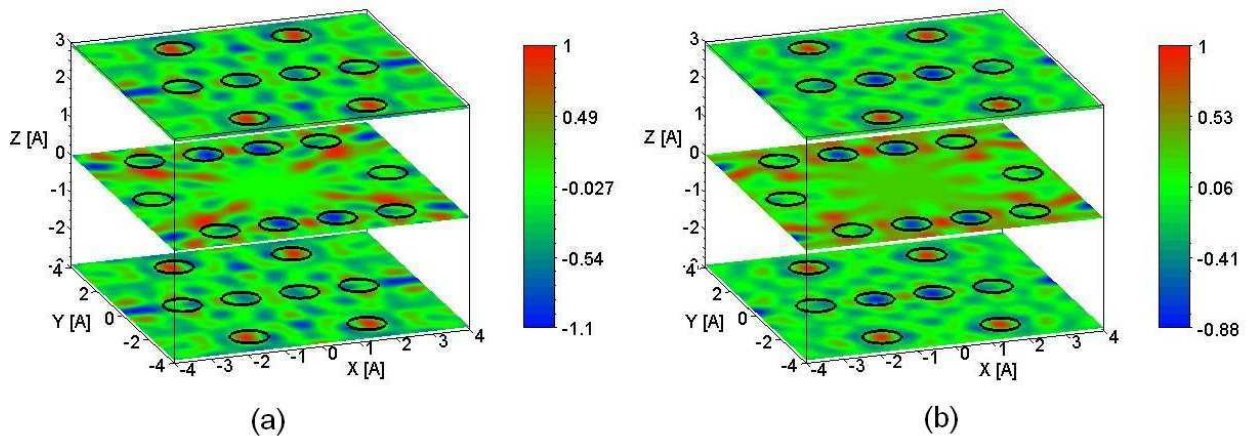
Figure 1. Real part of the reconstructed measured (a) and calculated (b) neutron hologram of SnCd sample.

The obtained arrangement of the Sn atoms surrounding the Cd one coincides with the regular Sn crystalline structure. No sign of the presence of Cd atoms in the interstitial position was observed. Consequently, at the level of achieved accuracy from the results it follows that Cd atoms prefer the substitutional positions instead of interstitial ones.

Reference
M. Markó, A. Szakál, Gy. Török, L. Cser: Construction and testing of the instrument for neutron holographic study at the Budapest Research Reactor, RSI, 81/10 105110, (2010)

B N C **Experimental Report**	*Experiment title* Structure study of rare earth substituted yttrium aluminium borate	*Instrument..* PSD *Local contact* E. Sváb
Principal proposer: J. Beregi and E. Sváb *Experimental team:* M. Fábián, Gy. Mészáros, J. Beregi, E. Sváb, MTA-SZFKI		*Proposal No.* *PSD_08_01_IH* *Date(s) of Exp.* *February 2008*

Objectives

Yttrium aluminium borate $YAl_3(BO_3)_4$ (YAB) single crystals have excellent non-linear optical properties, and doped YAB crystals have important applications in laser engineering. YAB crystals have suitable sites for some rare-earth elements at the Y^{3+} site (Er^{3+}, Nd^{3+}, Yb^{3+}, La^{3+}) or other doping ions at Al^{3+} site (Cr^{3+}, Ga^{3+}). The knowledge of the crystallographic parameters is important when characterising the optical properties of YAB crystals. The aim of this study was to investigate the crystallographic effect of the substitution of Er^{3+} and Yb^{3+} into $YAl_3(BO_3)_4$.

Results

$Y_{0.84}Er_{0.01}Yb_{0.15}Al_3(BO_3)_4$ single crystal was grown by top-seeded high temperature solution (flux) method. The single crystal was powdered into fine grains to obtain good powder spectrum suitable for Rietveld refinement. The neutron diffraction pattern are shown in Fig. 1.
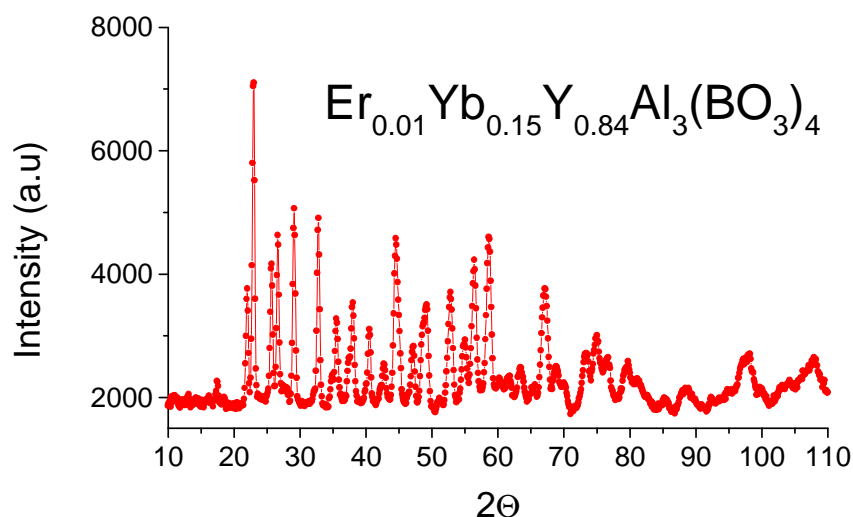
***Figure 1**. Neutron diffraction pattern ($\lambda_0=1.069Å$) of $Y_{0.84}Er_{0.01}Yb_{0.15}Al_3(BO_3)_4$*

The crystal structure of $YAl_3(BO_3)_4$ is rhombohedral with space group *R32*. The Y atoms, Al atoms and B atoms occupy trigonal prisms, octahedra, and triangles of oxygen, respectively. Our investigations have shown that the substitution of Y atoms by Er^{3+} and Yb^3 rare earth elements leaves the space group invariant, however, the lattice parameters and the atomic position parameters are different due to the differences in the ionic radii result. The results obtained by the Rietveld refinement are collected in Tables 1 and 2. The crystal strucrure is illustrated in Fig. 2.

Table 1. *Hexagonal lattice parameters in space group R32*

Composition	Lattice parameter (Å)	
	a	c
$YAl_3(BO_3)_4$	9.2785(1)	7.2257(2)
$Y_{0.84}Er_{0.01}Yb_{0.15}Al_3(BO_3)_4$	9.263186	7.211918

Table 2.*Atomic position parameters calculated by Rietveld refinement*

	$YAl_3(BO_3)_4$			$Y_{84}Er_{0.01}Yb_{0.15}Al_3(BO_3)_4$		
Atom (position)	**x/a**	**y/b**	**z/c**	**x/a**	**y/b**	**z/c**
Y, Er, Yb (3a)	0	0	0	0	0	0
Al (9d)	0.555(7)	0	0	0.554(3)	0	0
B(1) (3b)	0	0	0.5	0	0	0.5
B(2) (9e)	0.442(3)	0	0.5	0.442(1)	0	0.5
O(1) (9e)	0.850(8)	0	0.5	0.855(6)	0	0.5
O(2) (9e)	0.591(2)	0	0.5	0.589(3)	0	0.5
O(3) (18f)	0.449(4)	0.149(4)	0.521(1)	0.443(4)	0.153(4)	0.519(1)
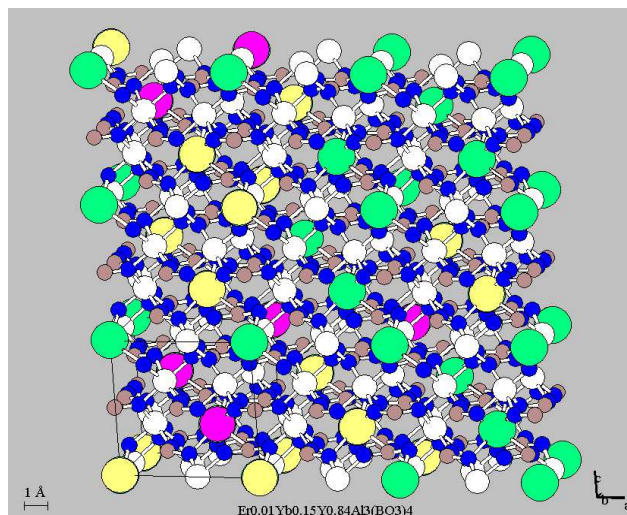
Figure. *2. Atomic structure of $Y_{0.84}Er_{0.01}Yb_{0.15}Al_3(BO_3)_4$*

B N C **Experimental Report**	*Experiment title* Neutron diffraction study of mixed oxides YCr$_x$Fe$_{1-x}$O$_3$	*Instrument.* PSD *Local contact:* E. Sváb
Principal proposer: Kiril Krezhov *Experimental team: M. Fábián, Gy. Mészáros, E. Sváb, MTA-SZFKI; S. Kovachev, K. Krezhov, Sofia/Bulgaria*		*Proposal No.* PSD_08_02_IC *Date(s) of Exp.* 2008

Objectives

Multiferroics are receiving wide attention in recent years. Besides important implications for novel electronic devices [1,2], the physics behind the complex magnetoelectric phenomena and the microscopic origin of multiferroicity is of great current interest [3]. The present neutron powder diffraction (NPD) study was aimed at obtaining of new results for the structure and magnetic phase transitions in the binary perovskite system YCr$_x$Fe$_{1-x}$O$_3$ (0<x<1) known for its unusual temperature and composition dependent magnetic behaviour [4-6]. In view of the weak biferroicity of YCrO$_3$ with transition at T_E =400 K to weak ferroelectric state much above the magnetic phase transition at T_N = 141 K to weak antiferromagnetic state, the evidence helps in improving our understanding of perovskite-like systems with noncollinear spin ordering.

Results

Powder samples with composition very close to the nominal formula x = 1.0, 0.875, 0.75, 0.67, 0.5, 0.33, 0.25,0.125, 0.0 (ICP analyses) were produced by solution combustion and characterized by thermo-gravimetric/differential thermal analysis (TG/DTA), X-ray diffraction (XRD) and magnetic measurements.
The main XRD peaks (Fig.1, Inset: limited angular part with reflections 311, 321, 240 and 042) are with nearly equal intensities and angular positions indicating that, similarly to YFeO$_3$ and YCrO$_3$, all the members are orthorhombic perovskites at RT.
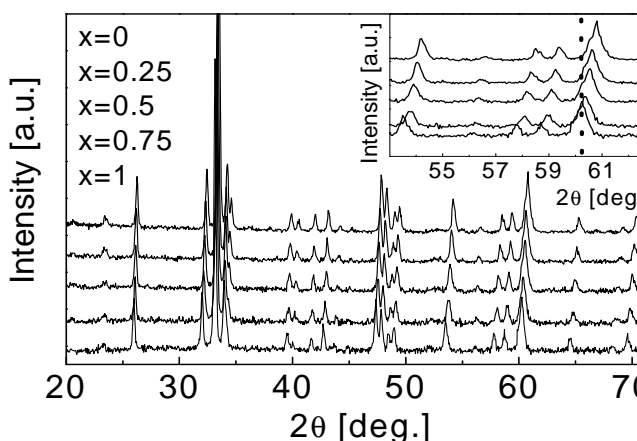
Figure 1. X-ray diffraction pattern

Figure 2 illustrates for $YCrO_3$ the crystal structure (Pnma) determination from a simultaneous refinement of the XRD (main) and NPD (inset) patterns at RT. Refinements of $YCrO_3$ data at RT in monoclinic P21/n, as used for density functional theory calculations in [8], do not produce better agreement factors.
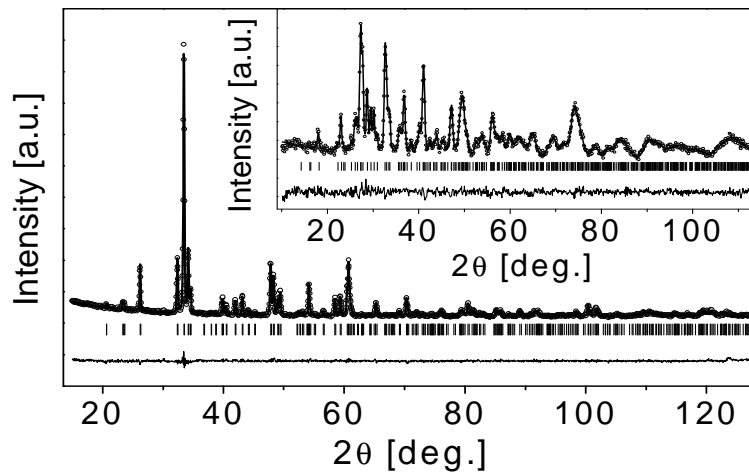
***Figure 2**. X-ray and neutron diffraction pattern and Rietveld refinement for $YCrO_3$*

In both $YFeO_3$ and $YCrO_3$ below the Neel temperature T_N=648 K and 141 K, respectively, the noncollinear antiferromagnetic (AFM) state Γ_4 ($G_cF_bA_a$) is established. The weak ferromagnetic (FM) constituent **F** observed is attributed to Dzyaloshinsky – Moriya (D-M) antisymmetric exchange leading to small canting between the spin sublattices [7]. Low angle part of RT NPD patterns and magnetization data give evidence for AFM ordering at RT for x≥0.75 and the weak FM component F increases with x. The unit cell volume expands monotonously with increasing x indicative of formation of a binary solid solution resulting from the random distribution over B-lattice sites of larger Fe^{3+} (half-field $t^3_{2g}e^2_g$, ionic radius ri= 0.645 Å) substituting smaller Cr^{3+} (empty t^3_{2g}, ri = 0.615 Å). Figure 3 shows that the G-ordering of $YFeO_3$ (x=0, inset) is preserved for x=0.875 (main). Thus, the average crystal structure of the system, including $YCrO_3$ is orthorhombic and centrosymmetric. In reasoning the biferocity of $YCrO_3$ the concept of local non-centrosymmetry was introduced [9].
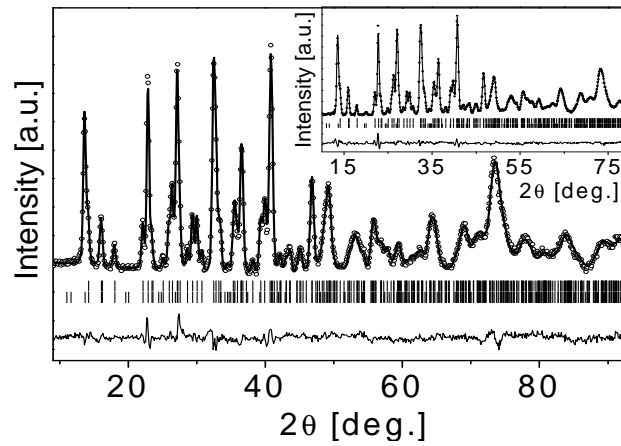
***Figure 3**. Neutron diffraction pattern and Rietveld refinement for $YCr_{0.875}Fe_{0.125}O_3$ (main) and for $YFeO_3$ (inset)*

References:

 [1] W. Erenstein, N.D. Mathur and J.F. Scott, *Nature* 442 (2006) 759 [2] R. Ramesh, N.A. Spaldin, *Nature Materials* 6(2007)21. [3] M. Fiebig, N.A. Hill, *Eur.Phys.J.* B71 (2009) 293. [4] A. Dahmani, M. Taibi, M. Nogues, J. Aride, E. Loudghiri, A. Belayachi, *Mater. Chem. Phys.* 77, 912 (2002). [5] A.M. Kadomtseva, A.S. Moskvin, I.N. Bostrem, B.M. Wanklyn, N.A. Khafizova, *Sov. Phys. JETP* 1202 (1977) 45. [6] S. Kovachev, D. Kovacheva, S. Aleksovska, E. Svab, K. Krezhov. *J. Optoelectr.&Adv. Mater.*, 11(10) (2009) 1549 [7] D. Georgiev, K. Krezhov, V. V. Nietz, *Solid State Commun.* 96, 535(1995). [8] C.R. Serrao, A.K. Kundu, S.B. Krupanidhi, C.N.R. Rao, *Phys. Rev. B* **72** (2005), 220101(R). [9] K. Ramesha, A. Llobet, Th. Proffen, C.R. Serrao, C.N.R. Rao, *J.Phys.:CM,* 19(10)102202

B N C **Experimental Report**	*Experiment title* High-temperature neutron diffraction study of the phase transition in a system of lead and bismuth based perovskites	*Instrument.* *PSD and MTEST* *Local contact:* *E. Sváb and* *L Kőszegi*
Principal proposer: Kiril Krezhov *Experimental team:* M. Fábián, E. Sváb, L. Temleitner, L. Kőszegi, SZFKI; *S.Kovachev, K. Krezhov,* Sofia/Bulgaria		*Proposal No.* BRR_219, *Date(s) of Exp.* 7-17.07.2009 5-17.10.2009

Objectives

The proposed neutron powder diffraction (NPD) study is focused on determining the details of the crystalline and magnetic structure of $Pb_{0.5}La_{0.5}Fe_{1-x}Mn_xO_3$ ($0 \leq x \leq 1.0$) and $Pb_{0.5-x}Bi_xLa_{0.5}FeO_3$ ($0 < x \leq 0.25$), less explored transition metal oxide systems due to difficulties in high-grade sample preparation. $Pb_yLa_{1-y}MnO_3$ ($y \leq 0.5$) are ferromagnets [1] with Curie temperature T_C increasing linearly with x to 355 K for x=0.5 [2] and display colossal magnetoresistance (CMR) effects [3] with an MR value of 50% in a field of 5.5 T at 330 K in thin films [4]. Doping of the Mn sites with Fe dramatically alters the material properties leading to wide scope of applications of $Pb_{1-y}La_yFe_{1-x}Mn_xO_3$ such as catalysts, electrode materials in solid oxide fuel cells, exhaust gas sensors, membranes for separation processes etc. [5-7].

Results

The powder samples with composition very close to the nominal formula (ICP analyses) were successfully produced by a specific solution combustion technique [8] and characterized by thermo-gravimetric/differential thermal analysis (TG/DTA), X-ray diffraction (XRD), magnetic measurements and Mössbauer spectroscopy (MS).

The neutron diffractometers PSD (λ=1.061 Å) and MTEST (λ=1.439 Å) were used. The allotted beam time was sufficient to take NPD patterns at 295 K and elevated temperatures on the system $Pb_{0.5}La_{0.5}Fe_{1-x}Mn_xO_3$ ($0 \leq x \leq 1.0$) only. The XRD analyses showed that the samples are single phases with apparently pseudo cubic perovskite structure. The XRD patterns could be indexed in rhombohedral space group R-3c but structure refinements using FullProf produced high χ^2. Susceptibility, TG/DTA and NPD data (Fig.1) evidenced that Néel temperature ($T_N \approx 555$ K, x=0) goes down with increasing x.
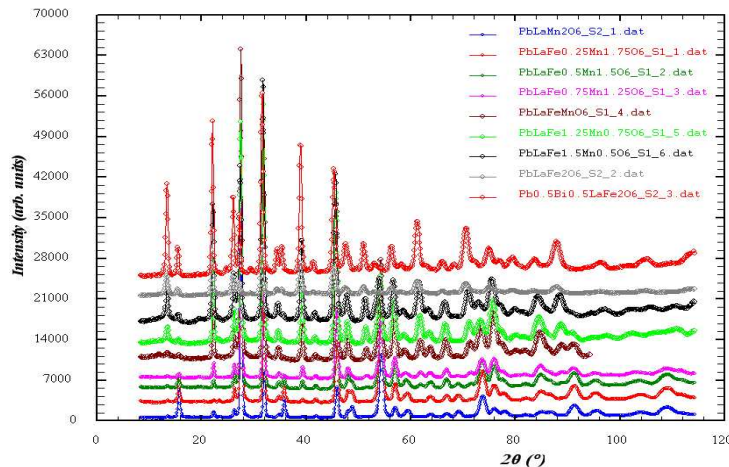
Figure 1. *Neutron powder diffraction pattern for $Pb_{0.5}La_{0.5}Fe_{1-x}Mn_xO_3$ ($0 \leq x \leq 1.0$) and for $Pb_{0.25}Bi_{0.25}La_{0.5}FeO_3$*

Simultaneous XRD and NPD Rietveld analyses showed that $La_{0.5}Pb_{0.5}FeO_3$ (x=0) is best described in orthorhombic Pnma space group (Fig. 2) in similarity with $LaFeO_3$.
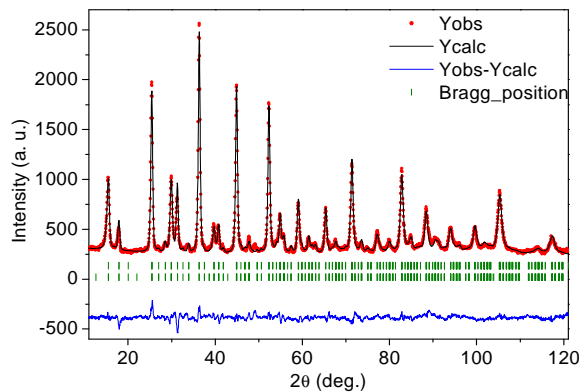
Figure 2. *Neutron diffraction pattern and Rietveld refinement for $La_{0.5}Pb_{0.5}FeO_3$*

The rest crystal structures have Imma symmetry (except R-3c for x=1) as exemplified with Fig. 3 for x=0.75. Though Mn^{3+} and Fe^{3+} are with practically identical ionic radius (0.645 Å), the doping affects the crystal structure: there are sizeable lattice deformations reflected in changes in unit cell volume, bond angles and cation-oxygen distances. Furthermore, the magnetic interactions are strongly influenced: the Mn rich compounds (x > 0.5) display ferromagnetism whereas those with high Fe content are canted antiferromagnets. The magnetic structure of x=0 is of G_xF_z-type with main component of the effective magnetic moment on the iron site $S_x = 3.6 \pm 0.2$ μ_B.

83
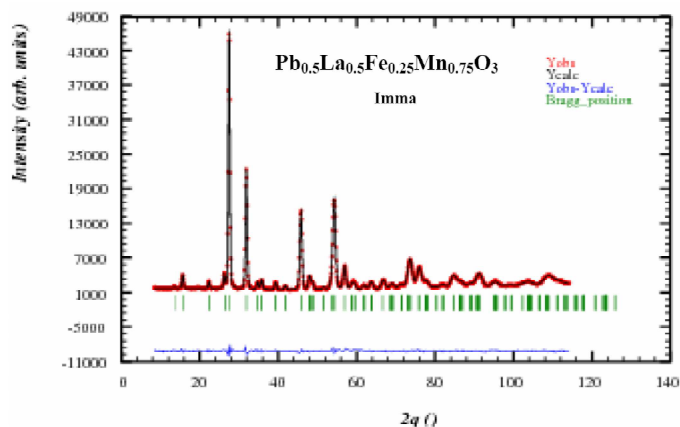
Figure 3. *Neutron diffraction pattern and Rietveld refinement for Pb$_{0.5}$La$_{0.5}$Fe$_{0.25}$Mn$_{0.75}$O$_3$*

References

[1] A. H. Morrish, B. J. Evans, J. A. Eaton, L. K.Leung, Can. J. Phys. 47, (1969) 2691; [2] E. Burzo, I.Balasz, I.G. Deac, M. Neumann, R. Tetean, Physica B 403, (2008) 1601; [3] Y. Tokura, Colossal Magnetoresistive Oxides, Gordon and Breach Science, Singapore, 2000; [4] C.N. Borca, S. Adenwalla, S.-H.Liou, Q.L.Xu, J.L. Robertson, P.A. Dowben, Mater. Letts 57, (2002) 325. [5] M. Kakihana, M. Arima, M. Yoshimura, N. Ikeda, Y. Sugitani, J. Alloys Compd. 283, (1999) 102; [6] M. Popa, J. Frantti, M. Kakihana, Sol. St. Ionics 154–155, (2002) 135; [7] A. Rinkevich, A. Nossov, V. Vassiliev, E. Vladimirova, J.Magn.Magn.Mater. 285, (2005) 118; [8] K. Krezhov, S. Kovachev, D. Kovacheva, E. Svab, G. Andre, F. Porcher, AIP Conf. Proc. 1203, (2009) 205.

B N C **Experimental Report**	*Experiment title* **Neutron diffraction study of multi-component sodium borosilicate waste glasses**	*Instrumet.* PSD *Local contact* M. Fábián
Principal proposer: M. Fábián and E. Veress *Experimental team:* M. Fábián, E. Sváb, Gy. Mészáros, SZFKI		*Proposal No* PSD_08_03_IH *Date of experiment* 2008

Objectives

Alkali borosilicate glasses have potential application in the nuclear industry as suitable materials for the immobilization of high-level nuclear waste. Structural characterization of these waste glasses is essential for understanding of glass durability. We have prepared and investigated multi-component sodium borosilicate waste glasses with the general composition of $(65-x)SiO_2 \cdot xB_2O_3 \cdot 25Na_2O \cdot 5BaO \cdot 5ZrO_2$, x=5-15 mol% (denoted as B5, B10 and B15), with the aim to clear up the correlation between structural characteristics and their thermal and glass stability. In these glasses SiO_2 and B_2O_3 are strong network formers, the alkali cations like sodium is the most widely used and investigated modifier, Ba ions with the large ionic radius are frequently used as modifier, addition of Zr has also been found very promising glass stabilizer due its strong charge compensating ability. The glass samples were isotopically enriched in [11]B (99.6%) in order to reduce the influence of the high neutron absorption [10]B present in natural boron. Glass compositions were synthesized by melting the previously homogenized powder mixtures and it was quenched by pouring it on a stainless steel plate. Powder samples of about 3-4 g each were prepared by powder milling of the quenched glasses in an agate mill for neutron diffraction measurements.

Results

Neutron diffraction structure factor, S(Q) was measured up to $Q_{max}=30 \, Å^{-1}$, and the experimental data were simulated by the reverse Monte Carlo (RMC) modelling (see Fig. 1a). A characteristic set of the partial atomic pair correlation functions, $g_{ij}(r)$ are displayed for the B15 glass in Fig. 1b.
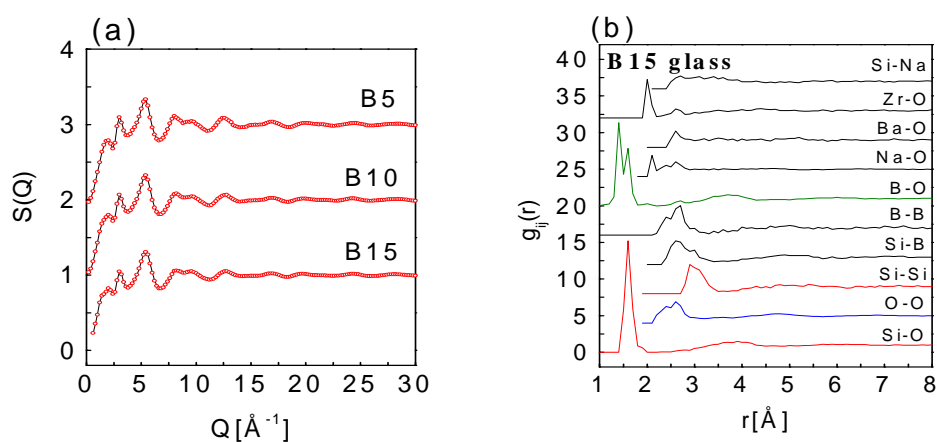
Figure 1. *a) Neutron diffraction total structure factors of the borosilicate glasses: experimental data (open circles) and RMC simulation (solid line); b) partial pair correlation functions.*

The Si-O distribution proved to be highly stable with characteristic first neighbour distances   at r_{Si-O}=1.60 Å and r_{Si-Si}=3.0 Å, the coordination number analyses have revealed network former SiO_4 units. The boron surrounding proved to be more complex. The first neighbour B-O distance shows two distinct distances at 1.40 and 1.60 Å and, both trigonal BO_3 and tetrahedral BO_4 units are present. A chemically mixed network structure is proposed including [4]B-O-Si and [3]B-O-Si chain segments, as it is displayed in Fig. 2. The O-O and Na-O distributions suggest segregation of the sodium boron and the mixed borosilicate network For more details see ref.[1].
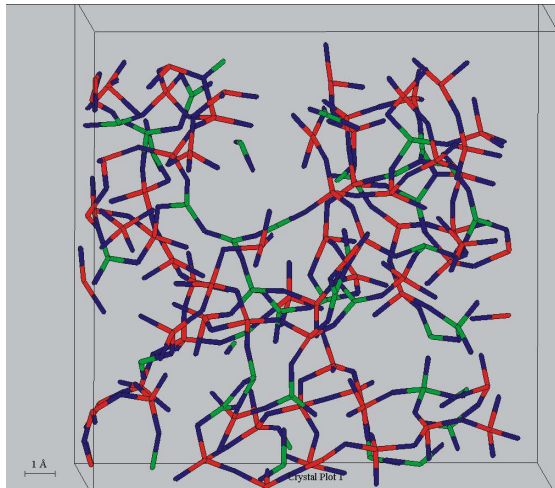
Figure 2. *Atomic configuration for the B15 sample.*
Illustration is for 500 atoms, where Si (red), B (green) and O (blue) bonds.

References

[1] M. Fábián, E. Sváb, Th. Proffen, E. Veress, *J. Non-Cryst. Solids;* **354**, 3299-3307, 2008

| **B N C** Experimental Report	*Experiment title* **Diffraction study of matrix glasses containing uranium with 10mol% B_2O_3 content**	*Instrument.* PSD *Local contact* M. Fábián
Principal proposer: M. Fábián and E. Veress *Experimental team:* M. Fábián, Gy. Mészáros, E. Sváb, SZFKI		*Proposal No* PSD_09_01_IH *Date(s) of Exp.* 2009. .

Objectives

The objective of this work is to develop a fundamental understanding of the structure of alkali borosilicate glasses, for the immobilization of high-level waste, excess plutonium, uranium and other nuclear waste. The composition of the investigated multi-component glassy specimens are $55SiO_2 \cdot 10B_2O_3 \cdot 25Na_2O \cdot 5BaO \cdot 5ZrO_2$ and the corresponding composition loaded with $30wt\%UO_3$, hereafter referred as B10 and UB10, respectively. For the study of uranium containing glass, complementary X-ray diffraction measurement is essential in addition to neutron diffraction experiment. X-ray diffraction data are dominated by contributions from heavier elements (*Ba, Zr, U*), while neutron diffraction gives information mainly on the light elements (*B, O, Si*).

Results

Neutron diffraction (ND) and high energy X-ray diffraction experiments have been performed. The experimental S(Q) data have been simulated by reverse Monte Carlo (RMC) method, characteristic fits are displayed in Fig 1.
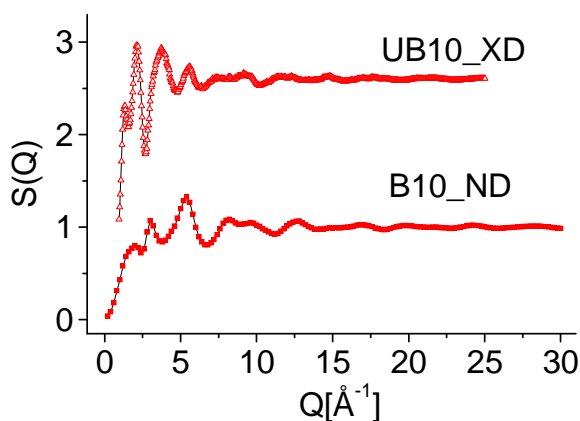
Figure 1. Experimental and RMC (solid line) structure factors for borosilicate B10_ND (red square) and UB10_XD (red triangle) glasses.

The basic network structure of the B10 and UB10 glasses proved to be fairly similar. The U-O pair distribution was achieved with a very good reproducibility, two well

resolved peaks appear at relatively short distances, centred at U-O1=1.84 Å and U-O2=2.24 Å, see Fig.2. The arrows show the two first neighbour distances, and the two others indicate the presence of intermediate short range order. The corresponding U-O1 and U-O2 coordination number distributions have been calculated by RMC algorithm, as they are displayed in Fig. 3a,b resulting in average numbers of $CN_{U-O1}=2.8$ atoms (interval 1.65-2.03 Å) and $CN_{U-O2}=2.7$ atoms (interval 2.03-2.65 Å). The total first neighbour U-O coordination number is 5.5 atoms. For more details see ref. [1].
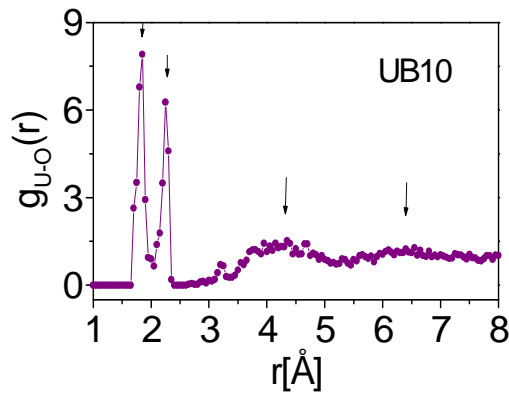
Figure 2. *Uranium-oxygen pair correlation functions in borosilicate UB10 glass.*
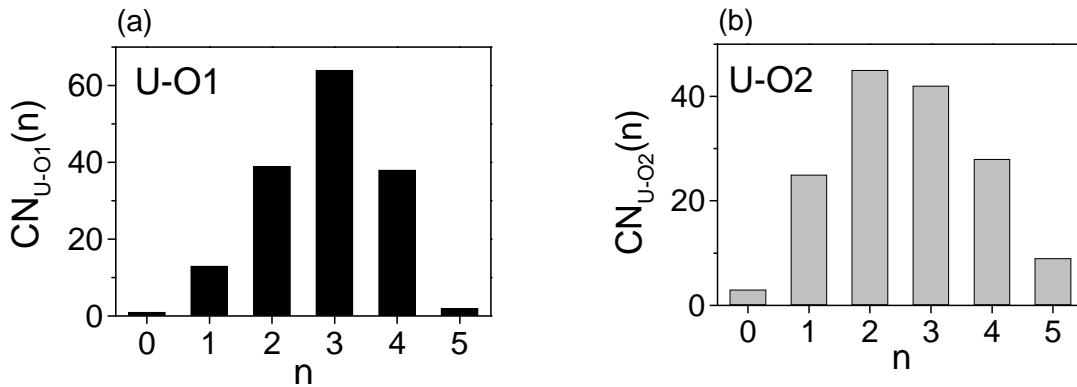
Figure 3. *U-O coordination number distribution for UB10 glass:*
a) U-O1; b) U-O2 atom pairs

References

[1] M. Fábián, Th. Proffen, U. Ruett, E. Veress, E. Sváb, *J. Phys.: Condens. Matter* **22** (2010) 404206 (8pp)

Objectives

Multi-component borosilicate glass has been widely accepted as a host matrix for the immobilization of high-level radioactive waste because of its ability to be processed at a significantly lower temperature than silicate glasses with comparable chemical durability. Structural characterization of these glasses is essential for understanding of glass durability. We are motivated in the investigation of borosilicate glass series with 15mol% B_2O_3 content, by adding step-by-step one additional element starting from the 4-component glass up to the 6-component uranium loaded glass.

We have performed a systematic neutron diffraction study for 4 samples with compositions:

(1) $60SiO_2*25Na_2O*15B_2O_3$;

(2) $55SiO_2*25Na_2O*15B_2O_3*5BaO$;

(3) $50SiO_2*25Na_2O*15B_2O_3*5BaO*5ZrO_2$;

(4) 70wt% $[50SiO_2*25Na_2O*15B_2O_3*5BaO*5ZrO_2]$+30wt%$UO_3$.

Results

The neutron diffraction structure factor, S(Q) data have been simulated by the reverse Monte Carlo (RMC) method. The fit proved to be very good, as it is illustrated in Fig. 1.
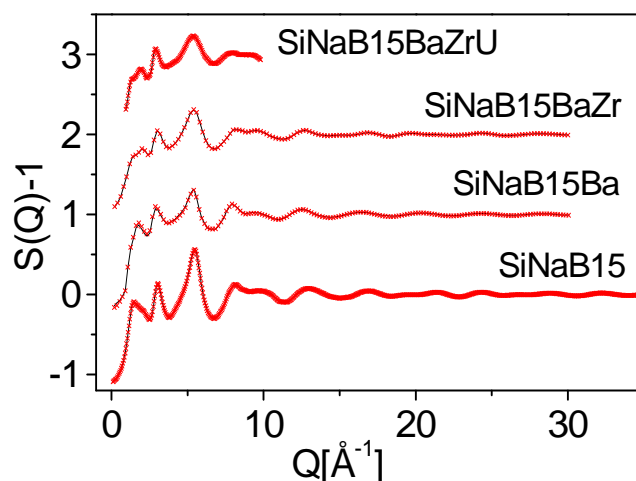
Figure 1*. Neutron diffraction structure factors, experimental data (red crosses) and RMC simulation (line).*

From the 3-dimensional atomic configuration generated by the RMC calculation, the most important partial atomic pair correlation functions, like the $g_{Si-O}(r)$, $g_{Si-Si}(r)$, $g_{B-O}(r)$, $g_{Na-O}(r)$, have been revealed, as they are shown in Fig. 2. The Si-O and Si-Si network proved to be highly stable, it consists of slightly distorted tetrahedral SiO_4 units with characteristic first neighbour distances at r_{Si-O}=1.60 Å and r_{Si-Si}=3.0 Å. The B-O surrounding proved to be more complex, two first neighbour

B-O distances at 1.30-1.40 and 1.60 Å were obtained. For the Na-O first distances two peaks at 2.1 and 2.6 Å were revealed, the intensity and position of the peaks depend on the actual composition of the samples, however, these values are very similar to each other. By adding new components, the structure of the multi-component glasses is stable and the basic network configuration is preserved.
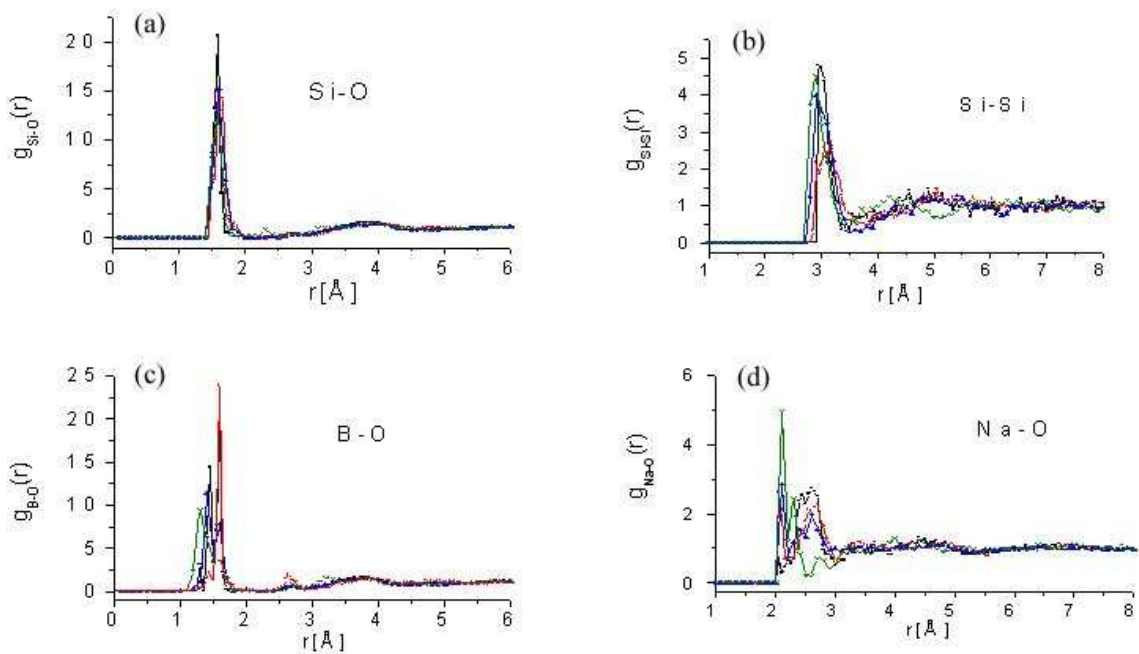
Figure 2. Partial pair distribution functions obtained by RMC simulation:
> *a) Si-O, b) Si-Si, c) B-O, d) Na-O atom pairs for the borosilicate glasses SiNaB15 (square),*
>
> *SiNaB15Ba (red circle), SiNaB15BaZr (blue triangle) and SiNaB15BaZrU (green crosses).*

B N C **Experimental Report**	*Experiment title* **Structure study of Ge-As-Se-Te chalcogenide glasses**	*Instrument.* PSD *Local contact* E. Sváb
Principal proposer: V. Pamukchieva *Experimental team:* M. Fábián, Gy. Mészáros, E. Sváb, SZFKI; V. Pamukchieva, Sofia/Bulgaria		*Proposal No.* PSD_08_04_IC *Date(s) of Exp.* 2008

Objectives

Chalcogenide glasses are transparent in the infrared region and exhibit high third order non-linear optical properties. Thus, they are very attractive as high-speed optical elements for application like data processing devices, electronic switches or optical memories. Among such materials is the quaternary Ge-As-Se-Te telluride system, which is in the focus of our interest.

Results

A neutron diffraction structure study has been performed on newly synthesized $Ge_{20}Sb_{20}S_{50}Te_{10}$ and $Ge_{27}Sb_{13}S_{50}Te_{10}$ chalcogenide glasses. Oscillations in the structure factor, $S(Q)$ have been measured with good sign-to-noise up to 35 Å^{-1}, the experimental $S(Q)$ data are presented in Fig. 1.
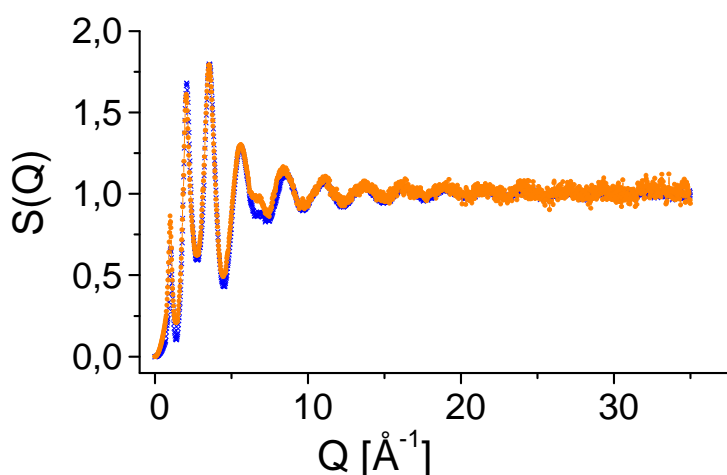
Figure 1. *Experimental structure factors for the $Ge_{20}As_{20}Se_{50}Te_{10}$ (blue cross) and $Ge_{27}As_{13}Se_{50}Te_{10}$ (orange circle) glasses.*

The reverse Monte Carlo simulation was used to model the 3-dimensional atomic configuration. The partial atomic correlation functions (see Fig. 2) and corresponding partial structure factors have been revealed. Several first and second neighbour distances, and coordination numbers have been calculated. We have established that several first neighbour atomic distances are overlapping at two characteristic distances, namely the

Ge-Ge, Ge-Se and As-Se are centred at 2.42 Å, while the Ge-Te, As-Te and Se-Te are centred at 2.60 Å. More details are described in ref.[1].
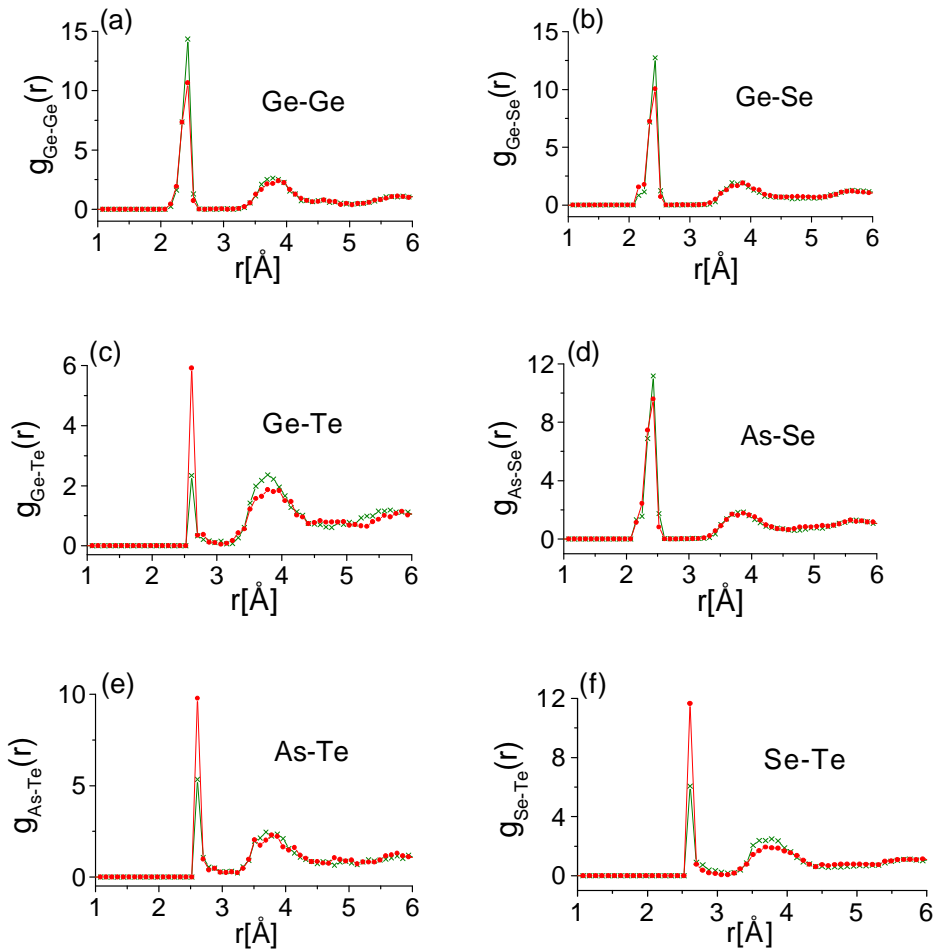
Figure 2. *Partial correlation functions obtained by RMC simulation: a) Ge-Ge, b) Ge-Se, c) GeTe, d) As-Se, e) As-Te, f) Se-Te atom pairs for chalcogenide glasses $Ge_{20}As_{20}Se_{50}Te_{10}$ (olive cross) and $Ge_{27}As_{13}Se_{50}Te_{10}$ (red circle).*

Reference

[1] M Fábián, E Sváb, S Vogel, V Pamukchieva, *Journal of Physics: Conference Series* **251** (2010) 012013

B N C Experimental Report	*Experiment title* **Structure study of As$_{40}$Se$_{60}$ and As$_{40}$Se$_{50}$Te$_{10}$ glasses**	*Instrument.* PSD *Local contact* E. Sváb
Principal proposer: Veselka Pamukchieva *Experimental team:* M. Fábián, Gy. Mészáros, E. Sváb, SZFKI; V. Pamukchieva, Sofia/Bulgaria		*Proposal No. BRR_218 Date(s) of Exp. June 2009*

Objectives

Chalcogenide glasses are perspective materials for practical application in optoelectronics as high-speed optical elements, for applications such as data processing devices, electronic switches, and optical memories. Among these glasses the As$_{40}$Se$_{60}$ and As$_{40}$Se$_{50}$Te$_{10}$ compositions are perspective materials for manufacturing optical fibers because of their low phonon energy, good transparency, low optical losses and good thermal and chemical stability.

Results

Neutron and high-energy X-ray diffraction measurements have been performed on As$_{40}$Se$_{60}$ and As$_{40}$Se$_{50}$Te$_{10}$ glasses. Both the traditional Fourier transformation technique and the reverse Monte Carlo (RMC) simulation of the experimental data have been applied to model the 3-dimensional atomic configurations. Using reasonable cut-off distances and conncetivity constraints in the RMC simulation procedure, we obtained very good agreement between the experimental and the calculated S(Q) curves, as it is illustrated in Figs. 1 and 2.
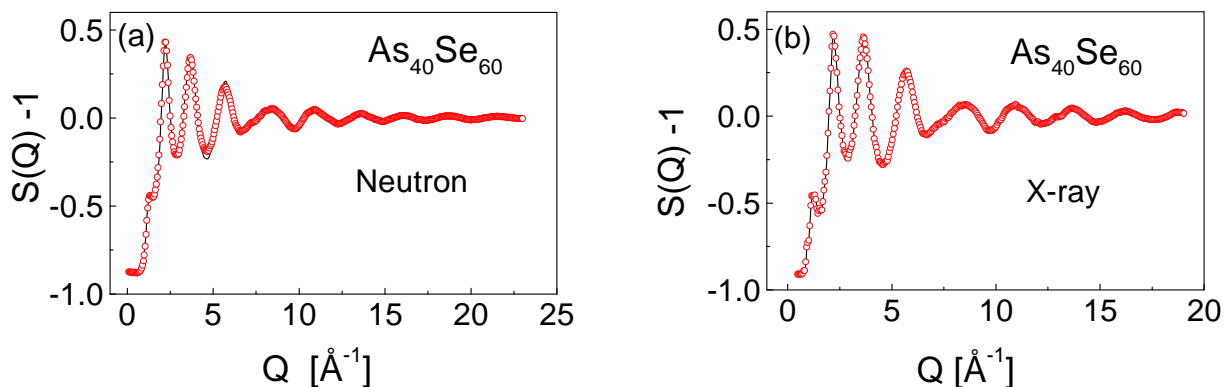
Figure 1a-b. *Neutron and X-ray experimental structure factors (open circles) and RMC model calculation (solid line) for As$_{40}$Se$_{60}$ glass.*

From the analysis of the partial atomic correlation functions and structure factors the first and second neighbour distances, coordination numbers and bond-angle distributions have been calculated. It is established that substitution of Se by Te does not change the basic

glassy network structure. For the As-Se bonding is revealed that the first neighbour distance is at 2.42 Å, the average coordination numbers are $CN_{AsSe}=2.6$ and $CN_{SeAs}=1.8$ atoms. The observed 2nd neighbour distance at 3.7 Å and 3rd neighbour distance at 5.6 Å for the As-Se bonds are evidence for medium range correlation in the glassy structure. For the As-As bonds the characteristic distance is at 3.7 Å, while for Se-Se at somewhat shorter distance 3.65 Å. For more details of the experimental conditions and results see ref. [1].
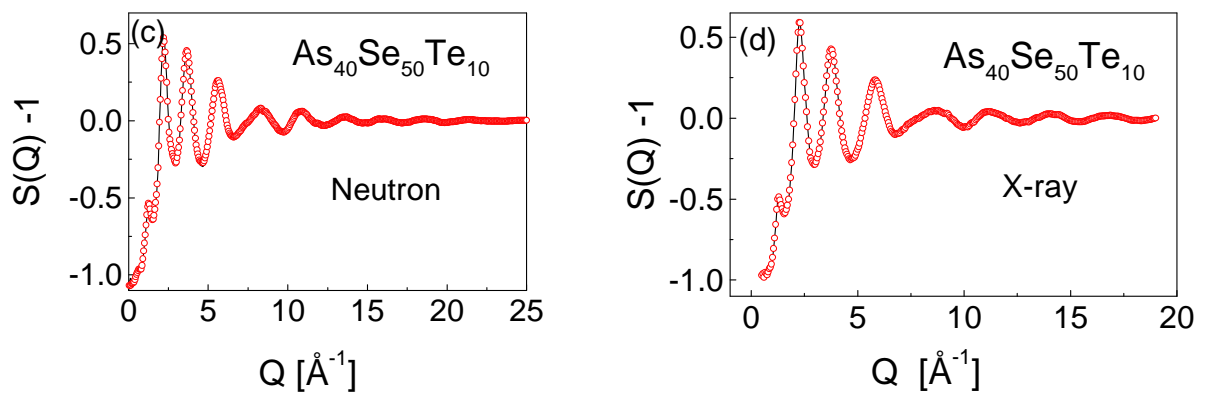
Figure 1c-d. *Neutron and X-ray experimental structure factors (open circles) and RMC model calculation (solid line) for As$_{40}$Se$_{50}$Te$_{10}$ glass.*

Reference
[1] M Fábián, E Sváb, V Pamukchieva, A Szekeres, S Vogel, U. Ruett, *Journal of Physics: Conference Series* **253** (2010) 012053

B N C **Experimental Report**	*Experiment title* **Study of the adsorption of corrosion products on structural materials by radiotracer method and quartz crystal microbalance (QCM)**	*Instrument.* *Gamma-spectrometry* *Local contact* *Ibolya Sziklai-László*
Principal proposer: Ibolya Sziklai-László, KFKI Atomic Energy Research Institute, HAS *Experimental team:R* Réka Répánszki, Zsolt Kerner, KFKI Atomic Energy Research Institute, HAS		*Experiment Number* *NAA_08_01_IH* *Date* 31. 12. 2009.

Objectives:

The aim of this work was to determine the extents of metal ion adsorptions of some corrosion products (Cr, Fe and Co) on the surfaces of structural materials (Zr1%Nb alloys and 08H18N10T stainless steel) of Paks NPP.

Results:

Radioisotopes ^{51}Cr, ^{59}Fe and ^{60}Co were prepared at the BRR. Experiments were carried out in electrolyte solution similar to reactor cooling water at room temperature. The concentrations of the soaking solutions were in the ranges belonging to the maximal coverage determined by QCM measurements. High-resolution gamma-ray spectrometry was used in the measurements. The adsorbed amounts on the metal surfaces were calculated by comparing with that of the standards made from the solutions with the same concentration. We determined the extent of the adsorption of the corrosion product ions on sputtered stainless steel and vacuum deposited zirconium and compared it with the results of QCM measurements. QCM can accurately measure the mass change but do not give information about the adsorbed ions. Using the radiotracer technique, we confirmed that the traced ions Co^{2+}, Cr^{3+} and Fe^{2+} can be adsorbed on the investigated surfaces and furthermore, we could also measure the quantity of the elements adsorbed. The amounts of Co, Cr and Fe adsorbed, were growing with their increasing concentrations in the solvents in the range of 4 - 20 mmol/dm^3 in most cases (Table 1), but a large variance of data was also observed. The adsorption of ferrite could not be measured on the sputtered steel surface by radiotracer method. More bi-chromate was adsorbed on Zr, and in the case of Co, the steel can adsorb higher amounts. At high solvent concentration maximal coverage was assumed and the maximal adsorbed mass (Δm_{max}) obtained from QCM measurements were in good agreement with that of the concentrations obtained by the radiotracer method in case of bi-chromate ion on both surfaces and in the case of Co on Zr. In the investigated system (with several components) the counterion can be adsorbed in place of the investigated one, or ion exchange can also take place on the surface (mainly the borate ions can be exchanged).

Table 1. Surface concentrations of ferrite, bi-chromate and cobalt ions on zirconium and stainless steel surfaces determined by radiotracer method and compared with the results obtained by QCM

Bulk concentration (mmol/dm^3)	Surface concentration (µg/cm^2)					
	Ferrite		Bi-chromate		Cobalt	
	Zr	steel	Zr	steel	Zr	steel
~ 4	0.15	<0.005	0.16	0.09	0.13	0.25
~ 8	0.15	<0.005	0.26	0.13	0.42	0.08
~ 12	0.23	<0.005	0.38	0.11	0.45	0.12
~ 20	0.17	<0.005	0.73	0.34	0.34	1.58
$\Delta m_{max,}$ QCM	0.48	0.53	0.80	0.46	0.44	0.40

Reference:

R. Répánszki, I. Sziklai - László, Zs. Kerner: Adsorption of corrosion and fission products on structural materials from the primary cicuit, Őszi Radiokémiai napok (2009) (in Hungarian). ISBN: 978-963-9970-01-4

B N C Experimental Report	Experiment title **Selenium and vitamin E concentrations in human milk and formula milk from Hungary**	Instrument. Gamma-spectrometry Local contact Ibolya Sziklai-László
Principal proposer: Ibolya Sziklai-László, KFKI Atomic Energy Research Institute, HAS Experimental team: Mária Ágnes Cser, Heim Pál Childrens Hospital Budapes, Dorotha Majchrzak University of Vienna, Austria		Experiment Number NAA_08_02_IH Date 30. 06. 2008.

Objectives:

The aim of this study was to determine the Se and vitamin E (α- and γ-tocopherol) contents of transitional and mature breast milk of healthy, well-nourished Hungarian mothers. For comparison, we determined the Se and vitamin E concentrations in milk-based formulas available in Hungary, in order to assess Se and vitamin E intakes in breast-fed and formula-fed healthy infants.

Results:

Se content was measured by instrumental neutron activation analysis (INAA). α-, and γ-tocopherol concentrations were determined by high performance liquid chromatography (HPLC). The mean Se concentration was 17.4 ± 2.8 µg/l in transitional and 13.8 ± 2.3 µg/l in mature milk. All of the starters (ST), the follow-on (FO) and the specialized formulas (SF) had lower Se content than breast milk (Table 1). Transitional breast milk resulted in a higher Se intake (14 µg/day) than mature milk (11 µg/day). The daily Se intakes in Hungarian infants were within the Recommended Dietary Allowance (RDA) range. The natural vitamin E contents of human milk were similar during early and late lactation. Mature breast milk had 3.30 ± 1.13 mg/l α-TE concentration and this was significantly higher than that of in ST (1.98 ± 1.57), and FO (1.77 ± 0.78), or in SF ready to feed preparations (1.03 ± 0.74) shown in Table 2. The present study suggests, that the formulas for the optimal development of young infants, should contain concentrations of these antioxidants on a level wich is comparable to that of the human milk.

Table 1. Selenium concentrations (µg/l) in Hungarian breast milk and different infant formulas

Samples of human milk and formulas	Mean ± SD	Median	Range
Transitional breast milk (n=12)	$17.4 \pm 2.8^*$	17.1	14.7 - 20.8
Mature breast milk (n=18)	13.8 ± 2.3	13.7	10.4 - 16.6
Starter formula (n=11)	12.2 ± 9.3	8.4	4.4 -34.3
Follow-on formula (n=19)	10.8 ± 4.8	8.4	6.7 - 22.9
Specialized formula (n=5)	10.4 ± 2.5	10.1	7.2 - 13.9

Level of significance in comparison to mature breast milk and formulas * $p < 0.05$

Table 2. Comparison of tocopherol equivalents (α- TE) in mature breast milk and in ready to feed formula solutions (mg/l)

Samples of human milk and infant formulas	Mean ± S.D.	Range

Mature breast milk (n=18)	3.30 ± 1.13*	2.11 - 5.18
Starters (n=6)[a]	1.98 ± 1.57	0.16 – 4.75
Follow-on (n=15)[a]	1.77 ± 0.78	0.61 – 3.31
Specialized (n=5)[a]	1.03 ± 0.74	0.44 – 1.96

Level of significance in comparison to all groups of formulas * $p < 0.05$

a α - TE concentrations calculated according to the dilution recommendations of the manufacturer's and expressed in mg/l.

Reference:

I. Sziklai-László, D. Majchrzak, I. Elmadfa, M.Á. Cser: Selenium and vitamin E concentration in human milk and formula milk from Hungary. J. Radioanal. Nucl. Chem. 279, (2), 585-590 (2009)

Objectives:

Thanks to the considerable penetration depth of neutrons and gamma-rays, PGAI is capable of detecting materials inside a container made of several centimetres of lead, aluminium or iron. Neutron radiography (NR) was used to locate and visualize the internal objects. The aim was the selective measurement of uranium in a sealed lead container.

Results:

Radiography-driven PGAI can be applied in the field of nuclear forensics as it does not destroy or degrade the confiscated evidence. The improved spatial resolution of PGAI can be better exploited if the neutron radiography shows us the sample parts to be analysed. The identification of uranium in lead, or the differentiation between Fe and Cu would not be possible using conventional X-ray radiography because of the similar mass absorption coefficients. Since the cross-sections of the elements for neutron capture and scattering vary widely, even materials with such similar atomic numbers give contrast in the NR image.

Using a set of NR images taken at different angles the 3D internal structure was determined with a resolution of a few hundred microns, but without any elemental information. The gamma-ray detection from the isovolume provided the elemental data. Based on the combined results we could to distinguish between nuclear and other materials, and we even managed to estimate the masses with a reasonable accuracy, without opening the container.

An example of a sealed container containing copper, iron, aluminium, and uranium oxide constituents can be seen in this figure: objects (Cu balls, U_3O_8 powder, Al cylinder, Fe screw), placed into a Pb container with a wall thickness of 7 mm. The radiographic image of the composite sample is shown as well.

The prompt-gamma spectra of the four objects show the evenly rising baseline of the farthest spectrum, a qualitative evidence for the presence of fissile materials.
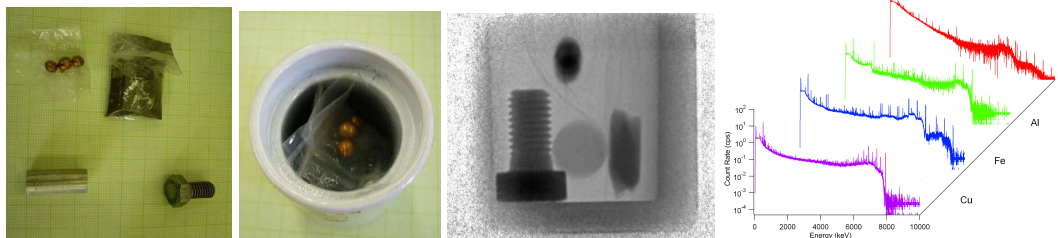
References:

Szentmiklósi, L., Révay, Z. and Kis, Z. *Neutrontomográfia és a PGAA módszer együttes alkalmazása tokozott uránminták háromdimenziós leképezése és analízise céljából*. MTA Izotópkutató Intézet, **OAH-ÁNI-ABA-10/07**, 2008, pp. 1-24.

B N C **Experimental Report**	*Experiment title* **Radiography-driven PGAI measurement on a copy of a original art objects**	*Instrument* *NIPS* *Local contact* *T. Belgya*
Principal proposer: T. Belgya – Institute of Isotopes-HAS *Experimental team:* T. Belgya, Z. Kis, L. Szentmiklósi, Zs. Kasztovszky – Institute of Isotopes-HAS		*Experiment Number* *NIPS_08_01_IC* *Date* March 2008

Objectives:

The ultimate goal of the EU FP6 Ancient Charm project was to apply the developed techniques to real art objects. Preparatory to measuring the valuable objects, tests were completed on copies of the original objects, called replicas.

Results:

The replica of a 6th century A.D. Merovingian disk fibula has rather complex structures with fine details and contains a number of elements as shown below.
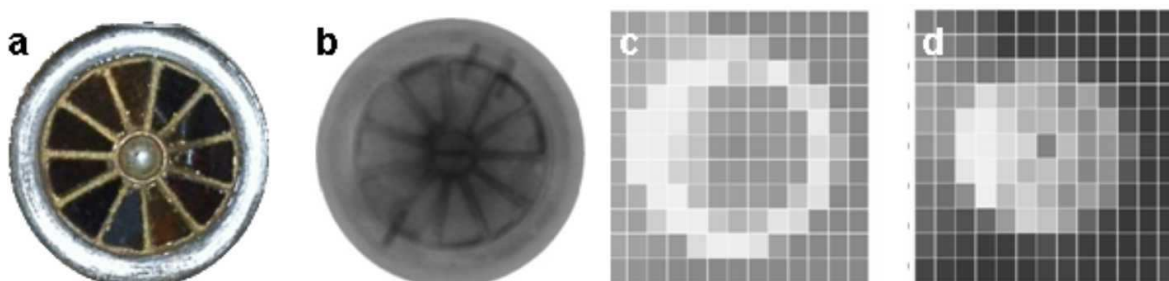
Fe and Cu are mapped in (c) and (d) panels of figure above: **(a)** The photo of the replica of a disc fibula (a Merovingian type of dress accessory with almandine inlays). **(b)** The neutron radiography of the replica. **(c-d)** The 2D element map of Fe (**c**) and Cu (**d**) made on the replica shows that the iron is concentrated at the perimeter, while the copper backing results in a more uniform distribution of the gamma-ray counts. A grid scanning of the replica was performed in the chord geometry with a step size of 3 mm, resulting in 143 measurement points.

The raw data presented are just semi-quantitative; they need to be corrected for self-absorption and self-shielding. The interpretation of the data becomes complex due to the neutron self absorption, the neutron thermalization and the photon attenuation of the object. These produce energy- and place-dependent gamma-ray intensity, which could be corrected for by means of iterative Monte Carlo simulations of which development is ongoing.

Reference:

Szentmiklósi, L., Kis, Z., Belgya, T., Kasztovszky, Z., Kudejova, P., Materna, T., Schulze, R. and Ancient Charm, C. A new PGAI-NT setup and elemental imaging experiments at the Budapest Research Reactor. NRC7 - Seventh International Conference on Nuclear and Radiochemistry, Budapest, Hungary 24-29 August 2008, (2008) 1-5

B N C **Experimental Report**	*Experiment title* **Sample holder family development for the study of the properties of super critical water by Dynamic Neutron Radiography**	*Istrument* RAD *Local contact* M. Balaskó
Principal proposer: T. Házi Gábor, MTA KFKI AEKI *Experimental team:* Márton Balaskó, László Horváth, Ákos Horváth Péter Tóth MTA KFKI AEKI		*Proposal No.* RAD_08_01_CW *Date(s) of Exp.* 01-11 2008.

Objectives

The supercritical water has an extraordinary feature. Its density changes dramatically above 370^0 C (~22 MP).This basic event can be studied by dynamic neutron radiography (DNR) but beforehand a special sample holder family has to be developped.

Results

  Four pieces sample holder were designed. The first two (KV-1 and KV-2) were made from high solidity structural steel. Both of them have 10 mm wall thickness and KV-1 contains of a 10 mm hole while KV-2 contains of 20 mm whole. They have concentric worm of screw plug system (M28 X 1,5) with metal sealing ring. The third sample holder (GR-2) was made from GR-2 type titanium alloy. Its dimensions were the similar to KV-2 but the wall thickness was 7 mm only. The application of the titanium alloy gave double advantages. The first was the higher solidity reduced the wall thickness gave better quality radiography picture. Additional the total macroscopic cross section of the titanium is the half of the iron only. It is meaning a better quality neutron radiography picture also. They are visible in Fig. 1. Later the plug system was modified to a flange style fixing with 8 X M6 screws (GR-2P). These three versions of the sample holder applied an up and down thermo-coax heating system for the good DNR visualisation of the middle part of the sample. However the gradient of the temperature distribution was a little much to the middle from the ends (50-60 ^{0}C on KV-2 and GR-2). The fourth version of the sample holder was made from GR-5 titanium alloy. Its dimensions were the similar to GR-2P but it contains a full-length thermo-coax heating system and its flange style plug system was fixed by 8 X M8 titanium screws. Its identification is GR-5H. The Fig.2. shows the picture of GR-5H and GR-2P sample holders with flange style plugs.

Reference

M. Balaskó, L.Horváth, Á. Horváth, P.Tóth and L. Kammel, Study of the behaviour of Super- Critical Water by Dynamic Neutron Radiography, Proc., Abstr., 6th ITMNR, Kobe University September 14-18, 2008.

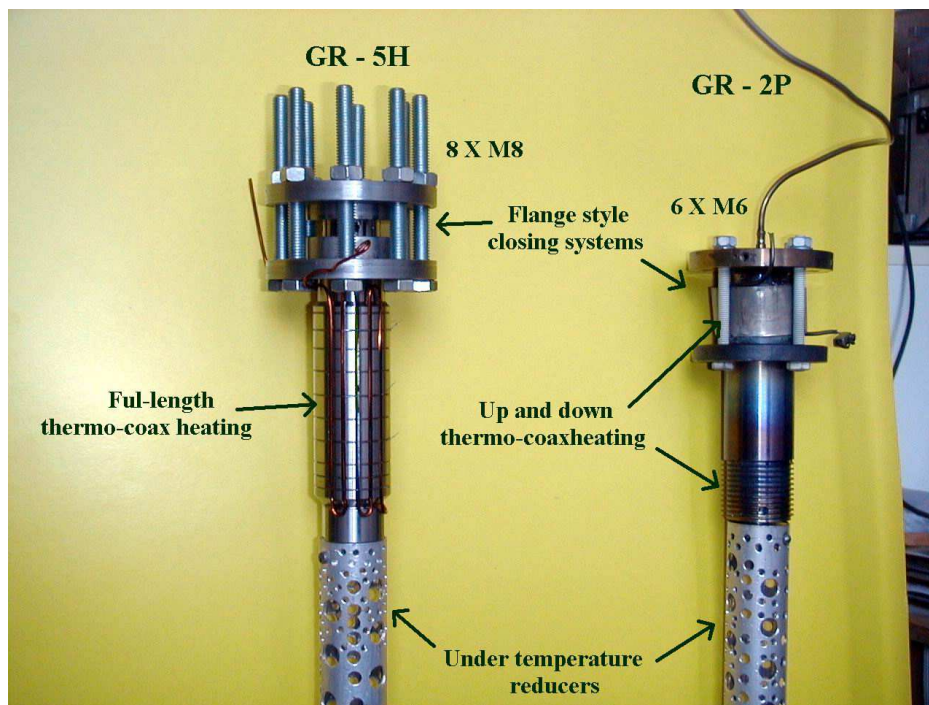Figure 1. Sample holders with concentric plugs

Figure 2. Flange style closing system on GR-5H and GR-2P sample holders

B N C Experimental Report	*Experiment title* **Study of the demaged sample of codex project by x-ray radiography**	*Proposal No.* RAD_08_02_CW *Local contact* M.Balaskó
Principal proposer: Zoltán Hózer *Experimental team:* Márton Balaskó and László Horváth MTA KFKI AEKI Budapest, Hungary		*Date(s) of Exp.* Febr, May 2008 *Date of Report* 11.06.2008

Objectives

The X-ray radiography (XR) inspection of the damaged sample of CODEX project was produced on the Dynamic Radiography station. Where the source of the X-ray radiation was MXR 300 type portable, industrial generator. The applied power was 295 kV and 2,5 mA. The focus distance was 1250 mm. The exposure time was 70 sec on BAS 20X40 MS Imaging Plate.

Results

The XR set up is visilized in the Fig.1. The task was to study the inner structure of the inspected, damaged CODEX sample. It was packed in a polyvinil chloride (PVC) tube, its diameter was 62 mm and its length was 1050 mm. The inside of the tube was filled up by artificial resin to fix the position of the sample. The radiography pictures were exposed in horizontal position of the PVC tube. Every five centimetres was marked by lead numbers from zero to 105 cm in 21 sections.

The crack of the resin in the PVC tube, collapsed zones of the bundle and the accumulated debris are observable on the composed XR picture in the Figure 2.

The composed XR picture gave useful information for the correct cutting surface contributing the further evaluation work.
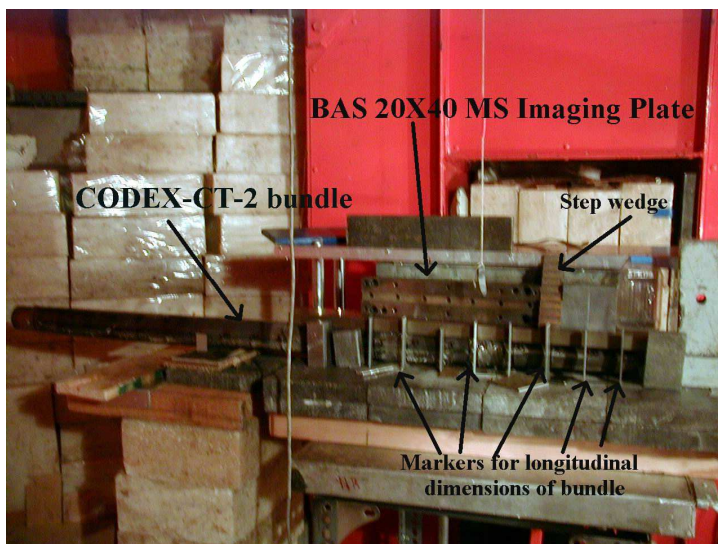

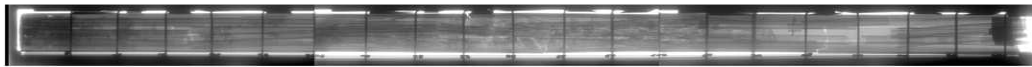Figure 1. Set up of the inspection of damaged CODEX sample

Figure 2. Composed XR picture of the damaged CODEX sample

Reference

Zoltan Hózer *, Marton Balasko, et al., Quenching of high temperature VVER fuel after long term oxidation in hydrogen rich steam, Annals of Nuclear Energy 37 (2010) 71–82.

B N C **Experimental Report**	*Experiment title* **Study of the behaviour of super critical water by** **dynamic neutron radiography, vibration diagnostics** **and acoustic emission**	*Proposal No.* Rad_08_03_NC *Local contact* M. Balaskó
Principal proposer: Gábor Házi *Experimental team:* Márton Balaskó, László Horváth, Ákos Horváth, László Kammel Péter Tóth MTA KFKI AEKI		*Date(s) of Exp.* 01-12. 2008. *Date of Report* 12. 10. 2009.

Objectives

The dynamic neutron radiography (DNR) is available to study the behavior of the water from the room temperature to the supercritical state at high temperature and at high pressure. Additional two other Non-Destructive Testing methods were used to complete the inspection technology, as vibration diagnostics (VD) and acoustic emission (AE). A special sample holder (GR-5H8t) was developed for the success of the investigation.

Results

The works were made on the well equipped measuring frame which is available for the wide range investigation of the supercritical water phenomena including the loss-of-coolant type accident also. The arrangement of the combined NDT is shown in Figure 1. It could remove the residual air above the water level and to process the heating procedure. When the temperature increased above 374°C the water level disappeared and the whole working area of the sample holder became homogeneous. This is the supercritical state of the water. The next step was the preliminary modelling of the loss-of-coolant type accident. The ventilation valve of the measuring frame was used three times. In the first case the opening time (V-1) of the valve was 1 sec. In the second case the opening time (V-2) of the valve was 5 sec. After these events the all ventilation procedures were followed dramatically changing of the pressure and the oscillation of the temperatures. In the next cases the opening time (V-3) was 10 sec. A crucial change was observable after the last ventilation procedure that the pressure stayed on zero and the sample holder was empty as it was observed by DNR [1]. The whole measuring procedure was followed by VD and AE techniques simultaneously. The Fig.2. shows characteristic of the noise during the V-3 ventilation process on a water-flow diagram where the horizontal coordinate is written by the frequency band (0 – 8 kHz), the perpendicular coordinate is given by the running time (0 – 350 sec). The running time was measured from the end of the V-2 ventilation process. The intensity of the noise is written by the form of the curves. The ventile valve was opened after 30 sec when the V-2 process was finished. The noise was very intensive and short (500 msec) in the 0-2 kHz band containing of three peak groups.

The Fig. 3. shows the most interesting part of the measurement by (AE) when was made modelling the conditions of a loss-of-coolant type accident. The changing amplitude of the AE events is written by the "A" curve. Its scale is visible on the left vertical coordinate in arbitrary unit. The average of the AE events is delineated by "B" curve. Its scale is visible on the right vertical coordinate of the Fig. 3. in arbitrary unit. The first peak (V-1.) on the curves from left was generated by the first opening of the ventil valve. The second peak (V-2.) was detected when the ventil valve was opened for the second time. The third peak (V-3) was written by the third opening of the ventil valve. The

drastic changing of the pressure (down and up again) generated many AE events. The running time of the measurement is written under the curves in arbitrary unit.
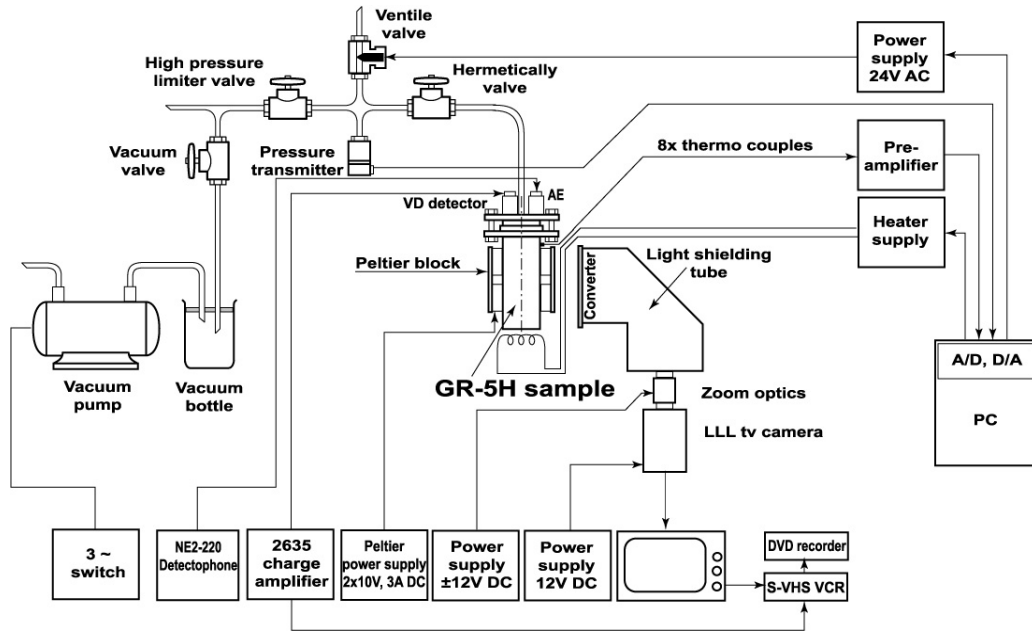

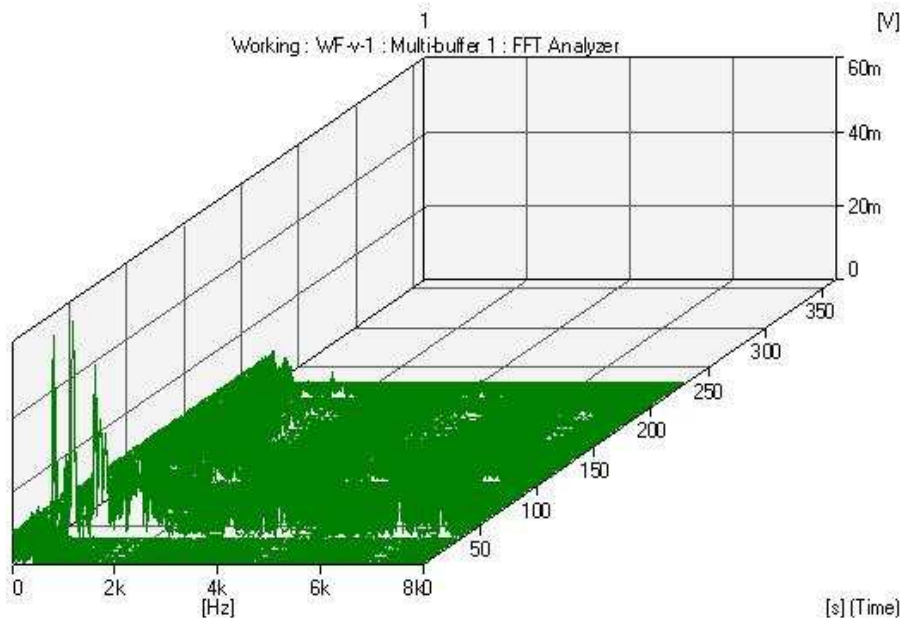Fig. 1. Arrangement of the combined NDT methods

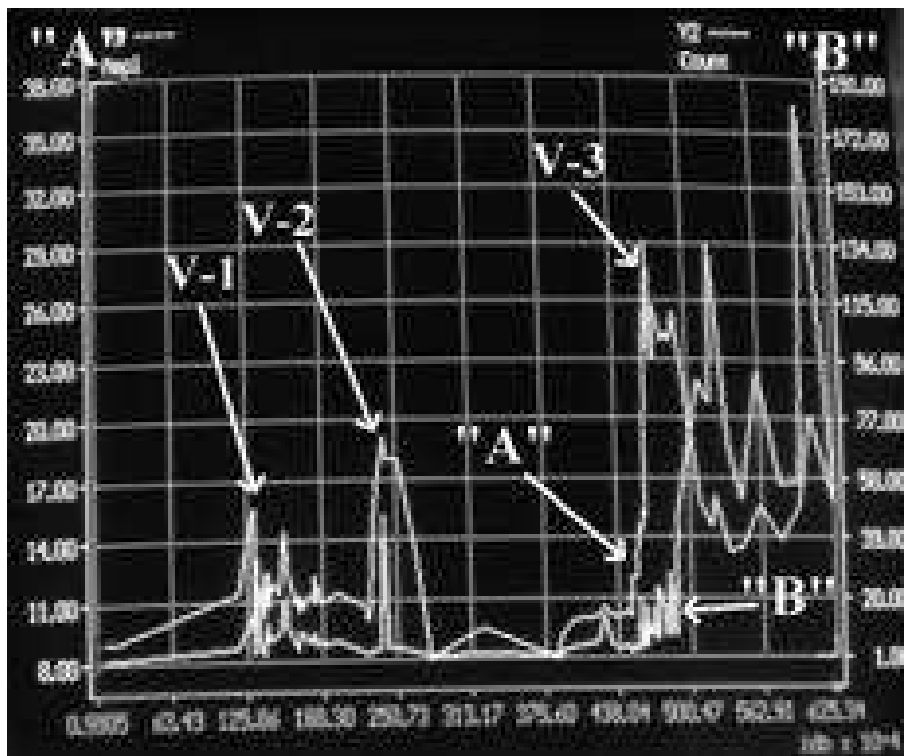

Figure 2. Water flow diagram of V-3 ventil process

Figure 3. Complete results of the AE measurement

Reference

 [1] M.Balaskó, L. Horváth, Á. Horváth, P. Tóth, Study of the behavior of super critical water by dynamic neutron radiography, Nucl. Instr. and Methods Phys. Res. A 605 (2009) 138-141

B N C **Experimental Report**	*Experiment title* **Comparison of the special properties of supercritical water by thermal – and cold dynamic neutron radiography**	*Proposal No.* RAD_08_04_IC *Local contact* M. Balaskó
Principal proposer: Gábor Házi[1] *Experimental team:*M. Balaskó[1], L. Horváth[1], B. Schillinger[2] and M. Mühlbauer[2] [1] MTA KFKI Atomic Energy Research Institute, Budapest, Hungary [2] Technische Universität München, Garching, Germany		*Date(s) of Exp.* May,July 2008 *Date of Report* 11.10.2008

Objectives

We have got an advantage to extend our investigation on the field of super critical water (SCW) by cold dynamic neutron radiography (CDNR) at the FMR II. research reactor.

Results

The interaction between the neutrons and the materials is depending on energy of neutrons. The attenuation coefficient of the low energy (cold) neutron beam lower on the metals then the thermal neutron beam's and its scattering components is lower also however it has very high sensitivity for the hydrogen contain of the materials. The Figure1. shows the heavy water in the GR-5H sample holder by CDNR (previously we hardly saw something by thermal dynamic neutron radiography, TDNR). The TDNR is better to observe the events of the SCW in light water as it is visible in the

Figure 2. Many new shade of difference were experienced by the high quality cold neutron beam and the two kinds of LLL cameras. The better resolution and the shorter exposure time of them served complementary results. The thermal DNR served a plenty of information about the behavior of light water in the sample holder.
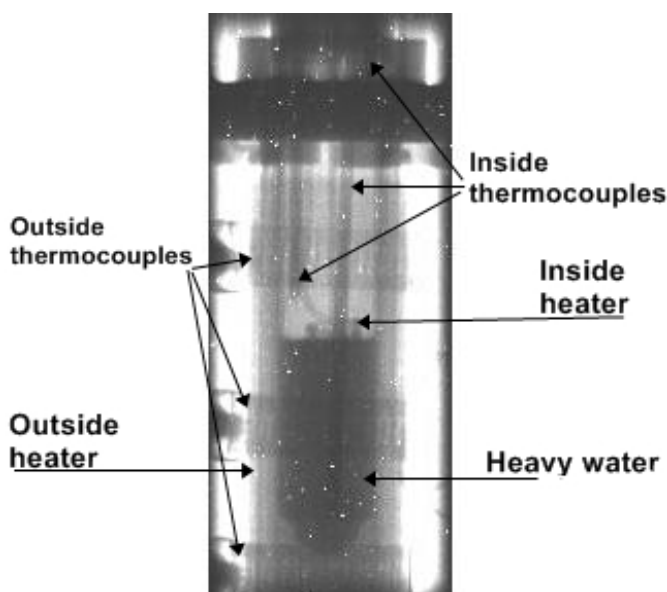

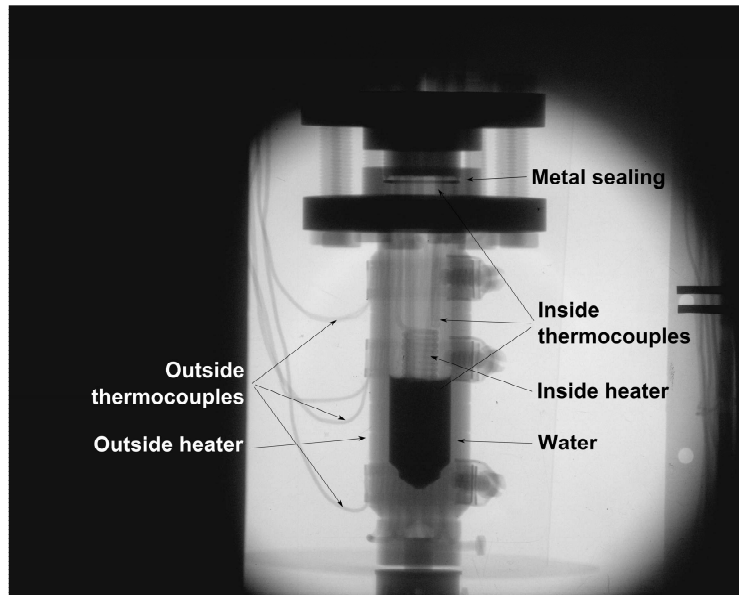Fig.1. Cold NR picture of GR-5H with 13 cm^3 heavy water on room temperature

Fig. 2. Thermal NR picture of GR-5H with 10 cm^3 light water on room temperature

Reference

M. Balaskó, L.Horváth, Á. Horváth, P.Tóth and L. Kammel, B. Schillinger, Study of special Properties of the Super Critical Water by Cooled Dynamic Neutron Radiography, Proc., Abstr.,6th ITMNR, Kobe University, September 14-18, 2008.

B N C **Experimental Report**	*Experiment title* **Complex neutron- and x-ray radiography inspection of neutron sources**	*Proposal No.* RAD_09_05_CW *Local contact* M.Balaskó
Principal proposer: Nguyen Cong Tam[2] *Experimental team*: Márton Balaskó[1], László Horváth[1] and Nguyen Cong Tam[2] [1]MTA KFKI AEKI Budapest Hungary, [2]IZINTA, Budapest, Hungary		*Date(s) of Exp.* Febr, May 2009 *Date of Report* 11.03.2009

Objectives:

To verify the position of the neutron sources in the holder pack (lead container)**.**

The X-ray - (XR) and the neutron radiography (NR) inspections of the source containers were produced on the Dynamic Radiography station (DRS). Where the source of the X-ray radiation was MXR 300 type portable, industrial generator. The NR pictures were exposed by the neutron beam of the DRS (neutron flux: 10^8 n/cm^2/sec, collimator ratio: 170). .

Results

Both the XR and NR picture were detected by IP technique using BAS 20X25 MS and BAS 20X25 ND type plates. The information were visible by BAS 2500 type reader and stored by Pentium-IV. PC.

Table I.

Exposure number	**Neutron source identificator**	**IP number**	**Energy [kV; mA]**	**Exposure time [sec]**
2011-01-01	Am-Li 1	088 ND	10^8 n/cm^2/sec	30
2011-01-02	Am-Li 1	160 MS	200; 2	60
2011-01-03	Am-Li 2	160 MS	200; 2	60
2011-01-04	Am-Li 2	088 ND	Auto radiogr.	360
2011-01-05	Am-Li 3	088 ND	Auto radiogr.	360
2011-01-06	Am-Li 3	160 MS	200; 2	60
2011-01-07	Am-Li 4	088 ND	10^8 n/cm^2/sec	360
2011-01-08	Am-Li 4	160 MS	220; 2	60
2011-01-09	Pu-Be 480 sz.	088 ND	10^8 n/cm^2/sec	360
2011-01-10	Pu-Be 480 sz.	160 MS	220; 2	60

The Table I. gives a survey about the exposure condition. The Figure 1. shows the XR picture of Am-Li 1 source but the lead container shadowed the inside structure but it is visible by NR picture in the Figure 2. The complementary characteristic of the two radiography technique gave useful results about the inner structure of the neutron sources.
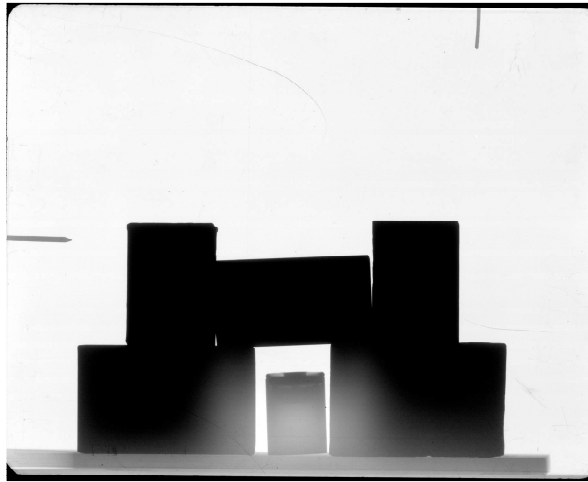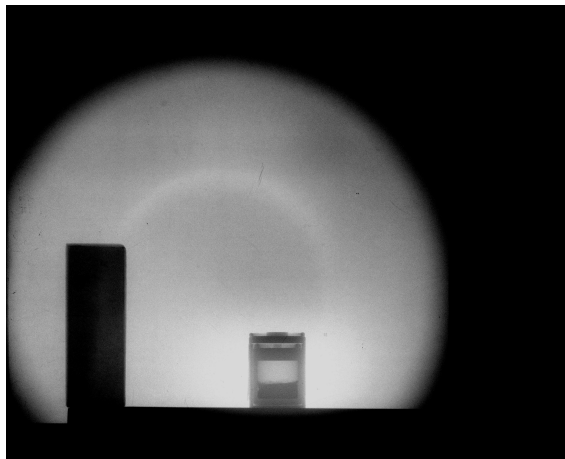
Fig. 1. XR picture of Li-Am 1 source

Fig. 2. NR picture of Li-Am 1 source

Objectives

Combined radiography inspection of Mi-2 helicopter rotor blade to study the life condition of this important part of the helicopter.

Results

The neutron radiography (NR) and X-ray radiography (XR) inspections of the Mi-2 helicopter rotor blade were produced on the Dynamic Radiography station (DRS). Where the source of the X-ray radiation was a Super Liliput type portable, industrial generator (140 kV; 5 mA). The NR pictures were exposed by the neutron beam of the DRS (neutron flux: 10^8 n/cm^2/sec, collimator ratio: 170). Both the XR and NR picture were detected by IP technique using BAS 20X25 MS and BAS 20X25

ND type plates. The imaging plates were red by BAS 2500 type scanner and the evaluation work was contributed by AIDA software. Figure 1. shows many details of the moisture in the honeycomb system of the rotor blade sector using the NR. Many important metal elements as anti-ice heating wires, flatter weight in the aluminium alloy spa are visible by the XR in the Figure 2. but the big water drops are observable also.
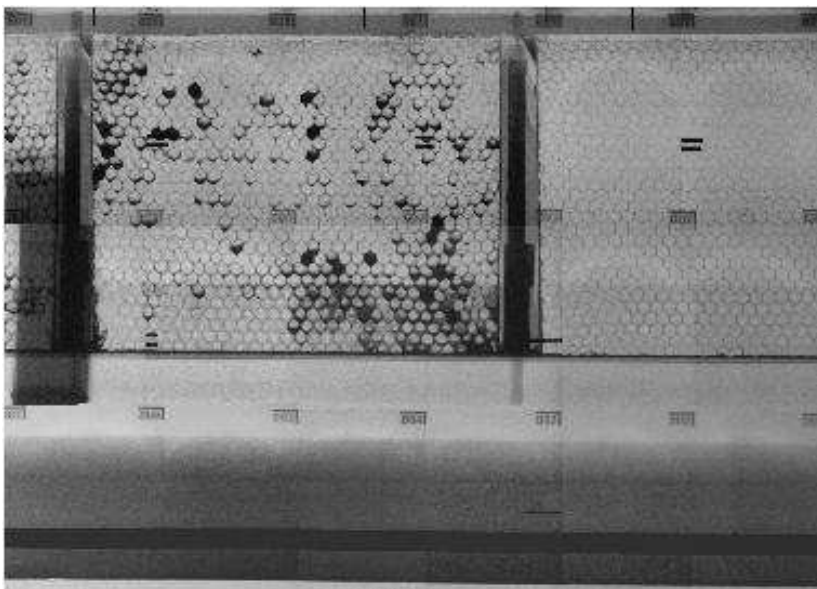

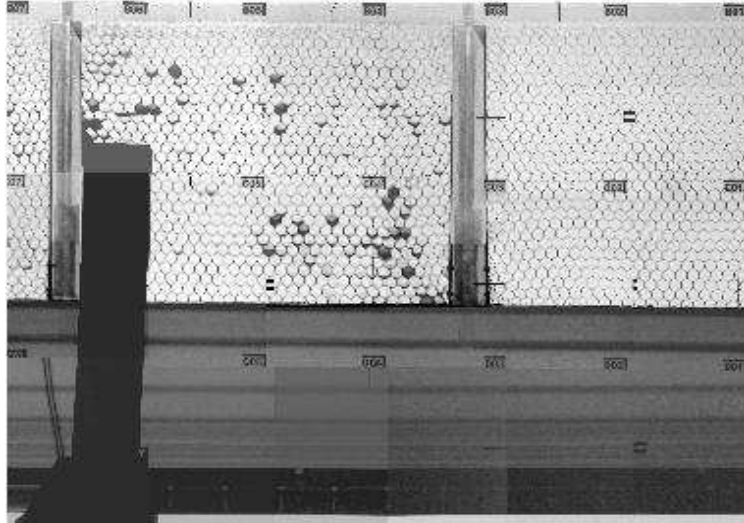Figure 1. Water distribution in the left sector is found by neutron radiography

Figure 2. Anti-ice heater and flatter weight in the aluminium spa are
shown by X-ray radiography

Reference

Márton Balaskó[1], G. Endröczi and L. Horváth, Application of combined NDT methods to study the helicopter rotor blades, International Symposium on NDT in Aerospace, Hamburg November 22-24. 2010, Abs. Booklet Tu.2.B.2. p. and CD-n, Edited Deutsche Gesellschaft für Zerstörungsfreie Prüfung E.V. és Fraunhofer EZRT, 8 p.

Objectives

Museum objects and those considered as cultural heritage are very often unique, aged, degraded and contain unknown contents, which can deliver information about the period of origin, the process of manufacturing and their application and use. The stucture of a group of the swords (from Early Iron Age) were study by X-ray radiography to contribute the determination of the production technology.

Results

Using the advantage of the complementary radiations of our Dynamic Radiography Station produced the X-ray radiography pictures of the swords. The source of the X-ray radiation was a Super-Liliput portable industrial X-ray generator (150 kV; 5 mA). The BAS-MS 20X40 type Imaging Plates were applied as detector screen. The all unsharpness of the arrangement is 100 micrometers. The imaging plates were red by BAS 2500 type scanner and the evaluation work was contributed by AIDA software. The visual picture of the investigated sword (Rhenen Seax 660C) is shown in Fig. 1. The X-ray radiography pictures were able to follow the efficiency of the production technology by the welding channel in the middle of the sword, as it is visible in Fig. 2.
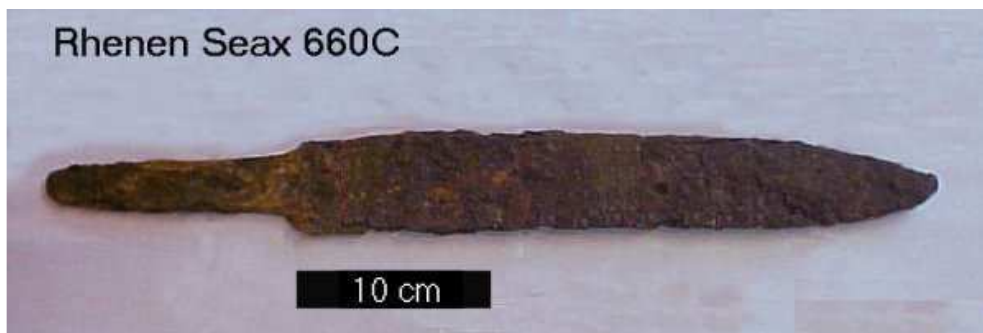

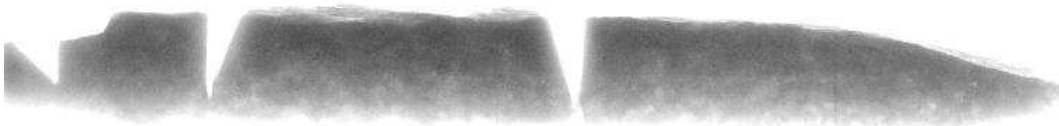Figure 1. The visual picture of number Rhenen Seax 660C sword

Figure 2. The XR picture of number Rhenen Seax 660C sword

Objectives

To study the water distribution in the Fuel Cell under operation by dynamic neutron radiography (DNR).

Results

Fuel cells (FC) are considered to be a very promising future option with respect to energy conversion process from chemical compounds towards electricity and in addition offer the possibility of environmental damage. The FC is consists of two electrodes sandwiched around an electrolyte. Oxygen (or air) passes over the "cathode" electrode and hydrogen over the "anode" electrode, generating electricity, heat and water. Hydrogen and oxygen are electrochemically combined to water as the reaction product, which is either withdraw from the reaction zone with the gas flow or accumulated in liquid phase inside the cell.

On the one hand, membrane hydration is required to maintain the proton conductivity. On the other hand, to much water will impede the access of gaseous reactants and this will limit the performance. Therefore the water management is critical topic for the advance of the FC technology. The DNR is an available non-invasive investigation of FC under operation with respect to the water distribution, as it is visible in Fig. 1. the arrangement of the DNR measurement for FC under operation. The neutron imaging is very helpful and powerful for two reasons: structural materials (graphite plates, metal elements, sealing) can be transmitted relatively easily by neutrons, and water delivers a high transmission contrast, even in small amounts. The Fig.2 shows the water distribution in the FC under

operation. The time schedule of the measurement is visible in Fig. 3. The changing of the output voltage was depending on the electric loading.
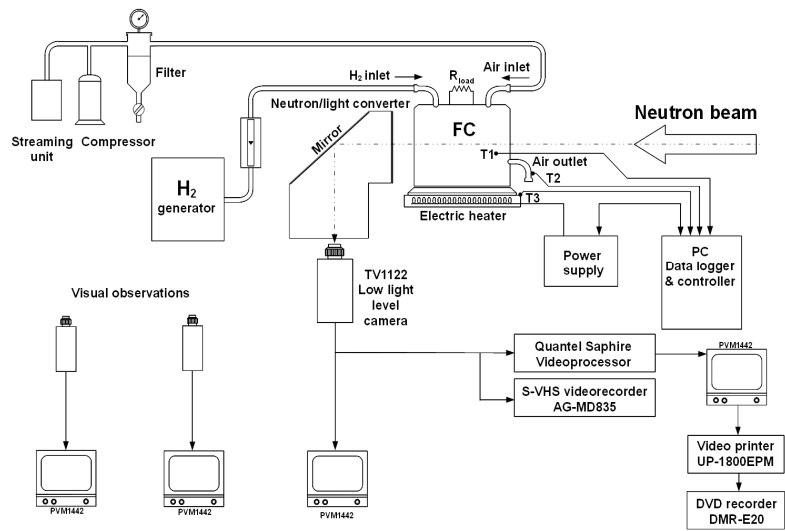
Figure 1. Arrangement of the DNR measurement for FC under operating
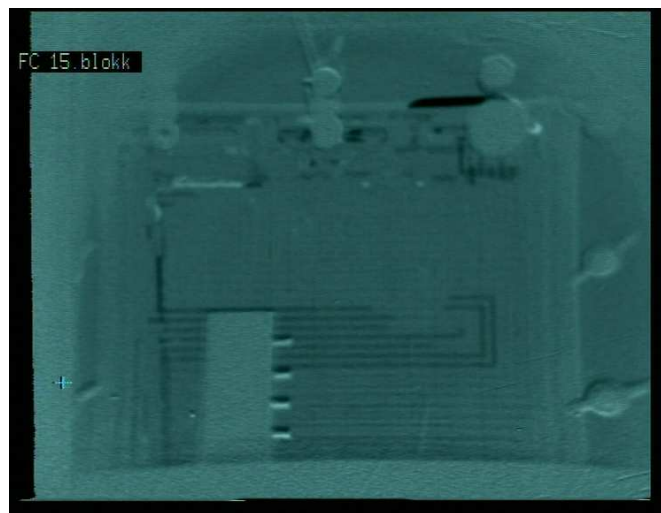

Figure 2. DNR picture of the water distribution in the FC under operation
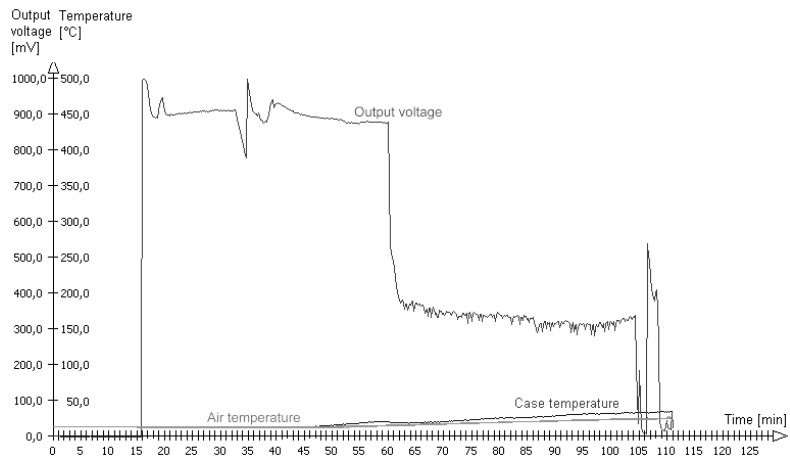
Fig. 3. The time schedule of the measurement

Reference

Balaskó Márton, Horváth László, Horváth Ákos, Kriston Ákos és Nemes Ákos: Tüzelőanyag cellák működés közbeni vizsgálata dinamikus neutron radiográfia alkalmazásával, Proc.abstr. RAKK-7, Eger 2011 April 12-14, editor: Dr. Trampus Péter, submitted.

B N C **Experimental Report**	*Experiment title* **DESIGN OF SUPER CRITICAL WATER LOOP**	*Proposal No.* RAD-09-09-NC *Local contact* M.Balaskó
Principal proposer: Attila Kiss[2] and Attila Aszódi[2] *Experimental team:* Márton Balaskó[1], László Horváth[1], Ákos Horváth[1], Kiss Attila[2] [1] MTA KFKI Atomic Energy Research Institute, Budapest, Hungary [2] BME Institute of Nuclear Technique, Budapest, Hungary		*Date(s) of Exp.* Oct., Dec. 2009 *Date of Report* 11.12.2009

Objectives

Important task to measure the streaming properties of the supercritical water in a closed circle loop.

Results

The supercritical water has an extraordinary feature. Its density is changing dramatically above 370 ^{0}C (~22 MPq). This basic event is available to study by dynamic neutron radiography (DNR). Four pieces sample holder were designed. The first two (KV-1 and KV-2) were made from high solidity structural steel and another two (GR-2 and GR-5H) were made from titanium alloy. A special equipment was designed for the repeatable conditions of the measurement procedure. The well equipped measuring frame and the sample holder family are available for the wide range investigation of the supercritical water phenomena including the loss-of-coolant type accident also in the volume of the sample holders.

We designed a closed circle loop which is available to study the main characteristics of the streaming SCW. The temperatures, pressures, difference pressures and mass flow will be measured. The DNR will be useful to optimize the structural elements of the loop also.

Reference

Balaskó Márton, Horváth László, Horváth Ákos, Kiss Attila és Aszódi Attila, Zárt húrokban áramló szuperkritikus víz tulajdonságainak vizsgálata dinamikus neutron radiográfiával,Proc., abst. RAKK-7, 2011 April 12-14, Eger, Editor: Dr. Trampus Péter (submitted).

Objectives:

Beside their many advantages the two dimensional position sensitive detectors are though not optimal for high resolution TOF diffraction at near back-scattering geometry; especially to detect short-wavelength neutrons. While the long detection path limits the q-resolution, their efficiency is weak due to the relatively low gas pressure. On the other hand, their main advantage – the good angular resolution – is unexploited in this case. After all, as the presented test-experiments improve, in a part of the high-angle region 2DPSD's can be used with perfect resolution and acceptable efficiency beside some disadvantages.

Results:

In time of flight powder diffraction (see an overview in [1])the value of d-spacing is calculated from the total time of flight t and the scattering angle, so that the function d/t can be imagined as a surface propagating in space (for a fixed d value) or as a set of fixed surfaces (for a set of different d-values) at a given moment (illustrated on ***Fig.1.*** for high scattering angles). It means that infinitesimal detectors placed on the same surface will capture neutrons scattered by equivalent diffraction planes at the same time (i.e. the same time channel). This phenomena is used out in the so called "time focussing technique" to reduce the size of the data set. In this technique flat detector plates (practically scintillators with photomultipliers) placed in this surfaces are used, so that the resolution is determined by the incoming beam and sample geometry only. The scintillator-photomultiplier system has many disadvantages including the prise. The elementary detector volumes of a 2D position sensitive detector generally are typically a few cm long small cross sectioned prisms, perpendicular to the front window. The resolution (i.e. the width of the Bragg peaks) depends on the pulse lengths, beam divergences, the sample size and the dimensions of the elementary detector volume (see right side of ***Fig.1*** where the mentioned parameters are represented by the vectors: $v\varDelta t$**ň**, $R\Delta\vartheta$**, s, h,** generalised as **r**$_i$ where v is the speed of the neutron, $\varDelta t$ the opening time of the pulse forming choppers, R is the sample-detector distance and **ň** the normal vector of the surface at the given point).

119

$$\frac{\Delta d}{d} = \frac{1}{L} \sqrt{\sum_i \left(\hat{\mathbf{n}}_{d/t} \Delta \mathbf{r}_i \right)^2}$$
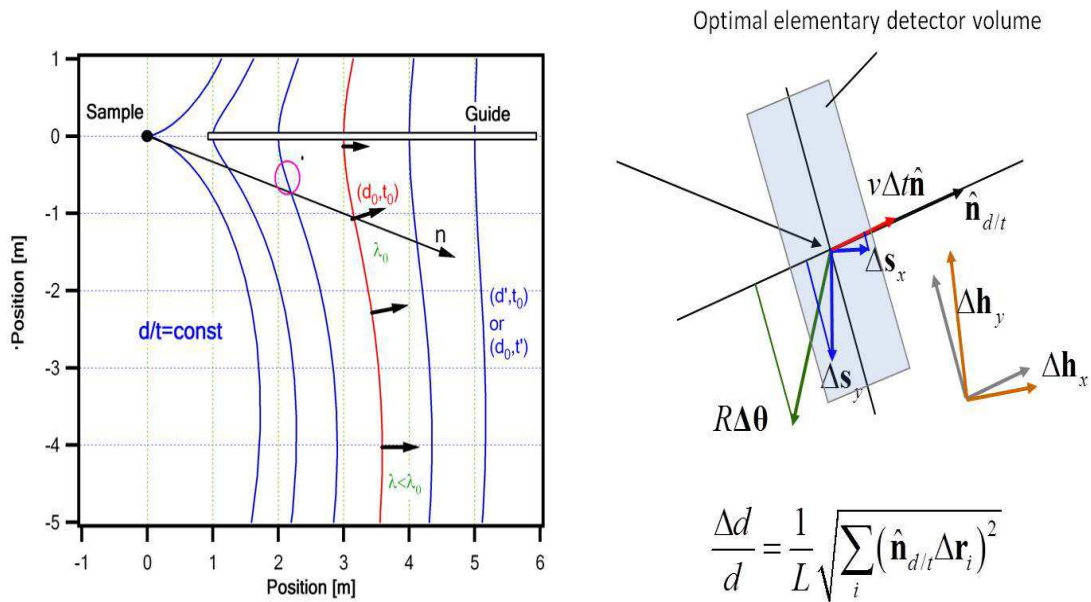
Fig.1. *See the text above.*

Facing the detector to the sample this volumes are not in the optimal position, but in proper orientation it can collect extremely good quality data, not only in the term of resolution but in efficiency too, since at inclined incidence the path length in the gas increases significantly without any decrease in the resolution, although it is true for the detector wall too. It is very important for short wavelengths neutrons, i.e. very high q-values. Has to note, that the data acquisition on TOF at BNC [2][3] is working in list mode, so the data volume does not depends on the size of the PSD matrix. The experiment presented here has improved that 2D PSD detectors can effectively be used to collect very good quality data in TOF powder diffraction at a large angular range too. (at low angles it is obvious). As test probe Al2O3 ceramic sample was used, and at optimal setup the resolution was practically the same what the incoming beam determines. On **Fig.2** the resolution measured with PSD is compared to that achieved with flat [3]He tubes. The used detector was a 256x256 pixel delay line detector with about 4 bar partial pressure of the absorbing gas.

Fig.2 *The measured resolution (Δd/d) with single and 2DPSD detectors.*

120
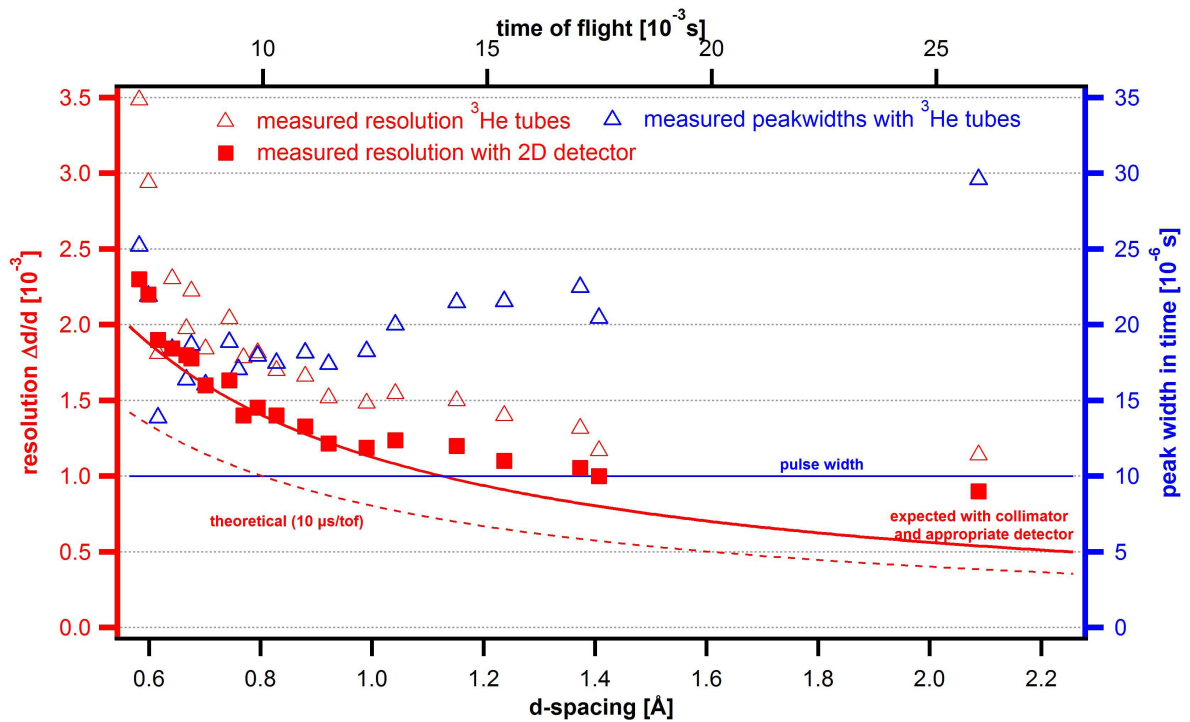
References:

[1] Aksenov V L, Balagurov A M "Neutron time-of-flight diffractometry" *Phys. Usp.* 39 897–924 (1996)

[2] Káli Gy, Sánta Zs, Bleif[*] HJ, Mezei F, Rosta L, Szalók[*] M; Commissioning of the high resolution TOF diffractometer at the Budapest Research Reactor; *Zeitschrift für Kristallographie*; Part 1 Suppl 26, 165-170, 2007

[3] Peters[*] J, Bleif[*] HJ, Káli Gy, Rosta L, Mezei[*] F; Performance of TOF powder diffractometers on reactor sources; *Physica B*; 385-386, 1019-1021, 2006

B N C **Experimental Report**	*Experiment title* Precise measurements of the fission neutron spectrum for application and fundamental investigation of the neutron emission mechanism.	*Instrument* *NIPS* *Local contact* *T. Belgya*
Principal proposer: *Edson Gonçalves F. Josef Hambst, JRC IRMM* *Experimental team:* F. Josef Hambst, Nikolai Kornilov, Imrich Fabry, Stephan Oberstedt, JRC IRMM, Geel, Belgium Tamás Belgya, Zoltan Kis, László Szentmiklósi, Institute of Isotopes HAS, Budapest, Hungary		*Experiment Number* *NIPS_08_03_IC* *Date* 23.09-03.10.2008

Objectives:

Neutron multiplicity, mean neutron energy, and emission spectrum for ^{235}U are crucial nuclear data. A model is based on the well-known assumption that all fission neutrons are emitted from accelerated fragments. This model has been successfully applied for practical applications. However, recent prompt fission neutron spectrum (PFNS) data (1980-2000), being in reasonable agreement with each other, do not agree with the model. The model cannot predict the macroscopic experimental data and benchmark experiments. For an investigation and solution to this problem, the Working Party on International Evaluation Cooperation (WPEC) of the OECD requested new high precision investigations of the PNSF in neutron-induced fission of ^{235}U. The motivation for this investigation was to verify some literature data measured over the past 20 years that contradict the Los Alamos model, as well as integral data, benchmark (K_{eff}) experiments, and recent spectral data taken at 0.5-MeV incident neutron energy.

Results:

A measurement of the ^{235}U PFNS was performed at the NIPS facilities at 100 K incident neutron energy. The measured spectra using three neutron detectors and a fission chamber (see Fig. 1) are in excellent agreement with each other. The average spectrum confirms literature data within the error bars in the neutron energy range of 0.7 to 10 MeV. However, the present PFNS shape cannot predict integral experimental data. It seems to be clear now that the disagreement between microscopic and macroscopic data is not connected with a systematic experimental error in the PFNS at low incident neutron energy.
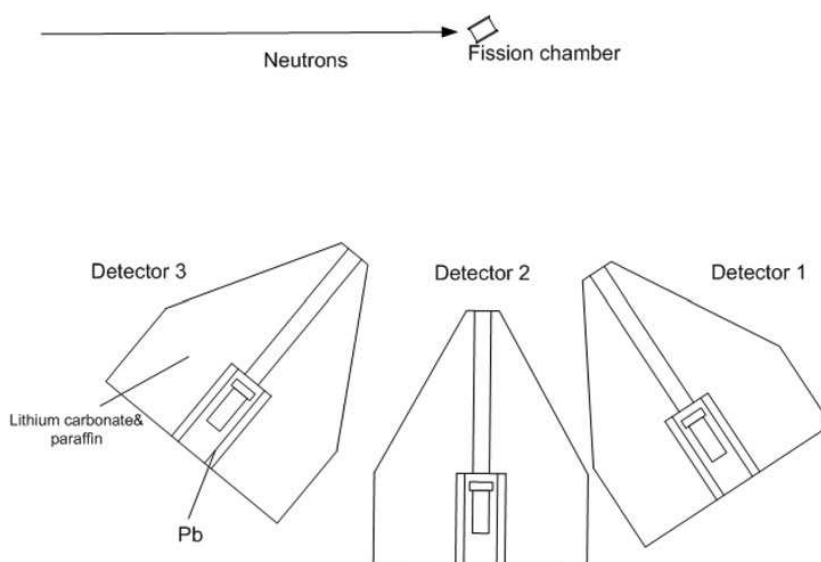
Fig. 1. Experimental setup.

References:

Hambsch, F.-J., N. Kornilov, S. Oberstedt, I. Fabry, T. Belgya, Z. Kis, L. Szentmiklosi, and S.P. Simakov. *A new measurement of the prompt fission neutron emission spectrum of 235U(n,f) Correlation of prompt neutron emission with fission fragment properties*. in *2nd EFNUDAT workshop*. Hotel Normafa, Budapest, 23-25 Sept. 2009, (2009) talk.

Fabry, I., F.-J. Hambsch, S. Oberstedt, T. Belgya, Z. Kis, L. Szentmiklósi, and S.P. Simakov. *Prompt fission neutron emission spectrum of 235U(n,f) at thermal energies*. in *2nd International Workshop On Nuclear Data Evaluation for Reactor applications (WONDER)*. CEA Cadarache Château, France, 29th September – 2nd October, 2009, (2009) talk.

Kornilov, N., F.J. Hambsch, I. Fabry, S. Oberstedt, T. Belgya, Z. Kis, L. Szentmiklosi, and S. Simakov, *The U-235(n, f) Prompt Fission Neutron Spectrum at 100 K Input Neutron Energy.* Nuclear Science and Engineering, **165**(1), 117-127 (2010).

BNC Experimental Report	Experiment title AMS Measurement of the Reaction ^{35}Cl(n,γ)^{36}Cl and its Relevance to Astrophysics and Nuclear Technology	Instrument PGAA Local contact T. Belgya
Principal proposer: A. Wallner, University of Vienna Experimental team: S. Pavetich, University of Vienna L. Szentmiklósi, Z. Kis, Institute of Isotopes HAS, Budapest, Hungary		Experiment Number PGAA_09_14_IC Date 14 Dec. 2009

Objectives:

^{36}Cl is a long-lived radionuclide ($t_{1/2}$ = 301000 a), which is dominantly produced via the reaction ^{35}Cl(n,γ)^{36}Cl. The seed nuclei of this reaction, the stable ^{35}Cl, act as a neutron poison in the nucleosynthesis processes during later burning phases of stars. This makes the reaction important for astrophysical calculations, aiming to reproduce the abundances of elements. Due to the long half-life of ^{36}Cl, the cross section and the production rate of the above reaction are also important for nuclear technology and nuclear waste management. The main goal of this work is the production of an independent ^{36}Cl/^{35}Cl standard for accelerator mass spectrometry (AMS)

Results:

Approaching our goal, NaCl pellets were irradiated at the TRIGA Mark II reactor at the ATI in Vienna and at the Budapest research reactor. The neutron flux was monitored via the reference cross section of ^{197}Au(n,γ)^{198}Au (gold foils attached to and gold powder homogenously mixed into the pellets) and determined by activity measurements on the foils and the pellets. With this data we calculated a ^{36}Cl/^{35}Cl ratio for the irradiated samples. The AMS measurements on these samples were performed at VERA (Vienna Environmental Research Accelerator), relative to a standard from ETH Zurich. The comparison of the ^{36}Cl/^{35}Cl ratio calculated from the activity measurements and measured ratios by AMS shows a systematic discrepancy of 5%. To determine the neutron capture cross section of ^{35}Cl, AMS measurements were performed on two samples, which were irradiated with neutrons of a Maxwell- Boltzmann energy distribution of 25 keV at the Forschungszentrum Karlsruhe as well. A preliminary mean value for the cross section is deduced by combining the AMS data and the neutron-fluence. The relevant cross section for nucleosynthesis in stars (MACS) was calculated by weighting the mean value for the cross section with a Maxwell-Boltzmann energy distribution of 25 keV.

References:

Pavetich, S., T. Belgya, M. Bichler, I. Dillmann, O. Forstner, R. Golser, F. Käppeler, Z. Kis, M. Martschini, A. Priller, P. Steier, G. Steinhauser, L. Szentmiklosi, and A. Wallner. *AMS measurement of the reaction 35(cl(n,g)36Cl and its relevance to astrophysics and nuclear technology.* in *60th Annual Meeting of the Austrian Physical Society, September 6-10, 2010* (Eds. Salzburg, Austria (2010), Talk.

Objectives:

Activation of ^{235}U samples in well-defined neutron geometry at IKI and subsequent counting of ^{236}U by Accelerator Mass Spectrometry (AMS) at the Vienna Environmental Research Accelerator (VERA). Advantage of this technique is that interference from fission channel is completely excluded. Therefore, results are important as an independent test of time-of-flight data obtained via prompt capture γ-rays.

Results:

At the NIPS and PGAA positions two uranium pellets, respectively, were activated under well-defined irradiation conditions. The U_3O_8 powder of typically 50-70 mg was homogeneously mixed with a few mg Au powder and pressed to pellets of 6 mm diameter ('U+Au'). In addition, thin Au foils were placed to form a sandwich of Au–U(+Au)–Au. The ^{197}Au(n,γ) thermal cross section value was used for the determination of the neutron fluence, assuming the same energy dependence of the capture cross sections from thermal to cold energies for uranium and gold.

The various pellets (50-80 mg) were grounded after the activation. A small fraction was directly used for AMS measurements of the ^{236}U/^{235}U isotope ratio without any pretreatment, i.e. for the direct measurement of ^{235}U(n,γ)^{236}U yield.
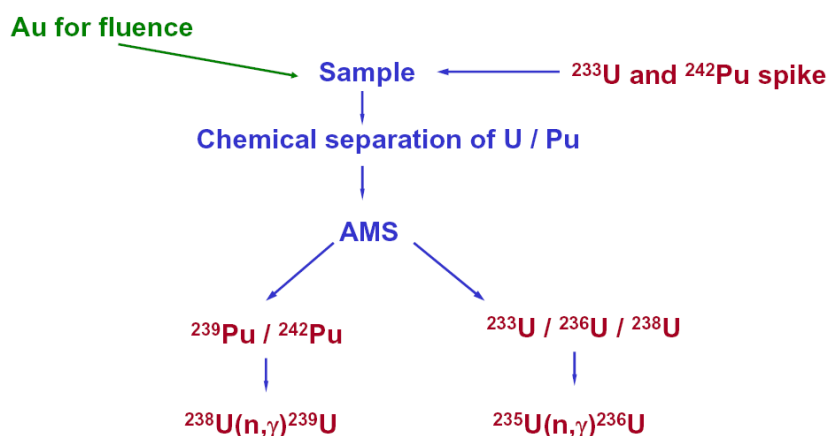
Fig. 1. Schematic view of the analytical strategy for preparation of AMS samples from the natural uranium samples.

^{235}U(n,γ)^{236}U: the ^{236}U data were normalized with VERA's in-house ^{236}U standard (known to ± 4%). We obtain a preliminary value for the thermal cross section of 103±5

barn, respectively, for the two samples. The final data will be compared to the better-known ^{233}U spike.

In case of ^{238}U(n,γ)^{239}U, the AMS data were obtained relative to the ^{242}Pu spike. Different sub-samples (the same as for U) were processed and gave individual ^{239}Pu/^{242}Pu ratios, which finally represent the ^{238}U neutron capture cross section values. This data is still under analysis.

References:
A. Wallner, T. Belgya, M. Bichler, K. Buczak, I. Dillmann, F. Käppeler, A. Mengoni, F. Quinto, P. Steier, L. Szentmiklósi, "Neutron-Capture Studies on ^{235}U and ^{238}U via AMS", accepted for publication

B N C Experimental Report	*Experiment title* **Characterisation of an enriched ^{96}Zr sample using PGNAA**	*Instrument* NIPS *Local contact* T. Belgya
Principal proposer: G. Tagliente, INFN Bari, Italy *Experimental team:* G. Tagliente, P.M. Milazzo, INFN Bari, Italy T. Belgya, L. Szentmiklósi, Z. Kis, Institute of Isotopes HAS, Budapest, Hungary		*Experiment Number* NIPS_09_01_IC *Date* 17-24 Febr. .2009

Objectives:

Characterization by PGNAA of an enriched sample of ^{96}Zr used in measurements at the n-TOF facility of CERN, and ^{Nat}Zr oxide powder to determine capture cross section of ^{96}Zr. In parallel experiments at IRMM on natural zirconium metallic discs were also analysed to determine there impurities.

Results:

The Al canned ^{96}Zr metal powder target obviously did not fill the volume inside the aluminium disc. It could be observed by shaking the target. We could perform two experiments without opening the sample. This was an important requirement due to the very high value (1 MEuro) of the target. In the first experiment, we measured the target close to the bottom relative to the gravity, where the powder thought to fill up the volume of the disc. In a second run, we measured the top, which were thought to be empty, to obtain the composition of the Al can.

The Ti and Hf contamination found in the sample can be easily explained because they are chemically similar to Zr. The others H, Cl can be due to the chemical processing of ZrO$_2$ powder. The origin of Ta is not known. Trace amount of B and Cd can be present in any material; they are observed due to their large cross section. The composition information from the Al disc manufacturer is also given and compare well only for half of the elements. In case of the other half (Ti, Cr, Mn, Fe) PGAA gives less than the cast values. Since the manufacturer did not give any precision indication, this is possible.

For determination of the cross section of ^{96}Zr we prepared a mixture of natural ZrO$_2$ and CHI$_3$ and irradiated for 147051.6 s. We have used the 443 keV transition following the ^{128}I beta decay as a comparator to the 743 keV transition following ^{97}Zr beta decay. The obtained 21.8 mb cross section is in good agreement with the old value of Mughabghab's compilation. The estimated uncertainty is about 3-4%.

Investigation of Zr disc of the old kind yielded a very clean Zr spectrum (free from the chemically similar Hf), while the manufactured two new discs contain small amount (0.36%) of Hf, which due to its high cross section rules the PGNAA spectrum thus useless for TOF experiments.

Thanks for the support of the EU FP6 EFNUDAT (No. 036443) project.

References:
T. Belgya, Report on "Characterisation of an enriched ^{96}Zr sample using PGNAA", 2009

B N C Experimental Report	Experiment title **Neutron capture and photon strength for 70 < A < 110**	Instrument *PGAA* Local contact *T. Belgya*
Principal proposer: *Arnd Junghans (FZD, Dresden)* *Experimental team:* *Ronald Schwengner, Andrija Matic, Evert Birgersson, Ralph Massarczyk, Institut für Strahlenphysik FZD* T. Belgya, Z. Kis, Institute of Isotopes HAS, Budapest, Hungary		Experiment Number *PGAA_09_14_IC* Date 06-16 Oct. 2009

Objectives:

A nuclear process of special importance for projects aiming for the transmutation of radioactive waste is the radiative neutron capture. Theoretical calculations of the process are performed using the Hauser-Feshbach formalism. For the incoming neutron channel optical potential is needed. The other ingredient is the photon strength function governing the γ-decay to low lying final states from the capturing resonances in the continuum. Here neutron reemission competes thus reducing the capture cross section. As far as the relevant spins allow, the gamma decay is mainly of electric dipole type. Only a very few stable nuclei have $1/2^-$ ground state which provides 1^- capture state for which we can directly compare the radiative neutron capture gamma-strength functions with elastic photon scattering strength functions. The corresponding pairs of nuclei and their reactions for comparison are ^{77}Se(n,γ)^{78}Se and ^{78}Se(γ,γ)^{78}Se; and ^{195}Pt(n,γ)^{196}Pt and ^{196}Pt(γ,γ)^{196}Pt. The aim of this measurement is to measure accurate radiative neutron capture spectra for these two nuclei.

Results:

Highly enriched targets of ^{77}Se and ^{196}Pt were irradiated with cold neutron beam at the PGAA station and the de-exciting gamma rays were measured with a BGO shielded HPGe detector transported from FZD. The same HPGe-BGO detectors were used to measure ^{78}Se(γ,γ) and ^{196}Pt(γ,γ) at the n-ELBE facility. To provide experimental spectra for high precision Monte Carlo (GEANT4) simulations of the detector response single and simple multi gamma-ray sources were also measured. For high energy calibration ^{14}N(n,γ) reaction was used. These measurements also provided high precision efficiency calibration. The calculations and simulations were made in Dresden, which will be a part of a PhD work. The obtained response and efficiency corrected spectra are show in Figure 1.
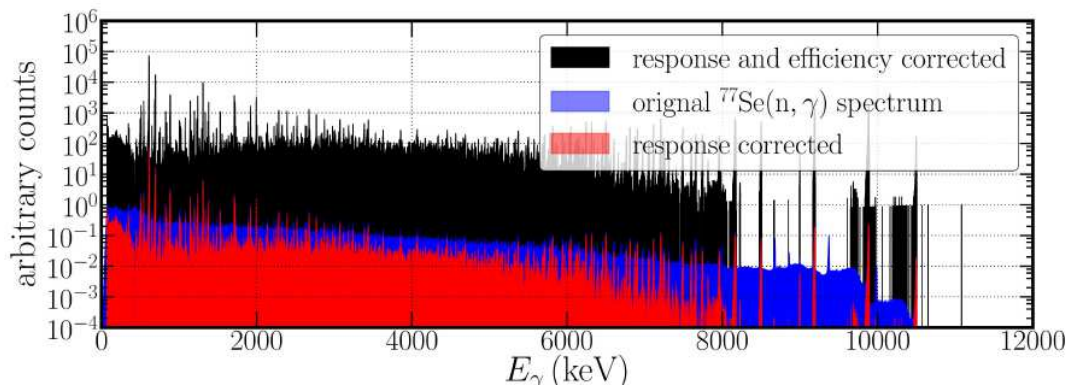
References:

Schramm, G. *Analysis and Simulation of* ^{77}*Se(n,γ) Spectra* in: *Kick-Off-Meeting European Research Infrastructures for Nuclear Data Applications (ERINDA) January 27 and 28, 201,* Helmholtz-Zentrum Dresden-Rossendorf, Bautzner Landstr. 400 | 01328 Dresden (2011), Talk.

Massarczyk, R., E. Birgersson, G. Schramm, R. Schwengner, T. Belgya, R. Beyer, E. Grosse, R. Hannaske, A.R. Junghans, A. Matic, L. Szentmiklósi, J. Weil, and A. Wagner. *Photon strength function deduced from photon scattering and neutron capture*. in *EFNUDAT User and Collaboration workshop: Measurements and Models of Nuclear Reactions, 25-27 May 2010*. Paris, France, (2010) EPJ Web of Conferences **8**, 07008

B N C **Experimental Report**	*Experiment title* **Measurement of thermal neutron induced γ-ray spectra of stable Fe and Ni isotopes**		*Instrument* PGAA *Local contact* T. Belgya
Principal proposer: F. Gunsing, CEA Saclay, France *Experimental team:* F. Gunsing, CEA Saclay, France, Claudia Lederer, Univ. Vienna T. Belgya, Z. Kis, Institute of Isotopes HAS, Budapest, Hungary			*Experiment Number* PGAA_09_13_IC *Date* May, July .2009

Objectives:

Characterization by PGNAA of enriched ^{54,56,57}Fe and ^{58,60,62}Ni samples used in measurements at the n-TOF facility of CERN. It is surprising that the cross sections of these important structural materials are known only 5-10% accuracy. Thus beside the composition of these highly enriched samples, their cross sections can also be improved.

Results:

All the samples, but ^{56}Fe and ^{62}Ni, came from CEA, Saclay, France. The ^{56}Fe and ^{62}Ni samples originated from Instituto de Fisica Corpuscular, Valencia, Spain and from Faculty of Physics, University of Vienna, Austria, respectively. The samples were measured in Spring 2009 at the PGAA station of the Budapest Research Center and returned for experiments to CERN.

The isotopic abundance of the main component of a sample was assumed to be exact for each sample. We obtained the following isotopic compositions:

Sample	^{54}Fe %	^{56}Fe %	^{57}Fe %	^{58}Fe %
Enriched in ^{54}Fe	99.77	0.2(1)	<0.05	<0.05
Enriched in ^{56}Fe	0.04(1)	99.94	0.02(1)	-
Enriched in ^{57}Fe	<0.1	0.7(1)	96.06	3.2(3)

Sample	^{58}Ni %	^{60}Ni %	^{61}Ni %	^{62}Ni %	^{64}Ni %
Enriched in ^{58}Ni	99.5	0.50(5)	<0.13	<0.02	<0.1
Enriched in ^{60}Ni	0.20(1)	99.31	0.40(5)	0.012(4)	<0.06
Enriched in ^{62}Ni	<0.02	0.043(9)	0.85(15)	97.95	1.11(15)

Hydrogen is always present in the examined spectra, their peak rates are higher to the current beam background measurement for all samples, and thus some parts belong to the samples as possible hydrogen contamination. Vanadium, manganese, and nickel can be found as trace in iron samples. The presence of copper in ^{56}Fe sample is strange. The cleanest sample is the ^{57}Fe due to our analysis. Phosphor was found in two nickel samples (^{60}Ni and ^{62}Ni). Their quantities (2–3 %) pose the possibility of a contamination during the sample preparation process.

The determination of the cross sections is still under evaluation; however, some preliminary results have already been presented.

References:

T. Belgya and Z. Kis, Report on "Measurements of compositions of enriched ^{54,56,57}Fe and ^{58,60,62}Ni samples", 2009

Kis, Z., T. Belgya, L. Szentmiklósi, and F. Gunsing. *Determination of the total neutron capture cross section for $^{58}Ni(n,\gamma)^{59}Ni$ reaction*. in 2nd *EFNUDAT workshop*. Hotel Normafa, Budapest, 23-25 Sept. 2009, (2009) talk.

Kis, Z., T. Belgya, L. Szentmiklósi, and F. Gunsing. *Determination of the total neutron capture cross section for 58Ni(n,γ)59Ni reaction*. in *EFNUDAT Slow and Resonance Neutrons, a Scientific Workshop on Nuclear Data Measurements, Theory and Applications, 23-25 September 2009* Budapest, Hungary: II-HAS, (2010) 121-126.

Objectives:

Periodic multilayers of different periods were prepared according to an algorithm proposed by the authors. The properties of such Ni/Ti multilayers are crucial in neutron supermirrors. The reflectivity properties of these systems were investigated using neutron reflectometry. Reflectivity of the manufactured multilayers was compared with the reflectivity of the proposed structure. In the first approximation, the results proved the main features of the manufactured multilayers to be close to the designed ones, but some deviance was also observed. The neutron optical importance of sputtered Ni/Ti multilayers suggests further investigations.

One of the authors, V. Ignatovich, proposed a new method for neutron supermirror design[1]. He recommends manufacturing periodic supermirrors composed of periodic stacks of bilayers. Samples were produced following Ignatovich's method and reflectivity measurements were performed on the obtained samples.

Results:

a.) Periodic multilayers: The investigated systems were periodic multialeyers consisting of 2, 4 and 8 Ni/Ti bilayers on glass substrates. The proposed thickness was 84 Å for Ni and 70 Å for Ti. The periodicity of the multilayers was chosen to have the Bragg peak at momentum transfer $q=2*q_{critNi}$, where q_{critNi} is the critical momentum transfer of the pure nickel surface. In neutron supermirrors the aim is to cover the widest possible q-range by the smallest number of bilayers. This requirement is fulfilled if $k_{Ni}l_{Ni}=k_{Ti}l_{Ti}=\pi/2$, where k_{Ni} is the wave vector in the Ni layer, l_{Ni} is the thickness of it, and similar requirement holds for the Ti layers.

The samples were produced by sputtering at Mirrotron Ltd., Budapest. The neutron reflectivity was measured at the constant wavelength ($\lambda=4.28°$Å angular resolution 0.5 mrad) reflectometer of BNC. X-ray reflectivity measurements were also performed on the samples. The fitting which gives acceptable agreement for neutron and X-ray measurements, reveals that the deposited Ni layers are thicker (96 Å), and the Ti layers are thinner (65.5 Å) than the proposed 84 and 70 Å. It is worth to note, that the fitting was performed using the assumption of the periodicity of our samples. Interesting observation that in the regime of satellite peaks between X-ray Bragg peaks good accordance of measured and calculated reflectivity was achieved only using the assumption, that the roughness is different for Ni on Ti (6Å) and Ti on Ni (9 Å) interfaces. It will be worth making a fit without the assumption of periodicity, and performing offspecular X-ray and neutron reflectivity measurements and diffraction.
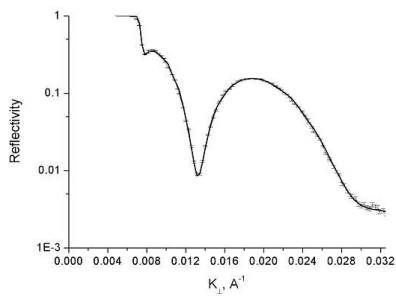
a.)
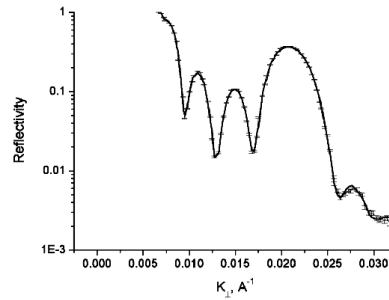
b.)
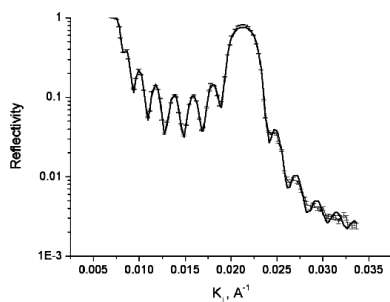
c.)

Figure 1. Results of the fitting of the reflectivity data for periodic chains of bilayers evaporated on a boronised float glass substrate. On Figures a) 2 bilayers film; b) 4 bilayers film; c) 8 bilayers film. There is a good correspondence between experimental curves and calculations that confirms the theoretical model. Discrepancies at the right end are caused by specific features of measurements, i.e. we used the PSD detector as a single detector integrating the intensity over all surface of the detector.

b.) Periodic supermirrors: Supermirror sample was produced at Mirrotron Ltd. with critical angle two times that of the Ni. The supermirror contains 58 bilayers, in 7 periodic stacks of Ni-Ti bilayers. Neutron reflectivity measurements show similar properties as the conventional supermirrors.

Future prospects

It is worth to make a fitting without the assumption of periodicity, and to perform offspecular X-ray and neutron reflectivity measurements and diffraction.

References

[1] I. Carron, V.K. Ignatovich, Phys.Rev A 67 (2003) 043610

[2] Bodnarchuck V, Cser L, Ignatovich V, Veres T, Yaradaykin S; Investigation of periodic multilayers; *JINR Comm*; E14, 127, 2009

133

B N C Experimental Report	*Experiment title* **Study of the reflectivity of neutron supermirrors influenced by surface oil layers**	*Instrument.* REFL *Local contact*
Principal proposer: T. Veres, L. Cser *Experimental team:T. Veres, L. Cser*		*Experiment Number* REFL_08_1_IH *Date* January 2008

Objectives:

The quality and possible deteriorations of neutron guides are problems of great importance for the neutron centers. Due to the multiple reflections, the reflectivity loss of neutron supermirrors (SM) has a severe effect on the quality of the guide. In the present work the influence of organic surface contamination (in our measurements: vacuum pump oil) was investigated.

Results:

One possible cause of reflectivity loss is the contamination of SM surface by hydrogen containing compounds (large incoherent scattering cross section), from vacuum pumps and the atmosphere. In our experiments vacuum pump oil was deposited on the surfaces of supermirror samples and the average film thickness was measured by weighing before and after deposition, the local one by optical interference. Inhomogenities, drop formation was observed by an optical microscope.

The reflectivity of the clean and oil covered supermirrors was measured at a constant wavelength (λ=4.2 Å) on the reflectometer of the Budapest Research Reactor.
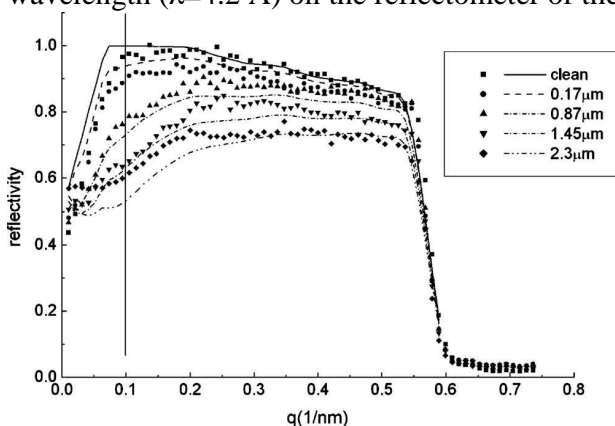
Figure 1. The measured (line) and calculated (dots) reflectivity of the supermirrors covered by different thicknesses of oil. (For q<0.1, the reflectivity is distorted by geometrical effects.)

Applying the Parratt method we calculated the reflectivity. On the figure we see the comparison of the measured and calculated reflectivities (the finite sample and slit sizes are taken into account). The drop formation can not be taken exactly into account; there is some deviation between calculated and measured values for the thickest oil films. Monte Carlo simulation of guides gives exponential decreasing of neutron yield in the function of the oil thickness.

References:

T. Veres, L. Cser: *Study of the reflectivity of neutron supermirrors influenced by surface oil layers* Review of scientific instruments **81** 063303 (2010)

	Experiment title	Proposal No.
B N C **Experimental Report**	Diffraction study of manganese, europium and cerium activated willemite phosphors prepared by sonocatalyzed sol-gel rout in presence of ethylene glycol.	TOF_ 2009_ 2_ IH *Local contact* *György Káli.*
Principal proposer: Cecilia Savii *Experimental team:* Zsombor S., György K.		*Date(s) of Exper.* 2008 *Date of Report* 2009

Objectives

Differently doped willemites are used as luminescent phosphor in cathode ray tubes, lamps and plasma display panels [1]. The conventional method to synthesize Zn_2SiO_4:Mn phosphor is the solid-state reaction which requires high firing temperatures and a milling process as a post-treatment procedure. In the present experiment zinc silicate phosphors obtained via ultrasonically assisted, sol-gel route in presence of ethylene glycol were studied by neutron diffraction. The xerogels were thermally treated at 1000 ºC. The comparison of the results, will be the basis for determination of the suitability of individual characterization method for determination of optimal conditions in order to obtain certain tailored materials with special properties.

Experiment

The target willemite phosphors corresponding to $2ZnO \cdot 1,1SiO_2 \cdot 0.085MnO$, were synthesized by sol-gel process, assisted and non assisted by an ultrasonic field, starting from: tetraethyl orthosilicate (TEOS, 99%, Fluka), ethylene glycol (Merck, for analysis), absolute ethanol (EtOH, Chimopar) zinc nitrate hexahydrate (Merck, extra pure), manganese (II) chloride tetrahydrate (Merck, for analysis) [2].
The synthesis parameters of samples are presented in Table 1.

Sample name	EtOH/ TEOS	HCl/TEOS	H₂O/TEOS	activator	APV	EG/TEOS
C8	15/1	0,02/1	11,3/1	0,062 moli Mn^{2+}($MnCl_2 \cdot 4H_2O$)	-	-
C10	15/1	0,02/1	11,3/1	0,062 moli Mn^{2+} ($MnCl_2 \cdot 4H_2O$) 0,02 moli Ce^{3+} ($Ce(NO_3)_3 \cdot 6H_2O$)	-	-
US2-M-11NAPV-Ce-Mn	15/1	0,02/1	11,3/1	0,085 moli Mn^{2+} ($MnCl_2 \cdot 4H_2O$) 0,02 moli Ce^{3+} ($Ce(NO_3)_3 \cdot 6H_2O$)	-	-
14_NAPV_Ce	15/1	0,02/1	11,3/1	0,06 moli Ce^{3+}	49000	-
US13-NAPV_Eu	15/1	0,02/1	11,3/1	0,085 moli Eu^{3+} ($Eu(CH_3COO)_3xH_2O$)	49000	-
6N_PE	15/1	-		0,085 moli Mn^{2+}($MnCl_2 \cdot 4H_2O$)	-	4/1

Results

Different resolution spectra in different *q*-range were collected. Low resolution spectra (rotation speed at 1,2 chopper 4000 rpm) from samples and pure willemite as reference were measured. In the case oh high resolution spectra (rotation speed at 1,2 chopper 11000 rpm) the effect of activators on willemite structure were demonstrated and will be compared with X-ray diffraction.

Data treatment and publication of the results is in progress.
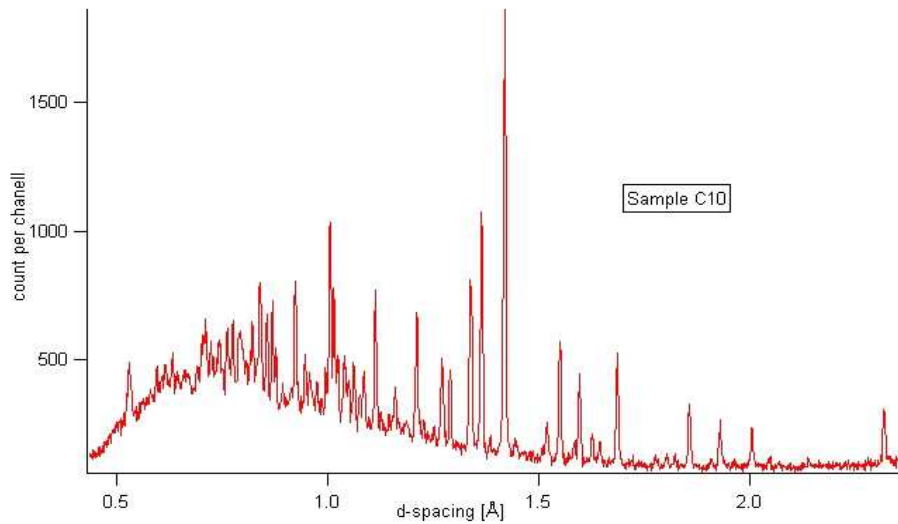
Fig.1 Time of flight diffraction pattern of C10 sample. Applied rotation speed at 1,2 chopper 4000 rpm.
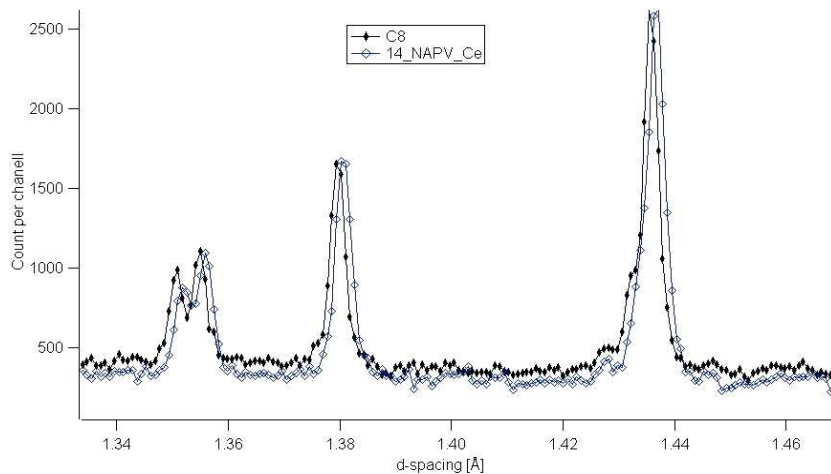
Fig. 2 Part of a diffraction pattern in high resolution mode. Applied rotation speed at 1,2 chopper 10000 rpm.

References

[1] Selomulya R., Ski S., Pita K., Kam C.H., Zhang Q.Y., Buddhudu S. (2003). Luminescence properties of $Zn_2SiO_4:Mn^{2+}$ thin-films by a sol-gel process. *Mater. Sci. Eng.* B100, p. 136-141.

[2] Lin C.C., Shen P. (1994). Sol-gel synthesis of zinc orthosilicate, *J. Non-Cryst. Solids.* 171, p. 281-289.

B N C **Experimental Report**	*Experiment title* **Time of flight experiments with neutrons in Bloch-states**	*Instrument.* *TOF* *Local contact* *György Káli*
Principal proposer: György Káli *Experimental team:György Káli*		*Experiment Number* *TOF_ 2008_ 1_ IH.* *Date 2008.05*

Objectives:

As it is well known from the dynamical scattering theory, neutrons that impinge on the surface of a perfect crystal in Laue geometry under Bragg condition can be scattered into degenerated standing wave states propagating along the reflecting planes. In special cases one component of the doublet can penetrate very deep into the crystal by anomalous transmission (Bormann effect). The objective of this experiment was to the apply that phenomenon as a non-destructive method to study or grade large sized silicon single crystals, and to measure the oxygen and precipitation diffusion in it [1]. The method would be somewhat similar to the electron and X-ray dark-field imaging and related techniques, but those methods are not applicable for large, almost perfect crystals produced nowadays. Those neutrons of special state have been investigated and used for long time in routine experiments (neutron interferometry) and in fundamental studies (e.g. EDM search, effective mass of neutron in crystal) but here the crystal itself is studied [2][3][4].

Results:

In the proposed experimental methods the slowly propagating standing wave would be used as a pair of two very monochromatic, almost opposite directed incoming beam. Lattice defects (interstitial atoms, precipitates and dislocations) can cause usual scattering processes (isotropic, small angle, Bragg and total reflection) measurable by proper detector system. The advantage of time of flight method is the possibility to separate these elastic effects from inelastic scattering. Although these very monochromatic beams are very weak, that is compensated by the large scattering cross-section of these kinds of processes, and for small angle scattering the usually disturbing incoming beam does not incidents on the detector, and in back scattering geometry the inelastic phonon scattering has a significant forbidden window.
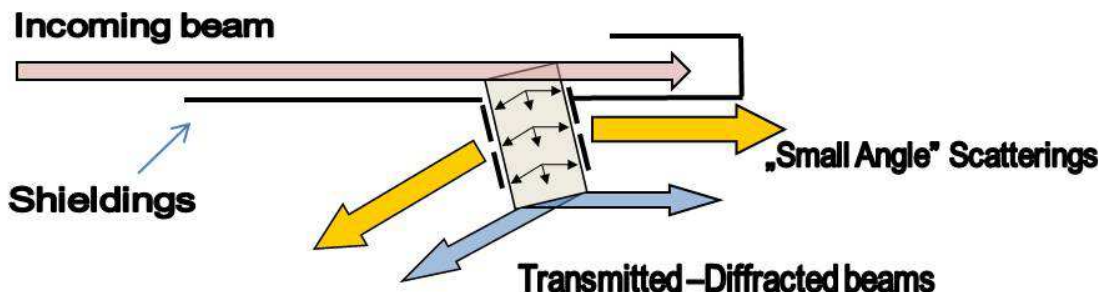
Fig.1. *Arrangement for the detection of secondary scattering*

In the present experiment large sized (app. 15 cm) silicon single crystals were used to measure the anomalous transmission of neutrons along different reflecting planes (parallel to 100, 110 and 111 planes) in room temperature. Since the transmission principally decays exponentially with the time the neutron spends in the crystal and the cross-section is principally proportional to it, an optimum exists depending on the applied reflection. The effect of the surface geometry (plane or cylindrical) and quality (polished - rough) and long time heat treatment was investigated too. The best result has been achieved on the 220 reflection as it was expected (taking into account also the spectrum of the incoming neutron beam). In this case (see *Fig.2*), at approximately $\lambda=4$ Å and $2\vartheta=175°$ the neutrons passed through the 15 cm thick crystal in 3 ms. Although this is much longer than the longest time published, the optimum was found to be around 1 ms (165°) or somewhat below it. Let us note, that in the above case (3 ms) the equivalent path length (the free neutron flights in the bulk during this time) is about 6 meter(!), and the equivalent wavelength of the moving standing wave packet in the direction of the propagation is 92 Å. Bragg and Laue reflections were detected separately moving the crystal a little bit in and out in the beam to satisfy one of the two conditions depending on the crystal geometry. Possible reflections from the surface between the front and back face were separated by proper shielding. Removing the shields no reflection comparable to the transmitted beam was measurable; the moderate increase belongs to secondary effects. The study can be continued with proper detector system.
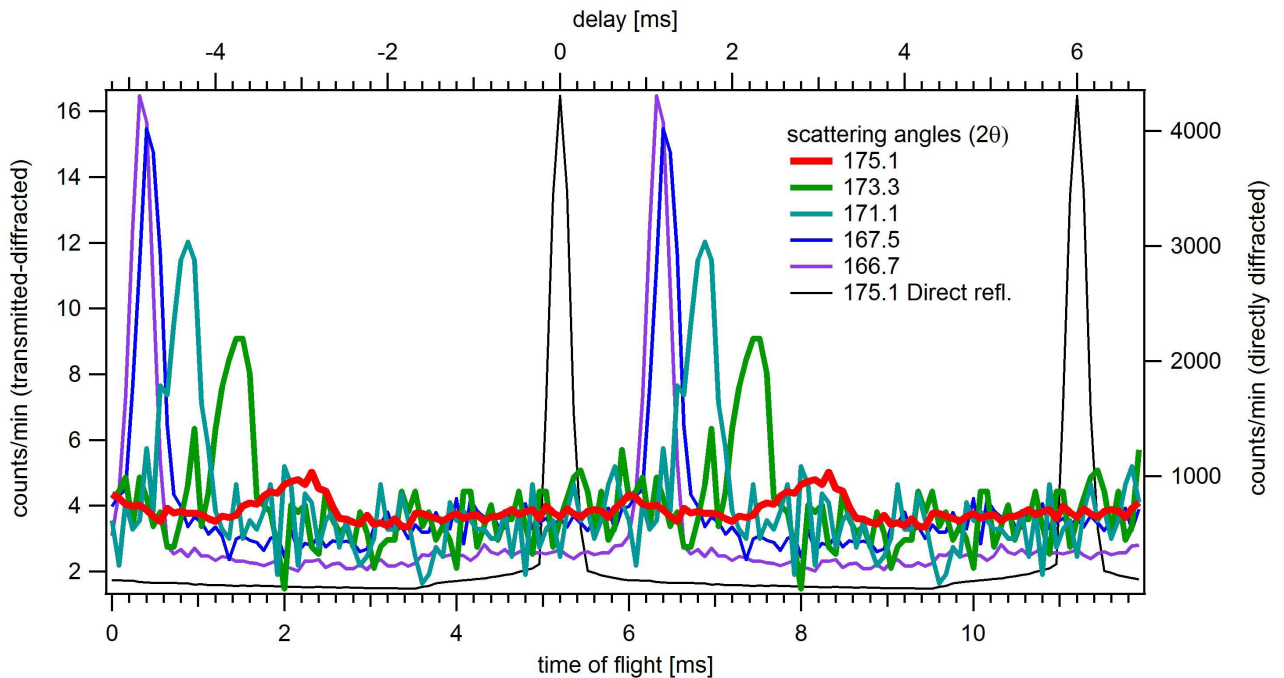
Fig.2. *The delay of the Laue reflected neutrons versus the scattering angles (29)*

References:
[1] Early Stages of Oxygen Precipitation in Silicon. Proceedings of the NATO Advanced Research Workshop, Exeter, U.K., March 26-29, 1996 Series: NATO Science Partnership Sub-Series: 3:, Vol. 17

[2] Structure Information from Anomalous Absorption Effects in Diffuse Scattering of Electrons. J. GJONNES AND R. HOmR, Acta Cryst. (1971). A27, 166

[3] Measurement of the neutron electric dipole moment by crystal diffraction. V.V. Fedorov et al., Nuclear Instruments and Methods in Physics Research A 611(2009)124–128

[4] Matter-wave interferometers: a synthetic approach. Ch.J. Bordé, In: P. Berman, Editor, Atom Interferometry, Academic Press (1997).

B N C Experimental Report	*Experiment title* Instrument development for residual stress measurements	*Proposal No.* ATHOS_08_2_IH *Local contact* Gy. Török
Principal proposer: Gy. Török *Experimental team:* Gy. Török		*Date(s) of Exper.* *June 2008* *Date of Report* 2011

Objectives *(Aim of the research in some sentences)*
The instrument development and tests for residual stress measurement on proven samples enable us to certify such kind of measurements to be carried out in BNC. First we tested the radial collimator transmission with 2D detector for residual stress measurements.

Results *(Description of concrete results, understandable also for non-experts of the field. Insert, if possible, a typical figure)*
Measurement of a Fe bar (1,1,0) with and without oscillating collimator (λ=1.86A). Collimator distance 250mm, window height 65 mm. Without collimator the window height is 110mm.
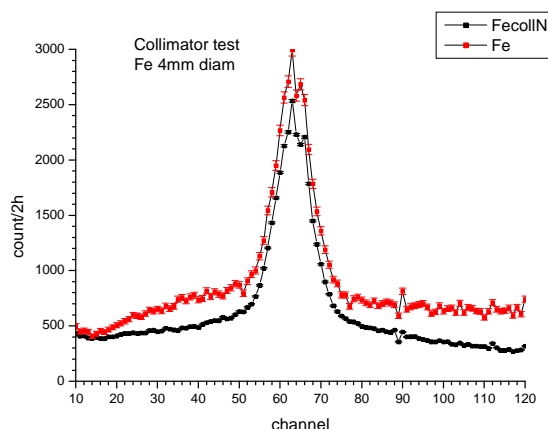
Comparison of spectrum of Fe nail with and without radial collimator.
(Transparency of collimator is better that 85%)

The peak ratio with and without radial collimation is about 85% - including geometrical factors. So we could test that the collimator quality is good. The movement of oscillation gives no artifacts. The background reduction is a factor of 2 in good measurement circumstances.

Future prospects *(Summary of the remaining problems to be solved, basis for the continuation of the work)*
More neutron tests with the full construction are planned in 2010.

B N C **Experimental Report**	*Experiment title* Residual stress measurement in furnace	*Proposal No.* ATHOS_08_03_IH *Local contact* Gy Torok
Principal proposer: Gy. Török *Experimental team:* Gy. Török		*Date(s) of Exper.* *June2008* *Date of Report* 2011

Objectives *(Aim of the research in some sentences)*

The furnace test measurement of residual stress on a benchmarked sample enables us to certify such kind of measurements carried out in BNC

Results *(Description of concrete results, understandable also for non-experts of the field. Insert, if possible, a typical figure)*

Neutron diffraction scans were made on steel samples at the ATHOS instrument.

The peaks correspond to the austenitic and Martensitic phase. Well displayed the growth of martensitic phase growing due to applied stress.

Fig 1.
The mechanical assembly of the furnace. We run the tensile test on the furnace.
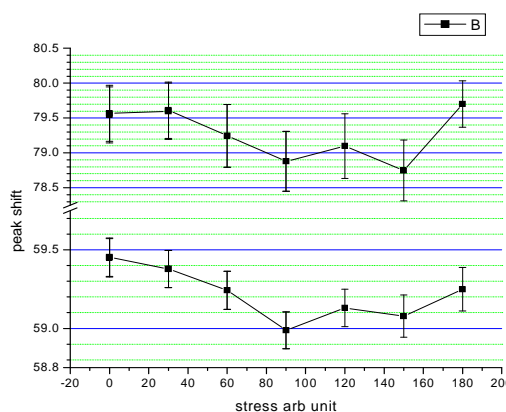
The peak shift of austenite (upper) and martensite phase. Here seen the ratio of elastic constants ~(1:4) and similar behaviour. Also the damage process is well displayed when the peak shift is not growing after stress (100) when other processes – like void formation became the main one.

Future prospects *(Summary of the remaining problems to be solved, basis for the continuation of the work)*
Neutron diffraction tests with the full construction including heating is planned to be carried out in 2010.

B N C Experimental Report	*Experiment title* Density of state measurement in BeZr amorphous material using a 2D detector set-up	*Proposal No.* ATHOS-_08_7_IC *Local contact* Gy. Török
Principal proposer: G. F. Syrykh, Kurchaton Institute of Atomic Energy *Experimental team: Gy. Torok*		*Date(s) of Exper.* *2008 okt1-nov20* *Date of Report:* 2011

Objectives *(Aim of the research in some sentences)*

The short-range order and dynamics of atoms, as well as the relationship between phonon and electron spectra of metallic glasses, are attracting major interest because of the unusual properties of these metastable systems. The amorphous Zr-Be system is interesting because of the large difference in atom sizes and masses; alloys can become amorphous in a wide range of compositions. So, it is possible to identify the structural and dynamics characteristics of the individual components. We have measured the BeZr amorphous material's density of state (DOS). In a previous measurement DOS was measured at higher energy transfer. Now we continue the scan at low energy. In Order to develop the neutron spectrometer's efficiency, we used a 2D detector setup shown in Fig1.

Results

Detector

The arrangement of measurement

Analyzer PG002
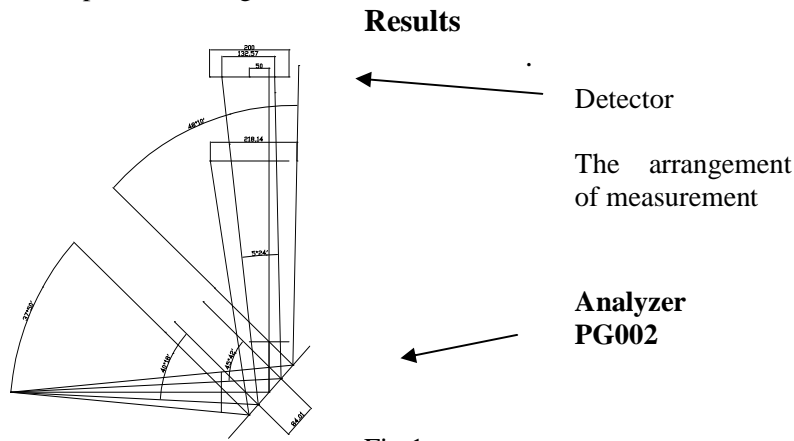
Fig 1.
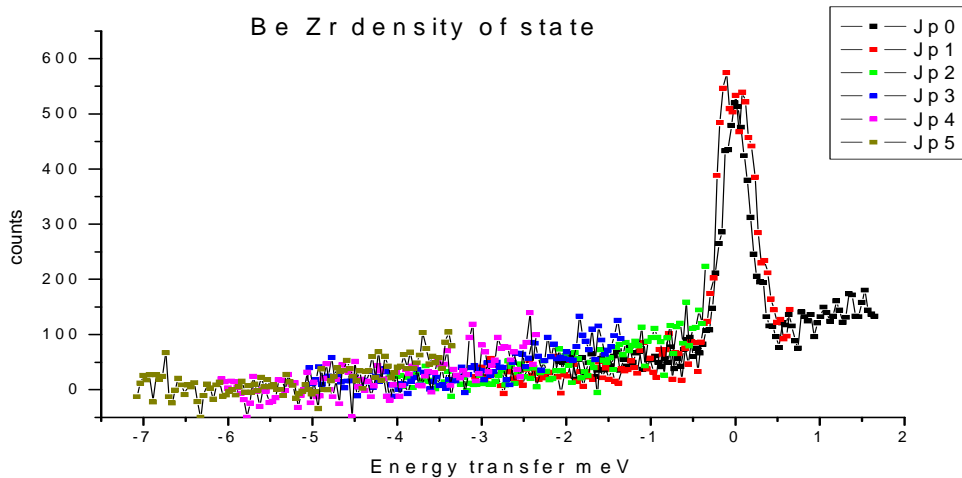
The measured density of state in $k_f = 1.8 A^{-1}$ fixed

143

According to the prediction of reference (below) we did not received a substantial inelasticity, i.e. any soft mode at a given energy transfer region.

References *(Published or accepted papers, research reports, conference lectures, seminars etc.)*
A.M. Bratkovsky, S.L. Isakov, S.N. Ishmaev, I.P. Sadikov, A.V. Smirnov, G.F. Syrykh, M.N. Hlopkin and N.A. Chernoplekov**,** Structure and dynamics of amorphous Zr-Be alloys, Journal of Non-Crystalline Solids 156-158 (1993) 72-75

Objectives

The experiment aimed to study water-soluble fullerenes and their association in the presence of salts in solutions. We studied the effect of chemical feature and concentrations of components to find appropriate regulation of structures of fullerene-containing systems for medical purposes.

Results

Water-soluble derivatives of fullerenes, $C_{60}(OH)_X$, and hydroxylated endofullerenes, $Gd@C_{82}(OH)_X$, have been studied in aqueous solutions with pH variation (pH = 5-7, addition of sodium citrate or sodium phosphate) in order to decode the mechanisms of fullerenes self-organization as induced by the van-der-Waals forces and hydrogen bonds between fullerene molecules those as usual demonstrate some trends to be ordered in cluster structures. These phenomena mean the reasons to consider fullerenes systems as an example of special cluster state of molecular matters. In the first SANS-experiments (25°C, neutron wavelength λ= 0.751 nm, λ = 0.386 nm, $\Delta\lambda/\lambda \sim 0.1$) there were examined the solutions of $C_{60}(OH)_X$ (number of hydroxyls X ~ 20) with concentration of these molecules C_F = 0.5 mg/ml in light water (pH=5). In following measurements the solution has contained additionally sodium citrate (c = 2.8 mg/ml) that provides pH = 6-7. In the last series of scattering experiments we added the higher amount of sodium citrate (c = 10 mg/ml) to achieve the magnitude pH = 7. The variation of salt concentration caused an increase of clustering in solutions that is clear visible in Fig.1 showing the behaviors of scattering cross sections $d\sigma/d\Omega = \sigma(q)$ versus momentum transfer q = 0.08-4.4 nm^{-1}. In all the solutions there was observed the formation of molecular clusters, and this process was intensified by the addition of salt. These clusters were globular structures. It is evident from the data analysis showed the scattering law

$$\sigma(q) = \sigma_o/[1+ (R_Cq)^2]^{D/2} + B, \qquad\qquad (1)$$

where σ_o is forward scattering cross section, $R_C \sim 16$-25 nm is the characteristic size of cluster (radius of molecular correlations inside a cluster), and B is the incoherent background arisen from light water.
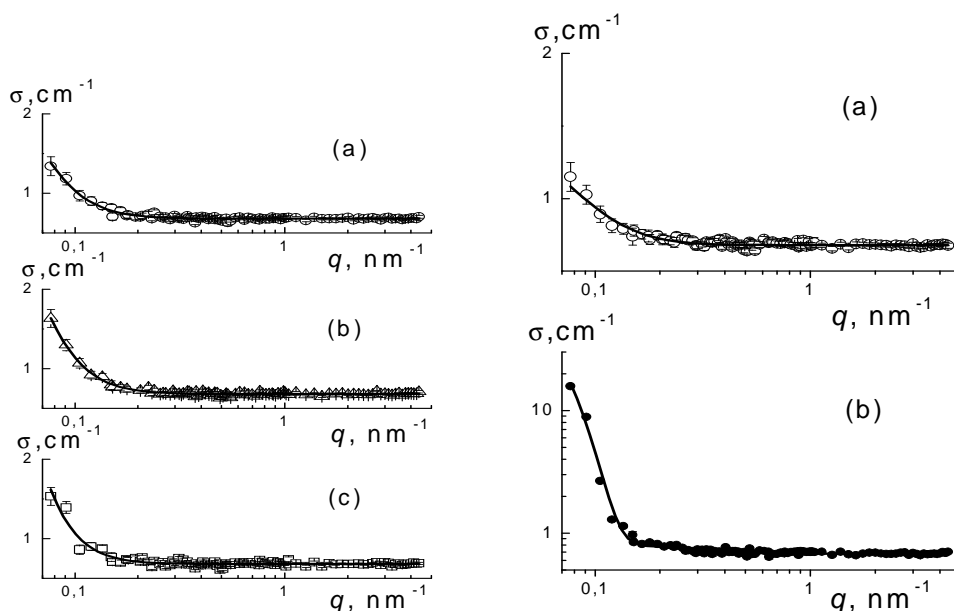
Fig.1. SANS from aqueous solutions of $C_{60}(OH)_X$ with different amounts of sodium citrate: a). c = 0, pH = 5; b). c = 2.8 mg/ml, pH = 6-7; c). c = 10 mg/ml, pH = 7. Lines are scattering functions (1)

Fig.2. Behaviors of cross sections vs. momentum transfer in solutions of $C_{60}(OH)_X$ with sodium phosphates: a). c = 0.6 mg/ml, pH = 7; b). c = 4.4 mg/ml, pH = 8.

As compared to the solution with citric salt, the systems $C_{60}(OH)_X + H_2O$ containing sodium phosphate revealed a strong association with formation two-level structures having characteristic scales few nanometers and about a hundred nanometer (Fig.2).

The system with small amount (c = 0.6 mg/ml) of sodium phosphate has not demonstrated any substantial deviation from the behavior of solutions containing citric salt (Fig1a). The q-dependence of the scattering is described by the function (1). Meanwhile, in the case of higher content of sodium phosphate (c = 4.4 mg/ml, Fig.2b) the scattering became stronger by two orders in magnitude in low-q region, and the q-dependence of scattering shows additional scattering (second part, Giunier model) except of contribution of small globular clusters (first part)

$$\sigma(q) = \sigma_o/[1 + (R_Cq)^2]^{D/2} + \sigma_G \exp[-(R_Gq)^2/3] + B. \qquad (1)$$

Here the first component does not differ from the function (1), and the second one depends on the forward cross section σ_G and the gyration radius R_G of large structures. Finally, the parameters of functions (1), (2) for solutions with different salts are displayed in Fig.3.
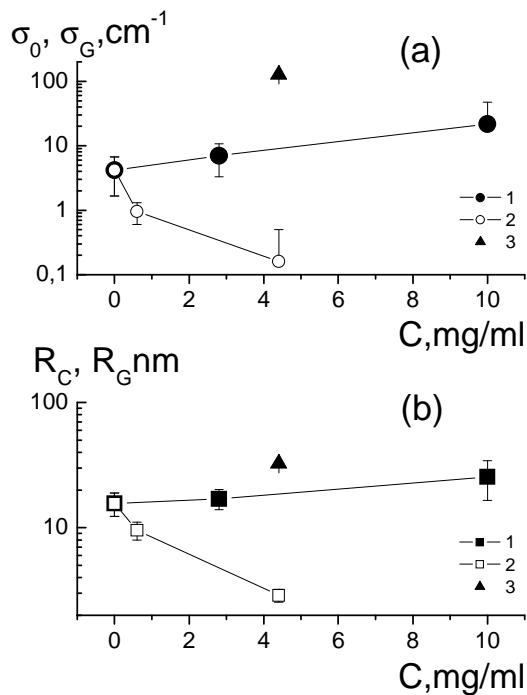
Fig.3. Parameters of scattering functions (1) and (2): forward cross sections (a) and radii (b).

Summarizing the obtained results, one should stress that the degree and forms of association of fullerenes in aqueous solutions can be varied using various additives those regulate the interactions of fullerenes (van-der-Waals forces, strength of hydrogen bonds). The evaluation of peculiarities of fullerenes association seems to be important for their medical applications: contrast agents in Nuclear Magnetic Tomography Diagnostics, carriers of medicine etc.

References

1. Lebedev V.T., Torok Gy., Nikolaev I.V., Kim. A.F. Ordering of hydroxylated fullerenes in aqueous solutions. Intern Conf. "Advanced carbon materials". Saint-Petersburg. 4-8 July 2011.

Future prospects

1. Problem of mechanisms of fullerenes ordering in biological media

2. Problem of nano-phase separation of fullerenes in solutions.

3. Problem of regulation of fullertenes' structures using various additives in solutions.

B N C **Experimental Report**	*Experiment title* Experimental study of mesoporous silica matrices microstructure behaviour versus sonocatalysed sol-gel processing variables, by using Neutron Scattering Techniques	*Proposal No.* **BRR_184** *Local contact* *Adel Len*
Principal proposer: Cecilia Savii *Experimental team:* Adél Len, Cecilia Savii		*Date(s) of Exper.* *04.10.2008* *Date of Report* *25.01.2011*

Objectives *(Aim of the research in some sentences)*

Silica sonogel samples showing peculiar properties were studied by SANS. The influence of two technological parameters, such as duration of sonication and influence of the ionic liquid content upon texture properties (pore size and shape, fractal character and density) of the prepared sonogels were followed.

Results

A. Silica sonogels prepared by ultrasonic field assisted sol gel process

Structural analysis of the dry gel samples pointed to the nonmonotonic dependence of the gel morphology and texture (pore size distribution, surface areas) on the total applied power.

Nitrogen adsorption isotherms indicated that the sample sonicated for two hours had a significantly different porosity distribution, than the other three samples. About 90% of the pores have an average dimension of about 3 nm, the fraction of microporosity (d < 2 nm) and macroporosity (d > 50 nm) being insignificant comparing to the same data of the other samples. Concerning the shape of the pores, all the samples, but the 2 hours sonicated one, exhibited a rather large difference between the porosity characteristics obtained from the adsorption and desorption branches of the nitrogen adsorption isotherms. Such difference is known to be related to the pore shape, actually to the ink bottle real shape of the pores. For the 2 hours activated sample both branches gave similar porosity data, suggesting that in this case the pore shape is closer to spherical and the microstructure is more ordered compared with the others.

Small-angle neutron scattering study

Small-angle scattering is caused by the inhomogeneous distribution of the material in the investigated sample volume. In our case, this inhomogeneity is related to the non-uniform distribution of the silica material and the pores, occurring on length scales 1–100 nm. The SANS measurements on the four dry gel powders samples have been performed on the SANS diffractometer operating at the cold neutron beamline at the Budapest Research Reactor. The data are depicted in the form of the scattered intensity in function of the magnitude of the scattering vector q. The scattering intensity has been registered over a q range 0.003–0.4 Å^{-1}, using two sample-to-detector distances and two incident wavelengths, 4 Å and 12 Å.

All samples display qualitatively similar scattering curves, which exhibit three characteristic regions. At lowest q, between 0.003 and 0.01 Å^{-1}, the scattered intensity has a power low behavior, which shows up as straight line in the double logarithmic presentation (Figure 1).
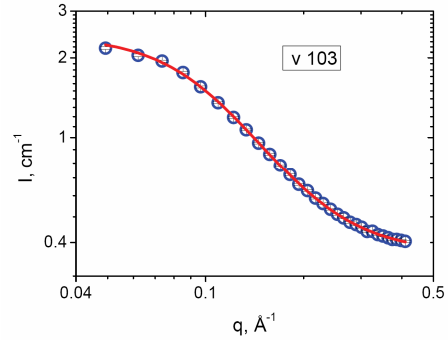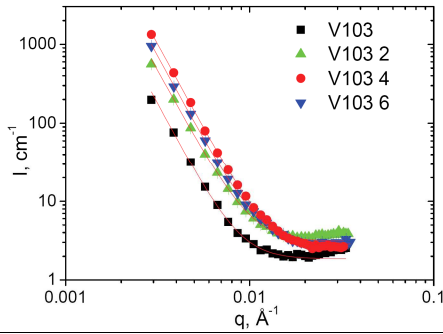
| **Figure 1.** SANS scattering data measured at low q (symbols), and the corresponding power law fits (lines) [1] | **Figure 2.** High q part of $I(q)$ data for the sample V103, fitted with the Posselt model [1] |

For the intermediate q, approximately between 0.01 and 0.08 Å^{-1}, a plateau is seen, which is followed by another decay in the high q range, up to 0.45 Å^{-1} (Figure 1). Such complex shape of the scattering curves indicates that spatial structures having different dimensions are seen. The quantitative analysis of the experimental data has been performed using some frequently used methods applicable for powder and gel like systems.

High q region The highest q region of the scattering curves corresponds to the smallest measured length scales. In our chase this has been in between 1–5 nanometers. The gelation process starts with the formation of the so-called primary structural units. They can be considered as spheres having rough surfaces. The corresponding model, proposed by Posselt [equation (1)], was applied to the high q part of the measured scattering data, and resulted in very good fits for all samples, as illustrated in Fig. 2. In equation 1 r corresponds to the nominal radius of the spheres, and Ds is the surface fractal dimension, characterizing the roughness of the surface.

$$I(q) = \frac{B}{1 + 0.22 (q^2 r^2)^{(6-Ds)}} + bg \qquad (1)$$

Low q region The lowest q region of the scattering curves reflects the structure at large size, roughly corresponding to 20–100 nanometers. In this size range, the gels exhibit a power law scattering, described and fitted by equation (2), with power exponent p ranging from 4.2 to 4.4.

$$I(q) = \frac{A}{q^p} + bg \qquad (2)$$

This indicates a complex structure, which cannot be described by either surface or volume fractal, often used for characterization of dry gel materials. In case of pure fractal structure, the power exponent should be less than 4, and $p = 4$ would correspond to a two-phase system (e.g. porous material) with smooth interfaces. It has been shown that $p > 4$ can reflect the situation of a two phase system as well, but the interface must have a gradual change of the density in the direction perpendicular to it. This is also similar to a two-phase system with a rough, but non-fractal, interface. In our case of dry silica gels, the scattering originates from the plausibly rough interface of the porous network of the aggregated primary structural units. The power exponents have been determined by least squares fitting of equation (2) to the scattering curves. The absolute integrated intensities (accounted for by the prefactor A) are proportional to the amount of the surfaces per unit volume. All samples exposed to ultrasonic treatment show an internal surface one order of magnitude higher than the non-treated sample. In this series, the 4 hours treated sample exhibits the largest surface. It should be noted, that unlike the gas adsorption techniques, the scattering measurement is equally sensitive to the surface of both the closed and the open pores. Unfortunately, without additional and precise knowledge of the pore structure, it is not possible to compare directly the surface and volume characteristics obtained from the two

different techniques, even though they are closely related to each other.

Conclusion

Structural analysis of the dry gel samples pointed to the nonmonotonic dependence of the gel structure (pore size distribution) on the total applied power. Both techniques, SANS and nitrogen adsorption, indicates that in given conditions, the duration of the sonication had an optimum value of 2 hours. The SANS results reveal the two-level complex structure of the gels. The characteristic size of the primary structural units were found to be 1.5–2 nm, while the secondary porous structure of the aggregated primary units, is seen to be above 20 nm [1].

Resuming, it can be inferred that by using a simple, low energy consuming methodology we obtained mesoporous materials having huge specific surface areas. They can be useful as matrices for guest materials which require separation, limitation of crystalline growth or preventing aggregation.

References *(Published or accepted papers, research reports, conference lectures, seminars etc.)*

[1] Savii C., Almásy L., Ionescu C., Székely N.K., Enache C., Popovici M., Sora I., Nicoara D., Savii G.G., Susan Resiga D., Subrt J., Štengl V.
Mesoporous silica matrices derived from sol-gel process assisted by low power ultrasonic activation,
Proc. Appl. Ceram., *PAC* 3, [1-2] 2009, 59-64

[2] Putz A-M, Ianãsi C., Dascãlu D., Savii C.
Acid Catalysed Silica Xerogels and Sonogels Synthesized with Buty-4-Methypyridinium Telrafluoroborate Ionic Liquid, *IJES* , Vol.a No.1 2010, 79-88.

B N C **Experimental Report**	*Experiment title* Structural study of water - in ionic liquid microemulsions by SANS	*Proposal No.* BRR_187 *Local contact* L. Almasy
Principal proposer: Mireille Turmine *Experimental team:* Mireille Turmine, Laszlo Almasy		*Date(s) of Exper.* June 2008 *Date of Report* January 2011

Objectives

Common surfactants form micelles in ionic liquids based on imidazolium cations. Besides, ionic liquid - in - oil microemulsions have been reported. Consisting of bmimBF$_4$, cyclohexane, and the non-ionic surfactant TX100. Earlier SANS studies of such microemulsions proved the formation of surfactant-stabilized dispersed nanodroplets with IL cores.

Water containing microemulsions are much more popular due to practical interest, however, no such systems with ionic liquids have been reported so far. Since ionic liquids show properties similar to oils or organic solvents, one could then expect the formation of water - in - ionic liquid type microemulsions. 1-hexyl-3-methylimidazolium perchlorate (hmimClO$_4$) is an IL immiscible in water. Addition of ionic or non-ionic surfactant in this IL allows the incorporation of water to the mixtures until approximately 10% in weight of water. We have determined the partial phase diagram for the microemulsions using several surfactants. The structure of these microemulsions is however completely unknown to date and we aimed to study it by small-angle neutron scattering

Results
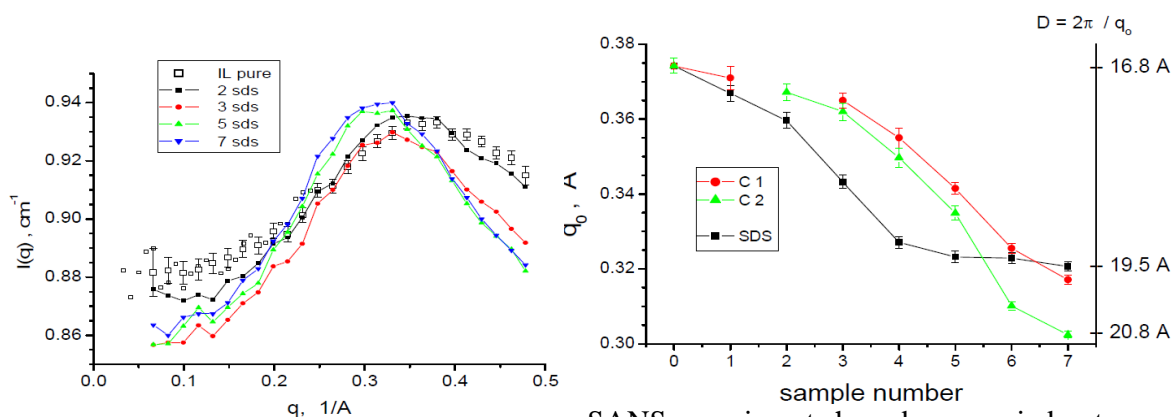
SANS experiments have been carried out on a series of mixtures of IL / surfactant / D$_2$O, varying the water content, and the amount and the type of the surfactant. All scattering curves show a broad interference peak, which is qualitatively similar to the structure factor of conventional micro-emulsions. In the same time, it is similar to the structure factor of the neat ionic liquid.

Increasing the water content, the peak position shifts to smaller q, indicating the structural change in the emulsion, this is similar to the behaviour of the conventional water-in-oil emulsions. Therefore, it can be assumed that the present system has a similar inner structure.

Objectives

The aim of experiment was to study macromolecular structure and self-assembly mechanisms of complex polymeric systems possessing the molecular groups or nanoparticles (sulfonated groups, e.g. SO_3Na, SO_3H and fullerene C_{60}) which play an active role in the formation of polymers and in the ordering of macromolecular ensembles in solutions.

Results

Protonated star-shaped polystyrenes with single and double fullerene C_{60} core and the hybrid stars with pairs of polar and non-polar arms (tertbuthylmetacrylate, polystyrene) have been studied in deuterated toluene ($20^{o}C$) by small-angle neutron scattering at low and moderate polymer concentrations ($c_1 \sim 0.01$ g/ml, $c_2 \sim 0.03-0.06$ g/ml) to evaluate the peculiarities of fullerene centre action on polymers self-assembly in solutions.

We found the cores composed of two fullerenes, linked via $Si(CH_3)_2$-bridge, to induce stars' anisotropic interactions and association into chain-like structures (correlation radius $\sim 400-600$ nm). Meanwhile the single-core stars of polystyrene and hybrids organize globular clusters (size $\sim 10^3$ nm) those geometry do not change significantly by polymer content variation.
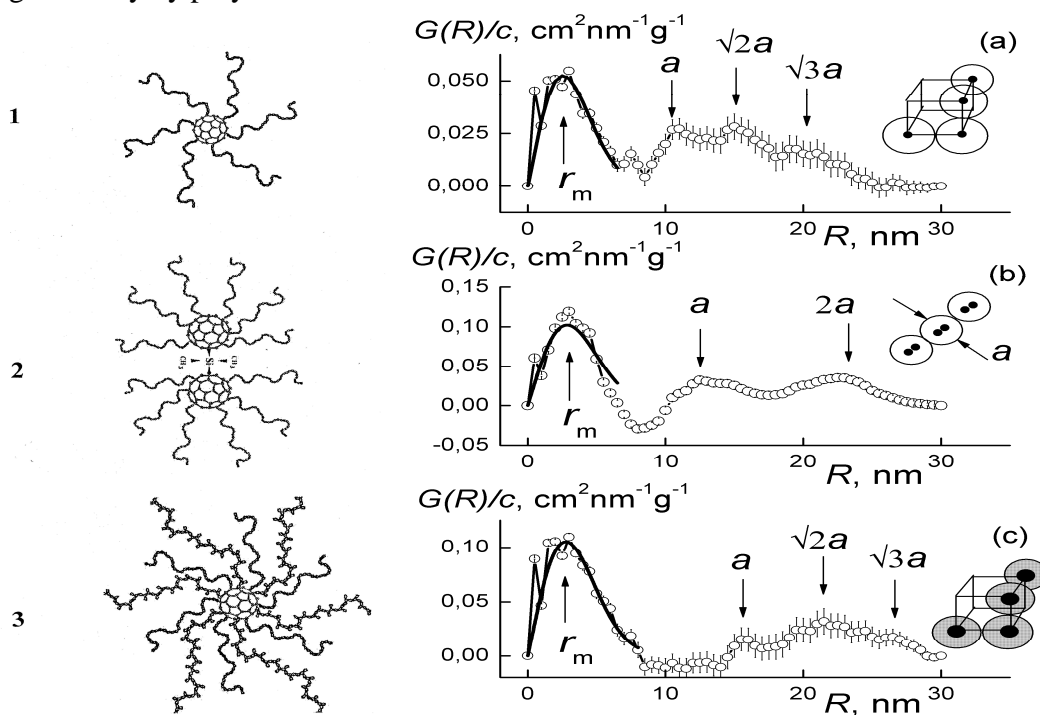
Star-shaped polymers: single-core 6-arm stars (1), double-core 12-arm stars and hybrids (3) with polar and non-polar arms.

Spectra of molecular correlations $G(R)/c$ in solutions of star-shaped polymers (concentration $c = c_2$): (a) – single-core 6-arm PS; (b) – double-core 12-arm PS; (c) – hybrids. Main maxima positions r_m correspond to stars' gyration radii found from the data approximation by correlation function (3). The secondary maxima indicate the characteristic distances between

The self-assembly of sulfonated polystyrene (molecular mass $1 \cdot 10^5$) with SO_3Na-groups has been studied in chloroform, D-toluene and benzene by SANS. As it was found, in chloroform the PS-chains containing 1.35 % mol. of ionic groups undergo the coil-globule transition induced by interactions of ionic groups.

At higher sulfonation level (2.6 % mol.) there was observed the transformation of coils into vesicles filled with solvent. The self-organization of ionomers in D-toluene is revealed in the formation of "effective chains" including up to ~ 7 macromolecules as dependent on the amount of SO_3Na-groups (0.5 − 5.8 mol. %). A following ordering leads to the association of "effective chains" to secondary clusters composed of 4-5 "effective chains".

ν = 0.5 mol. %   ν = 1. 35 mol. %   ν = 5.8 mol. %
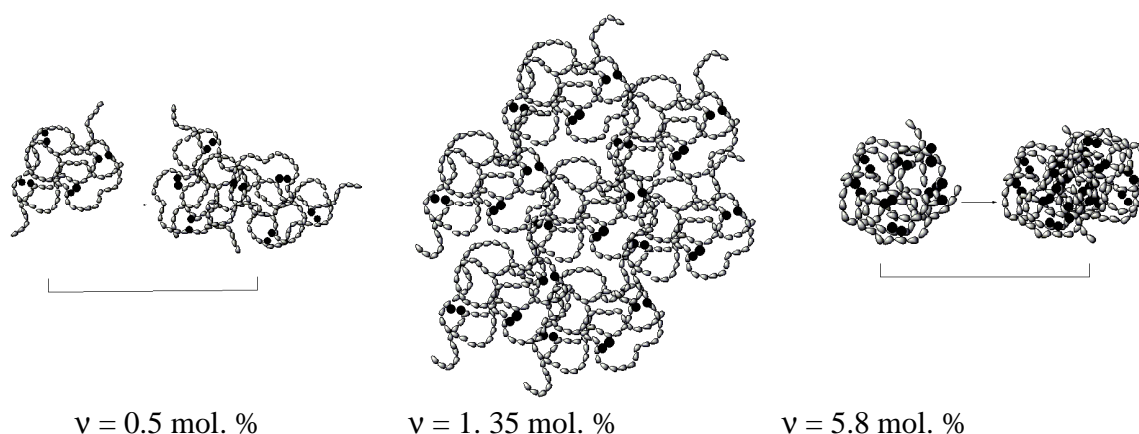
Formation of "effective chains" due to ionic groups association in D-toluene
(polymer content 1 g/dl).

Future prospects)
1. Problem of long-range action of fullerene on attached chains conformations.
2. Problem of nano-phase separation of the arms of different polarity in stars' volume and related structural peculiarities of star-shaped polymers.
3. Problem of perfect structures formation and study by SANS in ionomer's solutions to create membranes providing effective molecular separation in liquid mixtures.

References

1. Лебедев В.Т., Виноградова Л.В., Торок Д. Нейтронные исследования структурных особенностей звездообразных фуллерен (C_{60})-содержащих полистиролов в растворах. Высокомолек. соед. А. 2008. т.50. № 10. С. 1833-1841.

2. Lebedev V.T., Torok Gy., Melenevskaya E.Yu., Vinogradova L.V., Ivanova I.N. Poly(N-vinylcaprolactam)-C_{60} Complexes in Aqueous Solution. // Fullerenes, Nanotubes and Carbon Nanostructures. 2008. V. 16. N. 5-6. P. 603-609.

3. Lebedev V.T., Vinogradova L.V., Torok Gy. Structural Features of Star-Shaped Fullerene (C_{60})-Containing Polystyrenes: Neutron Scattering Experiments. // Polymer Science. Ser.A. 2008. V. 50. N 10. P. 1090-1097.

4. Lebedev V.T., Torok Gy., Vinogradova L.V. Neutron studies of structural peculiarities of star-shaped fullerene-containing polystyrenes in solution. 6th Intern. Symposium "Molecular order and mobility in polymer systems. June 2-6, 2008. St.-Petersburg. Russia. Proceedings. O-022.

5. Lebedev V.T., Torok Gy., Melnikov A.B., Vinogradova L.V., Orlova D.N., Lebedev V.M., Kulvelis Yu. V. Neutron studies of self-organization of ionomers to micellar and vesicular structures in solutions. 6th Intern. Symposium "Molecular order and mobility in polymer systems. June 2-6, 2008. St.-Petersburg. Russia. Proceedings. P-040.

6. Лебедев В.Т., Мельников А.Б., Виноградова Л.В., Торок Д. Нейтронные исследования самоорганизации в растворах иономеров на основе сульфированного полистирола. // Высокомолек. соед. А. 2009. Т. 51. № 3. С. 407-413.

7. Lebedev V.T., Melnikov A.B., Vinogradova L.V., Torok Gy. Neutron study of self-organization in solutions of ionomers based on sulfonated polystyrene. // Polymer Science. Ser. A. 2009. V. 51. N 3. P. 277-282.

8. Лебедев В.Т., Мельников А.Б., Виноградова Л.В., Торок Д. Особенности внутри- и межмолекулярной организации иономеров сульфополистирола в растворах по данным нейтронного рассеяния. // Высокомолек. соед. А. 2009. Т. 51. № 4. С. 572-581.

9. Lebedev V.T., Melnikov A.B., Vinogradova L.V., Torok Gy. Intra- and Intermolecular organization of Sulfopolystyrene Ionomers in Solutions: Neutron Scattering Studies. // Polymer Science. Ser. A. 2009. V.51. N 4. P. 372-381.

10. Torok Gy., Lebedev V.T., Vinogradova L.V., Orlova D.N., Shamanin V.V. Molecular correlations in bulk star-shaped polystyrene with fullerene C_{60} center. 9th biennial International Workshop "Fulerenes and Atomic Clusters". July 6-10, 2009. St.Petersburg, Russia. Abstracts, P. 38 (oral contribution).

11. Lebedev V.T., Vinogradova L.V., Torok Gy., Shamanin V.V. Long-range self-assembly in solutions of star-shaped polymers with fullerene C_{60} multifunctional centers. 9th biennial International Workshop "Fulerenes and Atomic Clusters". July 6-10, 2009. St.Petersburg, Russia. Abstracts, P. 140 (poster).

12. Lebedev Vasily, Vinogradova Lyudmila, Torok Gyula. Neutron scattering studies of structure and self-assembly of star-shaped polymers with fullerene centers in solutions. European Polymer Congress. July 12-17, 2009. Graz, Austria. Abstracts, P. 46 (oral contribution).

13. Лебедев В.Т., Торок Д., Мельников А.Б, Орлова Д.Н., Иванова И.Н. Молекулярная и надмолекулярная структура иономеров сульфированного

полистирола в растворах. // Поверхность. Рентгеновские, синхротронные и нейтронные исследования. 2009. № 8. С. 16-25.

14. Lebedev V.T., Torok Gy., Melnikov A.B., Orlova D.N., Ivanova I.N. Molecular and supramolecular structure of ionomers of sulfonated polystyrene in solutions. // J. Surface Investigation. X-ray, Synchrotron and Neutron Techniques. 2009. V. 3. N 4. P. 582-591.

15.Лебедев В.Т., Мельников А.Б., Török Gy., Виноградова Л.В. Самоорганизация сульфополистирольных иономеров в растворах в зависимости от полярности среды и содержания ионогенных групп в цепи. Пятая всероссийская каргинская конференция. "Полимеры 2010". 21-25 июня 2010. Москва. Тезисы. С.257 (приглашенный доклад).

16.Лебедев В.Т., Мельников А.Б., Török Gy., Виноградова Л.В. Гидродинамические свойства и структура иономеров полистирола с ионогенными группами SO_3Li в слабополярных растворителях. Пятая всероссийская каргинская конференция. "Полимеры 2010". 21-25 июня 2010. Москва. Постер С5-129. Труды конф. С.68.

17. Lebedev V.T., Vinogradova L.V., Torok Gy., Shamanin V.V. Long-range self-assembly in solutions of star-shaped polymers with fullerene C_{60} multifunctional centers. // Fullerenes, Nanotubes and Carbon Nanostructures, 2010. Vol. 18 Issue 4, P. 431-436.

18. Лебедев В.Т., Torok Gy. Виноградова Л.В. Механизмы самоорганизации звездообразных полимеров с мультифункциональными центрами ветвления на основе фуллеренов в растворах. XXI Совещание по использованию рассеяния нейтронов в исследованиях конденсированного состояния. Москва. Российский научный центр «Курчатовский институт», 16-19 ноября 2010 г. Тезисы. С. 26.

19. Лебедев В.Т., Torok Gy., Виноградова Л.В. Структура и надмолекулярные образования звездообразных гетеролучевых полимеров в дейтеротолуоле. // Высокомолек. соед. А. 2011. Т. 53. № 1. С. 15-26.

B N C **Experimental Report**	*Experiment title* **SANS-study of molecular complexes in solutions**	*Proposal No.* *SANS_09_01_IC* *Local contact* *Gy. Torok*
Principal proposer: V.T.Lebedev *Experimental team:* V.T.Lebedev, Kulvelis Yu. V., A.F.Kim , Gy. Török		*Date(s) of Exper.* *1-8 June 2009* *Date of Report* Date

Objectives *(Aim of the research in some sentences)*

The aims of research are related to the study of molecular complexes formation and behaviour in solutions as dependent on chemical nature (polymers, porphyrins, ferromagnetic particles, fullerenes) and other factors (concentration and polarity of components, molecular masses etc.).

Results *(Description of concrete results, understandable also for non-experts of the field. Insert, if possible, a typical figure)*

The present work is devoted to the complexes of nanoscale magnetic particles with sensitizer "photodithazine", being used for cancer photodynamic therapy, first synthesized and studied by small-angle neutron scattering (SANS). The photodithazine, chlorine e_6 derivative, first developed in 1998 in Russia as a photosensitizer for treating various types of tumours.

In order to increase the effectiveness of photodithazine and to decrease the side effects in treating, one should increase its concentration in tumour cells and decrease it in normal cells. For this purposes one of the solutions could become a magnet-guided sensitizer based on a photodithazine complex with magnetic particles. Such complex will concentrate in tumour more effectively when applying external magnetic field.

We studied the possibility of photodithazine complex with magnetic particles localisation on tumour cells, guided by external magnetic field. Magnetic fluids, based on magnetite particles covered with citric acid in water solution were synthesised and used in preparing complexes with photodithazine. One more component – pluronic F-127 (ethylenoxide and propylenoxide copolymer) – was added to ferrofluid samples to increase their effectiveness and biocompatibility. Pluronics are commonly used in medicine, in order to stimulate medicines penetration through biological barriers, and to increase accumulation of some anticancer antibiotics in tumour cells.

Complex structure and its dependence on the initial conditions of magnetic fluid synthesis have been studied by SANS. The structural features of nanoscale magnetic particles associated with photodithazine and pluronic were found. According to SANS data the complex represents nanoscale objects with magnetite core and pluronic shell (model scattering functions are shown in Fig.2).

The investigated complexes of magnetic fluid particles with photodithazine showed increasing the efficiency of treatment in cell experiments and also in subclinical tests on mice. Thus, a magnet-guided sensitizer for PDT, containing magnetite, photodithazine and pluronic has been developed. Applications of the studied system are under discussion.

Photodithazine
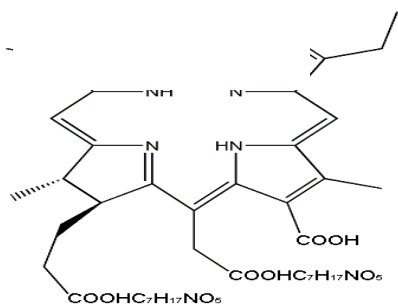
Fig. 1.
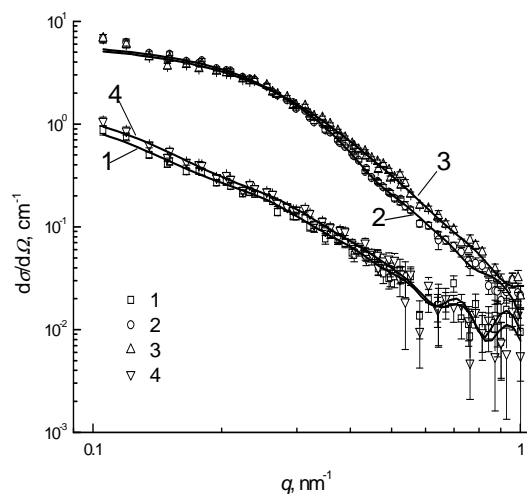
Fig.2.,

Neutron scattering cross section vs momentum transfer:
1 – ferrofluid based on magnetite;
2 – ferrofluid with pluronic;
3 – ferrofluid with pluronic and photodithazine;
4 – ferrofluid with photodithazine only. Lines are model scattering functions.

Future prospects *1. Problem of stabilization of colloids and study possible aggregation processes.*
2. Formation and studies of complexes for medicine using materials with photoluminescence properties.
3. Study the kinetics of absorption of biologically active substances on the surfaces of magnetic nano-particles.

References
1. Кульвелис Ю.В., Трунов В.А., Лебедев В.Т., Орлова Д.Н., Торок Д., Гельфонд М.Л., Мелик-Нубаров Н.С., Жиентаев Т.М. Разработка препаратов для повышения эффективности фотодинамической терапии. XX Совещание по использованию рассеяния нейтронов в исследованиях конденсированного состояния. РНИКС-2008. 13-19 октября 2008 г. Гатчина. Труды Совещания. С. 72.
2. Лебедев В.Т., Кульвелис Ю.В. Торок Д. Динамика воды в бинарных и тройных растворах ДНК и порфиринов. XX Совещание по использованию рассеяния нейтронов в исследованиях конденсированного состояния. РНИКС-2008. 13-19 октября 2008 г. Гатчина. Труды Совещания. С. 159.
3. Кульвелис Ю.В., Трунов В.А., Лебедев В.Т., Орлова Д.Н., Торок Д., Гельфонд М.Л. Комплексы феррожидкостей с фотодитазином и перспективы их применения в фотодинамической терапии. // Ж. Структурной химии. 2009. Т. 50. № 5. С. 981-985.
4. Кульвелис Ю.В., Лебедев В.Т., Трунов В.А., Иванова И.Н., Торок Д. Строение комплексов сульфированного тетрафенилпорфирина с поли-N-винилпирролидоном

по данным малоуглового рассеяния нейтронов. VII национальная конференция. Рентгеновское, Синхротронное излучения, Нейтроны и Электроны для исследования материалов. Нано-Био-Инфо-Когнитивные технологии. РСНЭ-НБИК 2009. 16-21 ноября 2009. ИК РАН-РНЦ КИ. Москва. 2009. Тезисы. С.37.

5. Kulvelis Yu.V., Lebedev V.T., Trunov V.A., Orlova D.N., Gelfond M.L., Török[3] Gy. Structure and properties of aqueous magnetic fluids for medical applications as magnetic antitumour medicines. Intern. Conf. "Physics of liquid matter: modern problems". May 21-24. 2010. Kyiv. Ukraine. Abstr. P.296.

6. Lebedev V.T., Torok Gy., Trunov V.A., Kulvelis Yu.V., Ivanchev S.S. NSE-study of water dynamics in gels composed of interpenetrating networks. Inter. Conf. "Physics of liquid matter: modern problems". May 21-24. 2010. Kyiv. Ukraine. Abstr. P.187.

7. Kulvelis Yu. V., Trunov V.A., Lebedev V.T., Orlova D.N., Torok Gy., Gelfond M.L. Structure of magnetically Guided Nanocarriers of the Photodithazine Sensitizer from Small Angle Neutron Scattering Data. Physics of the Solid State. 2010. V. 52. N5. P. 1040-1044.

8. Лебедев В.Т., Кульвелис Ю.В., Török Gy. Динамика воды в бинарных и тройных растворах ДНК и порфиринов. // ФТТ. 2010. Т.52. Вып.5. С. 1006-1010.

9. Кульвелис Ю. В., Трунов В. А., Лебедев В. Т., Орлова Д. Н., Török Gy., Гельфонд М. Л. Структура перспективных магнитоуправляемых носителей сенсибилизатора фотодитазина по данным малоуглового рассеяния нейтронов. // ФТТ. 2010. Т.52. Вып.5. С. 974-978.

10. Kulvelis Yu. V., Trounov V. A., Lebedev V. T., Orlova D. N., Török Gy., Gelfond M. L. Structure of Magnetically Guided Nanocarriers of the Photodithazine Sensitizer from Small Angle Neutron Scattering Data. // Physics of the Solid State, 2010, Vol. 52, No. 5, pp. 1040–1044. © Pleiades Publishing, Ltd., 2010.

11. Кульвелис Ю. В., Лебедев В. Т., Трунов В. А., Иванова И. Н., Торок Д. Строение комплексов сульфированного тетрафенилпорфирина с поли-N-винилпирролидоном по данным малоуглового рассеяния нейтронов. // Поверхность. Рентгеновские, синхротронные и нейтронные исследования. 2010. № 5. С.

B N C **Experimental Report**	*Experiment title* SANS study of the solutions of 3-methylpyridine in water – heavy water mixture	*Proposal No.* BRR_190 *Local contact* N. Székely
Principal proposer: Gábor Jancsó *Experimental team:* Gábor Jancsó, Noémi Székely		*Date(s) of Exper.* 28.02-04.03 2008 *Date of Report* 03.07.2008

Objectives

To perform SANS study of aqueous solutions of 3-methylpyridine (3MP) in the function of deuterium concentration of the solvent (water – heavy water mixture) and temperature in the scattering vector range $0.07 – 0.4$ Å^{-1}. The solutions are planned to be measured in the neighbourhood of the phase separation boundary. The results can be expected to provide information about the effect of deuterium substitution in the solvent on 3MP - 3MP and 3MP - solvent interactions and thus about the relationship between the phase separation and solution structure.

Results

The small-angle neutron scattering study on 3MP – water/heavy water mixtures (containing 30 weight% 3MP) was carried out in the function of deuterium concentration and temperature (see the table below).

t (^{o}C)						
45	x	x	x			
40	x	x	x	x		
35	x	x	x	x	x	x
25	x	x	x	x	x	x
D$_2$O (weight%)	50	60	70	80	90	100

The scattering curves were fitted to the Ornstein – Zernike model function of concentration fluctuations. As an example the fits are shown in the figure for the mixture with 70 weight% D$_2$O at 25 and 40 ^{o}C.
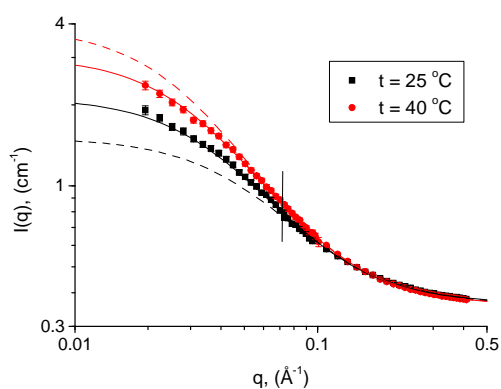
The measurements were carried out in the q range $0.07 - 0.4$ Å^{-1} for all mixtures and temperatures indicated in the table. For the checking of the low q behaviour of the scattering curves additional scattering experiments were performed on the mixture containing 70 weight% D_2O at 25 and 40 ^{o}C in the q range $0.02 - 0.1$ Å^{-1}. The figure above shows the fits to the scattering curves for the q range $0.07 - 0.4$ Å^{-1} (dashed lines) and those for the q range $0.02 - 0.4$ Å^{-1} (solid lines). It can be seen that including the low q scattering results significantly changes the shape of the scattering curves and thus the values of the forward scattering intensity.

Future prospects
For the reasons discussed above we would like to extend our investigation for all mixtures and temperatures studied before to the q range $0.02 - 0.1$ Å^{-1}.

| **B N C** **Experimental Report**	*Experiment title* **Cholesterol and sitosterol in egg phosphatidylcholine liposomes**	*Proposal No.* BRR_193 *Local contact* L. Almásy
Principal proposer Pavol Balgavý, Faculty of Pharmacy, Comenius University, Bratislava, Slovakia *Experimental team* Jana Gallová, Tanya Murugová and László Almásy		*Date of Experiment* June 2008 *Date of Report* Feb 2009

Objectives

We studied the effect of cholesterol and beta-sitosterol on structural parameters of bilayers composed of egg yolk phosphatidylcholine (EYPC).

Results
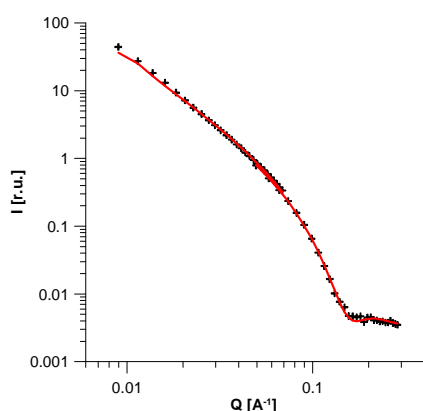
Cholesterol is ubiquitos constituent of mammalian membranes, beta-sitosterol is one of the sterols contained in plant membranes. Dietary beta-sitosterol is benefitial for human healt. We compared the effect of these two sterols on the EYPC bilayer.

Unilamellar liposomes composed of EYPC were prepared in the presence of 0-44.4 mol% of cholesterol or 0-41 mol% of beta sitosterol. SANS experiments were performed using two sample-detector distances (1.3 and 5.6 m) and at wavelength 5.9 A at 25 °C.

Fig. 1: SANS curve for multilamellar liposomes of EYPC+33.3 mol% of cholesterol together with the best fit.
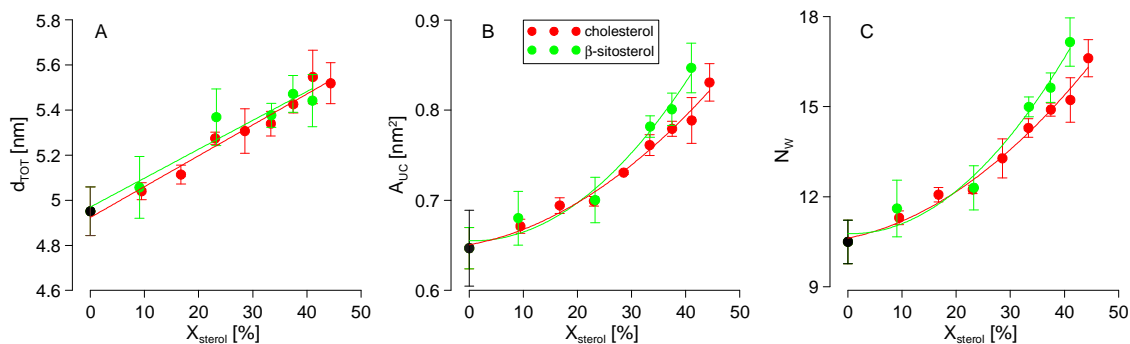
Fig. 2: Dependence of bilayer thickness d_{TOT} (A), area per unit cell A_{UC} (B) and number of water molecules N_W (C)

Bilayer structure was determined from SANS curve using a 3T model described by Kučerka et al. [1]. We have found that lipid bilayers thickness d_{TOT} increased linearly with increasing mol% of sterols. Both sterols influenced the bilayer thickness in the same manner in the range of experimental error. Sterols also increased the surface per unit cell A_{UC} (EYPC+fraction of sterol) at the lipid-water interface and number of water molecules in unit cell in the polar region. We were able to evaluate the partial area of EYPC, cholesterol and beta-sitosterol at the lipid-water interface (0.641 ± 0.010, 0.224 ± 0.015 and 0.275 ± 0.023 nm^2, respectively) according to Edholm and Nagle [2]. We suppose that larger partial area of beta-sitosterol in comparison with cholesterol is caused by bulkier side chain of beta-sitosterol. The partial areas of EYPC and both sterols do not depend on the concentration of sterol in the bilayer. This means that neither cholesterol nor beta-sitosterol have a condensing effect on the lipid-water interface.

References

[1] N.Kucerka, J.F.Nagle, S.E.Feller, P.Balgavy, Models to analyze small-angle neutron scattering from unilamellar lipid vesicles, Physical Review E 69 (2004)

[2] O.Edholm, J.F.Nagle, Areas of molecules in membranes consisting of mixtures, Biophys. J. 89 (2005) 1827-1832.

B N C **Experimental Report**	*Experiment title* SANS Study of Hybrid Materials Prepared by Gamma Irradiation	*Proposal No.* BRR_195 *Local contact* Meiszterics Anikó
Principal proposer: Fernanda Margaça *Experimental team:* Fernanda Margaça and Isabel M. Miranda Salvado		*Date(s) of Exper.* 11-13 July 2009 *Date of Report* 24 January 2011

Objectives

Hybrids are usually prepared by the sol-gel process. The authors prepared hybrid materials by gamma irradiation of a homogeneous mixture of the precursors, in the absence of solvents and water, using a ^{60}Co source. The final product was expected to have a different porosity from that of sol-gel prepared materials. The aim of the experiment was to obtain information on the materials structure at the nm scale.

Results Hybrid materials were prepared by gamma-irradiation of the mixture of the precursors. These were polyditmethylsiloxane (PDMS), S33, with average molecular weight 43500, tetraethylortosilicate (TEOS), and zirconium propoxide (PrZr). Samples with varying compositions have been measured by SANS. In this report the results obtained from samples with the composition, in weight %, shown in the Table below, are presented.

Composition	Sample
33S33 66TEOS 1PrZr	1Zr
33S33 65TEOS 2PrZr	2Zr
33S33 64TEOS 3PrZr	3Zr
33S33 62TEOS 5PrZr	5Zr
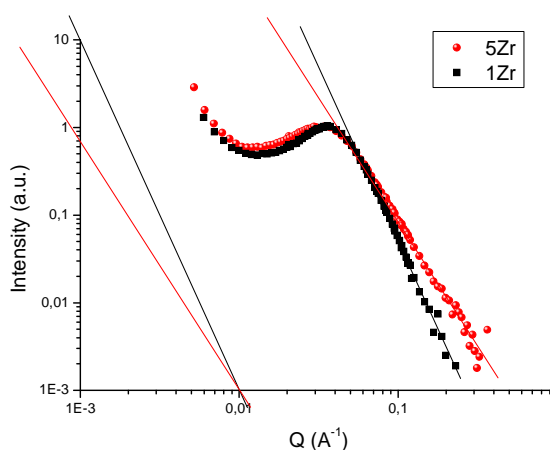
SANS results are shown in the above figure for the two samples with the smaller and the larger PrZr content. The spectra, in log-log plot, show a large scattering at low Q and a linear descent in the higher Q range. In the intermediate Q range a peak is present, in all spectra, attributed to a structure factor in the material structure. It was found that this peak position shifts to lower Q values as the content of PrZr increases whereas the slope value decreases from -4, the Porod slope associated to smooth surfaces, to -2.7 for the sample with the highest PrZr content. This latter value is associated to an open network of the mass fractal type. For the intermediate PrZr contents the slope was that associated to a surface fractal structure. These results show that the development of the inorganic matrix depends very strongly on the PrZr content in the precursors mixture. The matrix consists of a two level hierarchical structure - aggregates of small domains or particles, whose structure ranges from mass fractal to surface fractal or even smooth surface particles. Small pores between particles and large pores between aggregates are present.

162

In general this is the structure found in silica gels. The difference with the present hybrids prepared by gamma-irradiation is in the stronger dependence of the nanostructure on the Zr content.

References
A paper is being prepared for submission.

B N C **Experimental Report**	*Experiment title* Microstructural characterization by SANS of a car gear-shaft made from 20NiCRMo2 alloyed case hardening steel	*Proposal No.* BRR_205 *Local contact* Noémi Székely
Principal proposer: Massimo Rogante *Experimental team:* Massimo Rogante, Noémi Székely		*Date(s) of Exper.* *06-07/10/2009* *Date of Report* 05/01/2011

Objectives

A 20NiCRMo2 hardened steel car gear-shaft has been analysed by SANS, to know the structural characteristics at a micro- and nano-scale in correspondence of critical zones particularly fatigue- and/or crack-sensitive. The said high alloyed steel is a typical gear material for industrial applications, and it is normally submitted to heat treatment (case-hardening and hot oil quenching). Such components are subjected to the highest dynamic solicitations in power train engineering. The results are expected to supply indications on the effects of the considered thermal treatment on this gear-shaft, and to give a substantial support in the life assessment of the component.

Results

In a first step, three entire gear-shafts have been investigated - one before heat treatment, another after heat treatment (5-6 hours case-hardening - thickness ~ 0.7 mm - in atmospheric gas carburizing furnaces at ~900°C, using hot oil quenching), a third one after the finishing process successive to the heat treatment), adopting the following parameters: $\lambda = 4.12$ Å; sample-detector distance = 1.3 m, Q range = 0.0586-0.3672 (Å-1). The necessary calibrations have also been done (background, water, thickness, etc). Successively, the shafts have been sectioned into small portions, in correspondence of those critical zones particularly fatigue- and/or crack-sensitive, in order to achieve better SANS data: these samples showed a good scattering. A first series of SANS curves have been obtained for the mentioned samples, indicating a substantial difference between the not heat-treated and the heat-treated samples. These data will be fitted with appropriate model, thus further information on the possible inhomogeneities, size scale and distribution is being achieved in order to complete the data treatment. Fig. 1 refers to the measurement of a whole gear shaft, while Fig. 2 to the three samples cut from considered gear-shafts (before, after heat treatment and after the finishing process successive to the heat treatment respectively).

In Fig. 3 SANS graphs are reported, showing a well evidenced difference between the not heat-treated and the heat-treated shaft.

References

M. Rogante, Rogante Engineering Office and its contributions for the ESS Project, Presentation at the Symposium "The ESS Project: Opportunity for Italian Research?", Roma, 16/11/2010. http://ess-symposium.cnr.it/

Future prospects

The results obtained from the complete SANS data treatment are expected:

- to help studying the microstructural evolution of precipitates in the possible critical locations: the evaluation of shape and size of such precipitates can be particularly useful in order to locate the areas of maximum thermal alteration, and the expected changes of the precipitate characteristics can be important to be compared with the results of other investigations carried out by the manufacturer
- to give important information on the particles dimensions before and after the thermal treatment, and after the successive finishing process
- to supply useful indications on the effects of thermal treatment and the finishing process on the considered component, connecting the SANS results with the hardness and microstructural measurements (e.g., micrographs) already adopted by the manufacturer
- to help the quality enhancement of the heat treatment and give a support in the life assessment of the component.

Objectives

Elastomers filled with inorganic particles of nanometer size represent an attractive system for applications in modern technologies. Preparation of inorganic nanoparticles by precipitation of inorganic salts *in situ* in swollen elastomeric matrix represents a convenient method since it allows to control of size and content of the nanoparticles. For technological applications it is very important to have an information about the size, shape and space arrangement of the nanoparticles in the matrix. SANS suits very well to this purpose. In this project, hydrophilic epoxy networks filled with semiconducting CuO nanoparticles were prepared and their structure investigated by SANS.

Results

First, a series of hydrophilic epoxy networks was prepared by reaction of α,ω-diamino terminated polyoxypropylene-*b*-polyoxyethylene-*b*-polyoxypropylene (POP-*b*-POE-*b*-POP) Jeffamine ED2003 (number average of molar mass: $\overline{M_n}$ = 2000 g/mol) with diglycidyl ether of Bisphenol A propoxylate (PDGEBA). Hydrophilicity of the networks was controlled by initial stoichiometric ratio of reactive groups (amino and epoxy), $r = 2[NH_2]_0/[E]_0 = 1.00$ (EP1), 1.12 (EP2), 1.25 (EP3) and 1.50 (EP4). Nanophase separated structure of these networks consisting of water-rich and water-poor domains has been revealed by SANS [1].

Figure 1. Coherent SANS scattering patterns (coherent scattering intensity I_{coh} vs. magnitude of scattering vector q) obtained from the polymer nanocomposites filled with CuO: a) dry samples,
 b) samples swollen in H_2O.

In the next step, the samples of networks were swollen in aqueous solutions of $CuSO_4$ followed by precipitation of CuO by aqueous solution of KOH. Finally, the samples were washed in distilled water and dried.

The dry epoxy networks filled with CuO were subjected to SANS. Neutron scattering properties of Cu differ very much from the remaining elements present in the system, therefore SANS patterns shown in Fig. 1a reflect the space distribution of CuO particles precipitated in the environment of epoxy network. Scattering intensity is very

high in small q-region and decays monotonically with increasing magnitude of the scattering vector q. Coherent part of intensity scales approximately as $q^{-3.6}$ which corresponds to the scattering by surface fractals with surface fractal dimension $d_S = 6 - 3.6 = 2.4$. This parameter does not change with crosslinking density. Somewhat higher scattering intensity found for filled network EP4 is due to higher swelling degree and consequently higher amount of precipitated CuO in this network.

To get more information about the system, the networks filled were also swollen in H_2O and subjected to SANS to investigate the effect of swelling on the structure of CuO fractal aggregates. As shown in Fig. 1b, swelling causes a drop of the scattering intensity and formation of distinct scattering maximum at $q_{max} \approx 0.08$ Å^{-1} corresponding to the Bragg distance $D_B = 2\pi / q_{max} \approx 80$ Å. In high q-region scattering intensity scales as q^{-4} which corresponds to small CuO particles with compact surface formed by breakdown of fractal aggregates due to swelling of the system. The size of the CuO particles can be estimated roughly as $D_B / 2 \approx 40$ Å which is in good agreement with an estimate from scanning electron microscopy.

References

[1] Krakovský I., Pleštil J., Almásy L.: Polymer 47, 218 (2006)

Objectives *(Aim of the research in some sentences)*

The given experiment was performed as initial study of new type of magnetic fluids, namely functionalized magnetic nanoparticles and microgels which are suitable for applications in biomedicine and magnetic separation. Magnetic nanostructures were designed either as core-shell nanoparticles or microgels by applying procedures using water based magnetic nanofluids and different polymers as starting materials. The goal of present work was to study the structure of the dried magnetic microgel particles. Small-angle neutron scattering was used to find out the structural parameters of magnetic particles and its aggregates.

Results *(Description of concrete results, understandable also for non-experts of the field. Insert, if possible, a typical figure)*

The samples for small-angle neutron scattering (SANS) experiments were prepared using pyrrole monomers substituted with different molecular entities: COOH for FPCo8 and aminoacids for FPile. The dried magnetic particles of FPCo8 and FPile ferrofluids were studied. From SANS data (Fig.1) we can see that powders FPCo8 and FPile show similar structure at the scale 1-100 nm. Specific breaks in the curves at $q \sim 0.47$ and 0.71 nm^{-1}, respectively, makes it possible to use the Guinier approximation. Found parameters of the Guinier approximation are given in Fig.1. One can see that the particles in FPCo8 are larger than in FPile. Expected values of the radii of gyration from the polydispersity function found from EM patterns show larger values, which usually takes place when they are compared to SANS data. The relative difference between particle sizes in the two powders is the same for both the SANS and EM data. Deviations of the initial parts of the SANS curves from the Guinier approximation indicate that some kind of aggregation takes place in the system. At large q-values a power-law type of the scattering decrease is distinguished in both curves. The corresponding exponents point out the irregular surface whose fractal dimension, D_S, can be found as $D_S = 2.24$ for both samples.

Fig.1. SANS curves for samples FPCo8 and FPile. For convenient view the curve FPile is divided by factor of 5. Dashed lines show the Guinier approximations to specific breaks in the curves. Obtained radii of gyration are given. Straight solid lines are of power-law type approximated to the curves at large q-values. The corresponding exponent is shown.

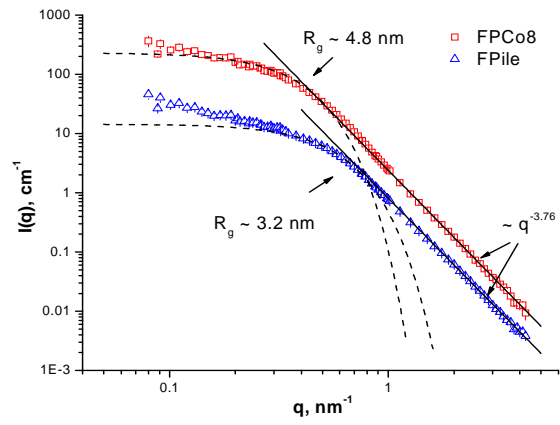| **B N C** **Experimental Report**	*Experiment title* Reorganization of C60 fullerene clusters in N-methylpyrrolidone after addition of various solvents by small-angle neutron scattering	*Proposal No.* BRR_210 *Local contact* N.Szekely
Principal proposer: O.A.Kyzyma, FLNP, Joint Institute for Nuclear Research, Dubna, Russia *Experimental team:* M.V.Avdeev, L.Rosta		*Date(s) of Exper.* May 2009 *Date of Report* Jul 2009

Objectives

It is known that some kind of transition from molecular to colloidal solutions takes place in fullerene solutions depending on the solvent polarity. Always the cluster growth in the discussed solutions is accompanied by the temporal solvatochromism (change in the absorption spectrum with time). The question under study in the present work is at what extent the solvatochromism is determined by the cluster formation. The addition of different solvents into the cluster solution C_{60}/NMP results in some effects, which correlate with reorganization of the initial clusters. The aim of this investigation was to study conditions for appearance of the new clusters after addition into the initial C_{60}/NMP solution various solvents (water, toluene (both miscible with NMP) or neat NMP) by means of small-angle neutron scattering.

Results

The proposed experiment provided the information about changes in the structure and size of fullerene clusters in the systems C_{60}/NMP after addition of various solvents with different polarity (toluene and water). The experimental SANS curves for C_{60}/NMP solution and C_{60}/NMP solutions after addition of toluene and water are presented in Fig.1. Addition of water or toluene leads to cluster reorganization in the system (appearance of the SANS signal in q range 0.1-0.6 nm-1). In contrast, the dissolution of C_{60}/NMP with pure NMP the SANS intensity does not show any increase for all dissolution rates. Vice verse, it decreases in according with the dissolution rate, thus proving that the detected signal is the tale of the scattering curve from large initial fullerene clusters (size up to 500 nm). So, the initial clusters do not change their structure after the dissolution of the system with NMP. Addition of water or toluene results in the formation of clusters with smaller sizes (in a range of 10-100 nm). Since the solvatochromism was observed in all cases of the dissolution (by water, toluene and NMP), the given SANS experiment indicates that the reason for the solvatochromic effects in the system C_{60}/NMP does not relate to the cluster formation, but rather to formation of some complexes between fullerene and solvent molecules.
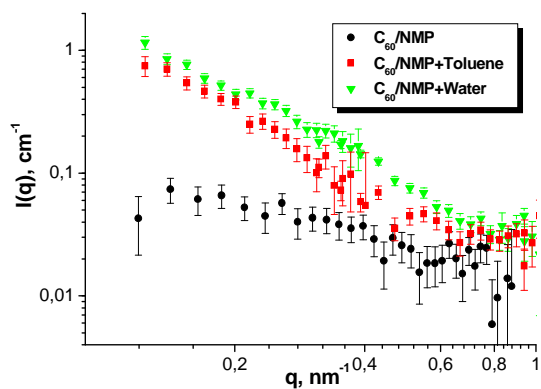
Fig. 1. SANS curves (refered to one concnetration) for C_{60}/NMP solution and C_{60}/NMP solutions after addition of toluene and water.

References *(Published or accepted papers, research reports, conference lectures, seminars etc.)*

1. O.A.Kyzyma, L.A.Bulavin, V.L.Aksenov, et al. *Fullerenes, Nanotubes and Carbon Nanostructures* 16 (2008) 610-615.
2. O.A.Kyzyma, L.A.Bulavin, V.L.Aksenov, et al. *Materials structure* 15 (2008) 17−20.
3. V.L.Aksenov, T.V.Tropin, O.A.Kyzyma, et al. *Phys. Solid State* 52 (2010) 1059–1062.

B N C **Experimental Report**	*Experiment title* Structural study of aqueous and methanolic solutions of methylpyridines	*Proposal No.* BRR_217 *Local contact* L. Almasy
Principal proposer: W. Marczak *Experimental team:* Bozena Czech, Kamila Kielek, Adel Len, Laszlo Almasy		*Date(s) of Exper.* June 2008,March 2009 *Date of Report* January 2011

Objectives *(Aim of the research in some sentences)*

Aqueous solutions have been extensively investigated due to the unique role of water in biological systems. Previous studies suggested strengthening of the three-dimensional structure of water around the molecules of methylpyridine isomers. 2,6-dimethylpyridine molecules interact with water through the O-H...N bonds that leads to formation of 1:1 water – amine complexes in the condensed phases. The clustering of methylpyridine in aqueous solutions probably consists of the association of these complexes rather than the hydrophobic association of the amine. Consequently, the supermolecular structures would depend on the solvent. In the methanolic solutions, the expected association would be weaker. Addition of ionic liquid is expected to influence the association process in both solvents. SANS experiments were performed to compare the magnitudes of the self association of the amines in the different solvents.

Results

SANS experiments have been performed on a series of binary and ternary mixtures at temperature 25C. The results evidence that inhomogeneities are present in heavy water solutions of 2,6-dimethylpyridine, 2-methylpyridine and pyridine at mole fractions of the amines up to 0.25. The scattering curves can be well approximated by the Ornstein-Zernike model:

$$I(q) = A/(1 + q^2 \xi^2) + bg,$$

where *A* is the magnitude of the *q*-dependent coherent forward scattering intensity, ξ is the correlation length of the fluctuations in the scattering length density and *bg* is a constant background term, accounting for the incoherent scattering contribution. The size of the microheterogeneities increases in the following order: pyridine – 2-methylpyridine – 2,6-dimethylpyridine. The stronger are the O–D...N bonds due to the CH_3 groups in the ortho position, the stronger is the co-operativity and the cluster contains more molecules.

An addition of the ionic liquid 1-butyl-3-methylimidazolium-bis (trifluoromethanosulfonyl)-imide to the mixture of 2,6-dimethylpyridine with water leads to the formation of spherical aggregates of layered structure.

Methanolic solutions are homogenous, the scattering curves are almost flat. This observation confirmed indirectly the role of water in the clustering of methylpyridines. Molecule of methanol, although capable of hydrogen bonding with the amines, cannot participate in larger structures because of the lack of protons that could form the next bonds. Thus, even if the amine – methanol complexes occur, they are incapable of further association.

Future prospects

Objectives

Our original objective was to study polyfluorene-polythiopheen block copolymer system. However, the block copolymer system turned complicated and to understand the block copolymer system well we decided to begin our analysie with the individual polythiophene block {poly[3-(6-trimethyl-ammoniumhexyl)thiophene] bromide} (P3TMAHT) in aqueous sodium dodecylsulfate (SDS). We will extend this study later by introducing polyfluorene block connected to P3TMAHT polymer.

Results

The experiment at BRR was very successful. Main findings (structural interplay of P3TMAHT in SDS and the subsequent optical transitions) are outlined in Fig. 1.

P3TMAHT was mixed with SDS or deuterated SDS to form P3TMAHT(SDS)x complex (x=the molar ratio of surfactant over monomer units) in D_2O and studied by small-angle neutron and X-ray scattering (SANS/SAXS) and optical spectroscopy. At room temperature, the phase transitions are observed from charged P3TMAHT aggregates with interparticular order to rodlike (x=1/5) and sheetlike particles (x=1/2-1) where rodlike (x=1/5-1/2) or sheetlike (x=1) polymer chains are embedded. Partial precipitation occurs at the charge compensation point (x=1). Ellipsoid particles, essentially SDS micelles modified by rodlike, dissolved polymer chains take place after this point (x=2-5). Polymer-SDS complexes (x=1/5-5) do not show interparticular order. Free SDS micelles dominate for x=20.

These transitions are followed by distinctive optical changes visibly observable as transitions from pale red (P3TMAHT) to turbid violet (rodlike and sheetlike aggregates) and orange-yellow (ellipsoid aggregates). Overall, the optical transitions are induced by increasing counterion fraction where both sterical and charge balance are changing. These will be interpreted in terms of structural transitions.

Future prospects

We have finished experimental work and are currently preparing a manuscript of this work. We have planned to extend these ideas to block copolymers and thermal measurements.
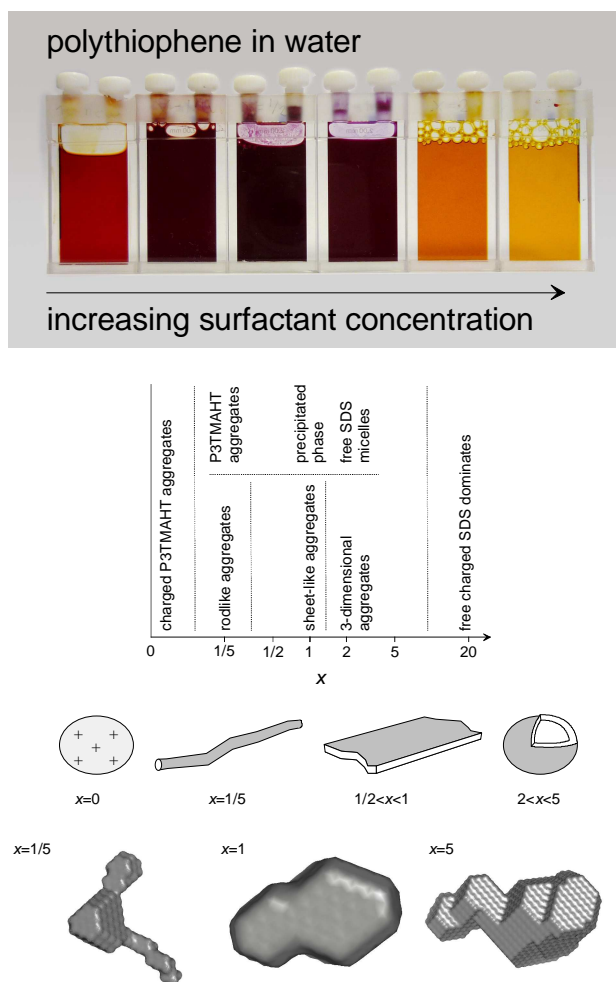

Fig.1. Above: Outlined phase diagram and structures of polymer-SDS particles. Below: Change of visual appearance with the increasing molar ratio *x*.

B N C **Experimental Report**	*Experiment title* SANS study of the structure of swollen copolymer networks	*Proposal No.* BRR-224 *Local contact* Noémi K. Székely
Principal proposer: Ivan Krakovský, Department of Macromolecular Physics, Faculty of Mathematics & Physics, Charles University, Praha, Czech Republic *Experimental team:* Noémi K. Székely		*Date(s) of Exp.* Oct 2009 *Date of Report* Jan 2010

Objectives

The goal of the experiment proposed is SANS study of the structure of block copolymer polymer networks swollen in selective solvents. The solvents used (CD$_3$OD) and (D$_2$O) differ in interaction with hydrophobic and hydrophilic blocks built in the networks.

Results

A series of copolymer epoxy networks was prepared by end-linking reaction of α,ω-diamino terminated poly(oxypropylene)-*b*-poly(oxyethylene)-*b*-poly(oxypropylene) (POP-POE-POP) Jeffamine ED600 (number average of molar mass: $\overline{M_n}$ = ca 600 g/mol), and diglycidyl ether of Bisphenol A propoxylate (PDGEBA) at various initial ratio of reactive groups $r=2[NH_2]_0/[E]_0$.

The networks prepared were swollen to equilibrium in deuterated methanol (CD$_3$OD) and heavy water (D$_2$O), respectively. Whereas methanol is good solvent for all the blocks built into the network (POE, POP and PDGEBA), water is good solvent for POE only. Consequently, SANS patterns of the networks swollen in CD$_3$OD and D$_2$O differ significantly as illustrated in Fig. 1. In methanol the scattering is governed by frozen and dynamic inhomogeneities, respectively, due to network connectivity and thermal movement of polymer segments [1]. By contrast, in water these contributions to SANS are superimposed
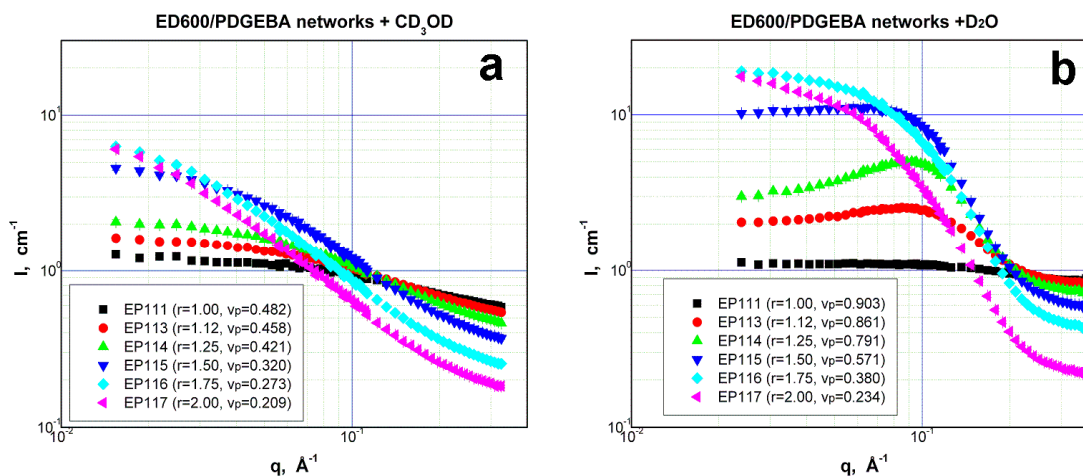
Figure 1 SANS scattering profiles obtained from the epoxy networks swollen to equilibrium in CD$_3$OD (a) and D$_2$O (b) at 25 ^{o}C, v_p denotes polymer volume fraction in swollen networks.

by inhomogeneities due to nanophase separation of the system into water-rich and water-poor domains [2]. A similar system prepared using much longer POE block in the diamine was investigated by us using SANS previously [2]. SANS patterns obtained from the copolymer epoxy networks swollen in D$_2$O were fitted well by Percus–Yevick model approximating structure of the system by dispersion of water-poor nanodomains of spherical shape in water-rich matrix. For the system studied in this project, it was found that the Percus-Yevick model fails in fitting SANS data. Another model, namely Teubner–Strey model

[3] based on different geometry of nanophase separated structure - locally lamellar order of nanophases – proved to be successful. Characteristic length of the structure as estimated from the position of scattering maxima in Fig. 1 is of the order of tens Å and increases with deviation of the network structure from perfect one expected for r=1.

Formation of the locally lamellar order can be attributed to the conservation of polymer network topology (linear chains of PDGEBA) and shorter length (lower content) of hydrophilic POE blocks in the epoxy networks.

References

[1] M. Shibayama: Bull. Chem. Soc. Jpn. 79, 1799 (2006)
[2] I. Krakovský, J. Pleštil, L. Almásy: Polymer 47, 218 (2006)
[3] M. Teubner, R. Strey: J. Chem. Phys. 87, 3195 (1987)

Objectives In photosynthesis, light energy is harvested by antenna complexes, which 'funnel' the excitation energy from the absorption of the 'dilute' photon flux to the photochemical reaction centers, the primary site of energy conversion. This is followed by a series of vectorial electron and proton transport. In green plants, this complex process occurs in a multilamellar membrane system. The system is constituted by essentially identical thylakoid membranes, a highly organized, laterally heterogeneous system consisting of stacked granal and unstacked stroma thylakoid membranes, which embed a large number of pigment-protein complexes and different redox components. Higher plant thylakoid membranes contain a protein kinase that phosphorylates certain threonine residues of LHCII, the main light-harvesting antenna complexes of photosystem II (PSII).

In this project we planned to investigate by small angle neutron scattering how phosphorylation of LHCII affects the dynamic architecture of the thylakoid membranes.

Results Intact thylakoid membranes were freshly isolated from *Pisum sativum* grown for 10-12 days in the greenhouse. Thylakoids were suspended in buffer, containing 50 mM Tris-HCl (pH 7.6), 10 mM NaCl, 10 mM $MgCl_2$, 10 mM NaF in D_2O, and were used within 10 min for phosphorylation or were stored on ice in this medium.

In the native photosynthetic system of higher plants the reduced state of the plastoquinone pool activates the kinase enzyme which is responsible for the LHCII phosphorylation. The reduced state of the plastoquionone pool can be achieved by illumination. However, in this project we used duroquinol induced phosphorylation, where duroqionol (in a final concentration of 4 mM) reduced the plastoquinone pool. ATP required for the phosphorylation was present in the phoshporylation buffer in 0.2 mM concentration. In order to differentiate between the effects of different treatments we investigated the membrane ultrastructure of thylakoids without duroquinol and ATP, in the presence of duroquinol and in the presence of duroquinol and ATP.

Neutron wavelength was set to 7.51 Å, sample detector distance was 5.6 m. In order to increase the signal to noise ratio and reduce the measuring time, samples were oriented with a magnetic field of ~ 0.7 T, oriented perpendicular to the neutron beam. Measuring time was 30 min for each sample. Structural information was obtained from radially averaged scattering curves (presented in Figure 1), after performing the usual background subtraction. The sum of a Gaussian and a power function was fitted for the scattering data as a function of the scattering vector, q. The former was accounted for the Bragg peak of the multilamellar membrane system, in this q range, of the stroma thylakoids, while the power function was ascribed to the polydispersity of the suspension. The characteristic repeat distances of the multilamellar system were calculated taking 2π over the q values corresponding to the peak position value of the Gaussian.

The measurements revealed significant, albeit not very large changes in the scattering. As obtained from the fits, the average repeat distances increased from 27.9±0.6 nm in the control to 31.0±0.7 and 30.7±0.1 nm in the duroquinol-treated and phosphorylated membranes, respectively (n=5). This increase in the repeat distances by duroquinol treatment can most probably be accounted for by a moderate swelling of the stroma thylakoid membranes. Results also show that phosphorylation resulted in ~ 20% decrease of the intensity of the Bragg peaks, suggesting decrease in the membrane order and corresponding decrease in the orientability. This latter effect was also observed in fluorescence polarisation experiments.
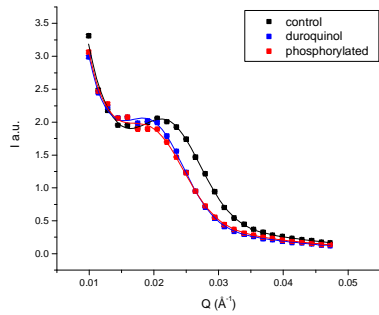
Fig. 1.: Radially averaged small angle neutron scattering curves from control, duroquinol treated and phosphorylated thylakoids. Continuous lines show the fitted model curves.

Reference The obtained results were published in „Effect of phosphorylation on the thermal- and light-stability of the thylakoid membranes, Zsuzsanna Várkonyi, Gergely Nagy, Petar Lambrev, Anett Z. Kiss, Noémi Székely, László Rosta and Gyözö Garab, Photosynthesis Research, Volume 99, Number 3, 161-171"

Future prospects The experiment revealed that SANS is a suitable technique to investigate structural changes in complex multilamellar membrane systems. Further experiments are being performed or planned in order to reveal the reorganizations of the thylakoid membrane systems in different wild type and mutant organisms during photosynthesis.

B N C **Experimental Report**	*Experiment title* SANS study of calcium silicate ceramics synthesized with acid catalysis	*Proposal No.* SANS_08_02_IH *Local contact* Anikó Meiszterics
Principal proposer: Anikó Meiszterics *Experimental team:* Anikó Meiszterics		*Date(s) of Exper.* February 2008 *Date of Report*

Objectives

In the present work the structure of calcium silicate synthesized with acid catalysis were studied by SANS. The changes in their supramolecular structure were followed in the function of temperature.

Results)

The acetic acid catalyst yields a very loose structure, the slope of the SAXS curves in log-log plot is close to -2 (Fig. 1). The SAXS investigations prove an open randomly branched structure for wet Ca silicate gel samples produced with acetic acid catalyst.

In the dried Ca silicate materials, aggregate structures can be identified (Fig. 1). The loose open randomly branched structure turns into a compact structure during the heat treatment. The rough surfaces of aggregates can be characterized with 2.2 – 2.6 surface fractal dimensions. The surface of aggregates becomes less rough by rising the temperature of heat treatment. The aggregates heated at 1300 °C have got completely smooth surface (Fig. 1).

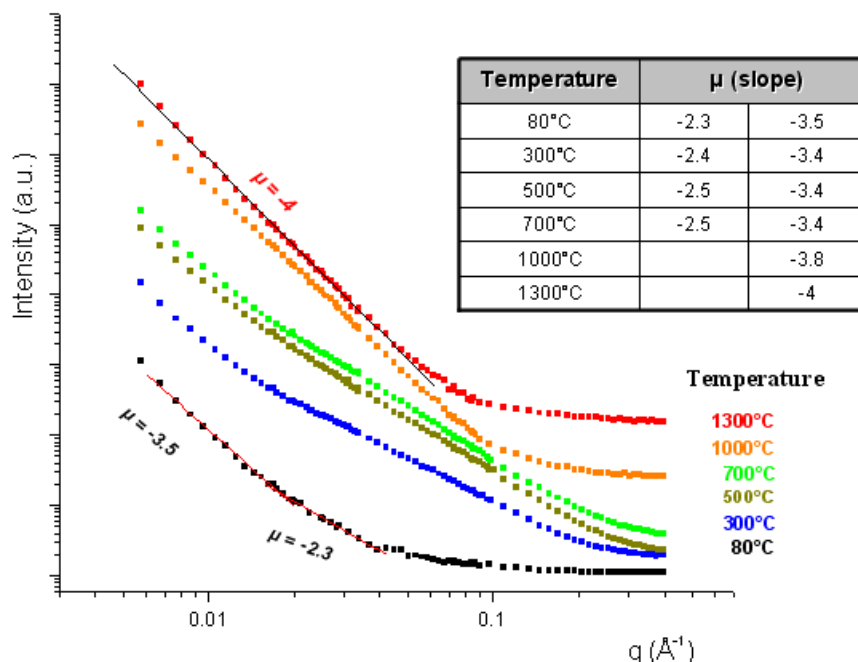| Temperature	μ (slope)	
80°C	-2.3	-3.5
300°C	-2.4	-3.4
500°C	-2.5	-3.4
700°C	-2.5	-3.4
1000°C		-3.8
1300°C		-4

Fig. 1. SANS curves for calcium silicate samples prepared with acetic acid catalyst

Objectives

Carbon nanotubes (CNTs) possess exceptional intrinsic mechanical and electronic properties, which makes them appealing as filler materials for nanocomposites. The expectations are the substantial enhancement in toughness, even at low filler loadings, as well as low percolation thresholds for electrical conductivity. Although these expectations were partially fulfilled, there are several limiting factors that make the CNT reinforced composites not to be able to fully exploit the potential offered by nanotubes. The substantial improvement of nanotube dispersion, as well as enhancing the interfacial load transfer, constitutes the key issues. However, while the load transfer between nanotubes and the matrix can be relatively easily improved by attaching functional groups to the nanotubes, unfortunately low dimensional nanoscale fillers are more difficult to disperse. Therefore, it is of particular importance to understand well the nature and structure of nanotube aggregates in the host matrix. Characterizing the dispersion of CNTs in ceramic composites by global methods is mandatory in order to understand in detail the structure of these composites. However, such a global characterization method has not yet been established. The dispersion of nanotubes in ceramic matrices is usually investigated by scanning electron microscopy (SEM) of fracture surfaces or transmission electron microscopy of thin slices from the composite. Although these methods are able to give some estimates about the dispersion grade of nanotubes and the typical size of the aggregates, the provided information is local and partial we lack the third dimension since only surfaces or very thin (100 nm) slices are imaged. Consequently, these methods provide little information about the internal structure of the aggregates themselves.

In this measurement, we applied neutron scattering experiment to deliver information about the global dispersion of nanotubes throughout the whole sample volume.

Results

The composite samples containing 3 wt % of single-walled carbon nanotubes (SWCNTs) were prepared by hot isostatic pressing at 1700 °C and 20 MPa. For a better dispersion of nanotubes, the powder mixtures together with the nanotubes were milled in a high efficiency attritor mill for 5 h before sintering. The SANS measurements were performed at the cold neutron research facility of the Budapest Neutron Centre. The Si_3N_4 ☐SWCNT samples were introduced in the SANS diffractometer with a sample to detector distance of 5.6 m and measured with a wavelength of 11.52 Å under ambient conditions. In order to investigate solely the dispersion of CNTs, we performed SANS measurement also after the nanotubes were burned out of sample. The plot in Fig. 1 shows the difference of the two measurements. This way we could get rid of the influence of scattering from porosities or other inhomogeneities intrinsic to the Si_3N_4 matrix. In the

case of interest for us, the scattering intensity usually obeys a power law behavior with an exponent that gives information on the dimensionality of the scatterers, which can also be a noninteger for disordered systems.

Based on the experience of SANS measurements of CNT dispersions in solutions and polymers, it is known that depending on their concentration, CNTs usually form loose disordered three dimensional networks. In this latter case the observed slopes range between values of -2 and -3, which correspond to disordered mass fractal distributions. However, for Si3N4 composites we measured slope values of -3.8 and -3.2, as can be seen from Fig. 1. These values not only indicate a quantitative difference but also a qualitative one since they no longer correspond to mass fractals but rather to surface fractals. A natural interpretation of this surface fractal behavior is that CNTs are surrounding the silicon nitride crystallites of the matrix, forming entangled networks on the surface of the grain boundaries. Indications that CNTs are disposed to assemble at grain boundaries have already been published based on the electron microscopy investigation of Al_2O_3 which is in good agreement with our results. What is more important is that our method provides a global characterization for the nanotube dispersion; therefore, we can conclude that the predominant majority of the CNTs in the silicon nitride matrix are located in positions surrounding grain boundaries. This model of nanotube networks surrounding grain boundaries also explains why these surface fractal behaviors are absent in SANS measurements of CNTs dispersed in solutions or polymer matrices, since grain boundaries only occur in crystalline materials. Furthermore, the breakpoint on Fig. 1 connecting the two lines with different slopes at the wave number value of 0.02 A^{-1} gives us the characteristic mesh size of 30 nm for the nanotube network entangled around a crystalline grain.

Based on these data we constructed a schematic model of CNT dispersion in Si_3N_4 matrices, which is shown in Fig. 1. Of course isolated CNTs can also be present in the sample but since neutron scattering is sensitive to the square of the mass, it is difficult to detect small objects in the presence of larger ones. One also has to be aware that our SANS measurements provide information on the 1–100 nm length scale. Ceramic grains and nanotube aggregates much larger than 100 nm are also present in the samples; however in order to characterize these features, ultrasmall angle neutron scattering experiments have to be performed.
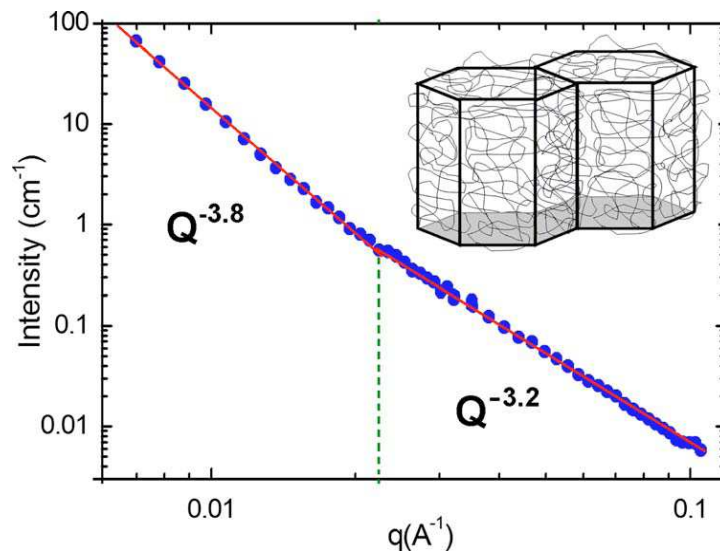
Fig. 1. Color online_ SANS spectra of Si_3N_4 □SWCNT nanocomposite revealing a power law behavior with decay rates indicating the surface fractal behavior of the nanotubes dispersed in the ceramic matrix. The inset shows the schematic structural model of Si_3N_4 □SWCNT nanocomposite constructed based on SANS data. The hexahedrons represent the Si_3N_4 crystallites, while the entangled curves represent the nanotubes surrounding them.

References

Orsolya Koszor, Levente Tapasztó, Márton Markó, and Csaba Balázsi, "Characterizing the global dispersion of carbon nanotubes in ceramic matrix nanocomposites" APL, 93, 201910 _2008_

Objectives

In the present work the structure of calcium silicate gel and ceramic systems were studied by SANS and compared with SAXS data. Their structural change dependence on ammonia concentration and temperature was observed.

Results

The supramolecular structures were studied by SAXS and SANS. The scattering data present in the samples synthesized under basic conditions are built up from aggregates (Figure 1). The aggregate structure is defined here as a random packing of colloidal particles. The SAXS and SANS curves follow the Porod`s law: The slope of the curves in a log-log plot is close to -4 (Table 1), which indicates large aggregated structures (Figure 1). The surface of the aggregates obtained by drying at 80 ºC is possibly slightly rougher with an increasing amount of NH_3 catalyst considering the slightly lower value for the slope in the log-log plot. However, in the size range above 50 nm, only aggregates with smooth surfaces can be confirmed by SANS (Table 1). A broad maximum can be observed in the SAXS curves for calcium silicate samples dried at 80 ºC (Figure 1, left image). The intensity of maximum increases and its position shifts to smaller q-values by rising molar ratio of NH_3. This indicates a growth of scattering units in a more basic medium.

If the systems are heat treated at 700 ºC, the elementary units are 3-D compact particles of 20-23 nm size, independent from the catalyst (Table 1). The heating leads to a slightly rougher surface visible by the slope differing from -4 in the log-log curve (Figure 1, right image). At lower molar ratios of NH_3, this seems to be more efficient (SANS curves in Figure 1). The size of the aggregates of elementary units obtained by heating at 700 ºC can not be determined with small angle scattering, as its size is larger than 100 nm.

References

A. Meiszterics, L. Rosta, H. Peterlik, J. Rohonczy, S. Kubuki, P. Henits, K. Sinkó, J. Phys. Chem. A, 2010. **114**, 10403

Table 1 Result of SAXS and SANS evaluation

Molar ratio of **NH₃ / Si**	SAXS				SANS	
	80 °C[1]		700 °C[1]		80 °C[1]	700 °C[1]
	slope[2]	size of elementary units (nm)	slope	size of elementary units (nm)	slope	slope
0.5	-4.0 ±0.05	– [3]	-3.7; -4.0[4]	20 ±1	-4.0 ±0.05	-3.2

1.0	-3.9 ±0.05	–[3]	-3.7	20 ±2	-4.0 ±0.05	-3.4
2.0	-3.9 ±0.05	–[3]	-3.4; -4.0[4]	20 ±3	-4.0 ±0.05	-3.4
3.0	-3.8 ±0.05	15 ±2	-3.4; -4.0[4]	23 ±2	-4.0 ±0.05	-3.6
5.0	-3.8 ±0.05	18 ±2	-3.4; -4.0[4]	23 ±1	-4.0 ±0.05	-3.7
10.0	-3.7 ±0.05	23 ±1	-3.5; -4.0[4]	20 ±2	-4.0 ±0.05	-3.8

[1]The gel samples were heat treated at 80 and 700 ºC, respectively.
[2]The slope of SAXS curve
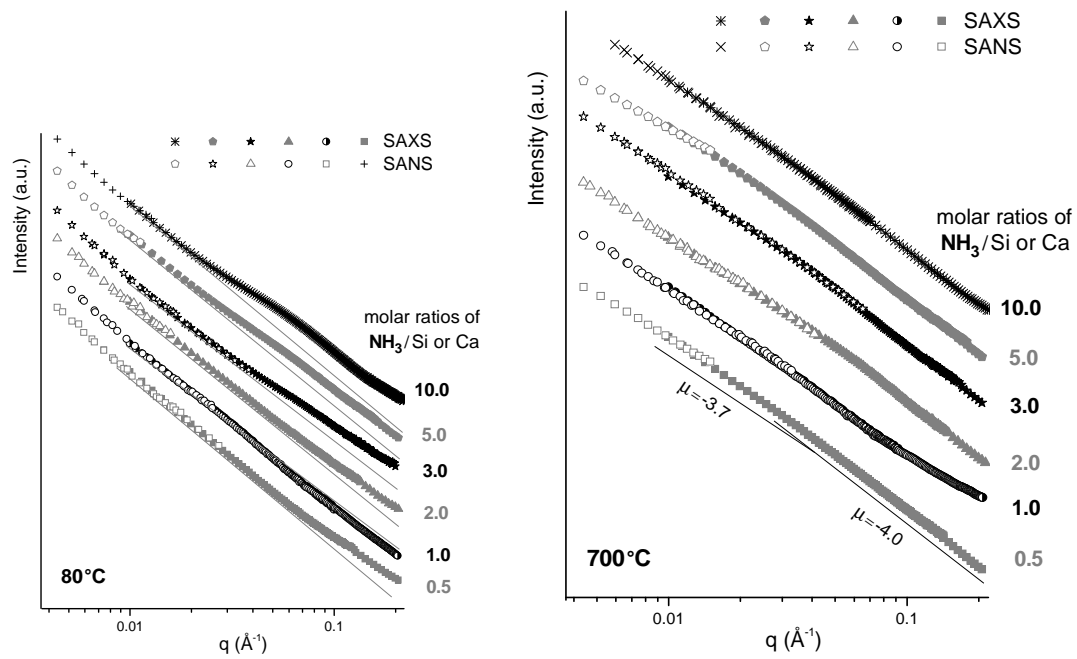
Fig. 6. SANS and SAXS curves for calcium silicate samples prepared with different NH_3 ratios and dried at 80˚C and 700˚C.

Objectives

The given experiment was performed as a continuation of the study of factors determining the stability of ferrofluids. The goal of the present work was to study the behaviour of free mono-carboxylic acids used in the stabilization of ferrofluids in non-polar solutions (d-decalin). Unsaturated bent oleic (OA) and saturated linear myristic (MA) and stearic (SA) acids were studied by small-angle neutron scattering (SANS) to find out the character of interaction in the system, as well as structural parameters of acids in the solution. Then, the interaction between acids was compared with that in d-benzene, which is actively used in non-polar ferrofluids either.

Results

The concentration of OA, MA and SA in d-decalin was varied in a range of 2-30 vol. %. The weak scattering from single acid molecules (Fig.1,a,b) was analyzed in terms of the Guinier approximation, which allowed to plot the forward scattering intensity and radius of gyration as a function of the surfactant concentration similar to d-benzene solutions [1]. The concentration increase for MA and SA results in vigorous growth of solution viscosity followed by the formation of a new jelly-like phase. We associate this effect with the transition into the liquid crystalline state, which is well-known in thermodynamics of stiff rod-like polymers. This transition starts at concentrations higher than 2 vol. % in SA solutions (Fig.1,c) and at concentrations higher than 10 vol. % in MA solutions (Fig.1,b). The characteristic size of aggregates (deviation from the Guinier law at small q values) can be roughly estimated as ~10 nm. For OA solutions no transition into the liquid crystalline state was observed in both benzene and decalin.
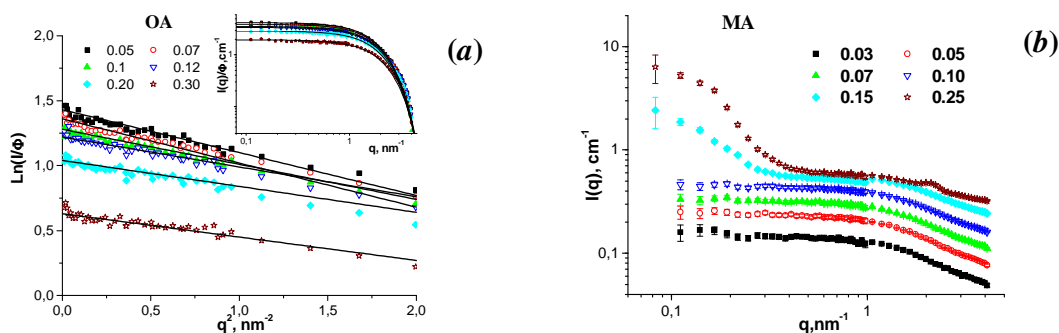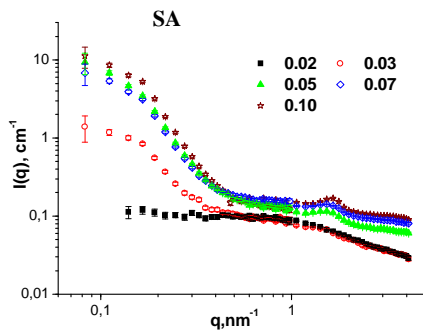
Fig.1. Experimental SANS curves from solutions of OA (*a*) (isotropic solutions); MA (*b*) and SA (c) (nematic-isotropic phase transition) in d-decalin. The curves are shown in absolute scale. Solid lines in (*a*) correspond to Guinier approximations.

References *(Published or accepted papers, research reports, conference lectures, seminars etc.)*
1. V.I.Petrenko, M.V.Avdeev, L.Almasy, et al. *J. Col. Surf. A* 337 (2009) 91.

B N C **Experimental Report**	*Experiment title* **SANS study of the elastomers filled with semiconducting nanoparticles**	*Proposal No.* SANS_2008_05_IC *Local contact* Noémi K. Székely
Principal proposer: Ivan Krakovský**,** Department of Macromolecular Physics, Faculty of Mathematics & Physics, Charles University, Praha, Czech Republic *Experimental team:* **Noémi K. Székely**		*Date(s) of Exp.* Dec 2008 *Date of Report*

Objectives

The goal of the experiment proposed is SANS study of the changes of structure which occur in first step of preparation of elastomers filled with semiconducting CuO particles.

Results

A series of copolymer epoxy networks was prepared by end-linking reaction of α,ω-diamino terminated poly(oxypropylene)-*b*-poly(oxyethylene)-*b*-poly(oxypropylene) (POP-POE-POP) Jeffamine ED600 (number average of molar mass: $\overline{M_n}$ = ca 600 g/mol), and diglycidyl ether of Bisphenol A propoxylate (PDGEBA) at various initial ratio of reactive groups $r=2[NH_2]_0/[E]_0$.

These networks were first swollen in $CuSO_4$ solutions in D_2O to prepare semiconducting nanoparticles of CuO in situ by precipitation with NaOH in the next step. Influence of CuSO4 concentration on the structure of the system was investigated.

Figure 1 shows changes of SANS patterns of one representative system (r=1.12) swollen in 0.1 M CuSO4 solution with time. Nanophase separation of the system into water-rich and water-poor domains has been revealed. The scattering peak moves to higher q-values, due to a slow diffusion of Cu^{2+} ions from water-rich to water-poor phase and complex formation with nitrogen atoms in the latter phase.

ED600/PDGEBA (r=1.12) in 0.1 M $CuSO_4$/D_2O
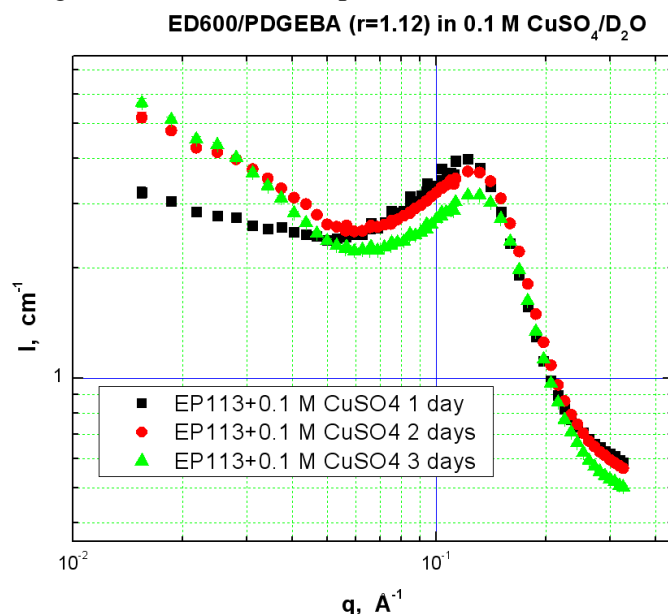
Figure 1 SANS scattering profiles of epoxy network EP113 swollen in 0.1 M CuSO4 in D_2O at different times.

Shift of scattering peak to higher q-values with increasing concentration of CuSO4 in the swelling solution was observed.

The results obtained were used in preparation of the systems studied later (see report BRR-207).

Comparison of the scattering curves of the non thickened and thickened samples having the same Ca content yielded significant differences in the pore structure of the thickened (exponent ~ 3.7) and non-thickened (exponent ~ 4) samples (see Fig. 1). One can say that the thickening process has a big influence on the inner structure of the aluminium foam precursors. Exponents of the fitted model curves indicated their fractal structures which conformed to the results obtained by optical microscopy but volume fractions could not be exactly determined because the scattering vector, q range, of the diffractometer was not wide enough towards the low q values (see Fig. 1).

Future prospects *(Summary of the remaining problems to be solved, basis for the continuation of the work)*
USANS measurements are going to be carried out in order to determine the specific surfaces.

B N C **Experimental Report**	*Experiment title* Structural study of ferrofluids prepared by different methods	*Proposal No.* SANS_2009_02_IC *Local contact* L. Almásy
Principal proposer D.E. Creanga *Experimental team* C. Nadejde, L. Almásy		*Date of Experiment* June 2009 *Date of Report* February 2011

Objectives

Suspensions of magnetite nanoparticles coated with oleic acid were obtained by applying two preparation methods, chemical co-precipitation of salt precursors and wet milling of micron size magnetite powder. The aim of the study is to compare the benefits and disadvantages of each methods regarding the ease of the preparation of the magnetic fluid, its quality. The fluids are characterized by various physico-chemical methods, densitometry, magnetization, X-ray diffraction, electron microscopy. Small angle neutron scattering is performed in order to assess the size and size distribution of the magnetite particles, and the quality of the fluid with respect to particle aggregation.

Experiments

Measurements of the original suspensions as well as suspensions diluted fivefold by kerosene have been measured at three instrument configurations, at room temperature. The concentrations of the original suspensions were about 2 percents in volume, according to densitometry data. The scattering intensities were analyzed by model of non interacting spherical scatterers, with a log-normal size distribution. The mean diameter of the particles in the two samples was 8.3 and 11.0 nm, and the polydispersity about

Fig. 1. SANS scattering data for colloidal dispersions of surfactant coated magnetite particles in kerosene. Solid curves are fitted models of spherical particles with log-normal size distribution.

0.30. Data for both samples follow the model behavior at intermediate and high scattering angles. At low angles a rather strong deviation from the theoretical model is seen for the sample prepared by co-precipitation, indicating the presence of an appreciable amount of aggregated particles.

References

1. C. Nadejde, D.E. Creanga, L. Almásy, M. Ursache-Oprisan, N. Apetroaie, V. Badescu

Experiments regarding the role of magnetic/non-magnetic stirring in the process of ferrophase preparation for stable magnetic fluids. Poster presented at conference TNT 2009, Trends in Nanotechnology, Barcelona, 2009.
2. D.E. Creanga, C. Nadejde, L. Almásy, E.V. Pomjakushina , M. Ursache-Oprisan: Chemical method versus wet milling in the preparation of soft magnetic colloids. Submitted to physica status solidi a.

B N C **Experimental Report**	*Experiment title* New 2D detector characterisation measurement	*Proposal No.* ATHOS_09_01_IH *Local contact* Gy Torok
Principal proposer:J. Orban, L.Cser *Experimental team: J. Orban, L.Cser, Gy. Török*		*Date(s) of Exper.* *Date of Report*

Objectives

In order to develop the neutron spectrometer's efficiency a two-dimensional position sensitive multi-wire prototype neutron detector has been designed and constructed at the Budapest Neutron Centre (BNC). The prototype is a ^{3}He and CF_4 filled position sensitive detector, with a sensitive area of 800 x 500 mm^2, having an average vertical position resolution of 3.8mm, horizontal position resolution of 3 mm and efficiency >74% at neutron wavelength λ=3.14 Å. The detector has a delay-line type readout. The electronic signals are digitized by a constant fraction discriminator and measured by a time-to-digital converter. For using this detector is necessary to measure the full characteristic of setup.

Results

We characterised this detector using the monochromatic beam of Athos instrument. The efficiency, position linearity, position resolution and effect of anode wires has been measured. The efficiency has been measured by a comparison using a reference, black detector tube. Other parameters have been measured by a 0.5 mm wide cadmium slit and a precision moving table.

The obtained value of the efficiency is 74.2±0.2 % at the neutron wavelength 3.14 Å.
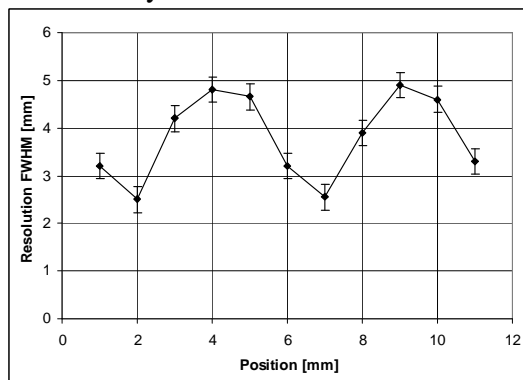
The vertical position resolution versus the relative slit position
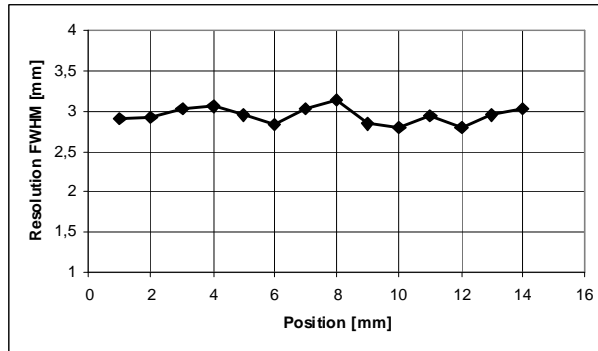
The horizontal resolution versus the relative slit position

The position resolution is mainly determined by the pressure of CF_4 limiting the ionization ranges of the charged particles. In our case the average longitudinal path range of the proton is 3.7 mm while that of the triton is 1.4 mm. A strong modulation is observed in vertical direction, due to the anode wire spacing, because the avalanche is created only close to the anode wires. As the anode wires are represented by continuous lines in the other direction, the horizontal resolution is more uniform. The average vertical position resolution is equal to 3.8 mm FWHM while the horizontal resolution is equal to 3 mm which values correspond to the expected ones.
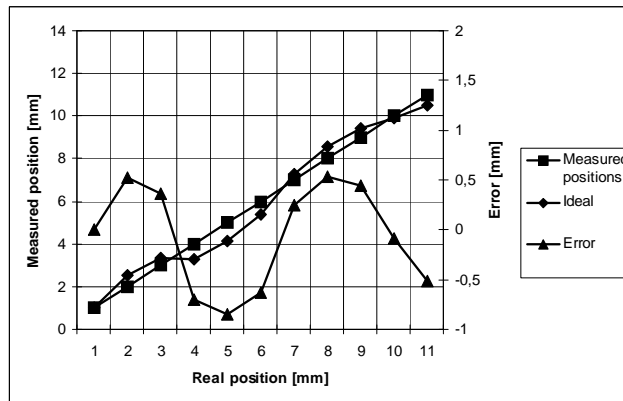
The result of the vertical position linearity: The slit position obtained from the measurement versus the real slit position, the error of the position linearity is modulated by the spacing of the anode wires
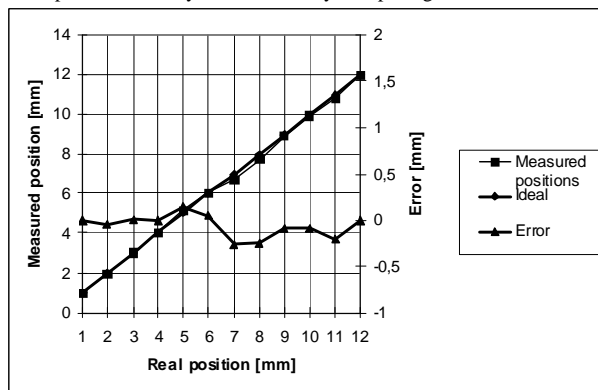
The result of the horizontal position linearity: The slit position obtained from the measurement versus the real slit position, the error of the position linearity is obviously not modulated by the discrete distribution of the anode wires

191

The position linearity has been also investigated (see Fig. 4 and Fig. 5). The anode wire spacing influences also the linearity accordingly the error of the position linearity is less in horizontal direction than vertical resolution. The maximum error is 0.67 mm vertically, 0.23 mm horizontally. The average of the absolute value of the error is 0,46 mm vertically and 0,1 mm horizontally.

References

Design and experimental results of a large, position sensitive, multi-wire prototype detector developed at BNC,
J. Orban, L. Cser, L. Rosta, Gy. Török and A. Nagy, Nuclear Instruments and Merthods A, Vol. 632, No. 1, 11 March 2011, Pages 124-127

Future prospects

We intend to optimize the anode wire spacing in order to decrease the fluctuation of the position resolution and position linearity orthogonally to the anode wires i.e. in the vertical direction.

6. INSTRUMENTS

6.1. NEUTRON CAPTURE GAMMA-RAY FACILITIES

Two instruments are located at the end position of the neutron guide NV1 – the prompt gamma activation analysis (PGAA) facility and the neutron induced prompt gamma-ray spectroscopy (NIPS) facility. The PGAA is used for non-destructive elemental analysis of samples by observing neutron-capture prompt gamma rays while the NIPS is designed for a wide range of experiments that involve nuclear reaction-induced prompt and delayed gamma radiations that include γ-γ-coincidences, neutron radiography, tomography, large-sample PGAA, as well as Prompt-Gamma Activation Imaging (PGAI).

The neutron guides have been recently upgraded with $2\theta_c$ supermirror guides [1] that improved the thermal-equivalent neutron fluxes at the PGAA and NIPS sample positions to 1.2×10^8 cm^{-2} s^{-1} and 4×10^7 cm^{-2}s^{-1}, respectively. Both beams are individually collimated to a cross-section of 2×2 cm^2 and the intensity of the incoming neutron flux is monitored and recorded with an ORDELA Model 4511 N neutron detector throughout the whole reactor campaign [2]. The spatial distribution of the beam flux is illustrated in Figure 1.
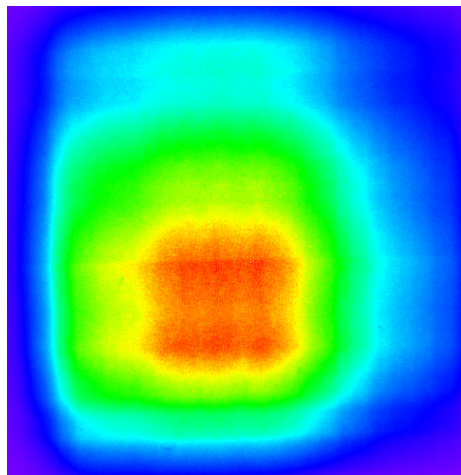
Figure 1. The 2×2 cm^2 collimated neutron flux profile at the sample position of the NIPS facility taken with a neutron radiograph equipment

For special experiments, a pulsed beam can also be used. Modulation in the order of milliseconds can be done by a revolving chopper blade [3], while longer on-off periods can be achieved with a fast beam shutter [2].

The experimental area is a 3×5 m^2 space at the rear end of the guide hall (see Figure 2). The neutrons enter the bunker and fly along the 3 m long evacuated aluminum tube across the experimental area, to the beam stop placed at the rear wall of the guide hall. The guided beam is divided into an upper and a lower beam. A pneumatic instrument shutter is used to control the entry of the neutron beam into the bunker while two computer-controlled secondary shutters are provided to allow independent operation of the two facilities. All sections of the modular aluminum flight tube can be easily removed

and reinstalled as needed. Collimators of appropriate sizes are used for the two beams. At present, the upper beam is used for PGAA measurements while the lower beam is used for NIPS experiments.

The PGAA target chamber is at 1.5 m distance from the end of the guide. A mechanism to create vacuum or gaseous atmosphere in the sample chamber is provided to decrease beam-induced background. To prevent scattering of neutrons to the PGAA sample from the lower beam, a layer of neutron absorber is placed below the sample. The targets are mounted to thin Al frames by Teflon strings. Optionally, an automated sample changer with a capacity of 16 samples can be used [2]. A neutron absorber beyond the PGAA target chamber stops the upper beam.

The NIPS station is positioned 1 m away from the PGAA station along the flight tube. This flexible setup can be used for several configurations. If several detectors are to be placed close to the sample, a narrow aluminum tube with the sample chamber is available. For measuring voluminous samples and scanning experiments, a 20×20×20 cm^3 sample chamber is used. If custom devices are to be built into the beam, a short flight tube without a sample chamber is the proper choice.

In addition to the in-beam facilities, a low-level counting chamber is also operational [2]. It has a background of about 1.5 cps and allows the accurate (off-line) measurement of the induced radioactivity.
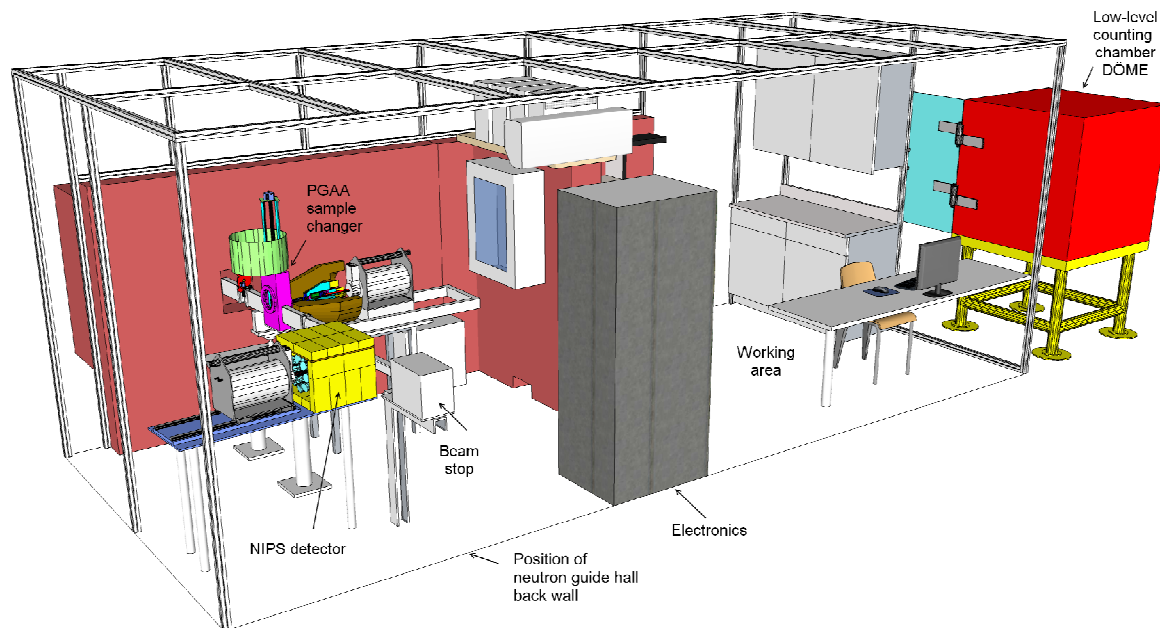
Figure 2. Layout of the PGAA-NIPS experimental area

6.1.1. The PGAA facility
Instrument reeponsible: Zsolt Révay

When a nucleus captures a neutron, the binding energy of the neutron is promptly emitted in the form of gamma radiation. This radiation is characteristic, in that the

195

energies of the gamma photons are specific to the nucleus, while their numbers are proportional to the quantity of that nuclide. By analyzing the energy spectrum of the emitted prompt gamma radiation, the isotopic and elemental contents of the irradiated sample can be determined. This is the essence of the prompt gamma activation analysis method.

The basic instrument of the PGAA facility consists of an n-type high-purity germanium (Canberra HPGe 2720/S) main detector with closed-end coaxial geometry, and a BGO Compton-suppressor surrounded by a 10 cm thick lead shielding. The sample-to-detector distance is adjustable, but it is typically 230 mm. By removing the front detector shielding the HPGe main detector can be placed as close as 12 cm to the target.

The BGO annulus and the catchers around the HPGe detect most of the scattered gamma photons. If the events from the HPGe and the BGO are collected in anticoincidence mode, Compton-supressed spectra can be acquired. With appropriate electronic gating, the HPGe-BGO gamma spectrometer can be also be used in annihilation-pair mode. An analogue or a digital spectroscopy amplifier can be used, depending on the preference of the user in terms of energy resolution and throughput. An Ethernet-based multichannel analyzer module (Canberra AIM 556A) with 2×16k memory collects the counts.

A user-friendly facility control program, "*Budapest PGAA Data Acquisition Software*", has been written for manual, semi-automatic, and unattended automatic batch measurements. This program controls the beam shutters, the sample changer and the data acquisition.

A schematic drawing of the sample chambers and the HPGe-BGO detector assembly is shown in Figure 3. The main parameters of the PGAA system are collected in Table 1.
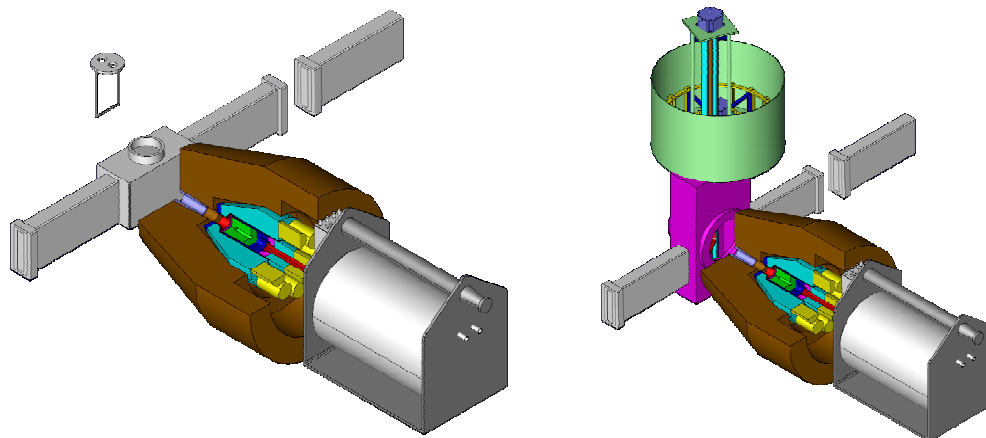
Figure 3. The PGAA facility, with the standard sample chamber (left)
and with the automated sample changer (right)

Table 1. Specifications of the PGAA facility

Beam tube:	NV1 guide, end position
Distance from guide end	1.5 m

beam cross section:	2×2cm^2, 1.4×1.4cm^2, 1×1cm^2, 42mm^2, 23mm^2, 10mm^2, 5mm^2, 1 mm wide slit
Thermal-equivalent flux at target:	$\approx1.2\times10^8$ cm^{-2}s^{-1} (in vacuum)
Vacuum in target chamber (optional):	≈1 mbar
Target chamber Al-window thickness	0.5 mm
Form of target at room temperature:	Solid, powder, liquid, gas in pressure container
Target packing at atmospheric pressure:	sealed FEP Teflon bag or vial
Activity of target after irradiation:	negligible
Largest target dimensions:	$4\times4\times10$ cm^3 / $7\times7\times0.5$ cm^3
γ-ray detector	n-type coax. HPGe, with BGO shield
Distance from target to detector window:	230 mm
HPGe window:	Carbon epoxy, 0.5 mm
Relative efficiency:	27% at 1332 keV (^{60}Co)
FWHM:	2.1 keV at 1332 keV (^{60}Co)
Compton suppression factor:	≈5 (1332 keV) to ≈40 (7000 keV)

The system is regularly calibrated for counting efficiency [4] and non-linearity [5]. This procedure results in a precision of about 0.5% for the relative efficiency curve, 1% for the absolute efficiency curve and a range of 0.005-0.1 keV for energy uncertainty for not very small peaks.

The complex γ-ray spectra are evaluated using Hypermet-PC [4-7]. A series of measurements has been completed at our PGAA facility to create a prompt gamma library for qualitative and quantitative analysis. The new gamma-ray energy and intensity data are accurate enough for the routine analysis [8-9]. An Excel macro (ProSpeRo) is used for the chemical analysis which compares the spectroscopic data library and the measured areas of the characteristic peaks [10].

6.1.2. The NIPS/NORMA facility

Instrument responsible:Tamás Belgya

The NIPS facility is located downstream of the PGAA facility at the end position of the neutron guide NV1. The neutron-induced prompt gamma-ray spectroscopy (NIPS)/Neutron Optics and Radiography for Material Analysis (NORMA) facility has been designed for a large variety of experiments involving nuclear reaction-induced prompt and delayed gamma radiations, including γ-γ-coincidences or neutron radiography, tomography, large-sample PGAA, as well as Prompt-Gamma Activation Imaging (PGAI) [11].

The beam arrives through a flight tube of 5×5 cm^2 cross section. This enables to place detectors very close to the target if needed. Alternatively a sample chamber with dimensions of 20×20×20 cm^3 is available for large-sample PGAA and position-sensitive applications. For this purpose an xyz-ω moving table can be introduced from the bottom of the sample chamber.

An n-type coaxial HPGe detector (Canberra 2318/S) equipped with a Scionix BGO Compton suppressor is used for the routine measurements. This latter can accommodate HPGe detectors with larger crystals (up to end cap diameter of 76 mm). The passive shielding is made of standard lead bricks. The specifications of the facility are listed in Table 3.

Table 3. Specifications of NIPS/NORMA facility

Beam tube:	NV1 guide, end position
Distance from guide end	2.6 m
Neutron beam cross section:	up to 2.5×2.5 cm^2
Thermal-equivalent flux at target:	≈4×10^7·cm^{-2}s^{-1}
Vacuum in target chamber:	Not available
Form of target at room temperature:	Solid, powder, liquid, gas in pressure container
Target packing at atmospheric pressure:	sealed FEP Teflon bag or vial
Activity of target after irradiation:	negligible
Largest target dimensions:	1.5×1.5×3.5 cm^3/20×20×20 cm^3
Distance from target to detector window:	minimum 25 mm, typical 250 mm
γ-ray detector	n-type coax. HPGe, with BGO shield
HPGe window:	Al, 0.5 mm
Relative efficiency:	23% at 1332 keV (^{60}Co)
FWHM:	2.1 keV at 1332 keV (^{60}Co)
Compton-suppression factor	≈3.5 (1332 keV) to ≈30 (7000 keV)

A four-channel, all-digital XIA Pixie 4 gamma spectrometer is set up to collect the counts. An integrated program for gamma spectrum acquisition, sample positioning and tomography is used to control the components of the system in a flexible way.
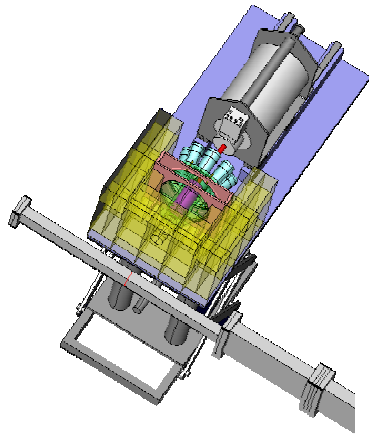
A) Element analysis of small samples
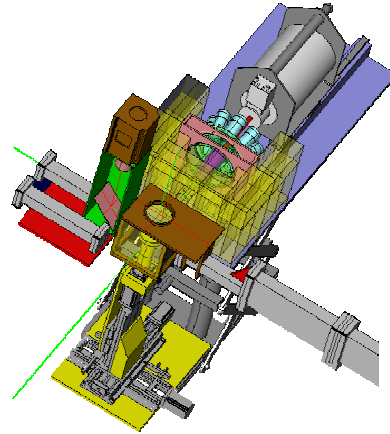
B) large-sample PGAA/position-sensitive element analysis with radiography-driven PGAA or PGAI (NORMA)
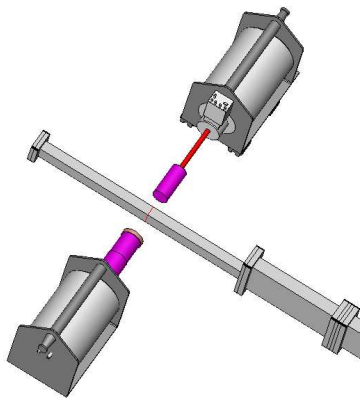
C) coincidence measurements with HPGe detectors
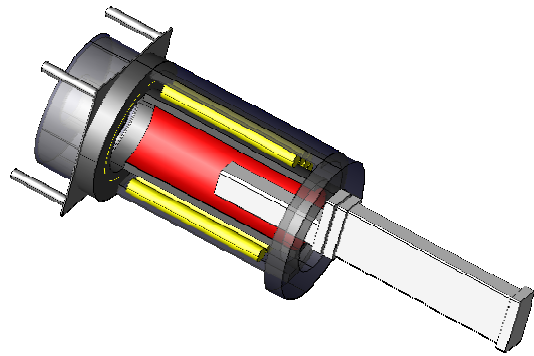
D) experiments with custom setups

Figure 4. Possible configurations of the NIPS/NORMA experimental station. The beam arrives from the lower-right corner of the images.

6.1.3. The low-level counting facility DÖME

In cooperation with the KFKI Atomic Energy Research Institute, a permanent low-level counting facility (referred as DÖME) has been established to assist the in-beam activation measurements, perform the off-line counting [12] of samples on a routine basis, and

enable the measurement of environmental samples with low activities during the reactor shutdown periods (see also in Figure 2) [2]. This consists of an iron chamber manufactured from pre-World War II steel, and is therefore free of any man-made radioactivity. The chamber with an internal dimension of $800{\times}800{\times}800$ mm^3 can accommodate the Canberra GR1319 HPGe detector with a Big MAC cryostat along its horizontal diagonal. This geometry allows sample-to-detector distances up to 250 mm. The wall of the chamber is 155 mm thick and has a graded shielding inside (Cd and Cu layers). As an option for measurement of low-energy lines with a better energy resolution, a Canberra Low Energy HPGe detector is also available. A Canberra DSA-2000 digital gamma spectrometer is used for the data acquisition.
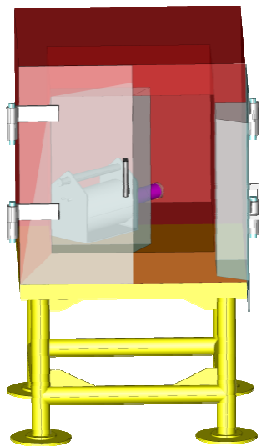
Figure 5. The low-level counting chamber DÖME.

References:

1. Zs. Révay, T. Belgya, L. Szentmiklósi, Z. Kis: *Recent developments in prompt gamma activation analysis in Budapest*, J. Radioanal. Nucl. Chem. 278 (2008) 643.

2. L. Szentmiklósi, T. Belgya, Z. Révay, Z. Kis: *Upgrade of the Prompt-Gamma Activation Analysis (PGAA) and the Neutron Induced Prompt-gamma Spectroscopy (NIPS) facilities at the Budapest Research Reactor*, J. Nucl. Radioanal. Chem., 286 (2010) 501-505.

3. L. Szentmiklósi, Z. Révay, T. Belgya: *An improved beam chopper setup at the Budapest PGAA facility*, Nucl. Instr. and Methods B, 263 (2007) 90-94.

4. G.L. Molnar, Z. Révay, T. Belgya: *Wide energy range efficiency calibration method for Ge detectors,* Nucl. Instrum. Meth. A 489 (2002) 140.

5. B. Fazekas, Zs. Révay, J. Östör, T. Belgya, G. Molnár, A. Simonits: *A new method for determination of gamma-ray spectrometer nonlinearity,* Nucl. Instr. Meth. A422 (1999) 469.

6. B. Fazekas, J. Östör, Z. Kis, G. L. Molnár, A. Simonits: *The new features of Hypermet-PC*, in: Proc. 9th International Symposium on Capture Gamma-Ray Spectroscopy and Related Topics, Budapest, Hungary, October 8-12, (G. Molnár, T. Belgya, Zs. Révay Eds.) Springer Verlag, Budapest/Berlin/Heidelberg, 1997, p. 774.

7. Z. Révay, T. Belgya, G.L. Molnár: *Application of Hypermet-PC in PGAA*, J. Radioanal. Nucl. Chem., 265 (2005) 261-265.

8. Zs. Révay, R.B. Firestone, T. Belgya, G.L. Molnár: *Catalog and Atlas of Prompt Gamma Rays in Handbook of Prompt Gamma Activation Analysis with Neutron Beams*, (G.L. Molnár ed.), Kluwer Academic Publishers, Dordrecht/Boston/New York, 2004, pp. 173–364.

9. Zs. Révay: *Calculation of uncertainties in prompt gamma activation analysis,* Nucl. Instrum. Meth A 564 (2006) 688.

10. Zs. Révay: *Determining Elemental Composition Using Prompt-gamma Activation Analysis*, Analytical Chemistry, 81 (2009) 6851-6859.

11. Belgya, T., Z. Kis, L. Szentmiklósi, Z. Kasztovszky, G. Festa, L. Andreanelli, M.P. De Pascale, A. Pietropaolo, P. Kudejova, R. Schulze, and T. Materna: *A new PGAI-NT setup at the NIPS facility of the Budapest Research Reactor.* J. Radioanal. Nucl. Chem. 278 (2008) 713-718.

12. L. Szentmiklósi, Z. Révay, T. Belgya, A. Simonits, Z. Kis: *Combining prompt gamma activation analysis and off-line counting*, J. Nucl. Radioanal. Chem. 278 (2008) 657-660.

6.2. SMALL-ANGLE NEUTRON SCATTERING DIFFRACTOMETER (Yellow Submarine)

Instrument responsible: Noémi Székely, Renáta Ünnep

The SANS diffractometer Yellow Submarine covers a Q-range from 0.003 - 0.5 Å^{-1} allowing to probe structures at length scales from 5 Å to 1400 Å. It has a wide range of applications from studies of chemical aggregation, defects in materials, surfactants, colloids, ferromagnetic correlations in magnetism, alloy segregation, polymers, proteins, biological membranes and macromolecules. The instrument is installed on the curved neutron guide No.2, with 4x4 cm^2 cross-section, made from supermirrors. The beam is monochromatized by a multidisc type velocity selector, the rotation speed can be tuned between 700 and 7000 rot/min (wavelength: 3 – 25 Å). The width of the transmitted wavelength distribution can be varied between 12% and 30% by changing the angle between the selector axis and the direction of the neutron beam. The beam-line has a 5 m long collimation system allowing the optimization of flux and resolution for different sample-to-detector distances.

Sample environment

In most of the experiments the samples are placed in an automatic sample changer having 6 positions. It can be thermostated from an external bath between –10 and 100°C. The sample changer can be removed, and a liquid nitrogen cryostat, electromagnet or a furnace can also be mounted in the sample position.

Detector

The scattered neutrons are detected by a 64 x 64 pixels (1cm x 1cm pixel size) two dimensional position sensitive LETI (Grenoble, France) detector filled with BF$_3$ gas.

Data acquisition

The control and data acquisition electronics and software have been made by Laboratoire Léon Brillouin, Saclay, France. The preliminary data treatment (circular averaging for isotropic samples, background subtraction, correction for transmission and sample thickness, and normalization to a standard, usually to 1 mm water) can be performed with a software package from LLB (isotropic –Regiso, Paresu; anisotropic - PXY).

Table 1.: Characteristic parameters of the SANS instrument *Yellow Submarine:*

Monochromator:	Mechanical velocity selector (Reference: L. Rosta: Physica B 174 (1991) 562)
Incident wavelength:	3 – 25 Å
Wavelength spread:	Adjustable between 12 – 30%
Transferred momentum	0.003 - 0.5 Å^{-1}

range:	
Neutron flux at the guide exit:	$5*10^7$ n/cm^{2}s
Sample-to-detector distance:	Continuously adjustable between 1.3 and 5.5 m
Detector:	2D position sensitive, 64 x 64 cm^2, filled with BF$_3$ gas
Sample environment	Thermostated sample changer, electromagnet, cryostat, furnace
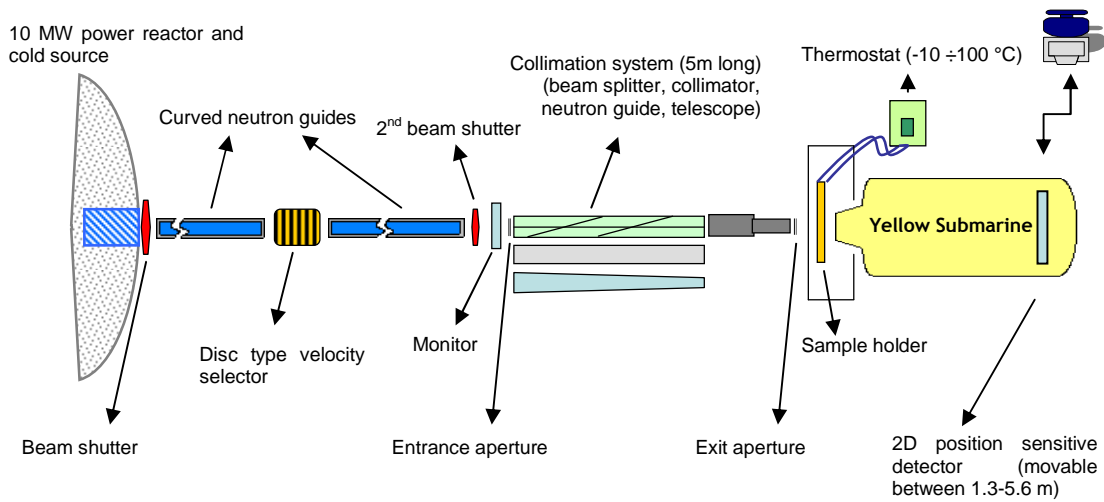
Scheme of the SANS diffractometer
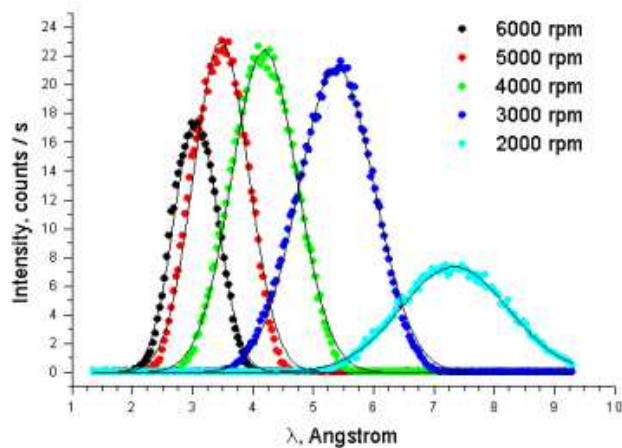
The wavelength distribution of neutrons transmitted by the selector.

6.3. GINA –NEUTRON REFLECTOMETER WITH POLARIZATION OPTION

Instrument responsible: László Bottyán

Triggered by the discovery of the giant magnetoresistance the increased interest in magnetic thin film analytical instruments resulted in a boom of Polarized Neutron Reflectomtery studies as well as in construction of a number of new neutron reflectometers with polarization option. Here we report on the "Grazing Incidence Neutron Apparatus" (GINA), the recently installed neutron reflectometer at BNC. The GINA reflectometer is open for Hungarian and international users throughout the year.

GENERAL OVERVIEW OF THE INSTRUMENT

The GINA reflectometer is a constant-energy angle-dispersive, vertical-sample instrument. The setup is displayed in Figure 1 and the operation parameters are summarized in Table 1. The focusing graphite monochromator MONO provides neutrons with wavelengths within the range of 3.2Å – 5.7Å and $\Delta\lambda/\lambda \approx 1\%$. The polarized neutron beam is produced by using a magnetized supermirror (P1) and an adiabatic radio-frequency (RF) spin flipper (SF1). The beam scattered on the sample may undergo spin analysis by an identical setup of a spin flipper and a spin analyzer (P2), and finally it is detected by a two-dimensional position sensitive neutron detector (DET). The incident intensity is monitored by a low efficiency (~0.1% at $\lambda = 4.6$Å) beam intensity monitor (IM). The components of the reflectometer are mounted on two heavy-load optical benches. The first one supports the beam shutter (BS), the IM, the beryllium filter (BF), the slit (S1) and the SM polarizer (P1), the adiabatic RF spin flipper (SF1) and the slit (S2). The

downstream end of the bench is fixed to the central sample tower ST and supports the various sample environment components (electromagnet, cryostat, etc.). The incident angle on the sample surface is set by the major (θ) goniometer of ST. The second bench – the 2θ-arm of the reflectometer – supports the slit S3, the spin flipper SF2, the spin analyzer P2, and the detector along with its electronics and dedicated control PC mounted underneath. The slit S4 in front of the detector is optionally used when data collection is restricted to specularly scattered
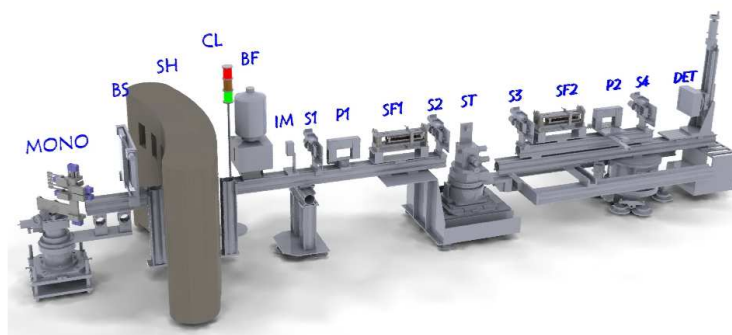
Figure 1. The layout of the GINA neutron reflectometer. For details see text.

neutrons. The 2θ-motion is driven by a wheel running on the marble surface while the corresponding air pads are activated. The wavelength may be changed by manually rotating the entire GINA setup around the turntable under the monochromator while air pads are activated and both arms float over the marble floor. At present, the available wavelengths are restricted to 3.2, 3.9, 4.6, 5.2 and 5.7 Å by the respective channels through the cylindrical concrete shielding (SH) around the monochromator assembly.

The monochromator MONO is located in a gap of the curved Ni/Ti SM guide 19 meters downstream the cold source, and comprises five highly oriented pyrolytic graphite crystals on small motorized 2-circle cradles for horizontal alignment and vertical focusing. Vertical focusing of the beam to the sample position doubled the intensity reflected by a 20×20 mm^2 sample at grazing incidence as compared to the non-focused case of parallel graphite crystals. Higher harmonics intensity is efficiently filtered by a Be block. The transmission of the filter is 41% and 87% for λ=4.6Å, without and with liquid nitrogen cooling, respectively.

Fine definition of the beam is maintained by the four slits. The blades are operated with a precision of 0.05 mm. Slit S1 defines the beam on the polarizer P1 to decrease the divergence thus increasing the polarization ratio. Slit S2 decreases the beam divergence on the sample and absorbs the neutrons scattered by the polarizer. With these optical elements the setup exhibits a relative Q-resolution of 10% to 2% for the available Q-range of 0.005 to ~0.25 Å^{-1}.

Polarized neutrons are produced by an Fe-Co/Si magnetic SM in transmission geometry (P1 in Figure 1). Spin analysis of the specularly reflected beam is performed by a single magnetic SM analyzer (P2) of identical construction with P1. The spin flippers are of adiabatic RF type [**Error! Bookmark not defined.**]: the flipper coil is placed in a

longitudinal gradient field of 20 – 40 mT/m, with a center field of 5.6 mT. The flipper coil is part of a resonant circuit, with typical values of effective RF current and bandwidth of 4 A and 4.5 kHz at the resonance frequency of 166 kHz.

Neutrons scattered by the sample are registered by a delay line type multi-wire proportional chamber with active area of 200×200 mm^2 and spatial resolution of 1.6 mm (FWHM). The detector is filled with a gas mixture of 2.5 and 3 bar partial pressures of ^{3}He and CF_4 , respectively, and it is encased in a boron-containing shielding for background suppression. A DASY TDC module (produced by ESRF, Grenoble) is installed in a slot of the PC dedicated exclusively to the detector data-acquisition and mounted on the 2θ-arm of the reflectometer. If no spin analysis is required, for further background suppression, an evacuated flight tube is mounted along the entire length of the 2θ-arm.

Parameter	Range
Wavelength	3.9÷5.1 Å in five steps
Present wavelength	4.6 Å
Max. scattering angle	$\geq\theta=35°$
Angular resolution ($\Delta\theta$)	0.003°
$\Delta\lambda/\lambda$	~1%
Background level	0.01 cps cm^{-2}
Detector	2D PSD, 200×200 mm^2
Detector spatial resolution	1.6×1.6 mm^2
Neutron flux at the monochromator position	4×10^5n$\times$cm$^{-2}\times$s^{-1}
Background reflectivity	$<7\times10^{-5}$
Overall polarization efficiency	0.895

TABLE 1 The operation parameters of GINA

MEASUREMENT CONTROL

The GINA hardware and control software are designed for maximum flexibility and remote controllability. In its full configuration, GINA comprises more than 30 remotely controllable stepping motors. θ- and 2θ-angles and precision slit positions are encoder-controlled. Hardware control is established via a USB multi-function data acquisition module to control the air compressor, the air pads, the temperature of the Be-filter, the beam shutter and control lights, the beam intensity monitor and various modular DC power supplies. The high voltage power supplies, the amplifiers, the discriminators and the ratemeters are of NIM standard. The control and detector PCs communicate via ethernet and with the stepping motor indexers as well as with the temperature controller via RS232 under the supervision of GINASoft written in LabView 2009. The program user interface is highly configurable and performs experiments including alignments, polarization and the sample environment control (flipper current and frequency, temperature, magnet current, etc.). Detector pictures and reflectivity data are efficiently viewed and manipulated during the data acquisition. Data and log information are saved in a clearly structured database format. Human control is facilitated by a web camera. Using remote desktop option, most operations can be performed remotely via internet from outside the experimental hall or even from a distant continent.

Figure 2 Partial view of the GINA reflectometer. Components are maked as explained in Figure 1 apart from the sample environment with the electromagnet (MAG) with mounted closed-cycle cryostat. The magnet weight is partially relieved by

SAMPLE ENVIRONMENT

GINA is dedicated to magnetic heterostructures, for studies requiring different environmental parameters, such as low temperature and occasionally high external magnetic fields. For room-temperature reflectivity measurements, the sample is held in position by vacuum. Two cradles and two perpendicular translators position the sample in the vertical plane and set the sample surface orientation. A closed-cycle cryostat (12 to 300 K range) can be mounted on the sample tower ST with (*cf*. Figure 2) or without the electromagnet. At GINA an air-cooled electromagnet is available, which generates magnetic fields up to 0.55 T for the pole distance of 40 mm that accommodates the 1.5" diameter cryostat housing. The optional water-cooled air core coil pair provides fields up to approx. 35 mT.

In summary, the GINA reflectometer is a versatile dance-floor-type, vertical sample, constant energy angle-dispersive instrument. Reflectivity ranges above four orders of magnitude have been measured. Further

205

developments including an environmental cell for membrane studies, a supermirror fan analyzer and further background suppression elements will be installed within the next two years.

6.4. THERMAL NEUTRON TREE-AXIS SPECTROMETER "TAST"

AND

NEUTRON HOLOGRAPHIC INSTRUMENT

Instrument responsible: Márton Markó, Alex Szakál

The thermal neutron three-axis spectrometer (TAST) at BNC is installed on the thermal neutron channel No.8 at the Budapest Research Reactor.

The TAST instrument provides moderate resolution (~1.0 meV) with sufficient intensity for use in a wide range of problems. It is ideally suited for the study of phonon and magnon dispersion curves in single crystals, phonon density of states for that large class of materials which contain hydrogen. Independent control of the momentum (Q) and energy transfer (E) is routine if required as opposed to the time of flight spectrometer in which Q and E are related by the instrumental configuration. Because of the limited number of other operational equipment the triple axis spectrometer is used in a multi purpose regime, e.g. for high-resolution diffractometry, strain analysis, quasielastic and inelastic scattering as well as for thermal beam irradiation and transmission tests.

The monochromatic beam is provided by a 90mm high doubly focusing multi-blade Cu monochromator. In order to supress the intensity of fast neutrons 15cm long sapphire single crystal is inserted in the primary shutter. For higher order filtering in the incident monochromatic beam a Ge analyzer can be used. The beam divergence is determined by thin film soller type mylar collimators coated with Gd_2O_3.

A highly efficient (90% at 1 Å) ^{3}He single counter of 1" diameter is applied as detector. A two dimensional position sensitive detector in medium resolution mode will be installed in 2005. Using this detector the efficiency of data collection will be raised about 40 times in quasielastic mode. For energy analyzing a focusing pyrolitic graphyte crystal assembly is used.

The spectrometer can be equipped by an Eulerian Cradle, or a goniometer that can hold various sample environment devices up to a weight of 100 kp. Starting from late 2005 TAST will be used also as a dadicated instrument for atomic resolution neutron holography measurements both in neutron or gamma ray detection modes.

Main parameters of the spectrometer :

Beam tube :	Channel No.8 (radial, zaphyre single crystal filter)
Monochromator :	Cu 200 (doubly focusing)
Analyser :	pyrolitic graphite 002 (horizontally focusing)
Detector	^{3}He single
Range of monochromator angle:	14°<2Θ< 90°
Range of analyser angle :	-100°< 2Θ < 120°

Range of crystal orientation : $0° < 2\Theta < 360°$
Angular resolution : $0.01°$
Flux at specimen at 1 Å: 2×10^6 n/cm^2/.sec
Beam size : $50 \times 50 / 10 \times 15$ mm^2 (depends on focusing)
Momentum transfer : $0.2 – 10$ Å^{-1}
Energy transfer : $1 - 60$ meV
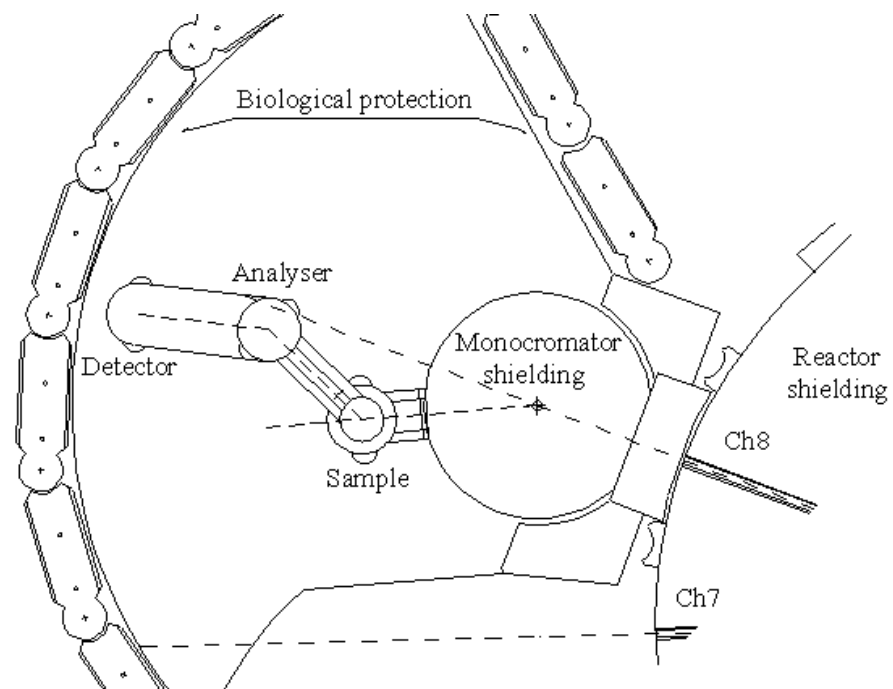
Figure 1. Layout of the thermal neutron three-axis spectrometer

New facility in our research activity: neutron holography setup

The principle and two ways of experimental realisation of atomic resolution neutron holography was proposed by László CSER (BNC). An international team lead by L. Cser has performed the first successful experiment proving the feasibility of the so called internal detector on a Pb-Cd single crystal. Neutron holography is a unique method for direct measurement of local lattice distortionss with sub-picometer accuracy. On the TAST instrument a dedicated holography setup was installed at the Budapest Reactor (Figure on the right). The first holographic spectra were recorded on an NH_4C_1 single crystal .
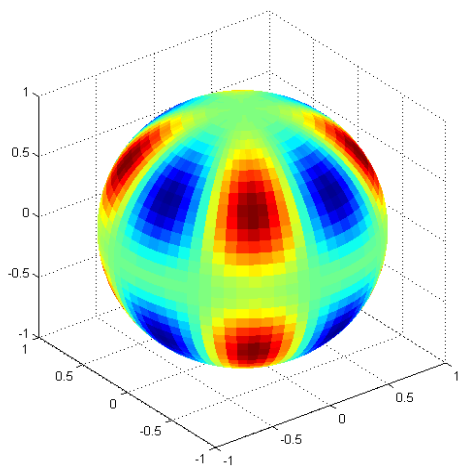
6.5. PSD - NEUTRON DIFFRACTOMETER
Instrument responsible: Erzsébet Sváb, Margit Fábián

The PSD neutron diffractometer is suitable for atomic structure investigations of amorphous materials, liquids and crystalline materials where the resolution requirements are not high. It is a 2-axis diffractometer equipped with a linear position sensitive detector system. The detector assembly is mounted on the diffractometer arm and it spans a scattering angle range of 25° at a given detector position. The entire diffraction spectrum can be measured in five steps.

The electronic control and data transfer systems have been refurnished in years 2008-2009.

Table 1. Characteristic features of the PSD diffractometer for two actual arrangements

Channel	thermal, 9T tangential	
Primary collimation	Soller-type : 20'	
Take-off monochromator angle facility	$-5° < 2\Theta_M < 45°$	
Monochromator and mosaicity	Cu(111), 16'	Cu(220), 20'
Monochromatic wavelength	1.069 Å	0.66 Å
Resolution, $\Delta d/d$	$1.2 \cdot 10^{-2}$	$2.4 \cdot 10^{-2}$
Flux at the sample position	$10^6 \, ncm^{-2}s^{-1}$	$10^5 \, ncm^{-2}s^{-1}$
Beam size at the specimen	10 mm×50 mm	
Scattering angle, 2θ	$5° < 2\Theta < 110°$	
Momentum transfer interval, Q	0.6-9.2 Å^{-1}	0.8-15.8 Å^{-1}
Monitor counter	fission chamber	
Detector system	- 3 linear position sensitive ^{3}He detectors - the detector assembly spans 25° scattering angle at a given position	
Data collection	Xilinx preprogrammed unit	
Data transfer and control	PC-AT with Eagle I/O card and a dedicated electronic device	
Remote control and file transfer	Windows programme package	

SOLLER COLLIMATOR-15'

NEUTRON BEAM

BORATED PARAFFIN

MONOCHROMATOR CRYSTAL
Cu <111> 16'

IRON RING

MONOCHROMATOR AXIS

SHIELDING SEGMENTS

COLLIMATOR SLIT 15X50 mm

COLLIMATOR SLIT 20X50 mm

CADMIUM SLIT

MONITOR COUNTER

SAMPLE AXIS WITH GONIOMETER

DETECTOR SHIELDING

Cd PLATED

^{3}He LINEAR POSITION
SENSITIVE DETECTORS

BORATED PARAFFIN

B_4C

1 m

M 1:20
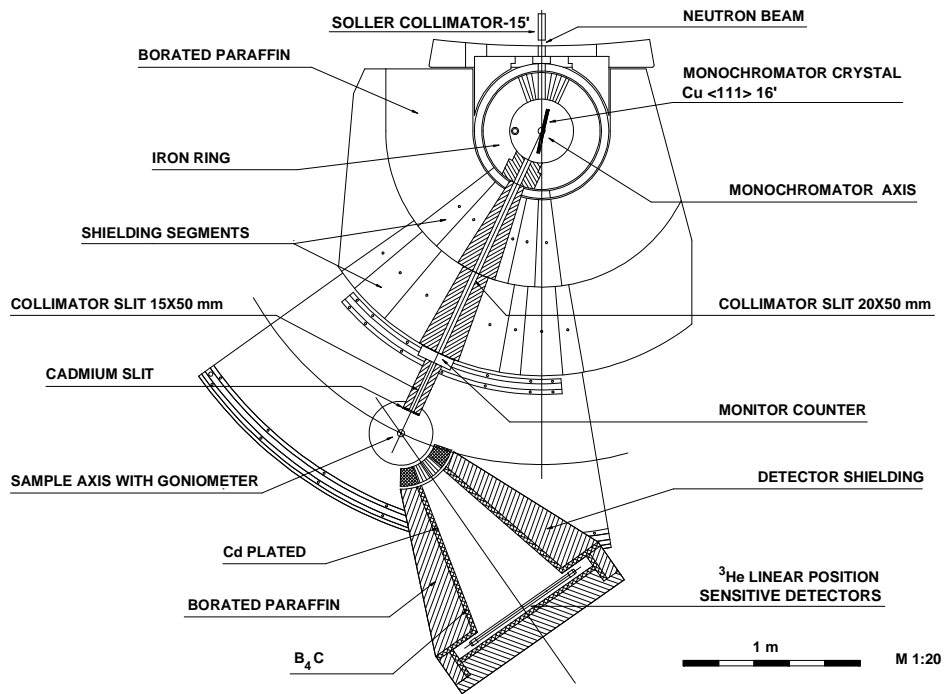
Figure 1. *Schematic arrangement of the PSD neutron diffractometer*
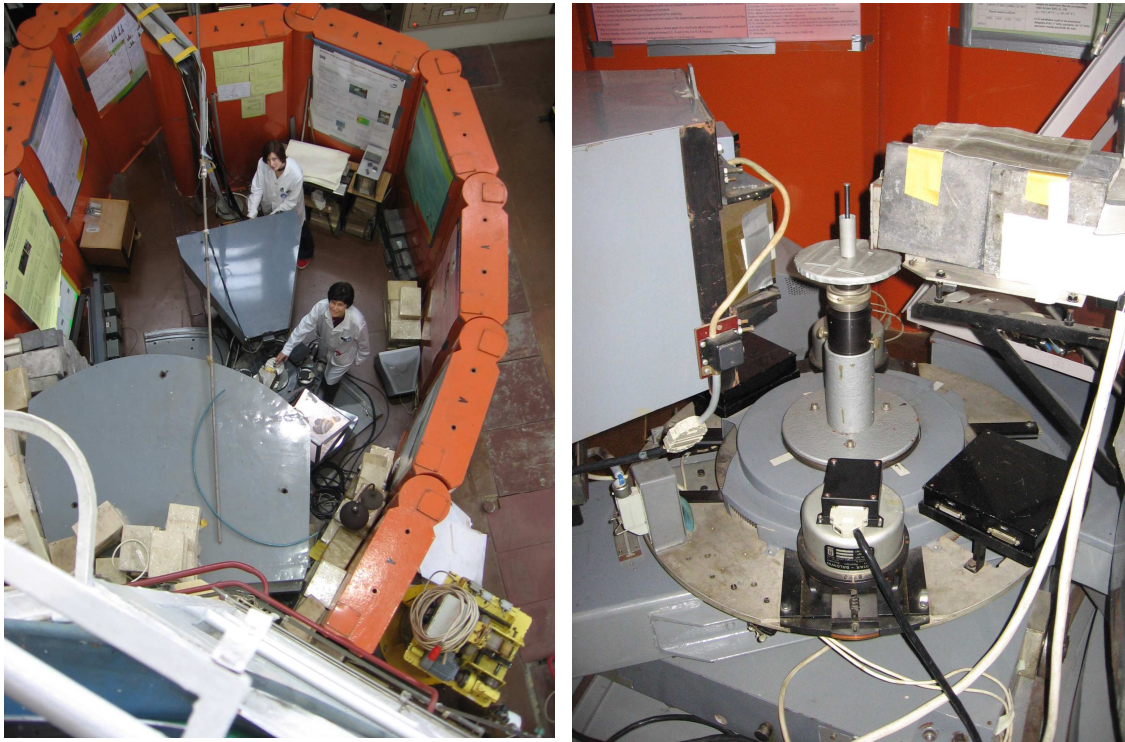
Figure 2*. Photographs taken from the PSD neutron diffractometer*

6.6. DYNAMIC RADIOGRAPHY STATION

Instrument responsible: Márton Balaskó

Neutron radiography utilizes transmission to obtain information on the structure and/or inner processes of a given object. It is used for various non-destructive test measurements. A dynamic radiography station has been built out visualize and analyse the flow of fluids, the evaporation and the condensation processes in closed metal objects, tube systems and other types of dynamic events.

Main parameters of the dynamic radiography station:

- Thermal channel: No. 2

„A"   ***In the conventional arrangement:***
- Complex pin-hole type collimator for neutron and gamma radiation with a collimation ratio of L/D = 170
- Neutron flux at the objects position: $6\ 10^7$ n·cm^{-2}·sec^{-1},
  behind of CD an In filter: $3 \cdot 10^6$ n·cm^{-2}·sec^{-1}
- Gamma intensity: ~ 8,5 Gy/h
- X-ray energy: 50-300 keV; 5 mA
- Variable beam diameter, with a maximum of 150 mm at the object position.
  Maximum surface for investigation: 700×1000 mm^2
- Maximum weight of the investigated object: 250 kg

„B"   ***In the extended inspection area (for study of helicopter rotor blades)***
- Maximum beam diameter: 185 mm
- Maximum surface: for investigation9750×700 mm^2
- Maximum weight of the investigated object: 200 kg
- Practicable to study, the efficiency of the moisture condition of the inspected objects, by a Moistening module is driven by a High pressure water pump
- Converters (radiation into light): for neutron radiography NE 426 scintillation screen with resolution of 100 μm; for gamma and X-ray radiography NaCs single crystal with resolution of 200 μm, or ZnS screen with resolution of 100 μm
- Variable filters: Cd, In
- Detection of the radiography image: low-light-level TV camera with a light sensitivity of 10^{-4} lux, imaging cycle is 40 msec, and a double cooled CCD camera (756 x 580 pixel), 10 bit.
- Radiography image is visualised on monitor, stored by S-VHS video recorder and DVD recorder and for further quantitative analysis a Quantel image processing system is used with Sapphire V.0.5 software, and an Iman β version software.
- Photo-luminescent Imaging Plates technique used by X-ray radiation or by neutron radiation with transfer method BAS IP-SR 20×25 and IP-SR 20x40[In and Dy (100 μm) foils]. The evaluation of exposed IP-s are by BAS 2500 reader unit used an AIDA picture reconstruction software.

Unique feature of the dynamic radiography station :

Our radiation sources give a possibility to study semi-simultaneously or simultaneously the investigated objects by neutron-, gamma- and X-ray radiography to use the all advantages of the complementary features of the different radiations. Simultaneously, other non-destructive inspection as vibration diagnostics and acoustic emission can be used.

6.7. HIGH RESOLUTION TOF POWER DIFFRACTOMETER

Instrument responsible: György Káli

The high resolution time-of-flight powder diffractometer (TOF) at BNC has been installed to a radial thermal neutron beam in a new guide-hall in collaboration with the Hahn-Meitner-Institut. According to Monte-Carlo simulation results [2-3] it was expected that this type of instrument can outperforms a conventional crystal monochromator powder diffractometer at continuous reactor source in the resolution range of $\Delta d/d = 1 - 5 \times 10^{-3}$. The other advantage to apply TOF monochromatization to neutron diffractometry on a continuous source is the variable resolution and intensity. A full diffraction spectrum can be gained within a variable bandwidth with ultrahigh resolution or with high intensity at conventional resolutions.

The monochromator system consists of a fast double and the two single choppers and a straight neutron guide with 2.5x10 cm cross section at the end. The double chopper is designed for a maximum speed of 12000 rpm. While in high resolution mode the very short - 10µs – neutron pulse and the 25m total flight path allows us to obtain a diffractogram with an accuracy of 10^{-3}Å (at back scattering mode) in a single measurement on polycrystalline materials, in low resolution mode liquid diffraction can be performed at good neutron intensity up to 15Å^{-1} scattering vector. As it was expected, the beam was contaminated with epithermal and fast neutrons because the straight guide is directed on the centre of the zone and the gadolinium coated chopper disks are transparent for them. Temporary silicon filters was applied with which the signal-noise ratio had been increased by a factor of 5-10.

The double disk chopper (Ch1 and Ch2) has two windows: a 1.5° opening for short pulses (10 µs) and a 15° window for long variable pulses (20–200 µs), and can be operated in parallel or counter rotating mode. The latter option is used to produce very short pulses at high speed. To minimize the opening time the neutron beam is reduced from 25 to 10 mm width at the position of the pulse choppers using a 4.5m compressor neutron guide section before and a same decompressor after them (see Figure1). Ch3 limits crosstalk between different pulses and Ch4 prevents frame overlap.

The instrument is working in back scattering mode to reach the best possible resolution. Until the planned detector (a 60x100 cm^2 2D detector) reach completion, a box of four ^{3}He tube is used with a 2.5MHz event recording board. Because of the much smaller surface, the box is placed closer (2m) to the sample opposite to the designed (3m). To achieve the maximum resolution the 2D position sensitive detector will be applied in combination with a bank of 32 pieces 6 mm thick pressed ^{3}He tubes . The data are acquired in so called list or time stamping mode: all the event on the detector, the chopper signs and optionally changes in the sample environment are registered with the time passed since the starting of the experiment. In this mode many uncertainties can be filtered out during the treatment and re-treatments.

References

1. H. J. Bleif, D. Wechsler and F. Mezei, 2000, *Physica B:*, V276-278, p 181-182

2. J. A. Stride, F. Mezei, H. -J. Bleif and C. Guy.,1997 *Physica B:*, V 234-236, p. 1157-1159,.

3. J. Peters, H.-J. Bleif, Gy. Káli, L. Rosta and F. Mezei, 2006, *Physica B:,* 385-86 1019-1021

4. Káli Gy., Sánta Zs., et al. 2006 *Proceedings of EPDIC10 Zeitschrift für Kristallographie*;
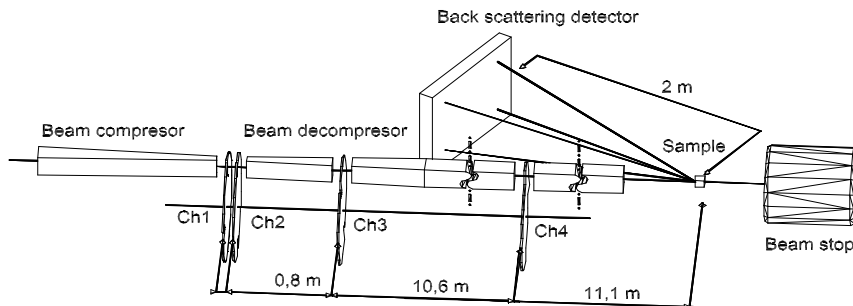
Figure1. Instrument Layout

Total flight path from chopper 1	L=25 m
Wavelength range	0.07-0.45 nm
Bandwidth in single experiment$\Delta\lambda$	from 0.4 nm to 0.08 nm (200 Hz)
Resolution $\Delta d/d$	1×10^{-3} at d=0.15 nm
Straight neutron guide cross section	25×100 mm^2
Coating	Supermirror NiTi, m=2
Beam flux at opened windows	4×10^7 neutron/s/cm^2
Pulse length	10-1000 µs
Max. speed for the double chopper	12000 rpm

Table1. Main parameters
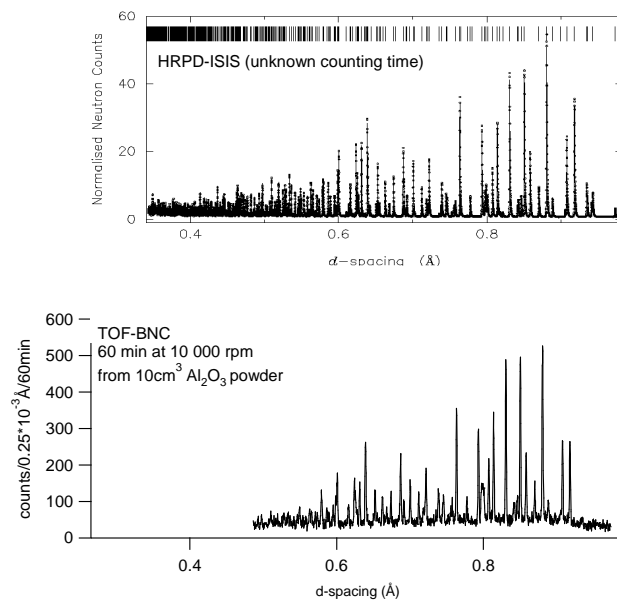
Figure2. A typical spectra in comparison wit HRPD at ISIS

6.8. REACTOR-NEUTRON ACTIVATION ANALYSIS

Instrument responsible: Rózsa F. Baranyai, Ibolya Sziklai-László

In spite of advanced nuclear analytical methods developed in the past two decades (PIXE, XRF, etc.) classic (n,γ) reactor neutron activation analysis (RNAA) is still preserving its role as a "workhorse" for the vast amount of analytical work. Combined with computerized high resolution gamma-ray spectrometry, RNAA offers mostly non-destructive, multi-element routine analysis needed in such areas as environmental monitoring, geochemistry, medicine and technological processes. Among its favourable characteristics negligible matrix effects, excellent selectivity and high sensitivity are worth mentioning (for about 75 elements less than 0.01 μg can be determined)

Instrumentation

Besides more than 40 vertical channels operated by the reactor staff, a pneumatic sample transfer system is also available at the Budapest Research Reactor. (Figure 1.)
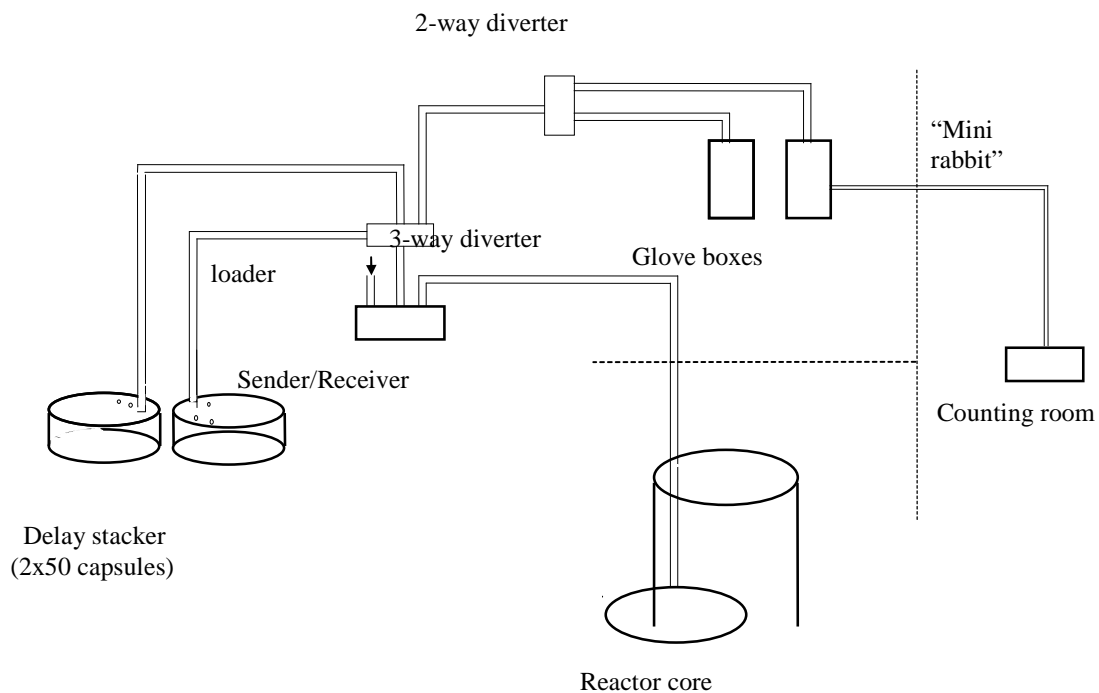
Figure 1. Schematic diagram of the multi-purpose pneumatic transfer system

The rather sophisticated but very versatile system includes:
- **Sender/Receiver Station** permitting capsule injection and programmable capsule transfer between the irradiation position and the station
- **Tubing system** (50 m long flexible polyprophylene) with photo detectors along the capsule pathway to control capsule position and speed

217

- **Aluminium irradiation end** (~5 m) equipped with a large variety of sensors to monitor capsule arrival at the irradiation position, cooling gas flow, humidity, temperature, etc.
- **Delay Stacker** (2 x 50 capsules) for decay of short-lived isotopes before counting
- **Drop-out Stations** for sample manipulation before counting
- **"Mini Rabbit" system** to transport radioactive samples to the counting room

The "rabbit" system operates by compressed air (2 bar). Capsules made of polyethylene can be cooled during irradiation with CO_2 in order to extend the irradiation period (over 20 minutes at present). The whole system is PC-controlled and the developed acquisition software allows a simple and user-friendly operation.

In the "B" vertical pneumatic tube, thermal neutron flux variation along the axis of the irradiation capsule is less than 5 %. As a rule, small samples and monitors are packed in 10 mm height x 8 mm dia. polyethylene vials in which less than 0.5 % flux inhomogenity can be expected during irradiation.

Neutron flux parameters have been measured with the "Bare Triple- Monitor" method using Zr foil, as well as Al-0.1%Au and Al-0.1% Lu wires. As seen in Table 1., channel "B" is fairly well thermalized ($f \approx 40$) and when representing the epithermal flux distribution with the $1/E^{1+\alpha}$ function, the α-value is positive.

MEASURED NEUTRON FLUX PARAMETERS IN THE PNEUMATIC TUBE "B"					
(Lattice position: 310-311-266, Date: 04-NOV-1997)					
$\Phi_S=n_{Cd}\cdot v_0$ "subCd flux" $[n/cm^2 \cdot s]$	$f=\Phi_s/\Phi_{epi}$ flux ratio	Φ_{fast} $[n/cm^2 s]$	α	T_n $[°C]$	NOTES
$6.0 \cdot 10^{13}$	36	$1.1\ 10^{12}$	0.033	57^*	Primary coolant temp: 50 °C

Instrumental, multielement neutron activation analysis makes perhaps the most stringent demands on the applied gamma-ray spectrometry. The measured spectra are often very complex, containing more than hundred peaks with many multiplets. Consequently, the importance of the quality of the applied hardware as well as the flexibility of the evaluation software can not be overemphasized.

In NAA practice, unknown samples are usually irradiated first for only a few minutes to "scan" possible major components and to gather information for planning the subsequent long irradiation. Short-time NAA usually results in "hot" samples with a number of fast-decaying isotopes (^{28}Al, ^{52}V, ^{49}Ca, ^{38}Cl etc.). A good quality spectrometer should, therefore, maintain spectrum quality at high and variable incoming rates while properly correcting all kind of pulse losses (dead time, pulse pile-up) to preserve the accuracy of quantitative analysis as well.

The block diagram of one of the three gamma-ray spectrometers is shown in Figure 2. All the setups incorporate now Westphal's Loss-Free Counting (LFC) modules with dual spectrum storage option.

Recently, conventional amplifiers and ADCs have been replaced with their digital counterparts (CI 2060) or with a standalone digital spectrum processor (DSpec^{PLUS}) in order to improve system characteristics (long time spectrum stability, rate-dependent resolution, etc.)
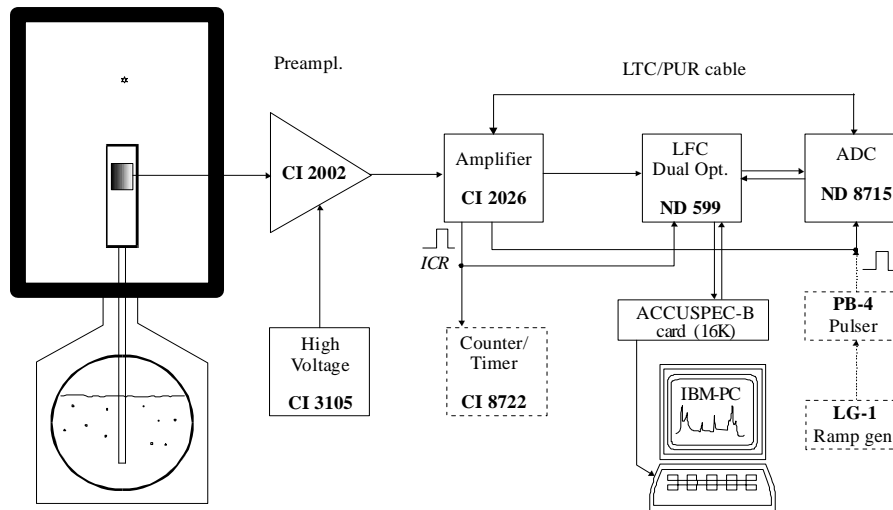
Figure 2. A gamma-ray spectrometer equipped with Dual Spectrum LFC module

Performance tests of the above mentioned gamma-ray spectrometers are carried out regularly. Sometimes factory engineers are consulted to check a built-in module (such as an ADC). For testing system parameters at high and varying counting rates, special homemade and certified isotopes should be made available. In Figures 3 and 4 some test results are shown.

D3-AEKI "TANDEM" LFC GAMMA SPEKTROMETER

Rate dependence of peak resolution and position

Detector: Canberra n-type HPGe (13%/1.7 keV) with RC preampl.
ADC: ND 583 8K/7µs, LFC: ND 599 (Dual), PET: 3 x 4.60 µs

Figure 3a. Peak centroid and resolution stability of AEKI detector D3 coupled to a conventional setup (amplifier + ADC) comprising a Dual LFC module
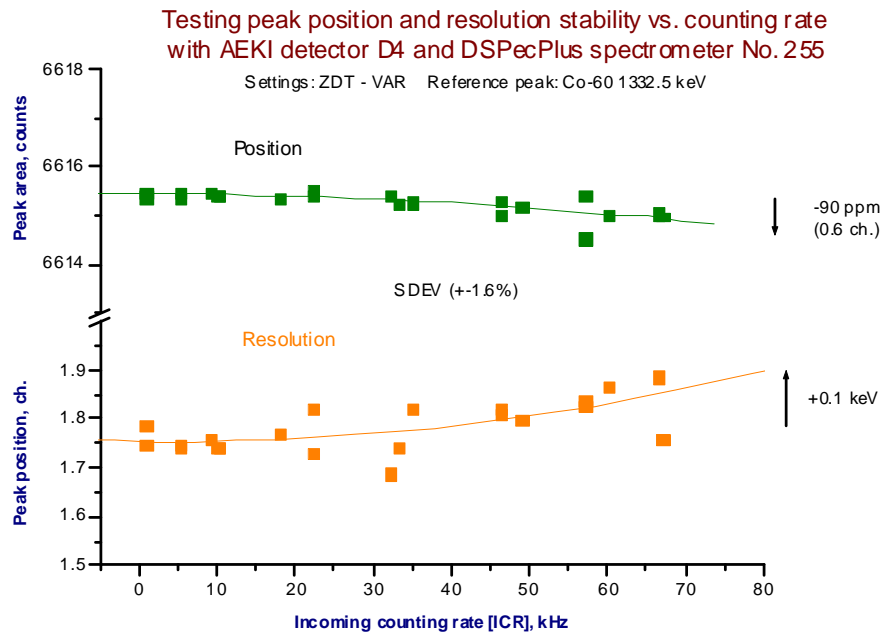
Figure 3b Peak centroid and resolution stability vs. counting rate of D4-AEKI detector with DSpec^{Plus}
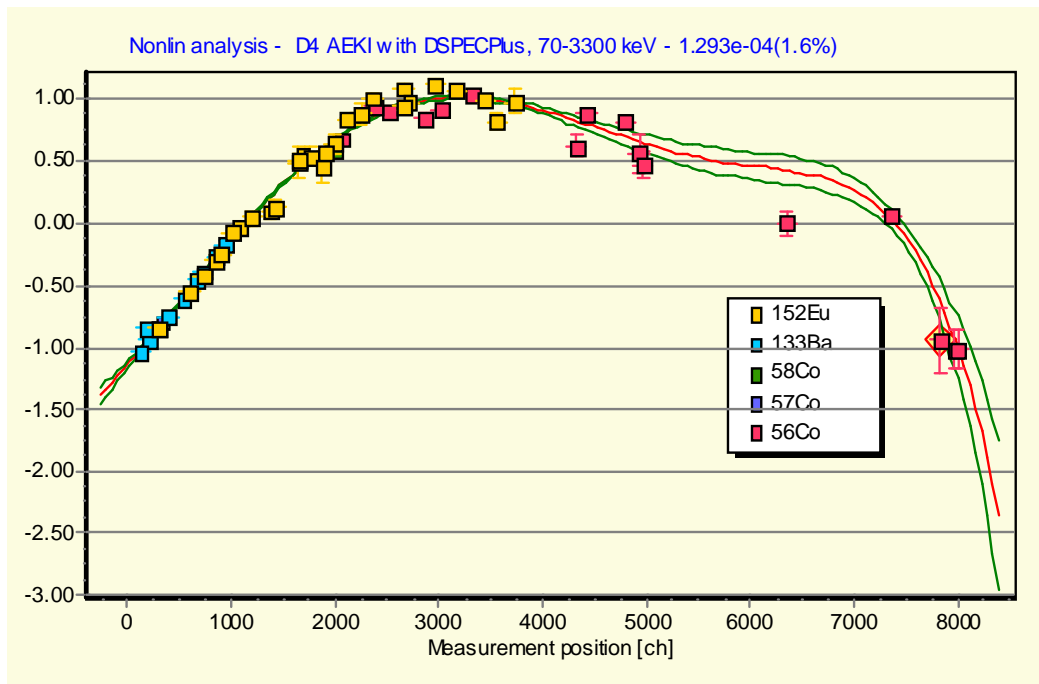
Figure 4. System nonlinearity with D4 detector and DSpec^{Plus}.

221

The recorded "tandem" spectra are evaluated with the program Hypermet-PC Ver. 5.0 which is fully compatible with the KAYZERO/SOLCOI program package used for concentration calculation.

Developments and applications

One important aspect of routine activation analysis is the simplification of the applied standardization procedure. A new method using compound nuclear constants (i. e. so called k_0-factors determined experimentally with high accuracy) was developed to eliminate standard preparations and errors originating from randomly selected nuclear data. In the course of a two decade co-operating research with the INW Gent University (Belgium), k_0-values and related nuclear data are now established for 140 (n,γ) reactions and the method is now opera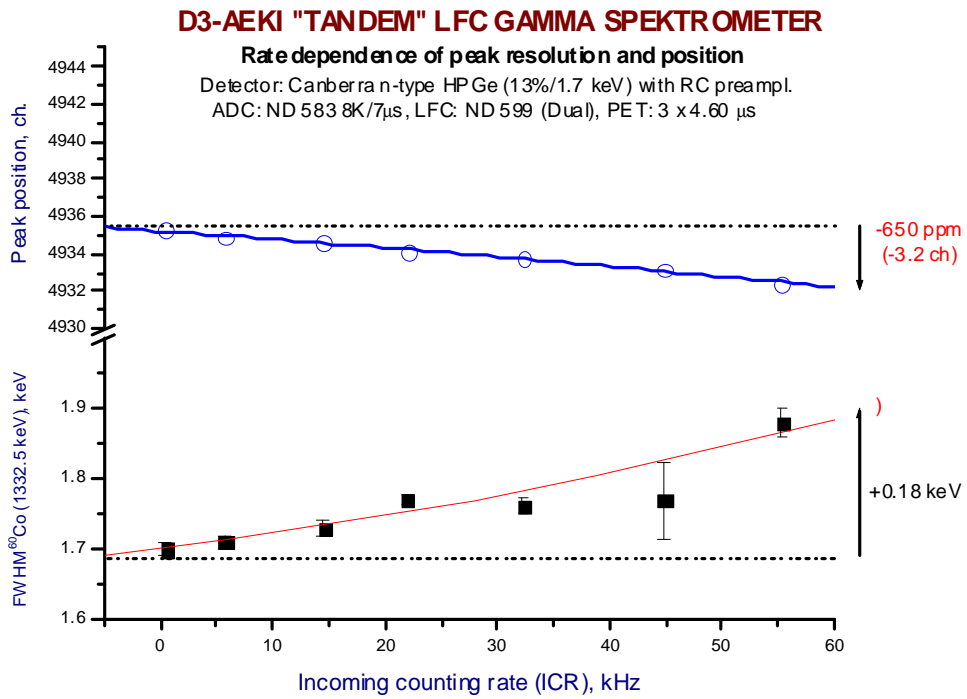tional in more than 50 NAA laboratories world-wide. In view of its large nuclear data library and its complex algorithms it was but logical that a computer code KAYZERO/SOLCOI was developed at DSM Research (The Netherlands) for k_0-NAA. In a framework of an EU COPERNICUS project the method is now tested and verified by analysing European multielement standard reference materials in five NAA laboratories. The latest compilation of recommended nuclear data for use in k_0-NAA is published in the Atomic Data and Nuclear Data Tables (Vol. 85 (2003) 47-67)

The INAA method described above was applied to study the concentration distributions of typical toxic heavy metals in small amounts of industrial type air particulate fractions. Generally, toxic components are distributed in two forms in the particulates, e.g. in a matrix involved form and in a surface deposited form of which the latter one can be considerably enriched. Within the scope of this project enrichment rates of about 18 toxic elements have been investigated in function of the sampling temperature.

The trace element content of vegetation growing inside the fertilizer plant and in the vicinity was investigated by neutron activation analysis method. We determined the degree of elemental enrichment in different plant species (carrot, potato) and soil samples collected on the premises of the plant and in some control area. Our results show that area is exposed to the emissions of the phosphate fertilizer industry. The specific pollutants emitted into the air by fertilizer plant are Sr, Cd, La, Ce, Sm, Tb, Yb, U and Th.

The nutritional importance of trace elements has grown rapidly during the last years mainly because of a better understanding of their biological functions. For determination of low concentration levels of Se INAA is very expedient a sensitive multielement technique which is valuable for both homogeneity testing and certification analyses due to its high precision and accuracy. INAA procedure using the ^{75}Se isotope was developed and the activation, decay and measuring scheme was optimized to the needs of the food samples and applied for the determination of Se levels in basic food ingredients. In addition the selenium state and its changes with age in children and adults living in three geographical regions of Hungary were studied

A nondestructive analytical method was developed to monitor the activity of the primary coolant of the Budapest Research Reactor. The activity of radionuclides in water and gas samples taken from the primary circuit have been measured for more than four years to monitor the technological parameters of the research reactor during normal operation. In the primary water samples 7 noble gas nuclides (Kr, Xe), 12 corrosion

(activation) products (Cr, Mn, Co, Fe, etc.), fission iodine and 8 other fission products and impurities (La, Sb, Ta, etc.) as well as radioactive components in the gas samples were determined routinely by high resolution gamma-ray spectrometry.

A non-destructive neutron activation analytical method was also developed for analysis of wear-components in liquid oil samples. More than 20 elements were determined and their enrichment rate studied in used lubricating oils from aircraft engines.

Epithermal neutron activation analysis (ENAA) was introduced to analyse geological and biological samples. The major advantage offered by epithermal neutron activation analysis is the substantial reduction of interfering matrix activities. Consequently, a number of important nuclides (^{75}As, ^{197}Au, ^{111}Cd, ^{100}Mo, ^{121}Sb, ^{124}Sn, ^{238}U) can be determined instrumentally with minimum delay.

7. EDUCATION

Graduate and postgraduate courses

2008-2009 Disorder in condensed phases (L. Pusztai, ELTE)

Laboratory practice and seminars

2008-2009 Laboratory practice in neutron diffraction (L. Pusztai, L. Temleitner, ELTE)

Ph.D. students

M. Fábián (ELTE): The structure of borosilicate glasses (Supervisor: E. Sváb)

Sz. Pothoczki (BME): Investigation of the structure of molecular liquids by neutron diffraction and computer simulation (Supervisor: L. Pusztai)

V. Mile (ELTE): Diffraction and computer simulation studies of structural disorder in molecular liquids and solids (Supervisor: L. Pusztai)

Dissertations, PhD

M. Fábián: Nátrium-boroszilikát alapú üvegek szerkezete: neutrondiffrakció és fordított Monte Carlo modellezés (Structure of sodium borosilicate based glasses: neutron diffraction and reverse Monte Carlo modelling, in Hungarian), PhD, ELTE, 2009.

8. EVENTS

(Workshops, Meetings, Conferences)

4th Reverse Monte Carlo Conference, 29 September – 03 October, 2009; Hotel Normafa, Budapest; organiser: L. Pusztai.

APPENDIX

EXPERIMENTAL STATIONS OF THE BNC

Acronym	Instrument	Current status	Responsible person phone: +361 392 2222 /EXT, e-mail
PSD	Powder diffractometer	scheduled, FP7	Erzsébet SVÁB /1418 svab@szfki.hu Margit FÁBIÁN/1466 fabian@szfki.hu
MTEST	Materials test diffractometer	scheduled, FP7	László KŐSZEGI /1469 koszegi@szfki.hu
SANS	Small angle scattering spectro-meter with XY detector	scheduled, FP7	Renata Ünnep/1447 runnep@szfki.hu
ATHOS	Three-axis spectrometer on neutron guide	scheduled, FP7	Gyula TÖRÖK/1439 torok@szfki.hu
TAST	Three-axis spectrometer on a thermal beam	scheduled, FP7	Márton MARKÓ/1416 marko@szfki.hu Alex SZAKAL/1416 szakal@szfki.hu
REF	Neutron reflectometer	scheduled, FP7	Tamás VERES /1738 veres@szfki.hu
DNR/SNR	Dynamic/static radiography	scheduled, FP7	Márton BALASKÓ /1434 balasko@aeki.kfki.hu
BIO	Biological irradiations	scheduled, FP7	József PÁLFALFI /1495,1671 palfalvi@aeki.kfki.hu
PGAA	Prompt activation analysis	scheduled, FP7	Zsolt RÉVAY /3143 revay@iki.kfki.hu
NIPS	Neutron Induced Prompt-Gamma Spectroscopy	scheduled, FP7	Tamás BELGYA /3234 belgya@iki.kfki.hu
TOF	Time-of-flight diffractometer	scheduled, FP7	György KÁLI/1439 kali@szfki.hu
GINA	Polarised Reflectometer	under installation	Laszlo Bottyan/2761 bottyan@nucssp.rmki.kfki.hu
BAGIRA	Controlled temper-ature irradiation rig	scheduled, FP7	Ákos HORVÁTH /3628 horvath@aeki.kfki.hu
RNAA	Fast-rabbit system and activation analysis	scheduled, FP7	Rózsa BARANYAI /1256 baranyai@aeki.kfki.hu

PUBLICATIONS

Articles

13. Teschner, D.; Borsodi, J.; Wootsch, A.; Révay, Z.; Hävecker, M.; Knop-Gericke, A.; Jackson, S. D.; Schlögl, R. *Science* **2008**, *320*, 86.

14. Révay, Z.; Belgya, T.; Szentmiklósi, L.; Kis, Z.; Wootsch, A.; Teschner, D.; Swoboda, M.; Schlögl, R.; Borsodi, J.; Zepernick, R. *Analytical Chemistry* **2008**, *80*, 6066.

15. Zs. Révay, T. Belgya, L. Szentmiklósi, Z. Kis: *Recent developments in prompt gamma activation analysis in Budapest*, J. Radioanal. Nucl. Chem. 278 (2008) 643.

16. L. Szentmiklósi, T. Belgya, Z. Révay, Z. Kis: *Upgrade of the Prompt-Gamma Activation Analysis (PGAA) and the Neutron Induced Prompt-gamma Spectroscopy (NIPS) facilities at the Budapest Research Reactor*, J. Nucl. Radioanal. Chem., 286 (2010) 501-505.

17. L. Szentmiklósi, Z. Révay, T. Belgya: *An improved beam chopper setup at the Budapest PGAA facility*, Nucl. Instr. and Methods B, 263 (2007) 90-94.

18. G.L. Molnar, Z. Révay, T. Belgya: *Wide energy range efficiency calibration method for Ge detectors,* Nucl. Instrum. Meth. A 489 (2002) 140.

19. B. Fazekas, Zs. Révay, J. Östör, T. Belgya, G. Molnár, A. Simonits: *A new method for determination of gamma-ray spectrometer nonlinearity,* Nucl. Instr. Meth. A422 (1999) 469.

20. B. Fazekas, J. Östör, Z. Kis, G. L. Molnár, A. Simonits: *The new features of Hypermet-PC*, in: Proc. 9th International Symposium on Capture Gamma-Ray Spectroscopy and Related Topics, Budapest, Hungary, October 8-12, (G. Molnár, T. Belgya, Zs. Révay Eds.) Springer Verlag, Budapest/Berlin/Heidelberg, 1997, p. 774.

21. Z. Révay, T. Belgya, G.L. Molnár: *Application of Hypermet-PC in PGAA*, J. Radioanal. Nucl. Chem., 265 (2005) 261-265.

22. Zs. Révay, R.B. Firestone, T. Belgya, G.L. Molnár: *Catalog and Atlas of Prompt Gamma Rays in Handbook of Prompt Gamma Activation Analysis with Neutron Beams*, (G.L. Molnár ed.), Kluwer Academic Publishers, Dordrecht/Boston/New York, 2004, pp. 173–364.

23. Zs. Révay: *Calculation of uncertainties in prompt gamma activation analysis,* Nucl. Instrum. Meth A 564 (2006) 688.

24. Zs. Révay: *Determining Elemental Composition Using Prompt-gamma Activation Analysis*, Analytical Chemistry, 81 (2009) 6851-6859.

25. Belgya, T., Z. Kis, L. Szentmiklósi, Z. Kasztovszky, G. Festa, L. Andreanelli,

M.P. De Pascale, A. Pietropaolo, P. Kudejova, R. Schulze, and T. Materna: *A new PGAI-NT setup at the NIPS facility of the Budapest Research Reactor*. J. Radioanal. Nucl. Chem. 278 (2008) 713-718.

26. L. Szentmiklósi, Z. Révay, T. Belgya, A. Simonits, Z. Kis: *Combining prompt gamma activation analysis and off-line counting*, J. Nucl. Radioanal. Chem. 278 (2008) 657-660.

27. M. Fábián, E. Sváb, Th. Proffen, E. Veress; Structure study of multi-component borosilicate glasses from high-Q neutron diffraction measurement and RMC modelling; *J. Non-Cryst. Solids*; 354, 3299-3307, 2008

28. M. Fábián, Th. Proffen, U. Ruett, E. Veress, E. Sváb, Uranium surrounding in borosilicate glass from neutron- and X-ray diffraction and RMC modelling, *J. Phys.: Condens. Matter* **22** (2010) 404206 (8pp)

29. D. Tzankov, D. Kovacheva, K. Krezhov, R. Puźniak, A. Wiśniewski, E. Sváb, M. Mikhov; Magnetic properties of Bi0.5Sr0.5FexMn1−xO3 (0.1≤x≤0.7); *Journal of Applied Physics*; **103**, 053910(7pp), 2008

30. S. Kovachev, D. Kovacheva, S. Aleksovska, E. Sváb, K. Krezhov; Structure and magnetic properties of multiferroic YCr1-xFexO3 (0≤x≤1*); J. Optoelectronics and Advanced Materials;* **11**, 1549 – 1552, 2009

31. V. Pamukchieva, A. Szekeres, E. Sváb, M. Fábián, Compositional dependence of the optical properties of new quaternary chalcogenide glasses of Ge–Sb–(S,Te) system; *Optical Materials*; 32, 45-49, 2009

32. V. Pamukchieva, A. Szekeres, K. Todorova, M. Fábián, E. Sváb, Zs. Révay, L. Szentmiklósi; Evaluation of basic physical parameters of quaternary Ge–Sb-(S,Te) chalcogenide glasses; *J. Non-Cryst Solids*; 355, 2485-2490, 2009

33. M Fábián, E Sváb, S Vogel, V Pamukchieva, Structure study of chalcogenide glasses from high Q-range neutron diffraction experiment and RMC modelling, *International Conference for Neutron Scattering ICNS99, 3-7 May 2009, Knoxville/USA, Journal of Physics: Conference Series* 251 (2010) 012013

34. M Fábián, E Sváb, V Pamukchieva, A Szekeres, S Vogel, U. Ruett, Study of As2Se3 and As2Se2Te glass structure by neutron- and X-ray diffraction methods, 16 ISCMP: Progress in Solid State and Molecular Electronics, Ionics and Photonics, August – September 2010, Varna, Bulgaria, *Journal of Physics*: *Conference Series* 253 (2010) 012053

35. Pamukchieva* V, Szekeres* A, Svab E, Fabian M, Revay* Z, Szentmiklosi* L; Spectral ellipsometric determination of the optical constants of multicompoment chalcogenide films of Ge-Sb-S-Te system; *J. Phys.: Conf. Ser.*; **113**, 012054(5pp), 2008

36. R. Szőke, I. Sziklai-László: Epiboron NAA: an option to analyze unfavorable matrices. *J. Radioanal. Nucl. Chem.*, **275,** 89-95 (2008).

37. Sziklai-László, D. Majchrzak, I. Elmadfa, M.Á. Cser: Selenium and vitamin E concentration in human milk and formula milk from Hungary. *J. Radioanal. Nucl. Chem.* **279**, (2), 585-590 (2009).

38. Pusztai L, Pothoczki Sz, Kohara* S; Orientational correlations in molecular liquid SnI4; *J. Chem. Phys.*; **129**, 064509/1-4, 2008

39. Temleitner L, Pusztai L, Akahama* Y, Kawamura* H, Kohara* S, Ohishi* Y, Takata* M, 'Orientational correlations in high-pressure fluid oxygen and nitrogen', *Phys. Rev. B* **78**, 014205/1-6, 2008

40. Pusztai L, Harsányi I, Dominguez* H, Pizio* O; Assessing the level of consistency between diffraction experiments and interaction potentials: A combined molecular dynamics (MD) and Reverse Monte Carlo (RMC) approach; *Chem. Phys. Letts.*; **457**, 96-102, 2008

41. Jóvári P, Kaban I*, Steiner J*, Beuneu B*, Schöps A*, Webb A*, Local order in amorphous $Ge_2Sb_2Te_5$ and $GeSb_2Te_4$, *Phys. Rev.*, B **77** 035202/1-6, 2008

42. Jóvári P, Yannopoulos* S N, Kaban* I, Kalampounias* A, Lishchynskyy* I, Beuneu* B, Kostadinova* O, Welter* E, Schöps* A; Structure of As_xTe_{100-x} ($20 \leq x \leq 60$) glasses investigated with EXAFS, X-ray and neutron diffraction and reverse Monte Carlo simulation; *J. Chem. Phys.*; in press, 2008

43. Pusztai L, Dominguez* H, Pizio* O, Sokolowski* S; Detailed structural analysis of a 2 molal aqueous rubidium bromide solution: A combined molecular dynamics and Reverse Monte Carlo approach; *J. Mol. Liq.*; in press 2008

44. Pusztai L, Pizio* O, Sokolowski* S; Comparison of interaction potentials of liquid water with respect to their consistency with neutron diffraction data of pure heavy water; *J. Chem. Phys.*; **129,** 184103/1-6, 2008

45. Pamukchieva* V, Szekeres* A, Sváb E, Fábián M; Compositional dependence of the optical properties of new quaternary chalcogenide glasses of Ge–Sb–(S,Te) system; *Optical Materials;* **32**, 45-49, 2009

46. Pamukchieva* V, Szekeres* A, Todorova* K, Fábián M, Sváb E, Révay* Zs, Szentmiklósi* L; Evaluation of basic physical parameters of quaternary Ge–Sb-(S,Te) chalcogenide glasses; *J. Non-Cryst Solids;* **355**, 2485-2490, 2009

47. Kovachev* S, Kovacheva* D, Aleksovska* S, Sváb E, Krezhov* K; Structure and magnetic properties of multiferroic $YCr_{1-x}Fe_xO_3$ ($0 \leq x \leq 1$); *J Optoelectronics and Advanced Materials;* **11**, 1549 – 1552, 2009

48. Pothoczki Sz, Temleitner L, Jóvári P, Kohara* S, Pusztai L; Nanometer range correlations between molecular orientations in liquids of molecules with perfect tetrahedral shape: CCl_4, $SiCl_4$, $GeCl_4$ and $SnCl_4$; *J. Chem. Phys.*; **130,** 064503/1-7, 2009

49. Pothoczki Sz, Pusztai L; Molecular liquid $TiCl_4$ and VCl_4: Two substances, one structure ?; *J. Mol. Liq.*; **145**, pp. 38-40, 2009

50. Vácha* R, Megyes* T, Bakó* I, Pusztai L, Jungwirth* P; Benchmarking polarizable molecular dynamics simulations of aqueous sodium hydroxide by diffraction measurements; *J. Phys. Chem. A;* **113**, pp. 4022-4027, 2009

51. Pusztai L, Dominguez* H, Pizio* O, Sokolowski* S; Detailed structural analysis of a 2 molal aqueous rubidium bromide solution: A combined molecular dynamics and Reverse Monte Carlo approach; *J. Mol. Liq.*; **147**, pp. 52-55, 2009

52. Ohara* K, Kawakita* Y, Temleitner L, Pusztai L, Kohara* S, Jono* A, Shimakura* H, Inoue* N, Takeda* S; Structural analysis of Lithium Lanthanum Titanate with perovskite structure; *phys. stat. sol. c;* **6,** 1004-1007, 2009

53. Mile V, Pusztai L, Dominguez* H, Pizio* O; Understanding the Structure of Aqueous Cesium Chloride Solutions by Combining Diffraction Experiments, Molecular Dynamics Simulations, and Reverse Monte Carlo Modeling; *J. Phys. Chem. B.*; **113**, pp. 10760-10769, 2009

54. Pizio* O, Pusztai L, Sokolowski* S, Sokolowska* Z; Solvation force between surfaces modified by tethered chains: a density functional approach; *J. Chem. Phys.*; **130**, 13401/1-10, 2009

55. Pizio* O, Dominguez* H, Pusztai L, Sokolowski* S; A core-softened model fluid in disordered porous media. Grand-canonical Monte Carlo simulation and integral equations; *Physica A.*;

388, pp. 2278-2288, 2009

56. Almásy L, Turmine[*] M, Perera[*] A; Structure of aqueous solutions of ionic liquid 1-butyl-3-methylimidazolium tetrafluoroborate by small-angle neutron scattering; *Journal of Physical Chemistry B*; **112**, 2382-2387, 2008

57. Füzi J; Direct measurement of cold neutron moderator spectra; *Nuclear Instruments and Methods in Physics Research A*; **586**, 41-45 2008

58. Füzi J; Quality assessment of in-pile guides by energy resolved neutron imaging; *Nuclear Instruments and Methods in Physics Research A*; **586**. 46-50, 2008

59. Füzi J; Neutron motion in magnetic fields; *Meas Sci & Techn*; **19**, 034013/1-6, 2008

60. Füzi J; Spectral accuracy of multiwire proportional counter detectors in time of flight regime; *Meas. Sc.i & Techn*; **19**, 034028/1-7, 2008

61. Hanski[*] S, Junnila[*] S, Almásy L, Ruokolainen[*] J, Ikkala[*] O: Structural and conformational transformations in self-assembled polypeptide-surfactant complexes; *Macromolecules*; **41**, 866-872, 2008

62. Heaton[*] ME, Rogante[*] M, Len A; A feasibility study for a SANS investigation of a heat cured and laser machined organic resin microturbine as used for airflow sensing; *Multidiscipline Modeling in Materials and Structures*, **4**, 155-162, 2008

63. Knaapila[*] M, Almásy L, Garamus[*] VM, Ramos[*] ML, Justino[*] LLG, Galbrecht[*] F, Preis[*] E, Scherf[*] U, Burrows[*] HD, Monkman[*] AP; An effect of side chain length on the solution structure of poly(9,9-dialkylfluorene)s in toluene; *Polymer*; **49**, 2033-2038, 2008

64. Kyzyma[*] OA, Bulavin[*] LA, Aksenov[*] VL, Avdeev[*] MV, Tropin[*] TV, Korobov[*] MV, Snegir[*] SV, Rosta L; Organization of fullerene clusters in the system C60/N-methyl-2-pyrrolidone; *Materials structure*; **15**, 17−20, 2008

65. Kyzyma[*] OA, Bulavin[*] LA, Aksenov[*] VL, Tropin[*] TV, Avdeev[*] MV, Korobov[*] MV, Snegir[*] SV, Rosta L; Aggregation in C60/NMP, C60/NMP/water and C60/NMP/toluene mixtures; *Fullerenes, Nanotubes and Carbon Nanostructures*; **16**, 610–615, 2008

66. Lebedev[*] VT, Török Gy, Melenevskaya[*] EY, Vinogradova[*] LV, Ivanova[*] IN; Poly(N-vinylcaprolactam)-C60 complexes in aqueous solution; *Fullerenes, Nanotubes and Carbon Nanostructures*; **16**, 603 – 609, 2008

67. Meiszterics A, Sinkó[*] K; Calcium silicate ceramics; *Colloids and Surfaces A: Physico-chemical and Engineering Aspects*; **319**, 143-148, 2008

68. Petrenko[*] VI, Bulavin[*] LA, Avdeev[*] MV, Aksenov[*] VL, Rosta L; Neutron investigations of the interaction of surfactant molecules in non-polar solvent; *Ukrainian Journal of Physics*; **53**, 229-233, 2008

69. Petrenko[*] VI, Bulavin[*] LA, Avdeev[*] MV, Aksenov[*] VL, Rosta L; Neutron investigations of magnetite-oleic acid-benzene ferrofluids stability with the excess of surfactant (in Ukrainian); *Journal of Physical Studies*; **12**, 3201-3204, 2008

70. Rosta L, Füzi J, Török Gy; Design of focusing SANS spectrometer at BNC; *Meas Sci & Techn*; **19**, 034008/1-5, 2008

71. Sinkó[*] K, Meiszterics A, Rosta L; Comparative study of calcium silicate bulk systems produced by different methods; *Progress in Colloid and Polymer Science*; **135**, 130–138, 2008

72. Vass[*] Sz, Pedersen[*] JS, Plestil[*] J, Laggner[*] P, Rétfalvi E, Varga[*] I, Gilányi[*] T; Ambiguity in determining the shape of alkali alkyl sulfate micelles from small-angle scattering data; *Langmuir*; **24**, 408-417, 2008

73. Bende[*] A, Almásy L; Weak intermolecular bonding in N,N'-dimethylethyleneurea dimers and N,N'-dimethylethyleneurea – water systems: The role of the dispersion effects in intermolecular interaction; *Chemical Physics*; **354**, 202-210, 2008

74. Koszor[*] O, Tapasztó[*] L, Markó M, Balázsi[*] Cs; Characterizing the global dispersion of carbon nanotubes in ceramic matrix nanocomposites; *Appl Phys Lett*; **93**, 201910/1-3, 2008

75. Füzi J; Neutron beam phase space mapping, In: *Modern Developments in X-Ray and Neutron Optics*; Eds.: Erko A, Krist Th, Idir M, Michette AG, Springer; 43-57, 2008

76. Krist* Th, Teichert* A, Kovács-Mezei* R, Rosta L; Neutron supermirror development, In: *Modern Developments in X-Ray and Neutron Optics*; Eds.: Erko A, Krist Th, Idir M, Michette AG, Springer; pp. 355-370, 2008

77. Avdeev[*] MV, Bica[*] D, Vekas[*] L, Aksenov[*] VL, Feoktystov[*] AV, Marinica[*] O, Rosta L, Garamus[*] VM, Willumeit[*] R; Comparative structure analysis of non-polar organic ferrofluids stabilized by saturated mono-carboxylic acids; *Journal of Colloid and Interface Science*; **334**, 37–41, 2009

78. Bodnarchuck[*] V, Cser L, Ignatovich[*] V, Veres T, Yaradaykin[*] S; Investigation of periodic multilayers; *JINR Comm*; **E14**, 127, 2009

79. Danilyan[*] GV, Granz[*] P, Krakhotina[*] VA, Mezei F, Novitsky[*] VV, Pavlova[*] VS, Russina[*] M,Shatalov[*] PB, Wilpert[*] T; Rotational effect of fissile nucleus in binary fission of ^{235}U induced by cold polarized neutrons; *Physics Letters B*; **679**, 25–29, 2009

80. Elnikova LV; Lattice model calculations on aqueous acetone and tetramethyl urea; *arXiv:0905.0600v1 [cond-mat.soft]*; 1-5, 2009

81. Kozhevnikov[*] SV, Ott[*] F, Paul[*] A, Rosta L; Resonances and off-specular scattering in neutron waveguides; *Eur Phys J*; **167**, 87-92, 2009

82. Lebedev[*] VT, Melnikov[*] AB, Vinogradova[*] LV, Török Gy; Intra- and intermolecular organization of sulfopolystyrene ionomers in solutions: neutron scattering study 1; *Polymer Science A*; **51**, 372–380, 2009

83. Lebedev[*] VT, Melnikov[*] AB, Vinogradova[*] LV, Török Gy; Neutron study of self-organization in solutions of ionomers based on sulfonated polystyrene 1; *Vysokomolekulyarnye Soedineniya A*; **51**, 407–413, 2009

84. Lebedev[*] VT, Török Gy, Melnikov[*] AB, Orlova[*] DN, Ivanova[*] IN; Molecular and supramolecular structure of sulfonated polystyrene ionomers in solutions; *Journal of Surface Investigation. X-ray, Synchrotron and Neutron Techniques*; **3**, 582–591, 2009

85. Lushnikov[*] SG, Svanidze[*] AV, Gvasaliya[*] SN, Török Gy, Rosta L, Sashin[*] IL; Fractal properties of lysozyme: A neutron scattering study; *Phys Rev E*; **79**, 031913, 2009

86. Markó M, Cser L, Krexner[*] G, Török Gy; Theoretical consideration of the optimal performance of atomic resolution holography, *Meas Sci & Techn*; **20**, 015502, 2009

87. Petrenko[*] VI, Avdeev[*] MV, Almásy L, Bulavin[*] LA, Aksenov[*] VL, Rosta L, Garamus[*] VM; Interaction of mono-carboxylic acids in benzene by small-angle neutron scattering, *Colloids and Surfaces A*; **337**, 91-95, 2009

88. Petrenko[*] VI, Avdeev[*] MV, Aksenov[*] VL, Bulavin[*] LA, Rosta L; Magnetic fluids with the excess of surfactants. Data of small-angle neutron scattering, *Journal of Surface Investigation. X-ray, Synchrotron and Neutron Techniques*; **3**, 161-164, 2009

89. Russina[*] M, Mezei F; First implementation of repetition rate multiplication in neutron spectroscopy; *NIM A*; **604**, 624–631, 2009

90. Savii[*] C, Almasy L, Ionescu[*] C, Szekely NK, Enache[*] C, Popovic[*]i M, Sora[*] I, Nicoara[*] D, Savii[*] GD, Resiga[*] DS, Subrt[*] J, Stengl[*] V; Mesoporous silica matrices derived from sol-gel

process assisted by low power ultrasonic activation; *Processing and Applications of Ceramics* **3**, 59, 2009

91. Székely NK, Jancsó[*] G; Small-angle neutron scattering and volumetric studies of dilute solutions of dimethylpropyleneurea in heavy water; *J Phys Chem A*; **113**, 2207-2211, 2009

92. Székely NK, Krakovsky[*] I; Dependence of nanophase separated structure of epoxy hydrogels on swelling conditions investigated by SANS; *Eur Pol J*; **45**, 1385-1390, 2009

93. Várkonyi[*] Zs, Nagy G, Lambrev[*] P, Kiss[*] AZ, Székely NK, Rosta L, Garab[*] Gy; Effect of phosphorylation on the thermal and light stability of the thylakoid membranes; *Photosynth Res*; **99**, 161-171, 2009

94. Mezei F, Rosta L; Hungary for ESS; *PSCA International Science & Technology*; **3**, 326, 2009

95. Aksenov[*] VL, Tropin[*] TV, Kyzyma[*] OA, Avdeev[*] MV, Korobov[*] MV, Rosta L; On fullerene cluster formation in nitrogen-containing solvents, *Physics of the Solid State*, accepted for publication

96. Avdeev[*] MV, Bica[*] D, Vekas[*] L, Aksenov[*] VL, Feoktystov[*] AV, Rosta L, Garamus[*] VM, Willumeit[*] R; Structural aspects of stabilization of magnetic fluids by mono-carboxylic acids, *Advanced Materials Research*, accepted for publication

97. Avdeev[*] MV, Tropin[*] TV, Aksenov[*] VL, Rosta L, Kholmurodov[*] MT; On fullerene cluster formation in carbon disulfide. Data of small-angle neutron scattering and molecular dynamic simulation, *Journal of Surface Investigation. X-ray, Synchrotron and Neutron Techniques*, accepted for publication

98. Feoktystov[*] AV, Avdeev MV, Aksenov[*] VL, Bulavin[*] LA, Bica[*] D, Vekas[*] L, Garamus[*] VM, Willumeit[*] R; Contrast variation in small-angle neutron scattering from magnetic fluid magnetite/myristic acid/benzene, *Journal of Surface Investigation. X-ray, Synchrotron and Neutron Techniques*, accepted for publication

99. Gomes[*] SR, Margaca[*] FMA, Miranda Salvado[*] IM, Falcao[*] AN, Almásy L, Teixeira[*] J; SANS investigation of PDMS hybrid materials prepared by gamma-irradiation, *Nuclear Instruments and Methods in Physics Research Section B*, accepted for publication

100.	Kulvelis[*] YV, Trunova[*] VA, Lebedev[*] VT, Orlova[*] DN, Török Gy, Gelfond[*] ML; Synthesis and structural study of ferrofluid complexes with photodithazine and their application in PDT, *Journal of Polymer Physics*, accepted for publication

101.	Petrenko[*] VI, Aksenov[*] VL, Avdeev[*] MV, Bulavin[*] LA, Rosta L, Vekas[*] L, Garamus[*] VM, Willumeit[*] R; Structure analysis of water-based ferrofluids by means of small-angle neutron scattering, *Physics of the Solid State*, accepted for publication

102.	Petrenko* VI, Avdeev* MV, Aksenov* VL, Bulavin* LA, Rosta L; Effect of surfactant excess in non-polar ferrofluids probed by small-angle neutron scattering, Advanced Materials Research, accepted for publication

103.	Avdeev* MV, Tropin* TV, Aksenov* VL, Rosta L, Kholmurodov* MT; Formation of fullerene clusters in carbon disulfide. Data of small-angle neutron scattering and molecular dynamics, Journal of Surface Investigation. X-ray, Synchrotron and Neutron Techniques; 2, 819-825, 2008

104.	Barna* IF, Imre* AR, Rosta L, Mezei F; Two-phase flow model for energetic proton beam induced pressure waves in mercury target systems in the planned European Spallation Source; Eur Phys J B; 66, 419–426, 2008

105.	Gomes* SR, Margaca* FMA, Miranda Salvado* IM, Falcao* AN, Almásy L, Teixeira* J; SANS investigation of PDMS hybrid materials prepared by gamma-irradiation, Nuclear Instruments and Methods in Physics Research Section B 266 (24) 5166-5170, 2008

106.   Knaapila* M, Garamus* VM, Almásy L, Pang* JS, Forster* M, Gutacker* A, Scherf* U, Monkman* AP; Fractal Aggregates of Polyfluorene-Polyaniline Triblock Copolymer in Solution State., Journal of Physical Chemistry B; 112, 16415–16421, 2008

107.   Füzi J; Neutron beam phase space mapping, In: Modern Developments in X-Ray and Neutron Optics, Eds: Erko A, Krist Th, Idir M, Michette AG, Springer (2008) 43-57

108.   Krist* Th, Teichert* A, Kovács-Mezei* R, Rosta L; Neutron supermirror development, In: Modern Developments in X-Ray and Neutron Optics, Eds: Erko A, Krist Th, Idir M, Michette AG, Springer (2008) 355-370

109.   Cser L, Krexner[*] G, Marko M, Sharkov[*] I, Török Gy; Neutron Holography, *Acta Phys Hung B* **26** (1,2) (2006) 189–194

110.   Mykhaylyk[*] OM, Kotsuruba[*] AV, Dudchenko[*] NO, Török Gy; Some signal effects in human erythrocytes on specific binding of free doxorubicin and doxorubicin conjugates with magnetite nanoparticles, *Ukrainskii Biokhimicheskii Zhurnal* **77** (4) (2006) 84-92

111.   Kulvelis* YV, Lebedev* VT, Török Gy, Melnikov* AB; Structure of the water-salt solutions of DNA with sulfonated scandium diphthalocyanine, PNPI preprint – 2669, 20 pages, Gatchina 2006

112.   Kulvelis[*] YV, Lebedev[*] VT, Török Gy, Melnikov[*] AB; Structure of the water salt solutions of DNA with sulfonated scandium diphthalocyanine, *Journal of Structural Chemistry* **48** (4) (2007) 740-746

113.   Lebedev[*] VT, Vinogradova[*] LV, Török Gy; Structural Features of Star Shaped Fullerene (C60) Containing Polystyrenes: Neutron Scattering Experiments, *Polymer Science Ser A* **50**, (10) (2007) 1090-1097

114.   Káli Gy, Sánta Zs, Bleif* HJ, Mezei F, Rosta L, Szalók* M; Commissioning of the high resolution TOF diffractometer at the Budapest Research Reactor; Zeitschrift für Kristallographie; Part 1 Suppl 26, 165-170, 2007

115.   Mezei F; New perspectives from new generations of neutron sources; C R Physique; 8, 909–920, 2007

116.   Weidlich* D, Cser L, Polzin* T, Cristiano* D, Zickner* H; Virtual reality approaches for immersive design; Cirp Annals-Manufacturing Technology; 56, 139-142, 2007

117.   Avdeev* MV, Bica* D, Vekas* L, Aksenov* VL, Feoktystov* AV, Marinica* O, Rosta L, Garamus* VM, Willumeit* R; Comparative structure analysis of non-polar organic ferrofluids stabilized by saturated mono-carboxylic acids; Journal of Colloid and Interface Science; 334, 37–41, 2009

118.   Bodnarchuck* V, Cser L, Ignatovich* V, Veres T, Yaradaykin* S; Investigation of periodic multilayers; JINR Comm; E14, 127, 2009

119.   Danilyan* GV, Granz* P, Krakhotina* VA, Mezei F, Novitsky* VV, Pavlova* VS, Russina* M,Shatalov* PB, Wilpert* T; Rotational effect of fissile nucleus in binary fission of 235U induced by cold polarized neutrons; Physics Letters B; 679, 25–29, 2009

120.   Elnikova LV; Lattice model calculations on aqueous acetone and tetramethyl urea; arXiv:0905.0600v1 [cond-mat.soft], 1-5, 2009

121.   Kozhevnikov* SV, Ott* F, Paul* A, Rosta L; Resonances and off-specular scattering in neutron waveguides; Eur Phys J; 167, 87-92, 2009

122.   Lebedev* VT, Melnikov* AB, Vinogradova* LV, Török Gy; Intra- and Intermolecular Organization of Sulfopolystyrene Ionomers in Solutions: Neutron Scattering Study 1; Polymer Science A; 51, 372–380, 2009

123. Lebedev* VT, Melnikov* AB, Vinogradova* LV, Török Gy; Neutron Study of Self-Organization in Solutions of Ionomers Based on Sulfonated Polystyrene 1; Vysokomolekulyarnye Soedineniya A; 51, 407–413, 2009

124. Lebedev* VT, Török Gy, Melnikov* AB, Orlova* DN, Ivanova* IN; Molecular and Supramolecular Structure of Sulfonated Polystyrene Ionomers in Solutions; Journal of Surface Investigation. X-ray, Synchrotron and Neutron Techniques; 3, 582–591, 2009

125. Lushnikov* SG, Svanidze* AV, Gvasaliya* SN, Török Gy, Rosta L, Sashin* IL; Fractal properties of lysozyme: A neutron scattering study; Phys Rev E; 79, 031913, 2009

126. Markó M, Cser L, Krexner* G, Török Gy; Theoretical consideration of the optimal performance of atomic resolution holography, Meas Sci & Techn; 20, 015502, 2009

127. Mezei F, Rosta L; Hungary for ESS; PSCA International Science & Technology; 3, 326, 2009

128. Petrenko* VI, Avdeev* MV, Almásy L, Bulavin* LA, Aksenov* VL, Rosta L, Garamus* VM; Interaction of mono-carboxylic acids in benzene by small-angle neutron scattering, Colloids and Surfaces A; **337**, 91-95, 2009

129. Petrenko* VI, Avdeev* MV, Aksenov* VL, Bulavin* LA, Rosta L; Magnetic fluids with the excess of surfactants. Data of small-angle neutron scattering, Journal of Surface Investigation. X-ray, Synchrotron and Neutron Techniques; 3, 161-164, 2009

130. Russina* M, Mezei F; First implementation of Repetition Rate Multiplication in neutron spectroscopy; NIM A; 604, 624–631, 2009

131. Savii* C, Almasy L, Ionescu* C, Szekely NK, Enache* C, Popovic*i M, Sora* I, Nicoara* D, Savii* GD, Resiga* DS, Subrt* J, Stengl* V; Mesoporous silica matrices derived from sol-gel process assisted by low power ultrasonic activation; Processing and Applications of Ceramics 3, 59, 2009

132. Székely NK, Jancsó* G; Small-Angle Neutron Scattering and Volumetric Studies of Dilute Solutions of Dimethylpropyleneurea in heavy water; J Phys Chem A; 113, 2207-2211, 2009

133. Székely NK, Krakovsky* I; Dependence of nanophase separated structure of epoxy hydrogels on swelling conditions investigated by SANS; Eur Pol J; 45, 1385-1390, 2009

134. Várkonyi* Zs, Nagy G, Lambrev* P, Kiss* AZ, Székely NK, Rosta L, Garab* Gy; Effect of phosphorylation on the thermal and light stability of the thylakoid membranes; Photosynth Res; 99, 161-171, 2009

135. Lebedev* VT, Vinogradova* LV, Török Gy, Shamanin* VV; Long-range self-assembly in solutions of star-shaped polymers with fullerene C60 multifunctional centers, Fullerenes, Nanotubes and Carbon Nanostructures, accepted for publication

136. Török Gy, Lebedev* VT, Vinogradova* LV, Orlova* DN, Shamanin* VV; Molecular correlations in bulk star-shaped polystyrene with fullerene C60 center, Fullerenes, Nanotubes and Carbon Nanostructures, accepted for publication

137. Füzi J, Török Gy; Features of position sensitive neutron detectors; In: Signal Processing and Electronics for Nuclear Spectrometry; Ed: Dytlewski N, IAEA Vienna; 51-66, accepted for publication

Conference proceedings

1. Sziklai-László, I. Kovács, N. Adányi, M. Á. Cser: Selenium intake, blood status in healthy Hungarian and American children, asthmatics and diabetics, all living in Budapest. Metal Ions in Biology and Medicine, Vol. **10**, 359-365 (2008) ISBN 978-2-7420-0714-1

2. I. Sziklai-László, I. Kovács, N. Adányi, D. Majchrzak, M. Á. Cser: Selenium and carotenoid intake in healthy and asthmatic Hungarian adolescents. Trace Elements in the Food Chain, Vol. 3, 21-25 (2009) ISBN 978-963-7067-19-8

3. R. Répánszki, I. Sziklai - László, Zs. Kerner: Adsorption of corrosion and fission products on structural materials from the primary cicuit, Őszi Radiokémiai napok (2009) (in Hungarian). ISBN: 978-963-9970-01-4

4. K. Krezhov, S. Kovachev, D. Kovacheva, E. Svab, G. Andre, F. Porcher, Neutron Diffraction Investigation of Pb0.5La0.5FeO3, *7th International Conference of the Balkan Physical Union*; doi:10.1063/1.3322423, *AIP Conf. Proc.* -- January, 2010 -- Volume **1203**, pp. 205-210,

5. S. Kovachev, D. Kovacheva, S. Aleksovska, E. Svab, K. Krezhov, Structure and Properties Investigation of Mixed Oxides YCr1−xFexO3 (0 ⋚ x ⋚ 1), *7th International Conference of the Balkan Physical Union*; doi:10.1063/1.3322418, AIP Conf. Proc. -- January, 2010 -- Volume 1203, pp. 199-204,

6. V. Pamukchieva, A. Szekeres, E. Svab, M. Fabian, Z. Revay, L. Szentmiklosi; Spectral ellipsometric determination of the optical constants of multicompoment chalcogenide films of Ge-Sb-S-Te system; J. *Phys.: Conf. Ser.*; 113, 012054(5pp), 2008

7. Balaskó* M, Sváb E, Kiss* Z, Tanács* A, Nagy* A, Kuba* A; Study of the inner structure of a damaged control rod by neutron-and X-ray radiography and discrete tomography; In: *Proc. of Contributed papers, 8th World Conference on Neutron Radiography, October 15-20, 2006, USA,* Ed. M.Arif & R.G.Downing, DEStech Publ.Inc. Pennsylvania, USA; pp. 294-303, 2008.

8. Balaskó* M, Sváb* E, Endrőczi* G, Tarnai* Gy, Molnár* Gy, Vigh* Z; Study of defects in helicopter rotor blade reference objects by neutron-, and X-ray radiography, vibration diagnostics and ultrasound testing; In: *Proc. of Contributed papers, 8th World Conference on Neutron Radiography, October 15-20, 2006, USA,* Ed. M.Arif & R.G.Downing, DEStech Publ.Inc. Pennsylvania, USA; pp. 304-312, 2008.

9. M. Fábián, E. Sváb, Th. Proffen, E. Veress, Structure study of simple and multi-component borate glasses (in Hungarian: Egyszerű és többkomponensű bór-üvegek szerkezetvizsgálata), Proc. EMT XIV. International Conf. of Chemistry, Cluj, Romania, November 2008 (Ed. Hungarian Technical Sc. Society Transylvania), pp. 48-53 (2008)

10. V. Pamukchieva, A. Szekeres, E. Svab, M. Fabian, Z. Revay, L. Szentmiklosi, Spectral ellipsometric determination of the optical constants of multicompoment chalcogenide films of Ge-Sb-S-Te system, 15th Int Summer School on Vacuum, Electrons and Ion Technologies, September 2007, Varna/Bulgaria, J.Physics: Conf. Series 113, 12054 (2008)

11. Rosta L; Neutron research for materials science and nanotechnology at the Budapest Neutron Centre, In: Proc of 1st Italian Workshop for Industry "Industrial Applications of Neutron Techniques", organised by Rogante Engineering, Civitanova Marche, Italy, 12-14 June 2008, accepted for publication.

12. Zamponi* M, Pyckhout-Hintzen* W, Wischnewski* A, Monkenbusch* M, Willner* L, Káli Gy, Richter* D; Molecular observation of branch point localization in star polymer melts; International Conference on Neutron Scattering, Knoxville, USA, 03.05 - 07.05.2009, accepted for publication

13. Zamponi* M, Pyckhout-Hintzen* W, Monkenbusch* M, Wischnewski* A,Willner* L, Richter* D, Káli Gy; Branch Point Motion in Star Polymer Melts; International Conference on Quasielastic Neutron Scattering: Paul-Scherrer-Institut, Laue-Langevin, Schweiz, 10.02- 13.02.2009, accepted

for publication

Ph. D. Theses

1. R. Szőke (ELTE): Study of the health effects of glass wool by traditional and nuclear methods. Ph.D. Theses (Supervisor: I. Sziklai-László

Books, Book Chapters

1. Jóvári P, Kaban I*; Structural study of multicomponent glasses by the reverse Monte Carlo simulation technique; Nanostructured Materials for Advanced Technological Applications; Ed. J. P. Reithmaier, P. Petkov, W. Kulisch, C. Popov; in press, 2008